DEVELOPMENT OF SHALLOW LANDSLIDE RUNOUT DISTANCE MODELS BASED ON CLIMATE CHANGE SCENARIOS (EOCENE FLYSCH FACIES, WESTERN BLACK SEA REGION)

İKLİM DEĞİŞİKLİĞİ SENARYOLARINA BAĞLI SIĞ HEYELAN YAYILIM MESAFESİ MODELLERİNİN GELİŞTİRİLMESİ (EOSEN FLİŞ FASİYESİ, BATI KARADENİZ BÖLGESİ)

MÜGE PINAR KÖMÜ

PROF. DR. CANDAN GÖKÇEOĞLU

Supervisor

Submitted to
Graduate School of Science and Engineering of Hacettepe University
as a Partial Fulfillment to the Requirements
for the Award of the Degree of Doctor of Philosophy
in Geological Engineering.

2024

To My Dear Mother and Father…

ABSTRACT

DEVELOPMENT OF SHALLOW LANDSLIDE RUNOUT DISTANCE MODELS BASED ON CLIMATE CHANGE SCENARIOS (EOCENE FLYSCH FACIES, WESTERN BLACK SEA REGION)

Müge Pınar KÖMÜ

Doctor of Philosophy, Department of Geological Engineering

Supervisor: Prof. Dr. Candan GÖKÇEOĞLU

Co- Supervisor: Prof. Dr. Hakan Ahmet NEFESLİOĞLU

May 2024, 178 pages

The shallow landslides, increased by climate change, currently rank high in the list of natural disasters that humanity frequently struggles with, posing significant irreparable problems for many societies. The aim of the dissertation is to test empirically-statistically developed shallow landslides runout distance models to estimate possible damages by shallow landslides for large area. Eocene flysch facies, cover a quite extensive area and determined considering the geological natural boundary in Western Black Sea region of Türkiye, are exceedingly active with respect to shallow landslides occurrence. The shallow landslide inventory for the studied region was primarily prepared. Considering that the field covers a very large area, the field was divided into three sub-basins in order to model more realistically. In addition, descriptive statistical evaluations on the sub-basin basis regarding the travel angle, depth and observed runout distance of the shallow landslides in the prepared inventory were separately made for each three sub-basins. The

testing of the runout distance probability assessment of shallow landslides requires to conduct the process of the detection of shallow landslides initiation points and their propagations. It is also necessary to generate a shallow landslide susceptibility map to allow for the most reliable prediction of possible initiation points of shallow landslides. Shallow landslides susceptibility maps were created using machine learning logistic regression method to determine the shallow landslide initiation points. This study was conducted based on two phases, one with Representative Concentration Pathway (RCP) scenario values and one without. Critical threshold values for shallow landslide initiations selected by considering shallow landslide susceptibility maps and RCP scenarios' precipitation values. In the initial analysis, it was assumed that only the shallow landslide susceptibility is required to be greater than 0.70 in order for the cell to be accepted as the shallow landslide initiations. In the reckon with RCP scenarios, it was assumed that if the cell's shallow landslide susceptibility value is greater than 0.70 and it receives more than 81 mm of precipitation according to the RCP rainfall scenarios, that cell is accepted as the shallow landslide initiations. In the second stage of the study, runout distance empirical probability models were prepared for both models with RCP scenarios and without RCP scenarios. The Flow-R 1.0.0 software was utilized by applying Modified Holmgren algorithm and Simplified Friction-Limited Model (SFLM) algorithm parameters, aiming to offer an empirical estimation of runout distances during the propagation process. Two types of parameter sets were created, namely the debris flow parameters model and the shallow landslide parameters model for runout distance estimation, and their comparative evaluations were conducted. The determination coefficients for predicting the maximum runout distance probability of shallow landslides and debris flows using the empirical runout distance model were found to be 0.62 and 0.64, respectively. When the obtained results are also assessed by reckoning with RCP scenarios, it is manifested that the possible shallow landslides initiations and their runout distances will decline in the future according to RCP scenarios.

Keywords: Shallow landslide, Debris flow, Empirical method, Runout distance, Flow-R, Climate change, RCP, Eocene flysch facies.

ÖZET

İKLİM DEĞİŞİKLİĞİ SENARYOLARINA BAĞLI SIĞ HEYELAN YAYILIM MESAFESİ MODELLERİNİN GELİŞTİRİLMESİ (EOSEN FLİŞ FASİYESİ, BATI KARADENİZ BÖLGESİ)

Müge Pınar KÖMÜ

Doktora, Jeoloji Mühendisliği Bölümü

Tez Danışmanı: Prof. Dr. Candan GÖKÇEOĞLU

İkinci Tez Danışmanı: Prof. Dr. Hakan Ahmet NEFESLİOĞLU

Mayıs 2024, 178 sayfa

İklim değişikliğiyle artan sığ heyelanlar, günümüzde insanlığın sıklıkla mücadele ettiği doğal afetler listesinde üst sıralarda yer almakta ve birçok toplum için telafisi mümkün olmayan önemli sorunlara neden olmaktadır. Bu doktora tezinin amacı, geniş alanlar için sığ heyelanların olası hasarlarını tahmin etmek amacıyla ampirik-istatistiksel olarak geliştirilmiş sığ heyelan yayılım mesafesi modellerini test etmektir. Türkiye'nin Batı Karadeniz Bölgesi'nde oldukça geniş bir alanı kaplayan ve jeolojik doğal sınır dikkate alınarak belirlenen Eosen Fliş Fasiyesi, sığ heyelan oluşumu açısından son derece aktiftir. Çalışılan bölge için öncelikle sığ heyelan envanteri hazırlanmıştır. Sahanın oldukça geniş alanı kapsadığı göz önüne alındığında daha gerçekçi olarak modelleme yapabilmek için saha 3 alt havzaya bölünmüştür. Tanımlayıcı istatistiksel değerlendirmeler, hazırlanan envanterdeki sığ heyelanların erişim açısına, kayma derinliğine, yayılım mesafesine yönelik havza bazında her 3 alt havza için ayrı ayrı yapılmıştır. Sığ heyelanların yayılım mesafesi olasılık değerlendirmesinin test edilmesi, sığ heyelan başlangıç noktalarının ve

onların yayılmalarının tespit edilmesi sürecinin yürütülmesini gerektirir. Sığ heyelanların olası başlangıç noktalarının en güvenilir şekilde tahmin edilebilmesi için sığ heyelan duyarlılık haritasının oluşturulması da gerekmektedir. Sığ heyelan duyarlılık haritaları, sığ heyelan başlangıç noktalarının belirlenmesi amacıyla makine öğrenimi lojistik regresyon yöntemi kullanılarak oluşturulmuştur. Bu çalışma, biri Temsili Konsantrasyon Yolları (RCP) senaryoları değeri olan, diğeri olmayan iki aşamaya dayalı olarak yürütülmüştür. Sığ heyelan başlangıç noktalarının kritik eşik değerleri, sığ heyelan duyarlılık haritaları ve RCP senaryolarının yağış değerleri dikkate alınarak seçilmiştir. İlk analizde hücrenin sığ heyelan başlangıcı olarak kabul edilebilmesi için yalnızca sığ heyelan duyarlılığının 0,70' ten büyük olması gerektiği kabul edildiği varsayılmıştır. RCP senaryoları dikkate alındığında, hücrenin sığ heyelan duyarlılık değeri 0.70' ten büyükse ve RCP yağış senaryolarına göre 81 mm' den fazla yağış alıyorsa o hücre sığ heyelan başlangıcı olarak kabul edildiği varsayılmıştır. Çalışmanın ikinci aşamasında RCP senaryolu ve RCP senaryosuz her iki model için de yayılım mesafesi ampirik olasılık modelleri hazırlanmıştır. Yayılım süreci sırasında yayılım mesafelerinin ampirik bir tahminini sunmayı amaçlayan Modifiye Holmgren algoritması ve basitleştirilmiş sürtünme sınırlı model (SFLM) algoritması parametreleri uygulanarak Flow-R 1.0.0 yazılımı kullanılmıştır. Yayılım mesafesi tahmini için moloz akması parametreleri modeli ve sığ heyelan parametreleri modeli olmak üzere iki tip parametre seti oluşturulmuş ve bunların karşılaştırmalı değerlendirmeleri yapılmıştır. Yayılım mesefesi ampirik modeli sonuçları, sığ heyelanların ve moloz akmalarının maksimum yayılma mesafesi olasılığını tahmin etmedeki determinasyon katsayıları sırasıyla 0.62 ve 0.64 olarak bulunmuştur. Elde edilen sonuçlar RCP senaryoları da dikkate alınarak değerlendirildiğinde, gelecekte olası sığ heyelan başlangıçlarının ve bunların yayılım mesafelerinin azalacağı ortaya çıkmaktadır.

Anahtar Kelimeler: Sığ heyelan, Moloz akması, Ampirik yöntem, Yayılım mesafesi, Flow-R, İklim değişikliği, RCP, Eosen fliş fasiyesi.

ACKNOWLEDGEMENTS

First of all, I would like to express my gratitude to my advisors. Since my master's thesis, I thank my advisor, Prof. Dr. Candan GÖKÇEOĞLU, who has never withheld his support and guidance from me in every difficult situation, who has always made my work easier with his practical and professional solutions through these challenging times. He has always been an exemplary person with his profound knowledge and attitude for me. I am very thankful to my dedicated co-advisor, Prof. Dr. Hakan Ahmet NEFESLİOĞLU, who has always been attentive and maintained professionalism through these hardest of times. His new and modern approaches guided my academic path. I have always felt very lucky to work with my co-advisor.

I would like to express my gratitude to my TIK members: Prof. Dr. Aykut AKGÜN and Assist. Prof. Dr. Emrah PEKKAN for their guidance, support and insight throughout the my TIK period. They always contributed valuable ideas to my dissertation with their innovative perspectives. I would like to thank the members of the examining committee, Prof. Dr. Taner Bekir SAN and Assoc. Prof. Dr. Nejan HUVAJ SARIHAN, for their valuable criticisms and remarks during my dissertation defence.

Special thanks to Turkish State Meteorological Service for having provided historical data.

I extend my gratitude to my dear grandmother (Pembe ÜNAL), who eagerly awaited my doctoral graduation but, unfortunately, couldn't witness it. She was very excited and happy about my Ph.D. journey. She had been one of my biggest supporters during this thesis process and throughout my life.

I am deeply thankful to my parents (Şengül KÖMÜ and Yusuf KÖMÜ) who enthusiastically supported and encouraged me to pursue my doctoral studies, helped ease the difficulties, and always enriched my life with their love. I want to write a little more detail for my parents: I am immensely grateful to my dear mother, who has played the most significant role in shaping the valuable qualities I have today. She brightens every moment of my life with her pure heart and honest nature. She has always been by my side, offering support in every situation and never hesitating to make any sacrifice for me. She constantly strives to make my life better. To my dear father, who has never spared any effort, always understanding, humorous, calm, and by my side in every circumstance, I thank you for all the support throughout my life.

Müge Pınar KÖMÜ
May 2024, Ankara

TABLE OF CONTENTS

LIST OF TABLES

LIST OF FIGURES

SYMBOLS AND ABBREVIATIONS

Symbols

E_{kin}^{i}	Kinetic energy of the cell in direction i
E_{kin}^{0}	Kinetic energy of the central cell
a	Independent variable
α	Travel angle
b	Coefficient
e	Exponential constant
ΔE_{pot}^{i}	Change in potential energy to the cell in direction i
E_{f}^{i}	Energy lost in friction to the cell in direction
H	Height difference
g	Gravitational acceleration
i	Direction
j	Direction
K	Consistency index (fluid's resistance to flow)
L	Travel distance
N	The normal stress on the running surface (ρhgcos(φ))
n	Flow behavior index
P	Probability of landslide occurrence
ρ	Density
ρ_i	Susceptibility value in direction i
ρ_0	Previously determined susceptibility value of the central cell

ρ_i^p	Flow proportion in direction (i) according to the persistence
ρ_j^p	Flow proportion in direction (j) according to the persistence
ρ_i^{fd}	Susceptibility proportion in direction i
ρ_j^{fd}	Susceptibility proportion in direction j
S	Frictional resistance
$\tan\varphi$	Gradient of the energy line
u	Flow velocity
Δx	Increment of horizontal displacement
Δh	Elevation differences between cells
∇P	Pressure gradient
τ	Shear stress
τ_0	Yield stress
μ	Viscosity
$\dot{\gamma}$	Shear rate.
ξ	Turbulent coefficient

Abbreviations

A	Altitude
AI	Artifical Intelligence
AR5	Fifth Assessment Report
CCSM4	Community Climate System Model
CD	Closed Depression
CI	Convergence Index
CMIP5	Climate Model Intercomparison Project

CNBL	Channel Network Base Level
CND	Channel Network Distance
DEM	Digital Elevation Model
DL	Deep Learning
GIS	Geographic Information System
GPP	Gravitational Process Path
IPCC	Intergovernmental Panel on Climate Change
İRAP	Provincial Disaster Risk Reduction Plan
Lat.	Latitude
Long.	Longitude
LR	Logistic Regression
ML	Machine Learning
M	Earthquake Magnitude
NDVI	Normalized Difference Vegetation Index
ProDF	Progressive Debris-Flow Routing and Inundation Model
PGA	Peak Ground Acceleration
PLC	Plan Curvature
PRC	Profile Curvature
RAMMS	Rapid Mass Movements Simulation
RCP	Representative Concentration Pathway
RF	Random Forest
SA	Slope Aspect
SFLM	Simplified Friction Limited Method
SG	Slope gradient
SLF	Slope Length Factor
SRTM DEM	Shuttle Radar Topography Mission Digital Elevation Model

SVM	Support Vector Machine
TA	Travel Angle
TRIGRS	Transient Rainfall Infiltration and Grid-Based Regional Slope Stability
TWI	Topographic Wetness Index
UTM	Universal Transvers Mercator
VD	Valley Depth

1. INTRODUCTION

The maps prepared to include runout distances as part of an integrated study of shallow landslides and Representative Concentration Pathway (RCP) scenarios document the runout distances in the Western Black Sea region (Eocene flysch facies) of Türkiye with combining effects of climate change in this dissertation. This chapter primarily aims to provide insight into the dissertation's motivation, highight the main problem, pose research questions, specify the research scope, summarize the purposes and objectives, give detail information about research's materials and methodology, and present the organization of the dissertation by summarizing chapters.

1.1. Motivation

Shallow landslides are considered to be natural disasters capable of causing noteworthy tragedies by rocking the countries in today's world. Shallow landslides may actually lead to millions economic damage to tangible resources and numbers of casualties each year (Froude and Petley, 2018; Haque et al., 2019; Luino et al., 2022). For instance, the news of roads being partially buried due to shallow landslides has been increasingly prevalent in social media or television channels' news bulletins. With rapidly advancing technological capabilities, having more detailed information about the most current shallow landslides, which are also widely covered in the media, is crucial for future advanced studies (Pennington et al., 2022). Considering this information, the necessity of scientifically researching ways to overcome negative effects of shallow landslides has emerged. Society might get rid of the possible destructive effects of the shallow landslide disasters in the least possible and safest way with researching on shallow landslide runout distances. Runout distance predictions are so essential to shallow landslide studies for quantifying the detrimental effects of them in a possible disaster event that prolific researchers have been eager to enhance the existing knowledge in this field (Guthrie and Befus, 2021; Goetz et al., 2021; Vegliante et al., 2024). Runout distance can be explained that when the landslides start to mobilize, how far lanslides can travel by reaching maximum velocity (Ray et al., 2022). No developing runout strategy will be effective in improving runout distance achievement, unless researchers analyze shallow landslides' triggering factors accurately and consistently. There is a significant connection between

shallow landslides, climate change, and heavy rainfall. When heavy rainfalls are triggered by climate change, heavy rainfall leads to shallow landslides (Tiranti, Nicolò and Gaeta, 2019; Zhu et al., 2021a; Asada and Minagawa, 2023; Jemec Auflič et al., 2023; Smith et al., 2023; Song et al., 2023; Tiranti and Ronchi, 2023). Due to rapid climate change, observation of an increase in shallow landslide activity needs rapid adaptation and detailed plans in order to eliminate the negative effects of shallow landslides. When the existing various approaches on shallow landslides are combined with runout distance information, stronger foundational data will be provided for further advanced studies. For instance, shallow landslides susceptibility maps should include much information such as runout distances of shallow landslides so that society or government can effectively take precautions to be one step ahead in facing natural disaster threats of shallow landslides. In other words, the runout information of shallow landslide is obviously key marker of country's resilience. Although the landslide susceptibility is popular research topic in the landslide literature, the runout of landslide probability has frequently not been studied due to its uncertainties and challenging nature.

It is clearly revealed that a comprehensive map, which includes not only shallow landslide susceptibility and but also consists of their runout distances, can help to progress country's standing on the global stage about disaster management with respect to its landslide disasters resilience improvements. Based on this information, it should prioritize selecting more exposed to disastered locations for mapping the runout distance of shallow landslides in areas where shallow landslides frequently occur. Small-scale especially flow type of landslides frequently triggered in the Western Black Sea Region because of heavy rainfalls (Duman et al., 1998; Ocakoglu, Gokceoglu, and Ercanoglu, 2002; Can et al., 2005; Akgun, Gorum and Nefeslioglu, 2021). Eocene flysch facies are interesting and distinctive study area, where notable and significant observations can be made, in terms of abundance of shallow landslides occurrence. Thus, Eocene flysch facies, which are situated in the Western Black Sea Region, will be troughly tested in terms of shallow landslides such as their runout distances in this dissertation. It is note that Eocene flysch facies were actually chosen by considering based on natural geological boundaries to investigate the shallow landslide tendency. Preparation of the shallow landslide inventory map was actually a primary step that can examine shallow landslides in the study region in terms of their statistical descriptions. Satellite images and Google

Earth images allowed the observation of the shallow landslides in order to prepare the landslide inventory map. The shallow landslide susceptibility map was also prepared by using Machine Learning (ML) Logistic Regression (LR) to adapt to the technological developments. The determination of threshold of the shallow landslide's susceptibility constituted the determinant factor in this study. The use of empirical-statistical method, which offers researchers more practical researches, to examine shallow landslide runout distance was preferred runout calculation method due to its low cost. Shallow landslides' geometry and energy relationships, which indicate the line between failure initiations and their reached locations, and size were evaluated with empirical statistical method in this study. Angle of reach ("Fahrböshung") or Travel Angle (TA), is generally preferred method and depends on Simplified Friction Limited Method (SFLM), was used as the empirical method to analyse the runout distances in this study. Runout flow direction was estimated with Modified Holmgren (Horton et al., 2013) algorithm in this research. Flow-R 1.0.0 software (Horton et al., 2013), which can combine the SFLM and Modified Holmgren flow direction algoritms, was used in the empirical runout distances analyses in the dissertation.

Moreover, the exploration of connections between these previous mention steps and climate change is a highly valuable approach. Over the years, awareness of climate change has been better improved than it was in the past. Many researchers studied on relationships between landslide and climate change (Gariano and Guzzetti, 2016; Ciervo et al., 2017; Peres and Cancelliere, 2018; Park and Lee, 2021; Araújo et al., 2022; Lim and Kim, 2022; Wijaya et al., 2022; Guo et al., 2023; Jakob and Owen, 2023; Jemec Auflič et al., 2023; Kim, Jung and Kim, 2023; Nefros et al., 2023; Tiranti and Rochi et al., 2023; Park et al., 2024). However, shallow landslide runout relations and climate change relations have yet not been discussed. It was critical to tie a link between shallow landslides and climate change considering the precipitation data. The increasing prevalence of extreme rainfall events possessed a major concern because of its potential adverse effects such as triggering of shallow landslides events in the Eocene flysch facies. Increasing awareness about climate change RCP scenarios precipitation values had become a key priority in runout distances of shallow landslides in this study scope. This research suggests that, rather than scrutinizing on runout distance analyses only without

RCP precipitation, runout distance prediction should also be investigated through RCP precipitation scenarios in order to improve the perspective of future landslide hazard map.

Despite its difficulties, this thesis investigates not only the possible current runout distance of shallow landslides but also examine future possible shallow landslide runout distance in the Eocene flysch facies by considering climate change scenarios' precipitations effects. Thus, this dissertation might foster and deploy the next researches about the shallow landslide runout and climate change combinations applications. In fact, this thesis can also mainly highlight the importance of maps which include the shallow landslide runout distance information in the Eocene flysch facies. Additionally, the results of this thesis will not only support development of susceptible maps in terms of shallow landslide runout distance but also guide good practises with respect to investigation of incorporating the relationships between climate change and future hazard maps which also include future possible shallow landslide runout distance. Therefore, the present research can also provide as a valuable reference for researchers conducting future empirical runout distance analyses of shallow landslides. The main stages of the present research are (i) to scrutinize and test the empirical-statistical model for the shallow landslide runout distance in Eocene flysch facies, (ii) determine possible shallow landslide initiations for both the stages that include RCP precipitation scenarios and those that do not and (iii) generate the probable maximum runout distances of shallow landslide maps for both the stages that include RCP precipitation scenarios and those that do not for each determined period. In the following sections, the fundamental steps, including the definition of main problem, scope and objectives, goals, materials, methods, and thesis organization, have been examined separately to better specify basic stages of dissertation.

1.2. Problem Statement

Determining the dissertation problem statement is critical for the rest of the thesis structure and organization. It is clearly observed that many shallow landslides have occurred in the Western Black Sea Region in recent years due to the change in climatic conditions. Heavy rains in Eocene flysch facies trigger many shallow landslides across the region. Considering the potential in the region, runout maps are needed in order to be affected by all the negativities that may occur such as loss of life and property in the least

possible way. However, there is no information about runout distances on maps in Türkiye. Therefore, in this dissertation, it is aimed to reach a comprehensive assessment by including the runout distance on the maps for Eocene flysch facies.

1.3. Research Questions

Specific questions, which are chosen for this research topic in order to reduce uncertainties, are listed in the following:

i. How to improve the knowledge of runout distances of shallow landslides in the Eocene flysch facies economically and practically?

ii. Is it possible to observe the effect of changing climate on shallow landslide runout distance with future climate scenarios?

1.4. Research Scope and Purposes

It is possible to notice that the shallow landslide activity is increasing day by day both in Türkiye and in the world. When the recent studies are examined, it is seen that many researchers are very interested in shallow landslides due to the unexpected destructive impacts of the pending. It is clearly noticed that the quality of the studies has increased considerably with the developing technology. Nevertheless, the shallow landslide runout distance investigation is not common and missing on the susceptibility maps which are prepared in Türkiye. The precipitation data related to climate change are also included in the study to attempt to improve and expand the level of the study by envisoning in the coming years. Therefore, when this study is successfully completed, a very important and original development will be made in determining the shallow landslide runout distance in order to contribute to the landslide literature. To progress a detail comprehension of runout distances of shallow landslides and of the influence of the using empirical methods and climate changes on runout distance results, empirical-statistical modelling is executed in this study. In order to give better understand of the research scope and purposes, research objectives are also listed the form of the smart goals setting in the following sub-chapter.

1.5. Research Objectives

Objectives of the dissertation are listed below in order to develop runout models in Eocene flysch facies.

- Introduce Eocene flysch facies formation and analyse their characteristics,
- Analyse satellite and Google Earth images of the study area in terms of occurrence of shallow landslides,
- Prepare the shallow landslide events inventory map for the study area,
- Visualize the shallow landslides inventory in Eocene flysch facies,
- Prepare descriptive statistical analyses for the shallow landslide inventory,
- Prepare the shallow landslide susceptibility map by using ML logistic regression,
- Identify potential shallow landslide initiations,
- Decide critical parameters of the runout distance assessment in the empirical approach,
- Present simulation results and analyse them,
- Evaluate climate scenarios by considering precipitation data to examine the effects of climate change, and prepare spatial distribution of modelling of the RCP precipitation data in Geographic Information System (GIS) environment,
- Discover new possible shallow initiations by reckoning with RCP precipitation scenarios,
- Examine the future runout distance of shallow landslides by using the empirical-statistical method with same determined parameters.

The main contribution of this dissertation can be stated that by the end of study, researchers will have gained a comprehensive understanding of how relationship between future RCP precipitation scenarios and landslides runout distances predictions in the shallow landslide assessment can be important to resilience. Additionally, embracing software technology in both susceptibility mapping and runout assessment significantly boosted study success and visualisations, making it pivotal aspect of modern landslide assessment.

1.6. Materials

The research success is mostly depending on the available data set. Data sources are listed in Table 1.1 which offers a synopsis of data obtained from public open sources, the published literature and tecnical reports. Even though this study consists of many stages, the field studies and examination of satellite images or Google Earth images constitute the primarily part of the study in order to develop the landslide inventory database. Prepared landslide inventory will also be analysed in terms of considering multiple attributes. Therefore, it is very significant to rigorously work on these stages as the other stages will be based on these stages. Not only landslide inventory is critical for runout assessment but also development of the shallow landslide susceptibility model by using ML is also critical in terms of determination of the possible source areas in order to determine runout distances. Table 1.1 has a high level of importance in preparation of susceptibility maps and determination of landslide initiations.

Table 1.1. Data sources in this study.

Data Type	**Source**	**Data Resolution /Scala**
DEM	SRTM DEM	25 m
Land Use	CORINE Land Cover (CLC 2018 version is v.2020_20u1)	50000 m^2
NDVI	Copernicus Open Access Hub (https://scihub.copernicus.eu/dhus/#/home)	10 m
Geology	Eocene flysch facies from Akbaş et al. (2011) 1:1.250.000 Türkiye Geological Map	1:1.250.000
Geology	Türkiye Landslide Inventory Map, 1/500.000 scale Zonguldak Section (Duman et al., 2005a, 2005b)	1:500.000
Daily historical precipitations record	Turkish State Meteorological Service	-
RCP scenarios precipitations	NCAR (https://gis.ucar.edu/inspector)	105 km

Software have been utilized for the professional evaluation of the materials used in the thesis. Google Earth Pro, GIS software (ArcGIS 10.8.2, QGIS 3.30.1, SAGA GIS 7.8.2), and Flow-R 1.0.0 were used for performing data analysis and scientific computations. Python 3.11 (via the Spyder), is the programming language, was also used in this study.

1.7. Methodology

This study methodology is a multifaceted to stem from a range of interconnected steps. First, the shallow landslide susceptibility map preparation by using machine learning Logistic Regression (LR) is the fundamental part. Second, selection of the critical threshold values to determine possible shallow landslide initiations by checking shallow landslide susceptibility map and RCP scenarios precipitation values is very critical step of this study. Third, shallow landslide runout distance empirical methodology, which depends on the flow direction and SFLM (travel angle), is applied on the detected possible shallow landslide initiations to forecast the possible runout. The empirical runout analyses are implemented with the assistance of Flow-R 1.0.0 software. Finally, relevant parameter configuration is adjusted in order to obtained accurate models in the runout distance assessment. Flow diagram of the research frame is illustrated in Figure 1.1. It provides a general perspective of the relationship between the different dissertation steps.

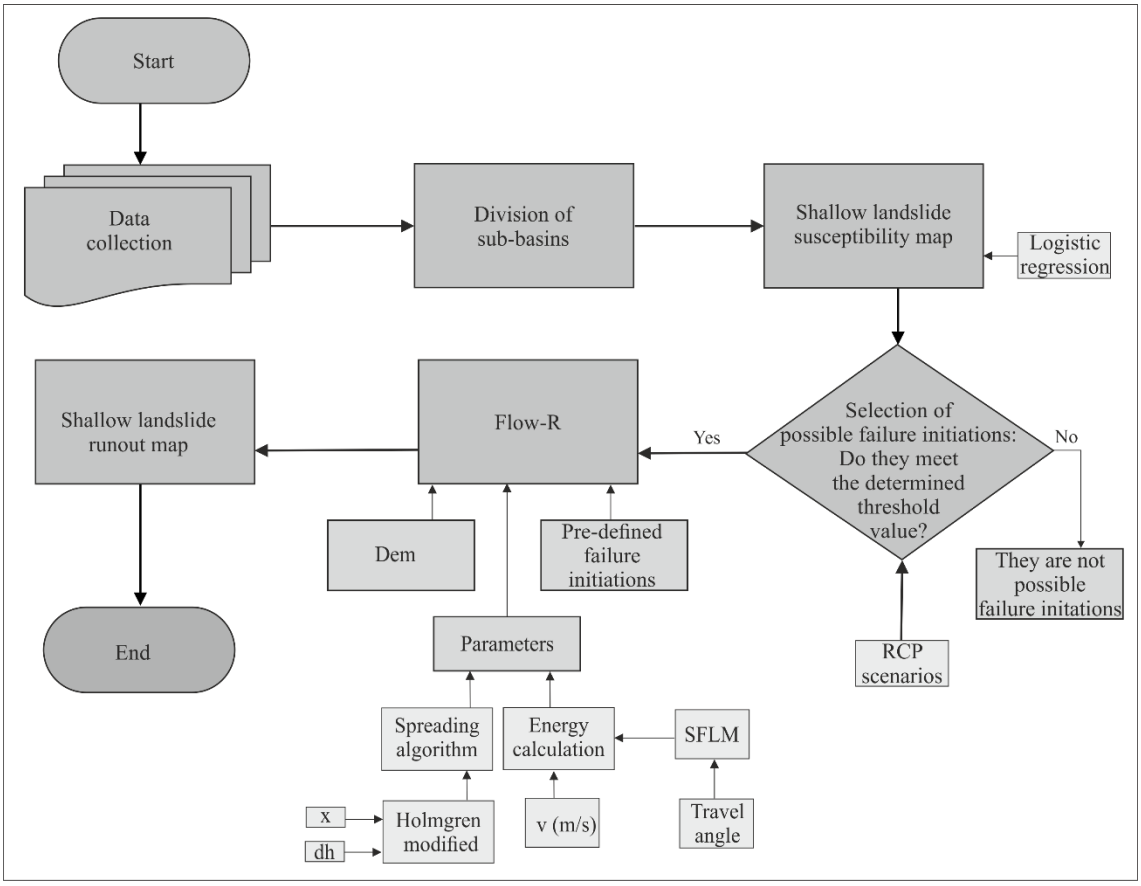

Figure 1.1.The process flow diagram representing the main stages of the shallow landslide runout distance assessment in this study.

1.8. Organization of the Dissertation

Dissertation framework can be summarized as follows:

- ***Chapter* 1** is an introduction chapter. It introduces the motivations, research problem statement and questions, scope, purposes and objectives. Data and methodology are also presented in this chapter.

- ***Chapter* 2** is an overview of the literature review.

- ***Chapter* 3** gives information about the characterization of study area in terms of its location, geomorphological characteristics, geology, land use and vegetation, seismicity and climate and rainfall characteristics of the study area. Division of sub-basins is also illustrated in this chapter.

- ***Chapter* 4** presents the shallow landslide inventory and susceptibility maps. Necessary statistical descriptions are also presented in this chapter.

- ***Chapter* 5** describes the runout analysis of shallow landslides in terms of their initiation's detections and propagations.

- ***Chapter* 6** presents the assessment of shallow landslide runout distance by including RCP climate change precipitation scenarios. Climate change scenarios precipitation data are assessed by considering the study area climate conditions. Runout maps are prepared by considering these shallow landslides initiation changes. Shallow landslide frequency changes are also evaluated.

- ***Chapter* 7** is a discussion chapter. It is critical to summarize and evaluate the results. Benefits and limitations of the study are also emphasized in this chapter.

- ***Chapter* 8** is a conclusion chapter. Recommendations of future works are also suggested and evaluated in this chapter according to simulation results.

- References are presented in the end of the dissertation.

2. LITERATURE REVIEW

This chapter is extensively prepared to assess the stage of the literature concerning fundamental concepts for the study.

2.1. Shallow Landslides

Landslides are globally known as natural disasters (Froude and Petley, 2018; Bellugi et al., 2021). If the latest natural disaster events are examined, it is not surprise to reach that of all the various kinds of natural disasters, shallow landslides increasingly tend to be catastrophic disasters that societies strive for the most. Therefore, considering the frequency of shallow landslides disasters that have occurred in the world, it is expected that researchers will contribute more to studies on this subject in order to provide effective resilience against disasters. Shallow landslides are generally triggered by heavy rainfalls (Guo et al., 2021; Zhou et al., 2022; Ortiz-Giraldo, Bitero and Vega, 2023; Guo et al., 2023; Song et al., 2023; Thomas et al., 2023). Although shallow landslides are generally triggered by heavy rainfalls and earthquakes, it is possible observe that human activities also cause shallow landslides. The surge in shallow landslides caused by human activity (such as mining and road construction) has been observed in recent years compared to previous years (Maki Mateso et al., 2023). Tanyaş et al. (2022) also allege that road construction leads to shallow landslides occurrence as if shallow landslides are triggered by the earthquake with a magnitude of 6. The latest some examples of studies conducted on the earthquake indicuded shallow landslides are Fan et al. (2023), Salinas-Jasso et al. (2023) and Yunus et al. (2023). The earthquake induced shallow landslides are also affected by antecedent rainfalls (Martino et al., 2022). To elaborate on the concept of shallow landslides, it is necessary to recall the definitions of landslide and debris flow closely associated with shallow landslides. In accordance with Cruden and Varnes (1996), a landslide is the downward displacement of rock, debris, or soil by gravitational forces. Debris flow is also defined as very rapid landslide type (Varnes, 1978). Debris flow is a flow type landslide which is composed of soil, rock and water (Colorado Geological Survey). Liang et al. (2021) attempted to illustrate potential relationships between landslide and debris flow by using machine learning supervised method of Random Forest (RF) in the preparation stage of landslide susceptibility mapping. Shallow landslides are

generally defined as movements occurring within a limited depth. Shallow landslides' depth has been recognized as different values such as less than 3 or 5 m in recent studies. For instance, while shallow landslides depths are defined as less than 5 m in studies Zaruba and Mencl (1969), Duman et al. (2005b), Li et al. (2020a), Keles and Nefeslioglu (2021), Durmaz et al. (2023), Maki Mateso et al. (2023), Wang et al. (2023) and Djukem et al. (2024), shallow landslides depths are less than < 3 m in the studies Cascini, Ciurleo and Di Nocera (2017), Shirzadi et al. (2017), Shirzadi et al. (2018), Troncone, Pugliese and Conte (2022), Zhou et al. (2022), Song et al. (2023) and Thomas et al. (2023).

Shallow landslides may be transformed into debris flows in the downstream regions with accumulating additional channel sediments (Stancanelli et al., 2017; Ortiz-Giraldo, Bitero and Vega, 2023; La Porta et al., 2023; Thomas et al., 2023). Debris flows tend to selectively channelize, frequently streaming from open slopes into pre-existing concavities and channel networks (Rosser et al., 2021). Debris flows often stem from shallow landslides in the majority of cases (Cuomo, 2020). It has also been observed in recent studies that shallow landslides and debris flows have been evaluated separately within the same study. For instance, shallow landslide and debris flow susceptibility maps were separately prepared in the study of Liang et al. (2021) in order to detect hazard areas. In addition, shallow landslides and debris flow were studied separately on propagation simulations in order to get accurate hazard chain prediction in the study of Zhou et al. (2022).

Increases in the frequency of shallow landslides associated with climate change may lead to big problem in many countries. Therefore, many researchers continue to elaborate on researching on shallow landslides. The shallow landslide inventory represents the spatial distribution of past landslides which are triggered factors such as precipitation and earthquake (Licata et al., 2023). In the following sub-chapter, the shallow landslide susceptibility map will be discussed.

2.2. Shallow Landslide Susceptibility Map

Landslide susceptibility mapping indicates on spatial distribution of anticipating possible landslide occurrence (Merghadi et al., 2020; Achu et al., 2023). Due to necessity of

enhancing resilience to disasters, it is also required to create a landslide susceptibility map, which commonly enable to handle the mitigation stage within disaster management scope. If literature is reviewed about landslide susceptibility maps, it is observed that GIS, remote sensing, quantitative techniques, frequency ratio, logistic regression analysis, artificial neural network analysis, fuzzy logic and ML methods have been used to preparation of landslide susceptibility in the studies. The rapid advancement in Artificial Intelligence (AI) technologies have created a huge and perpetual improvement in preparation of the landslide susceptibility map. There are main ML methods which are supervised, unsupervised, deep learning and reinforcement methods (Sun, Bocchini and Davison, 2020; Tehrani et al., 2022). Many types of ML methods have been favoured for preparation of the shallow landslide susceptibility map in the recent studies. It should be remarked that choosing appropriate machine learning methods in landslides susceptibility performance in a study may affect the success of the study. LR (Sevgen et al., 2019; Xion et al., 2020; Nhu et al., 2020; Qiu et al., 2022; Zhang et al., 2022a; Zydroń, Demczuk, and Gruchot, 2022; Song et al., 2023; Liu et al., 2024; Gu et al., 2023), Logistic Model Tree (Nhu et al., 2020; Naemitabar and Asadi, 2021; Ling et al., 2022; Ghasemian et al., 2022), RF (Adnan et al., 2020; Karakas et al., 2020; Nam and Wang, 2020; Pradhan and Kim, 2020; Xion et al., 2020; Wang, Liu and Liu et al., 2020; Naemitabar et al., 2021; Akinci, 2022; Ghasemian et al., 2022; Nnanwuba et al., 2022; Zhang et al., 2022a; Zydroń, Demczuk, and Gruchot, 2022; Ansar et al., 2023; Hussain et al., 2023; Song et al., 2023; Kaya Topacli, Ozcan and Gokceoglu, 2024; Liu et al., 2024; Unal, Kocaman and Gokceoglu, 2024), SVM (Adnan et al., 2020; Nhu et al., 2020; Nam and Wang, 2020; Wang et al., 2020; Xion et al., 2020; Naemitabar and Asadi, 2021; Akinci, 2022; Qiu et al., 2022; Gu et al., 2023; Kumar and Sarkar et al., 2023), XGBoost (Zhang et al., 2019; Pradhan and Kim, 2020; Can, Kocaman and Gokceoglu, 2021; Nnanwuba et al., 2022) are main supervised method to decide landslide susceptibility in studies. Deep Learning (DL) is also used in landslide susceptibility mapping (Zhan et al, 2019; Nam and Wang, 2020; Pradhan and Kim, 2020; Azarafza et al., 2021; Ado et al., 2022; Nikoobakht et al., 2022; Zhang et al., 2022a; Hussain et al., 2023; Mondini et al., 2023). Literature reviews indicate that RF is also frequently used ML method in the assessment of the landslide susceptibility. Nevertheless, LR machine learning will also be used in the studies in order to predict landslide prone areas. LR is deemed to be satisfactory for shallow landslides

susceptibility mapping in this thesis. Following equations, Equation 2.1 and 2.2, represent the utilized equations of the logistic regression landslide probability of occurrence.

$$P = 1 / (1 + e^{-y}) = e / (1 + e^{y}) \quad (2.1)$$

$$y = b_0 + b_1a_1 + b_2a_2 + \cdots\ldots + b_na_n \quad (2.2)$$

In this context, P represents the probability of landslide occurrence, varying between 0 and 1, with "e" denoting the exponential constant (Menard, 1995). In other words, when the pixel value of 1 shows landslide-prone areas, the value of 0 represents non-landslide areas. It can be grasped from the equations that the "a" value represents the independent variables, while the "b" coefficient denotes the regression coefficients associated with the independent variables. In contrast to a and b, y represents a dependent variable.

2.3. Runout Analysis Methods

Due to increasing severe shallow landslides hazard possibilities, that runout distance topic has virtually unrestricted potential for researching is extremely intriguing to researchers seeking to bring out the best method with respect to study conditions and its limitation. Runout distance can be defined that the distance between landslide' start and end points line, which indicates the landslide path of the movement and influenced by material properties and slope geometry, accounts for landslide runout distances (Zahra, 2010; Cuomo, 2020). The flow type of landslide such as a debris flow' horizontal distance length is called debris flow runout (Ortiz-Giraldo, Bitero and Vega, 2023). In order to assess behaviour of shallow landslides after following their initiations, runout analyses are necessary to be performed. A runout distance is influenced by controlling the factors are topography, geology, material properties, land cover etc. (Zahra, 2010; Guthrie and Befus, 2021). Prediction of landslide runout distance can be modelling by empirical-statistical methods, numerical methods and physical methods. In addition, a data-driven approach for estimating of shallow landslide runout was applied in the research of Giarola et al. (2024).

2.3.1. Empirical-Statistical Methods

Landslide initiation and its final location are empirically-statistically described by using landslide geometry or energy relationship. Angle of reach method is commonly used the empirical model in the studies (Di Napoli et al., 2021; Ju et al., 2022; Marchesini et al., 2024). The angle of reach, which also called fahrböschung angle (Heim, 1932) and travel angle (Cruden and Varnes, 1996) is measurement of the angle of line between initiation source and displaced mass (Corominas, 1996; Luna, 2012) (Figure 2.1). While L shows the travel distance, H represents the height difference between the shallow landslide initiation and maximum runout distance (Di Napoli et al., 2021) (Figure 2.1). "α" also denotes the reach angle in Figure 2.1 and Equation 2.3. Reach angle can be calculated from Equation 2.3. Landslide volume, movement type and topographic limitations along the travel line affect the reach angle (Corominas, 1996).

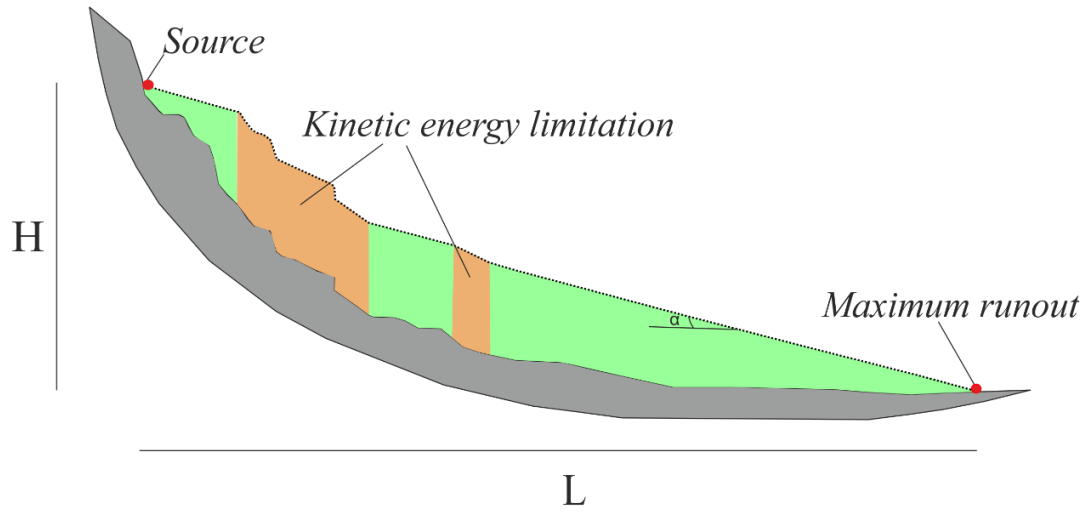

Figure 2.1. Reach angle and kinetic energy limitation (Modified after Horton et al., 2013 and Di Napoli et al., 2021).

$$\alpha = \tan^{-1}(H/L) \quad (2.3)$$

Moncayo and Ávila (2023) estimated landslide runout distance by using simple and multiple regression techniques depends on empirical relationships. Determination of the spatial distributions of the past landslides requires both field works and image interpretations (Luna, 2012). Field observation and image interpretation have also an important role in preparation of the empirical runout model with respect to analysing characteristic of past landslides' travel angle and velocity. The simultaneous utilization

of advanced technologies, which were increasingly added continuous innovations by researchers, along with empirical methods for runout distance investigation, is an important opportunity brought by the era.

Combining ML and empirical statistical method have been carried out a wide range of research studies. For instance, a novel terrain matching-targeted machine learning model was utilized to predict landslide runout distance and path in the study of Ju et al. (2022). Di Napoli et al. (2021) combined machine learning and ensemble approach with reach angle method to decide landslide runouts. They claimed that the empirical-statistical method is suitable for quick assessments. Tian, Xu and Li (2023) utilized Bayesian approaches to develop the empirical debris flow runout model by employing multichain method ($DREAM_{(ZS)}$ algorithm) and single chain (M–H algorithm). In addition, photogrammetric techniques may enhance the success of shallow landslide contemporary runout analyses. For instance, Roman Quintero et al. (2024) explored the utilization of geometric approximations for assessing landslide runout distances, employing photogrammetric techniques to characterize morphology of specified study area.

Furthermore, incorporating geometric approaches alongside assessing kinematic parameters such as velocity can greatly enhance the effectiveness of runout distance implementation (Falconi et al., 2023). Energy calculation and geometric relationships were used together in many studies (Horton et al., 2013; Park, Lee and Woo, 2013; Pastorello, Michelini and D'Agostino, 2017; Pradhan et al., 2016; Rahman, Ahmed and Di, 2017; McCoy, 2019; Sturzenegger et al., 2019; Do, Yin and Guo, 2020; Polat and Erik, 2020; Ali et al., 2021; Bera, Melo and Guru, 2021; Charbel and El Hage Hassan, 2021; Giano, Pescatore and Siervo, 2021; Jiang et al., 2021; Liu et al., 2022; Putra et al., 2022; Xu et al., 2022; Sharma et al., 2023) (Figure 2.1). Steger et al. (2022) also studied on data-driven approaches based on geomorphometric analyses to simulate debris flow runout. Vegliante et al. (2024) used the Legros equation (Legros, 2002) to find shallow landslide runout. Equation 2.4 shows the Legros equation (Legros, 2002) that L represents the extent of the runout in a planar direction, and V stands for the volume of the initial area of activity (Vegliante et al., 2024). a and b also represent the coeffcients in Equation 2.4.

$$L = aV^b \tag{2.4}$$

2.3.2. Numerical Methods

Various numerical methods have been studied for shallow landslides and debris flows. A flow type of landslide flow can be examined as a non-Newtonian fluid motion (Hong, Jeong and Kim, 2020). Unlike Newtonian fluids, non-Newtonian Fluids focus on material properties in addition to density and viscosity. Motion of fluids contains two kinds of equivalent descriptions which are Eulerian and Lagrangian. Both of them can be used in the runout distance calculations. Navier-Stokes equation (Equation 2.5) and depth averaged equations are critical equations of applying of the numerical methods to simulate fluid mobility. Depth-averaging the Navier-Stokes equations enable to examine debris flow simulation economically (Kang, Hong and Jeong, 2021). These equations can solve the rheologies.

$$\rho\,(\partial\vec{v}/\partial t+\vec{v}\cdot\nabla\vec{v})= -\nabla P +\rho\vec{g} + \mu\nabla^2\vec{v} \tag{2.5}$$

Rheology explores the interplay between the viscosity and shear stress experienced by a debris flow (Khan et al., 2021). Rheological model is also used to define material property of debris flow which can be obtained from back-analysis (Cuomo, 2020). Bingham (Equation 2.6), Herschel Bulkley (Equation 2.7) and Voellmy Equation (2.8) rheologies are recurringly used for debris flows in the studies. Equation elements' explanations were given in Table 2.1. While Bingham and Herschel Bulkley rheologies are obtained from considering the studies of Kang, Hong and Jeong (2021), Xia and Tian (2022) and Paul et al. (2023), Voellmy equation is also obtained from RAMMS software online page under the title of debris flow theory of the friction parameters.

$$\tau = \{\tau_0+ \mu \cdot|\dot{\gamma}| \text{ if } |\tau| > \tau_0 \text{ or, } 0 \text{ if } |\tau| \leq \tau_0\} \tag{2.6}$$

$$\tau = \tau_0 + K \cdot |\dot{\gamma}|^n \tag{2.7}$$

$$S = \mu N + ((\rho g u^2) / \xi) \tag{2.8}$$

The shear stress (τ) is calculated by using the yield stress (τ_0), viscosity (μ) and shear rate ($\dot{\gamma}$). “K” and “n” are also index values. Furhermore, frictional resistance (S) is obtained by using not only relations between the viscosity and normal stress (N) but also combining the relations between multiple elements which are density (ρ), gravitational acceleration (g), velocity (u) and turbulent coefficient (ξ).

Table 2.1. Equations' element clarification.

Equation element	Explanation
∇P	Pressure gradient
τ	Shear stress
τ_0	Yield stress
μ	Viscosity
$\dot{\gamma}$	Shear rate
K	Consistency index (fluid's resistance to flow)
n	Flow behavior index
S	Frictional resistance
ξ	Turbulent coefficient
N	The normal stress on the running surface ($\rho hg\cos(\varphi)$)
ρ	Density
u	Flow velocity
g	Gravitational acceleration

Numerical analyses have changed and promoted greatly with the event of using software. Software, which were a superb success and improvement from a technological point of view, are tools to easily apply the numerical methods with using these equations and rhelogies in the studies. For instance, RAMMS: DEBRIS FLOW (DF) uses Eularian equations by applying Voellmy rheology, DAN3D employs Lagrangian equation and different rheologies. Moreover, Xu et al. (2023) employed the Coupled Eulerian–Lagrangian (CEL) method to estimate run-out distances in their debris flow runout assessment. The researchers have fostered significant numerical models by using

appropriate software and rheologies in their studies. Landslide runout distances are successfully predicted with help of numerical model DAN-W software by using Voellmy rheology for debris flow and frictional rheological model in the sliding source area (Yang et al., 2019). Numerical model in order to inspect runout of debris flow by applying Voellmy rheology in RAMMS: DF software in the studies of Calista et al. (2020), Abraham et al. (2021), Dash, Kanungo and Malet (2021), Vicari, Nordal and Thakur (2021), Mikoš and Bezak (2021), Oh et al. (2021), Zhou et al. (2022), Alene et al. (2023) and Bolliger, Schlunegger, and McArdell (2024). Numerical simulation was also applied to research into runout distance by using Debris-2D in the study of Chae et al. (2020). REEF3D code, which is a numerical model depending on Navier-Stokes equation in three-dimensions and developed in NTNU by Marine Civil Engineering group (Clark, 2018), was used to determination of runout distance in the study of Fornes et al. (2017) and Clark (2018). The Navier–Stokes momentum equation and continuity equation by considering the rheology of Herschel–Bulkley was used to simulate initiation and deposition of the debris flows and landslides in the study of Hong, Jeong and Kim (2020). In addition, debris flow runout simulations were completed by FLOW-3D which employs 3D Navier–Stokes equations using the finite difference method in the study of Zhang et al. (2021). r.avaflow depends on Voellmy rheology was used in the study of Fischer et al. (2020), Zhao, Amann, and Kowalski (2021) Baggio, Mergili, and D'Agostino (2021), and Zhao and Kowalski (2022). LPF^{3D}, which depends on Newtonian fluid, investigates three-dimensional landslide runout for flow-like landslide (Gao et al., 2023a). Its results were also verified with not only flume test but also real landslides in the study of Gao et al. (2023a). Debris flow runout prediction was also applied by using SFLOW, which solves shallow-flow model and the finite volume method, in the study of Li et al. (2020b). PFC3D software was used to numerically model flow type landslides movement by evaluating runout distances stages (Gao et al., 2023b). Comprehensive shallow landslide maps containing numerically calculated runout distances have been developed by using various combined stages in some studies. For instance, shallow landslides and debris flow hazard prediction were prepared by using combined with Transient Rainfall Infiltration and Grid-Based Regional Slope Stability (TRIGRS) and Rapid Mass Movements Simulation (RAMMS) (Zhou et al., 2022). RASH 3D, which depends on numerical modelling by calculating depth-averaged balance equations with considering Bingham rheology, and TRIGRS were used together during the scope of study to find runout

distance in the research of La Porta et al. (2023). Adjusted rainfall information, which is obtained by using a supervised machine learning method RF, and RAMMS were combined to forecast the debris flow in the study of Oh et al. (2021). Landslide hydrodynamic triggering model and the Pudasaini model (Pudasaini, 2012) were used together to simulate the shallow landslide motion under rainfall conditions in the study of Yin, Zhou and Peng (2023). The analysis of the landslide's runout characteristics and the conversion of energy is conducted using numerical model in the study of Li et al. (2022). Numerical model results were also verified with video recording in the study of Li et al. (2022).

2.3.3. Physical Methods

Flume tests, often in association with physical method, are principally conducted under controlled conditions in the laboratory by analysing of the flow rates, channel geometries, and material compositions for the landslide runout estimation. Proper identification of flow type of landslides runout was carried out by flume test, which is the physical method, in the studies of Baselt et al. (2021) and Gao et al. (2023). Video records are also strongly support to prepare an effective physical model. For example, videos are critical to find velocity of debris flow (Clark, 2018). The combined use of physical modeling with numerical models has been common in recent studies. For instance, Zhu et al. (2021b) combined numerical and physical model in an attempt to understand the failure mechanism. The studies (Clark, 2018; Melo, van Asch and Zêzere, 2018; Gan and Zhang, 2019) employed a combination of both physical flume testing and numerical methods to examine runout distances. Runout distances were numerically calibrated using rheologies by considering previous experimental flume test runout results in these studies. Despite physical models' results are more realistic than numerical models result (Zhu et al., 2020), it is arduous to reflect the real-time condition of the field in the laboratory (McDougal, 2017; Tang, Gratchev and Ravindran, 2023). Physical methods can not reconstruct the 3D topography due to scaling effects (Wei, Cheng and Dai, 2023). In fact, it is very difficult to perform the landslide events to repeated anymore at the same conditions in terms of adjusting their sensitivity of the measurement's accuracy. In addition, it is hard to perform physical modeling of runout distance in large areas because it is necessary to observe many events for accurate modelling (Goetz et al., 2021).

2.3.4. Comparisons of Runout Methods

While prediction of runout distance is the rife solution to negative effects of shallow landslides in almost every country, there is ongoing debate whether empirical methods might be more effective alternative. This part of the research has covered why the empirical method was chosen to use in the following analyses by comparing the both methods. There is no universally adopted method for runout analysis because each study has its own set of limitations and advantages. In other words, it is difficult to claim that one method can be superseded the other method because it depends on study requirements and conditions. Therefore, study conditions should be analysed more carefully in order to detect the suitable method.

Recent researches' results suggest that empirical-statistical runout methods in the analyses can lead to easy and practical work satisfaction and even enhanced reaching general and realistically simple approach by spending less time for computation. Although researchers are revolutionizing landslide runout strategies with helping of technology, the empirical method is still frequently preferred method so that it can provide profound results at runout distance studies without not having at a high level of expertise of statistic. Profuse dataset may bring successful estimation in empirical-statistical method. In fact, sufficient data sets obtained from field observations about clues of past landslides have given opportunity to predict future runout distances by using empirical-statistical method (Clark, 2018).

In addition, researches about studying with statistical-empirical and numerical models have developed in an extraordinary fashion thanks to improvement of software. A software enables to keep up with predicting possible future hazards by providing realistic simulations and visual data (Komu, Nefeslioglu and Gokceoglu, 2024). Runout distance can be empirically-statistically estimated with software having potent capabilities such as Flow-R (Horton et al., 2013), DFLOWZ (Bertie et al., 2014), DebrisFlow Predictor (Guthrie and Befus, 2021) and Progressive Debris-Flow Routing and Inundation (ProDF) model (Gorr et al, 2022), whereas RAMMS (Christen, Kowalski and Bartelt, 2010) DAN3D (Hungr and McDougall, 2009), r.avaflow (Mergili, Krenn and Chu, 2017) and

TITAN2D (Pitman et al., 2003) have been robust numerical software in order to predict runout distance in recent studies.

In general, statistical methods are accepted as powerful and easy (Chen et al., 2020a). Instead of only focusing of advantages of the empirical-statistical method, it is necessary to underline the disadvantages of this method for an objective decision. The previous studies evidences substantiate that approximate runout results are obtained in empirical-statistical methods. In addition, lack of the data is prone to errors because the empirical statistical correlation reliability is decreasing (Chen et al., 2020a). In addition, despite possessing extensive datasets, it is important to acknowledge the potential for errors or inaccuracies in the obtained results by using an empirical method. The precise evaluations may also prove challenging in a complex environment with using statistical-empirical methods (Komu, Nefeslioglu and Gokceoglu, 2023). Neglection of the initial material leads to conceptual uncertainty in the empirical method studies (Milledge et al., 2019). Not including volume information may also cause bias in the analyses. Unlike empirical-statistical method, numerical analyses have discriminant capabilities to characterize the effects of initial volume in simulations (Peruzzetto et al., 2020). It is noteworthy that due to computational complexities and their costly (Motamedi, 2013), numerical analyses should be guided by experts with strong knowledge and experience in terms of numerical methods (Khalkhali and Koochaksaraei, 2019). Allocating additional time to the calculation of runout distances in numerical analyses is necessary due to trying variety of rheological parameter options (Peruzzetto et al., 2020). Consequently, these analyses may not be suitable for studies requiring rapid decision-making. Unless rheology parameters of an of the shallow landslide event is explicitly stated, the event might not be realistically represented with numerical methods due to importance of the precision (McDougall, 2014; Melo, van Asch and Zêzere, 2018). It is highly valuable to complete the study with a more limited input dataset and budget (Melo et al., 2018).

To sum up, a simple, publicly available model that can provide accurate results for researchers is often the ideal option for many important studies. When considering the advantages of using empirical models, it is not surprising that they have been widely preferred in this study and in other recent studies.

2.3.5. Previous Works

It should not be forgotten that runout distance is a very current topic that is open to research and needs improvements. In this section, while it is focused on the previous studies about runout distance by statistically empirically modelling, it will be also evaluated how has the academic publication interest trend of empirically–statistically runout distance evolved from in recent years. Empirical-statistical runout method applied studies compiled between 2011 and 2024 are shown in Table 2.2.

Among the international researches focused on empirical investigation of landslide runout distance up to 2024, although *Landslides, J. Mt. Sci., Engineering Geology* and *Remote Sensing* have several publications related to this topic, scholarly journals showing the most favourite attentions in this topic are *Nat. Hazards Earth Syst. Sci* and *Natural Hazards* (Table 2.2).

The bar charts show numbers of studies about empirical-statistical approach for landslide runout distance at the landslide literature in the world from 2011 to 2024 (Figure 2.2). Figure 2.2, is good indicators of understanding the interest and progress in empirical landslides runout distances in terms of years, indicates that the interest in empirical runout distance researches has increased especially in the years 2021 and 2022. In fact, 2021 reached the highest number of publications about considering landslide runout distance by using the empirical method.

Landslide empirical runout studies have appeared as top priority in terms of studied current topic in landslide literature in recent years for many countries. Figure 2.3. shows the studies about using empirical method to scrutinize landslide runout with respect to country. Although Italy is the lead in academic contributions of this topic because of especially frequently occurrence of this type of landslide in this country, Canada and China contribute in the empirical runout landslide investigation as significant as Italy (Figure 2.3).

Table 2.2. Previous studies about empirical-statistical runout method.

Authors	Year	Published in	Country
Baumann	2011	Pan-Am CGS Geotechnical Conference	Argentina
Park, Lee and Woo	2013	International Journal of Innovative Research in Science, Engineering and Technology	Korea
Horton et al.	2013	Nat. Hazards Earth Syst. Sci.	Switzerland
Krikitos and Davies	2015	Landslides	New Zealand
Polting et al.	2016	Austrian Journal of Earth Sciences	Austria
Blais-Stevens and Behnia	2016	Natural Hazards	Canada
Gregoretti, Degetto and Boreggio	2016	Journal of Hydrology	Italy
Pradhan et al.	2016	Geocarto International	Korea
Pastorello, Michelini and D' Agostino	2017	J. Mt. Sci.	Italy
Sharir, Simon and Roslee	2018	ASM Sc. J.	Malaysia
Melo et al.	2018	Nat. Hazards Earth Syst. Sci.	Portugal
Mergili, Schwarz and Kociu	2019	Landslides	Austria
McCoy	2019	7th International Conference on Debris-Flow Hazards Mitigation	USA
Sturzenegger	2019	7th International Conference on Debris-Flow Hazards Mitigation	Canada
Do, Yin and Guo	2020	Geomat. Nat. Haz. Risk	Vietnam
Polat and Erik	2020	J. Mt. Sci.	Türkiye
Peruzzetto et al.	2020	Geosciences	Hong Kong
Bera, Melo and Guru	2021	Bulletin of Engineering Geology and the Environment	India
Ali et al.	2021	Natural Hazards	Pakistan
Charbel and El Hage Hassan	2021	Geo-Eco-Trop.	Lebanon

Table 2.2. continued. Previous studies about empirical-statistical runout method.

Author	Year	Published in	Country
Di Napoli et al.	2021	Water	Italy
Giano, Pescatore and Siervo	2021	Remote Sensing	Italy
Goetz et al.	2021	Nat. Hazards Earth Syst. Sci.	Chile
Gutrie and Befus	2021	Nat. Hazards Earth Syst. Sci.	Canada
Jiang et al.	2021	Frontiers in Earth Science	China
Liu et al.	2021	Geoscience Frontiers	Norway
Paudel, Fall and Daneshfar	2021	Geotech. Geol. Eng.	Nepal
Wallace and Santi	2021	Environmental & Engineering Geoscience	USA
Arghya, Hawlader and Guthrie	2022	Geohazard 8 Conference	Canada
Apriani et al.	2022	Tahun	Indonesia
Gorr et al.	2022	Landslides	Italy
Liu et al.	2022	Remote Sensing	China
Putra et al.	2022	RISET Geologi dan Pertambangan Indonesian Journal of Geology and Mining	Indonesia
Xu et al.	2022	Geoenvironmental Disasters	China
Hien et al.	2022	VNU Journal of Science: Earth and Environmental Sciences	Vietnam
Ju et al.	2022	Engineering Geology	China
Sharma et al.	2023	Natural Hazards	India
Falconi et al.	2023	Natural Hazards	Italy
Giorala et al.	2024	Catena	Italy
Vegliante et al.	2024	GeoHazards	Italy
Roman Quintero et al.	2024	Sustainability	Colombia
Marchesini et al.	2024	Engineering Geology	Italy

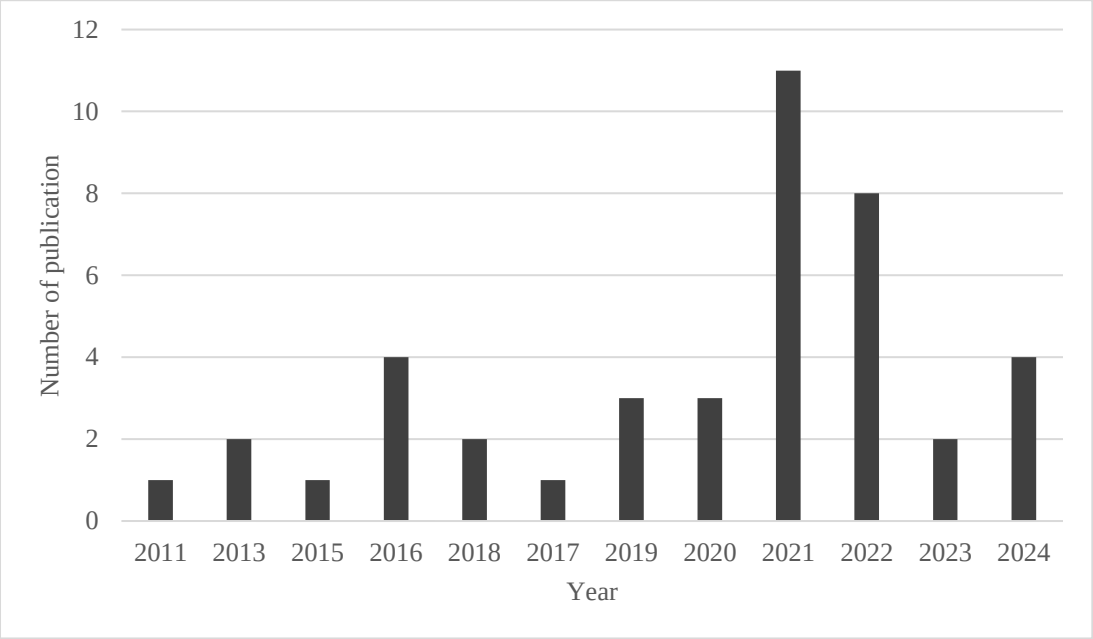

Figure 2.2. Empirical method runout interest in literature in terms of years.

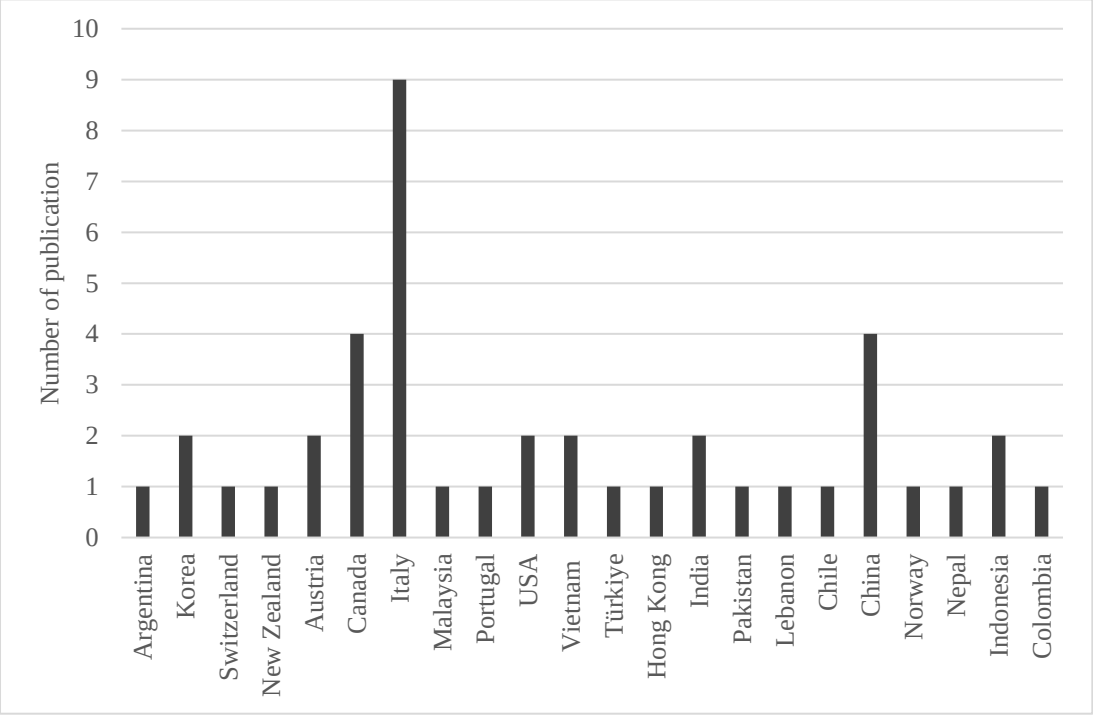

Figure 2.3. Empirical method runout interest in literature in terms of countries.

The keywords of recent researches, especially those focusing on empirically landslide runout, have also been examined. Keywords such as “runout, runout distance runout path, runout zone propagation” were frequently chosen in the researches (Kritos and Davies, 2015; Poltnig et al., 2016; Gregoretti, Degetto and Boreggio, 2016; Pradhan et al., 2016; Sharir, Simon and Roslee, 2018; Melo, van Asch and Zêzere, 2018; Mergili, Schwarz and Kociu, 2019; McCoy, 2019; Do, Yin and Guo, 2020; Polat and Erik, 2020; Peruzzetto et al., 2020; Bera, Melo and Guru, 2021; Di Napoli et al., 2021; Paudel, Fall and Daneshfar, 2021; Wallace and Santi, 2021; Apriani, Credidi and Khala, 2022; Gorr et al., 2022; Liu et al., 2022; Ju et al., 2022; Falconi et al., 2023; Sharma et al., 2023; Giarola et al., 2024; Roman Quintero et al., 2024; Vegliante et al., 2024). It is not surprising that “runout” is the frequently preferred as a keyword in the studies; thus, it is an index of the popularity status of this research topic.

“GIS” was the other frequently used keyword in landslide runout analyses (Park, Lee and Woo, 2013; Kritikos and Davies, 2015; Poltnig et al., 2016; Gregoretti, Degetto and Boreggio, 2016; Pradhan et al., 2016; Mergili, Schwarz and Kociu, 2019; Polat and Erik, 2020; Charbel and El Hage Hassan, 2021; Di Napoli et al., 2021; Liu et al., 2022; Paudel, Fall and Daneshfar, 2021; Wallace and Santi, 2021; Vegliante et al., 2024). With the developing technology, it is seen that GIS is widely used, as in many areas, together with the existing methods. However, it is clear that there are points that still need attentions. For example, Mergili (2008) and Mergili et al. (2008) stated that there is a required for an algorithm that needs flow direction in studies where GIS is combined with an empirical-statistical approach. It is also important to determine the correct flow algorithm for the study area. Researchers also combined different methods with GIS in their studies to examine the propagation distance. For instance, the investigation of runout analysis for shallow landslides involved the application of specialized GIS tools, utilizing an empirical approach on a basin scale within the context of the study on Vegliante et al. (2024).

A keyword “susceptibility” (Park, Lee and Woo, 2013; Kritikos and Davies, 2015; Melo, van Asch and Zêzere, 2018; Mergili, Schwarz and Kociu, 2019; Sturzenegger et al., 2019; Polat and Erik, 2020; Bera, Melo and Guru, 2021; Di Napoli et al., 2021; Giano, Pescatore

and Siervo, 2021; Xu et al., 2022; Marchesini et al., 2024) was frequently used in the runout studies.

Keywords such as “landslide” (Kritikos and Davies, 2015; Sharir, Simon and Roslee, 2018; Do, Yin and Guo, 2020; Peruzzetto et al., 2020; Hien et al., 2022; Ju et al., 2022, Sharma et al., 2023; Roman Quintero et al., 2024), “debris flow” (Kritikos and Davies, 2015; McCoy, 2019; Sturzenegger et al., 2019; Giano, Pescatore and Siervo, 2021; Xu et al., 2022; Hien et al., 2022; Ju et al., 2022; Vegliante et al., 2024; Marchesini et al., 2024), “shallow landslide” (Poltnig et al., 2016; Di Napoli et al., 2021, Liu et al., 2021; Giarola et al., 2024), and “mudflow” (Charbel and El Hage Hassan, 2021) were also used in the empirical landslide runout studies. These keywords indicate that empirical models applied in previous studies have generally been used for flow-type landslides in order to investigate runout distance.

In addition, a number of scientific studies have scrutinised how to estimate runout distance using software. They used various software in the analysis. There is an empirical software called Flow-R, developed by the University of Lusanna, which was written in MATLAB using these algorithms, which allows automatic source area identification and evaluation of spread coverage in debris flow or shallow landslides (Horton et al., 2013). Guthrie and Befus (2021) developed a physical-empirical software called "DebrisFlow Predictor" that can reach the propagation distance by modelling the complex behavior of the debris flow. In addition, Progressive Debris-Flow Routing and Inundation model (ProDF) (Gorr et al., 2022) is also empirical model software in order to inspect runout. Flow-R and DebrisFlow Predictor, are both empirical models, are compared in the study of Arghya, Hawlader and Guthrie (2022), DebrisFlow Predictor might be indicated as providing better landslide hazard assessment. DebrisFlow Predictor requires the user-defined failure initiations (Arghya, Hawlader and Guthrie, 2022). Unlike DebrisFlow Predictor, Flow-R offers an opportunity in detecting a landslide initiation (Arghya, Hawlader and Guthrie, 2022). 'Debris Flow Predictor', and estimates the area, volume and depth along the landslide path for shallow landslides and fast flowing type landslides with using 5 m spatial resolution (Guthrie and Befus, 2021). The ability to perform runout

simulations even for very small cells can be expressed as the most significant strength of the program.

Another issue that researchers are interested in today is contributing to the studies with machine learning. Considering this information; with the increasing interest in machine learning, it is not a surprise to realize that many researchers also benefit from machine learning in their studies on shallow landslides. Shirzadi et al. (2018) mentioned that using machine learning to develop quantitative models that predict landslides spatially has become more popular in recent years. Shallow landslide modelling (Liu et al., 2021) has been successfully applied with machine learning method in their studies. With the rapidly changing technological developments, especially recently, shallow landslide propagation distance sensitivity has started to be investigated in more detail by using machine learning and expert systems. Machine learning has been used in recent runout studies (Di Napoli et al., 2021, Liu et al., 2021; Hien et al., 2022; Ju et al., 2022; Sharma et al., 2023).

“Reach angle or travel angle” is critical for empirical runout studies (Horton et al., 2013; Park, Lee and Woo, 2013; Poltnig et al., 2016; Pastorello, Michelini and D’Agostino, 2017; Rahman, Ahmed and Di , 2017; Sharir, Simon and Roslee, 2018; Kaafarani et al., 2019; McCoy, 2019; Mergili, Schwarz and Kociu, 2019; Paudel, 2019; Sturzenegger et al., 2019; Do, Yin and Guo, 2020; Ali et al. 2021; Bera, Melo and Guru, 2021; Charbel and El Hage Hassan, 2021; Jiang et al., 2021; Paudel, Fall and Daneshfar, 2021; Di Napoli et al., 2021; Pradhan, 2021; Putra et al., 2022; Xu et al., 2022; Sharma et al., 2023). Perla’s friction model was also empirically used for debris flow runout distance in the studies (Fischer, Keiler and Zimmermann, 2016; Goetz et al., 2021; Polat and Erik, 2020; Giano, Pescatore and Siervo, 2021). The travel angle is more frequently preferred alternative friction model for runout assessment in studies (Poltnig et al., 2016; Rahman, Ahmed and Di, 2017; Sharir, Simon and Roslee, 2018; Kaafarani er al., 2019; Mergili et al., 2019; Sturzenegger et al., 2019; Di Napoli et al., 2021; Paudel, Fall and Daneshfar, 2021; Pradhan et al., 2021; Marchesini et al., 2024). In this part of research was pinpointed current empirical runout researches.

By using a set of probability rules over the Digital Elevation Model (DEM), a completely predictive model has been developed to determine the deposition, path selection and propagation behavior for flowing type landslides (Guthrie and Befus, 2021). Melo et al. (2019) also proposed a simple cellular automata model to determine propagation in shallow slides. The spread was determined using the probability density function (Guthrie and Befus, 2021). The propagation path is determined according to the random walk theory based on Monte Carlo simulation by using The Gravitational Process Path ((GPP) Wichmann, 2017) model (Goetz et al., 2021). The flow path was determined by following the steepest path from the potential source area in the study of Sharir, Simon and Roslee (2018). Marchesini et al. (2024) also used the random walk theory implements Monte Carlo simulation identify probable source areas and observe their runout by using reach angles. GIS software enable to visualize both flow directions and runout distances in the analyses. For instance, flow path is visualized with the SAGA-GIS software in the study of Goetz et al. (2021). ArcGIS software was also used in the studies in order to visualize the runout. "Field of View" tool developed in ArcGIS was used in the study of Kaafarani et al. (2019). A tool that can calculate propagation distance called "Add-In" has been developed to be used in ArcGIS (Poltnig et al., 2016). Data from the modular "r.landslides.statistics", which examines the regional probability function, and "r.randomwalk", which uses Monte Carlo simulation, which evaluates the orientation of the flow, were combined by using GRASS-GIS software in the study of Mergili, Schwarz and Kociu (2019). In addition, Statistical R software was also used to visualize the runout distance in the study of (Goetz et al., 2021). Mergili, Schwarz and Kociu (2019) pointed out that landslide spread analyses make important contributions to hazard and risk assessment. Runout distance is also important for planning the land use areas and determining the necessary priorities against the hazards (Kritikos and Davies, 2015).

This dissertation involves detailed research on previous works that utilized the Flow-R software. 19 interesting Flow-R software used studies, were pooled from after the detail literature review, were listed in Table 2.3 between the years 2013 and 2024. It was interpreted from Table 2.3 that the choice to focus on debris flow was frequently preferred research topic in order to investigate on the runout distance in the listed publications. These studies have goals at minimizing the hazards negative effects in the communities and providing proficient prevention by offering effective visualisation in a practical sense.

It is easily noticeable from Table 2.3 that these studies have generally focused on landslides exhibiting flow type characteristics.

Unlike using debris flow runout studies with Flow-R, Ali et al. (2021) and Noël et al. (2023) also used Flow-R software to rockfall runout simulation. Horton et al. (2021) also suggested suitable parameters for rockfall runout examination.

The other differences between the studies can also be discernible from Table 2.3. For example, determining the initiations of shallow landslides and the method to be applied during propagation are differently promoted in the studies. Although many researchers conduct their runout distance research based on user defined shallow landslide initiations, which they have determined themselves, many researchers have also utilized the advantage fostered by the Flow-R software by using automatically detected shallow landslides initiations (Table 2.3). While flow direction was also generally thrived with Holmgren or Modified Holmgren in studies, SFLM was also the most preferred method during the propagation stage in the previous studies (Table 2.3).

Different spatial resolutions of DEMs have been used in the Flow-R studies. For instance, 5 m (McCoy, 2019; Do, Yin and Guo, 2020; Giano, Pescatore and Siervo, 2021), 10 m (Park, Lee and Woo, 2013; Charbel and El Hage Hassan, 2021; Jiang et al., 2021), 12 m (Ali, Haider and Abbas, 2021), 12.5 m (Xu et al., 2022), 20 m (Polat and Erik, 2020; McParland et al., 2021) and 30 m (Ali et al., 2021; Liu et al., 2022) were utilized.

As seen in the literature studies, several researchers have been trying to calculate and measure runout distance with using Flow-R. The main aims of these works are to make use of limited information efficiently thanks to the Flow-R software. It should be noted that even the best models can achieve a generalized view of reality. Therefore, the awareness that a generalized approach will be reached at the end of this study has emerged.

Table 2.3. The previous studies which used the Flow-R software.

Authors	Research	Landslide Initiations	Runout Method	Flow Direction Algorithm
Horton et al. (2013)	Debris flow runout susceptibility map	Initiations detected by Flow-R	SFLM	Holmgren Modified
Park, Lee and Woo (2013)	Debris flow runout susceptibility map	Initiations detected by Flow-R	SFLM	Holmgren Modified
Pastorello, Michelini and D'Agostino (2017)	Debris flow runout susceptibility map	User-defined initiations by considering flow accumulation and slope gradient	SFLM	Holmgren Modified
Pradhan et al. (2017)	Shallow landslide runout susceptibility map	User-defined initiations	SFLM	Holmgren
Rahman, Ahmed and Di (2017)	Landslide runout susceptibility map	User-defined initiations	SFLM	Holmgren Modified
McCoy (2019)	Debris flow runout susceptibility map	User-defined initiations	SFLM	Holmgren Modified
Sturzenegger et al. (2019)	Debris flow runout susceptibility map	User-defined initiations	SFLM	Holmgren Modified
Paudel (2019)	Debris flow runout susceptibility map	User-defined initiations by considering landslide susceptibility map	SFLM	Holmgren Modified
Do, Yin and Guo (2020)	Landslide runout susceptibility map	Initiations detected by Flow-R	SFLM	Holmgren Modified
Polat and Erik (2020)	Debris flow runout susceptibility map	User-defined initiations by considering landslide susceptibility map	Perla	Holmgren Modified
Ali et al. (2021)	Debris flow runout susceptibility map	User-defined initiations with remote sensing and slope gradients distributions	SFLM	Holmgren
Bera, Melo and Guru (2021)	Debris flow runout susceptibility map	User-defined initiations with GPS and multi-temporal satellite images like Google earth, GeoEye-1 and worldview-2	SFLM	Holmgren
Charbel and El Hage Hassan (2021)	Mudflow runout susceptibility map	Initiations detected by Flow-R	SFLM	Holmgren
Giano, Pescatore and Siervo (2021)	Debris flow runout susceptibility map	Initiations detected by Flow-R	Perla	Holmgren Modified
Jiang et al. (2021)	Debris flow runout susceptibility map	Initiations detected by Flow-R	SFLM	Holmgren Modified
Liu et al. (2022)	Landslide runout susceptibility map	User-defined initiations with previos studies and D-InSAR technology	SFLM	Holmgren modified
Putra et al. (2022)	Debris flow runout susceptibility map	User-defined initiations with sentinel images	SFLM	Holmgren modified
Xu et al. (2022)	Debris flow runout susceptibility map	Initiations detected by Flow-R	SFLM	Holmgren Modified
Sharma et al. (2023)	Debris flow runout susceptibility map	Initiations detected by Flow-R	SFLM	Holmgren Modified

2.4. Flow Direction Algorithm and Simple Friction Limited Model (SFLM)

In this part of thesis, it is delved into the flow direction algorithm and SFLM algorithm, crucial for the empirical Flow-R software. It is important to use the correct algorithm according to the environmental conditions, because not every algorithm is suitable for study requirements. Investigation may also require the use of different flow algorithms for debris flows, shallow landslides and rockfalls to represent more realist to flow. For instance, Holmgren (1994), Modified Holmgren (Horton, 2013), D8 (O'Callaghan and Mark, 1984; Jenson and Domingue, 1988), D∞ algorithm (Tarboton, 1997), Rho8 algorithm (Fairfield and Leymarie, 1991), multiple flow direction approach (Quinn et al., 1991), Freeman (1991) approaches are commonly used algorithms for debris flows (Horton et al., 2013).

x parameter is incorporated the into the multiple flow direction method by Holmgren (1994) in his algorithm, enabling a more detailed examination to be conducted. Although in Equation 2.9 elements' explanitons are also accounted for in Table 2.4, it is necessary to summarize them that while $\tan\beta_i$ and $\tan\beta_j$ represent the change in slope gradient between cells, ρ_i^{fd} indicates the susceptibility proportion in determined direction (Horton et al., 2013). x, has the highly critical role in the equation, is the variable parameter that controls the variable deviation in Equation 2.9. As indicated by Equation 2.9, the variable x may range from 1 to infinity.

$$\rho_i^{fd} = \frac{(\tan\beta_i)^x}{\sum_{j=1}^{8}(\tan\beta_j)^x} \quad \forall \quad \left\{ \begin{matrix} \tan\beta > 0 \\ x\ \varepsilon\ [1;+\infty] \end{matrix} \right\} \tag{2.9}$$

In the Modified Holmgren algorithm proposed by Horton et al. (2013), the height of the central cell alters due to the change of the gradient values of the "dh" parameter. The most important difference between Holmgren and Modified Holmgren is the parameter dh. Paudel (2019) stated that the modified Holmgren algorithm can be used for both multiple flow directions and single flow directions. In this study, it is planned to use modified Holmgren (1994) flow direction algorithm.

The D8 algorithm was developed for eight flow directions (Paudel, 2019). Although the spread data is unrealistic because the algorithm adopts straight flow, it can be useful if a brisk approach is desired (Horton et al., 2013).

While the D∞ algorithm allows to make sense of small spreads, it has been stated that it is insufficient in some special conditions (Horton et al., 2013). Nevertheles, it was sucessfully used to estimate shallow landslide spread in the study of Kritos and Davies (2015). While the Rho8 algorithm is considered as a stochastic approach, it causes incomplete deterministic results (Erskine et al., 2006; Horton et al., 2013). It has been stated that very large diffusion results can be achieved with the multiple flow direction approach (Huggel et al., 2003; Horton et al., 2013).

Since the slope direction changes frequently in the field, the function is required to determine the new direction according to the initial slope gradient (Paudel, 2019). Horton et al. (2013) named this function as the persistence function shown in Equation 2.10. While ρ_i^p indicates the persistence flow rate in the i direction; $a_{(i)}$ is the angle from the previous flow direction (Horton et al., 2013). The "w" persistence value can be determined proportionally, according to Cosine and Gamma applications.

$$\rho_i^p = w_{a(i)} \tag{2.10}$$

By combining the direction and persistence algorithms, Equation 2.11 is obtained to determine the sensitivity. ρ_i, the sensitivity value in the i direction; ρ_i^{fd}, flow direction algorithm according to flow rate; ρ_i^p, persistence flow rate; ρ_0, represents the sensitivity value of the predetermined central cell (Horton et al., 2013).

$$\rho_i = \frac{\rho_i^{fd}\rho_i^p}{\sum_{j=1}^{8}\rho_j^{fd}\,\rho_j^p}\,\rho_0 \tag{2.11}$$

SFLM is characterized by the minimum angle of motion relative to the maximum possible propagation pattern. It should be emphasized that the minimum angle applied here is used

in many studies as "reach angle" or "fahrböschung angle" used in the literature. Horton et al. (2013) approach adopts a principle using energy-based flow direction algorithms. The debris flow is experimentally calculated starting from the predefined source cells derived from the DEM. In addition, while making propagation distance evaluations; flow mass is accepted as a unit value and energy loss is entirely due to friction (Horton et al., 2013; Paudel, 2019). While the flow analysis takes place at the cell level, it is checked whether the flow can reach other cells (Horton et al., 2013). The energy required for the flow to go from one cell to another must be adequate. While the equation created by considering the energy between the cells is expressed in Equation 2.12, the explanations of the elements included in the equation are shown in Table 2.4.

$$E_{kin}^{i} = E_{kin}^{0} + \Delta E_{pot}^{i} - E_{f}^{i} \tag{2.12}$$

The angle applied here is the angle of the line connecting the source area or possible failure initiations to the farthest point reached by the debris flow or shallow landside (Figure 2.1) (Horton et al., 2013). As can be seen in Equation 2.13, a small angle of motion will reach a greater spread. Table 2.4 accounts for the elements of Equation 2.13.

$$E_{f}^{i} = g\Delta x \tan\varphi \tag{2.13}$$

Considering the energy units, the unit of the gravitational acceleration (m/s^2) will be the unit of the operation (m^2/s^2), considering that the horizontal displacement increment unit is “m”. This unit is known as the joule. In order to determine the maximum runout distance, minimum travel angle and maximum speed can be selected. Field observations about the travel angles which are obtained from past landslides allow researchers to prepare data in order to reach more real conditions for study area. The velocity equation (Equation 2.14) is constructed in order to avoid the consequences of improbable propagation distances caused by unrealistic amounts of energy during propagation. According to equation, Δh is the height difference between the center cell and the cell in the i direction; V_0, initial speed; V_{max}, indicates the maximum speed limit (Horton et al., 2013).

$$V_i = \min\left\{\sqrt{{V_0}^2 + 2g\Delta h - 2g\Delta x \tan\varphi}, V_{max}\right\} \quad (2.14)$$

In addition to the SFLM, similar Perla model algorithms are also used to evaluate the friction loss (Horton et al., 2013). It has been stated that both models can reach the same spread areas with similar parameter selections (Jaboyedoff, Rudaz and Horton, 2011; Horton et al., 2013). The velocity reached at the end of the motion in the i direction is represented by V_i, together with the Perla nonlinear friction law-based equation of motion (Horton et al., 2013). This equation is shown in Equation 2.15. Equations 2.16 and 2.17 show how the elements of equations in Equation 2.14 are obtained.

$$V_i = (a_i\omega(1 - e^{b_i}) + {V_0}^2 + e^{b_i})^{\frac{1}{2}} \quad (2.15)$$

$$a_i = g(\sin\beta_i - \mu\cos\beta_i) \quad (2.16)$$

$$b_i = \frac{-2L_i}{\omega} \quad (2.17)$$

"ω" represents (mass/friction). While the unit of friction is Newton (kgm/s^2), mass is expressed in kg. In this case, the unit ω is (s^2/m). Friction parameter is shown with μ. While the parameter L_i indicates the length of the segment, its unit is (m). In this situation the unit of the parameter shown with is m^2/s^2. β_i is also included in the equation as the angle of inclination (Horton et al., 2013). Initial speed is denoted by V_0, while g denotes gravitational acceleration (Horton et al., 2013). In the study of Polat and Erik (2020), μ and w were chosen as 0.02 and 200, respectively. The descriptions of the equation elements used in the equations are elaborated in Table 2.4.

Table 2.4. Explanations of the symbols in the equations (Horton et al., 2013).

Symbol	Explanation
$\tan\beta_i$	Slope gradient between cell and the cell in the i direction
$\tan\beta_j$	Slope gradient between cell and the cell in the j direction
ρ_i	Susceptibility value in direction i
ρ_0	Previously determined susceptibility value of the central cell
ρ_i^p	Flow proportion in direction (i) according to the persistence
ρ_j^p	Flow proportion in direction (j) according to the persistence
ρ_i^{fd}	Susceptibility proportion in direction i
ρ_j^{fd}	Susceptibility proportion in direction j
i	Direction
j	Direction
E_{kin}^i	Kinetic energy of the cell in direction i
E_{kin}^0	Kinetic energy of the central cell
ΔE_{pot}^i	Change in potential energy to the cell in direction i
E_f^i	Energy lost in friction to the cell in direction
g	Acceleration because of gravity
Δx	Increment of horizontal displacement
$\tan\varphi$	Gradient of the energy line
Δh	Elevation difference in between the central cell and the cell in direction i
ω	Mass to friction
L_i	Length of the segment
V_0	Initial velocity
V_{max}	Maximum velocity
V_i	End of the motion velocity

2.5. Climate Change Scenarios

In this section, the relationship between climate change scenarios and landslides will primarily be investigated. Gariano and Guzetti (2016) stated in the special report published by the Intergovernmental Panel on Climate Change (IPCC) that the change in heavy rainfall due to climate change will affect landslides in some regions. Stoffel, Tiranti and Huggel (2014) claimed that the formation and size of mass movements will also change along with changes in temperature and precipitation. Jakob and Owen (2021) pointed out that extreme precipitation events might trigger frequency of landslides according to IPCC (2020) climate model. Jakob and Lambert (2009) underlined that shallow landslides and debris flow will be affected by climate change in terms of occurring frequency. In fact, in the study of Jakob and Lambert (2009) despite debris flow frequency will increase averagely about 10% at the late century, approximately 30% increase of number of debris flow will also be possible in some region at the late century. Utilizing RCP scenarios is an important advancement to further investigate the relationship between climate change and landslides (Wang et al., 2024).

IPCC's Fifth Assessment Report (AR5) scenarios give an opportunity to analyse climate change effects in the literature. It should be remembered that RCPs represent climate change scenarios based on greenhouse gas emissions integrated by the IPCC (Demircan, 2017). RCPs are RCP 2.6/3.0, RCP 4.5, RCP 6.0 and RCP 8.5. RCP 2.6 is determined as low, RCP 4.5 medium-low, RCP 6.0 medium-high, RCP 8.5 high (Moss et al., 2008). The expected future CO_2 limits for each model is a very important criterion when evaluating model scenarios. ~1370 ppm, ~850 ppm, ~650 ppm and ~490 ppm will be CO_2 concentrations for RCP 8.5, RCP 6.0, RCP 4.5. and RCP 3/2.6 scenarios in 2100, respectively (Moss et al., 2008). While the worst scenario expected to happen can be evaluated as RCP 8.5, the more moderate RCP 4.5 scenario stands out as a viable scenario in studies. In this study, it is also planned to continue studies for precipitation data of RCP 4.5 and RCP 8.5 climate scenarios.

Climate scenario simulations by using climate model such as Climate Model Intercomparison Project (CMIP5) and the Community Climate System Model (CCSM4) enable to explore the variations in precipitation. RCP 4.5 and RCP 8.5 scenarios are also

generally preferred scenario to scrutinize the relationships between climate and landslide (Bernardie et al., 2021; Jemec Auflič et al., 2023; Volpe et al., 2023). The landslide susceptibility was also prepared by considering RCP 4.5 and RCP 8.5 rainfall scenarios in some studies. For instance, Park and Lee (2021), Yunus et al. (2021), Wijaya et al. (2021), Ageenko et al. (2022), Araújo et al. (2022), Nefros et al. (2023), Pham et al. (2022) and Chen et al. (2023) prepare landslide susceptibility maps in order to closely examine climate change impact by using RCP 4.5 and 8.5 scenarios. Random forest (RF) was used a supervised machine learning method to prepare the landslides susceptibility in the studies of Park and Lee (2021), Yunus et al. (2021), Ageenko et al. (2022) and Janizadeh et al. (2023). In addition, when Park and Lee (2021) and Ageenko et al. (2022) compared machine learning method in order to prepare the landslide susceptibility map including RCP scenarios, they find that RF is the best alternative supervised method in terms of high accuracy. Mohamed-Yusof et al. (2024) also used SVM for preparation the landslide susceptibility map of the by reckoning with RCP 4.5 and RCP 8.5 scenarios. Furthermore, Chen et al. (2023) used RCP 4.5 and 8.5 scenarios in the landslides hazard predictions. Kim et al. (2015) claimed that potential landslides hazards will increase if RCP 4.5 and 8.5 scenarios are considered. Peres and Cancelliere (2018) predicted a decrease in the probability of triggering future landslides using Monte Carlo simulations for RCP 4.5 and 8.5 scenarios because of reducing of precipitation duration and depth. With the inclusion of the precipitation effect of climate change scenarios in this study, an important step will be taken in order to make a detailed hazard assessment of shallow landslides. Climate change scenarios are critical in order to evaluate effects of the trends of varying precipitation in terms of analysing landslide runout behaviour impacts within the scope of this thesis.

As can been seen from previous sentences, the relation of the RCP 4.5 and RCP 8.5 precipitation scenarios and landslides occurrence are debatable topic in researchers. It should be dwelled on shallow landslides occurrence under future RCP 4.5 and 8.5 precipitation scenarios trends for effective hazard analysis. In spite of searching of relation between RCP scenarios and landslide occurrence has been studied, it has not yet combined with the investigation of landslide runout behaviour. It is necessary to correlate RCP scenarios with precipitation data and the existing precipitation data in the region by downscaling in order to establish a relationship with climate change. In other words,

downscaling is necessary to predict mix conditions which are local climate condition and global climate condition. According to the literature, researchers use dynamic and statistical scale downscaling methods to conduct a more detailed and realistic study of the region they work in. Considering that both methods have advantages and limitations, the method to be used should be painstakingly selected according to the research content and scope. Statistical downscaling is generally useful downscaling methods for climate change studies because of their low cost (Tzabiras, Loukas, and Vasiliades, 2016). Tzabiras, Loukas, and Vasiliades (2016) also state that statistical downscaling considers the empirical quantitative relationships between the global–scale climate variable and local-scale climate variable. While local-scale climate variables accepted as predictands, global–scale climate variable accepted as predictors. Tzabiras et al. (2016) mention that dynamical downscaling is mainly focused on preparing comprehensive regional climate model. Demircan et al. (2017) evaluated the future precipitations trend for 2016-2099 by using a local climate model (RegCM4.3.4) depends on dynamical downscaling. The model outputs show that precipitation amounts will generally decline in Türkiye (Demircan et al., 2017). However, Gumus et al. (2023) claimed that although a decreasing trend in annual total precipitation for 30-year periods has been observed, an increase in maximum precipitation is anticipated in the Black Sea region with respect to their analyses.

3. CHARACTERIZATION OF THE STUDY AREA

To provide a characterize the study area, at least six fundamental issues should be addressed properly: (i) Location, (ii) Geology, (iii) Seismicity, (iv) Land use and vegetation, (v) Climate and precipitation, and (vi) Division of sub-basins and their geomorphological characteristics.

3.1. Location

Eocene flysch facies which are situated at the Western Black Sea Region between latitudes **41° 1'7.54"**to **41°40'0.94"** North, and longitudes **31°38'58.05"**to **32°29'55.30"** East in Türkiye (Figure 3.1). Indeed, this formation is located on between two cities which are Zonguldak and Bartın.

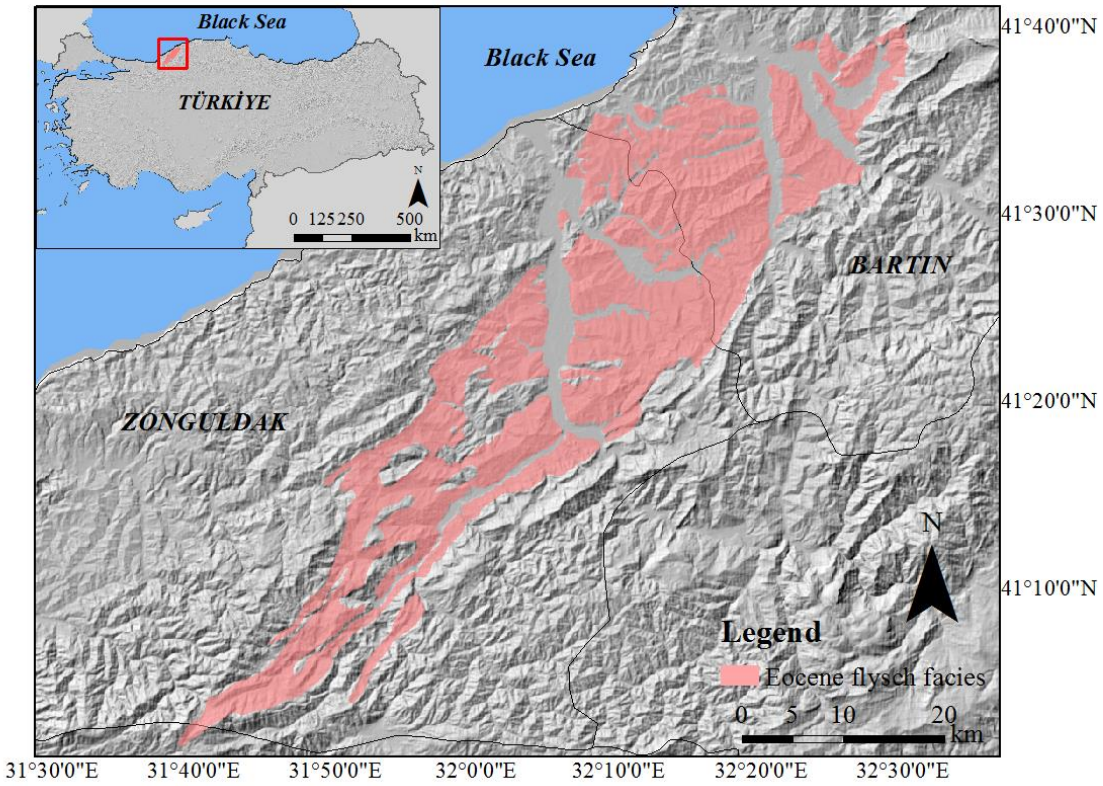

Figure 3.1. Location map of the study area: The boundary of Eocene flysch facies was modified after Akbas et al. (2011) and Duman et al. (2005a).

The Eocene flysch facies has an area of about 877 km^2, the terrain is generally low in the northeast and high in the southwest (Figure 3.2). Figure 3.2 shows that the distance between the study area east and west parts is approximately 103 km.

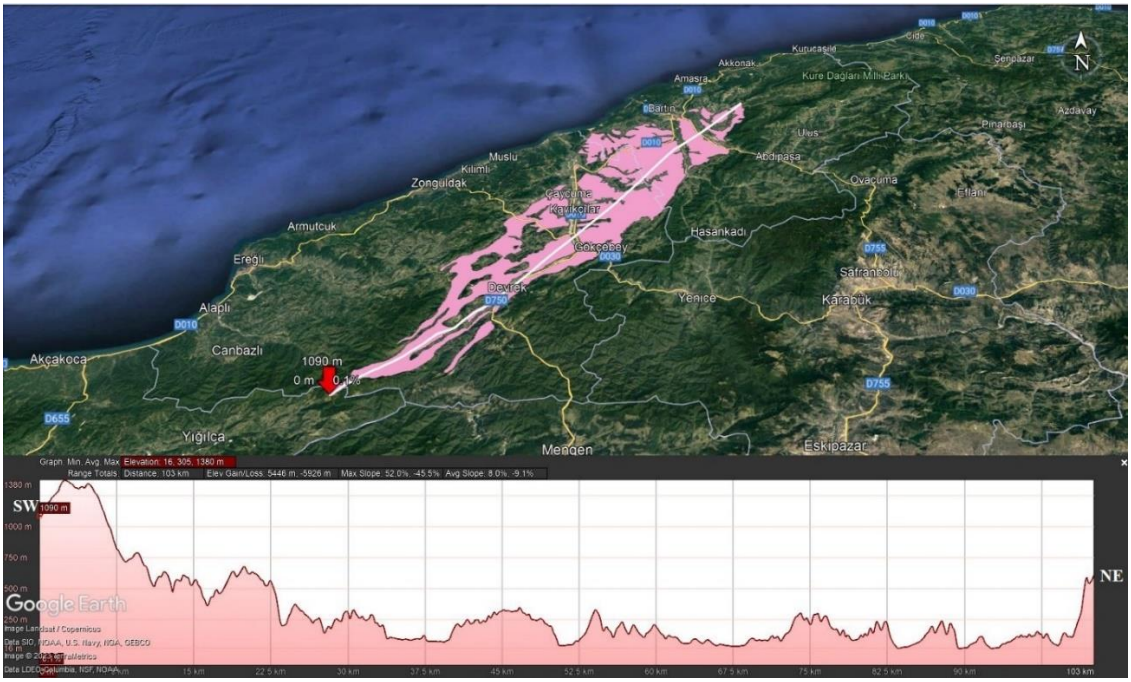

Figure 3.2. Cross section of the Eocene flysch facies in terms of altitude profile.

Major transportation roads mainly include three main type lines: the state roads, village roads and railway road in the study area. The state roads of D755, D010, D750 and D030 pass through the boundaries of the working area (Figure 3.3). Karabük-Zonguldak Railway pass through the Hacılar village, located in the Eocene flysch facies. Railway can be examined from the zoomed-in image inside the red square in Figure 3.3.

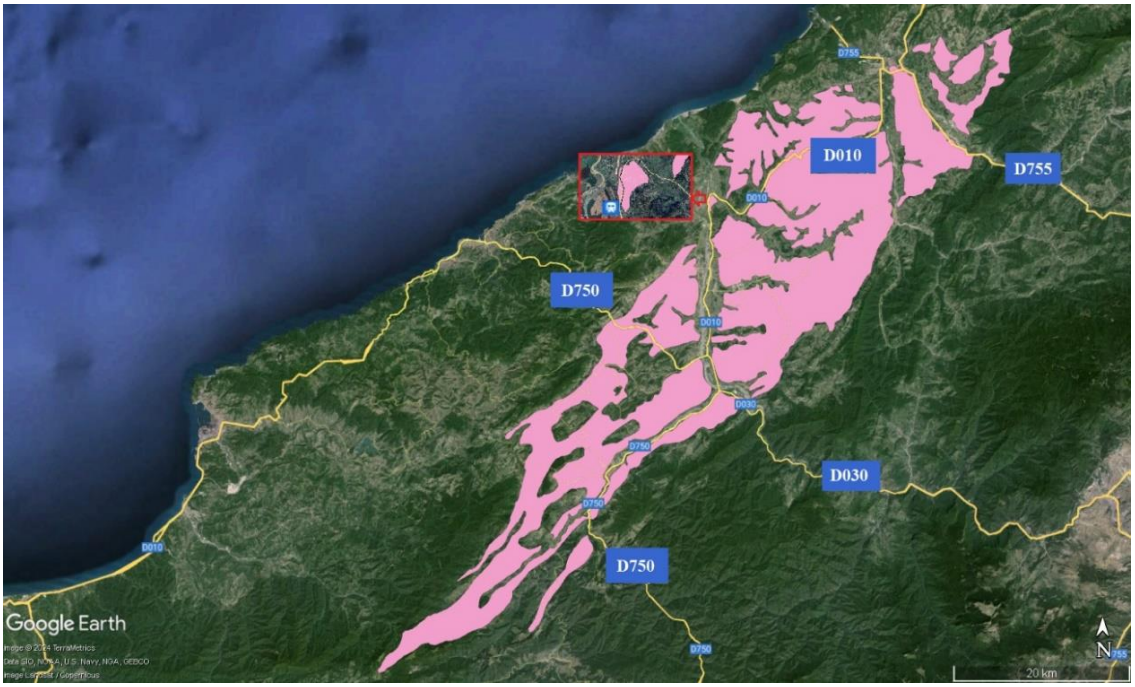

Figure 3.3. Major transportation roads in Eocene flysch facies.

Akgün et al. (2021) stated that Eocene flysch facies formation although their surrounding is accepted as a rugged topography, this formation has low topographic values. The projection coordinate system is set to: “WGS 1984 UTM Zone 36N”. Topographic parameters which are altitude and slope gradient were derived from Digital Elevation Model (SRTM DEM data, WGS 1984 UTM zone 36N) in order to collect evidence with respect to evaluating the study by using ArcGIS software. It is possible to say that results substantiate the real field conditions. The altitudes in Eocene flysch facies increase from north to south (Figure 3.4). In fact, altitude is high in the southwestern part with a maximum altitude of over 1574 m. Slope gradient is an important parameter in the onset of examination of study area in terms of landslide because relationships between slope gradient and landslide occurrence are inextricably intertwined. The slope gradient map was divided into five classes: 0° –7°, 7° – 12°, 12° – 18°, 18° – 26° and >26° (Figure 3.5).

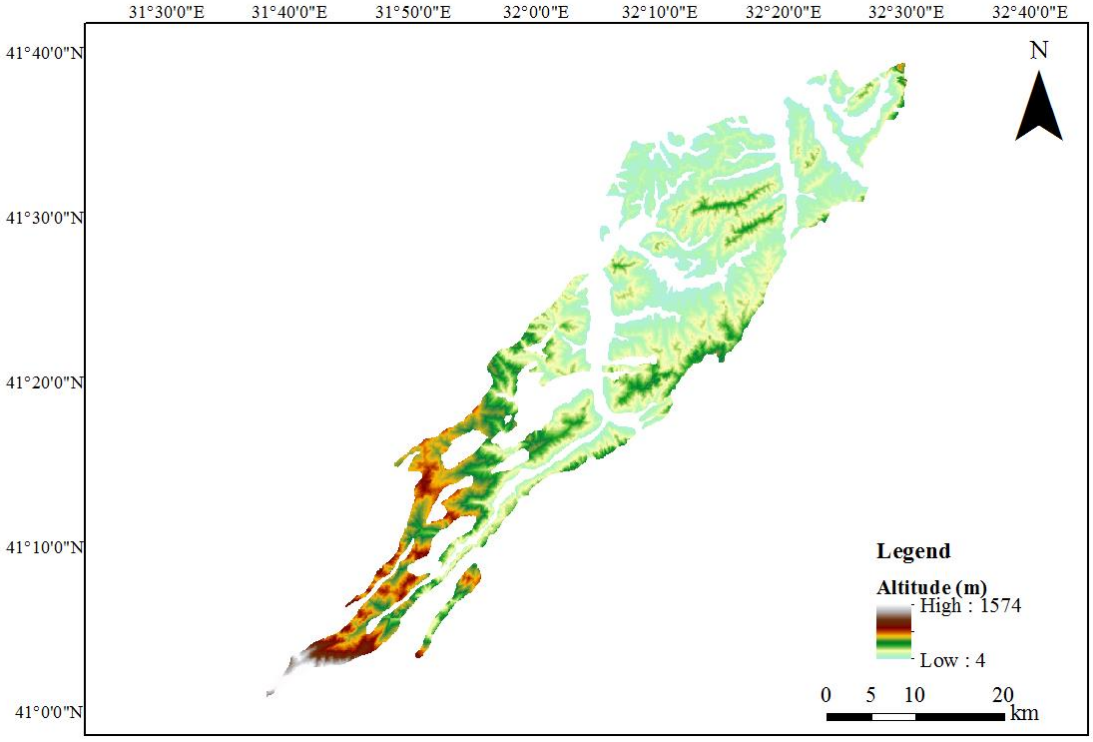

Figure 3.4. The altitude map of the Eocene flysch facies.

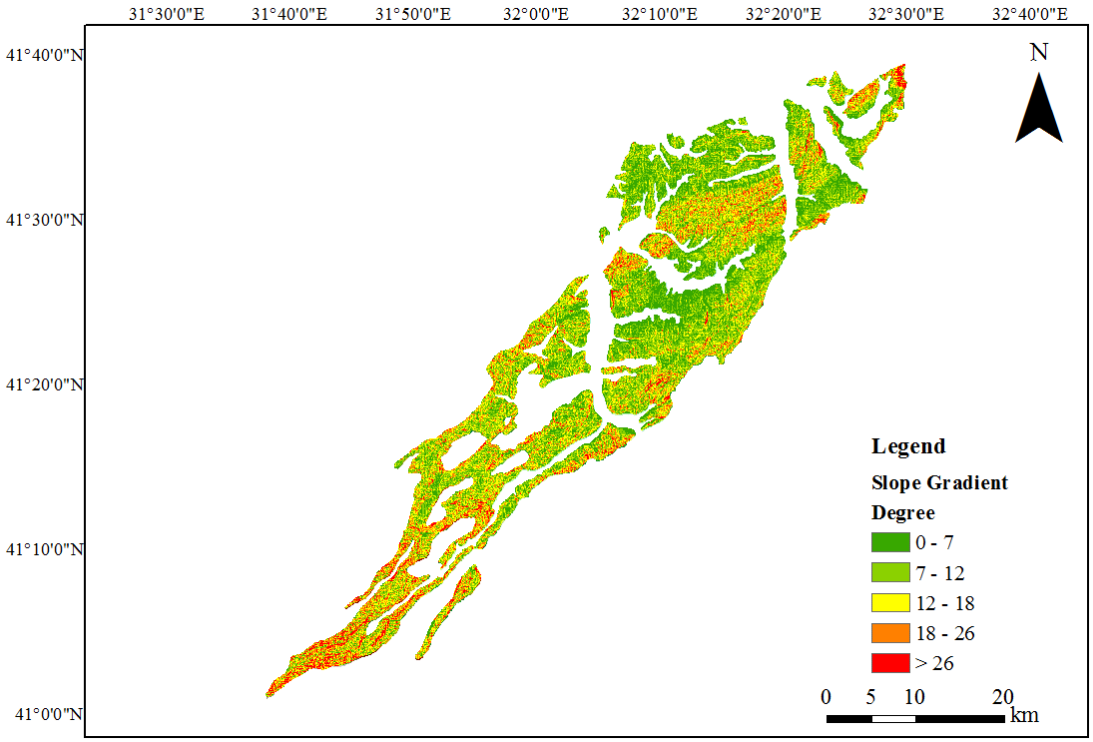

Figure 3.5. The slope gradient map of the Eocene flysch facies.

3.2. Geology

Study location was determined as according to natural geological borders. This study area consists of Eocene-aged clastics and carbonates (Akbaş et al., 2011). Geological map of the Eocene flysch facies (Akbaş et al., 2011) which was obtained from MTA Earth science portal is given in Figure 3.6.

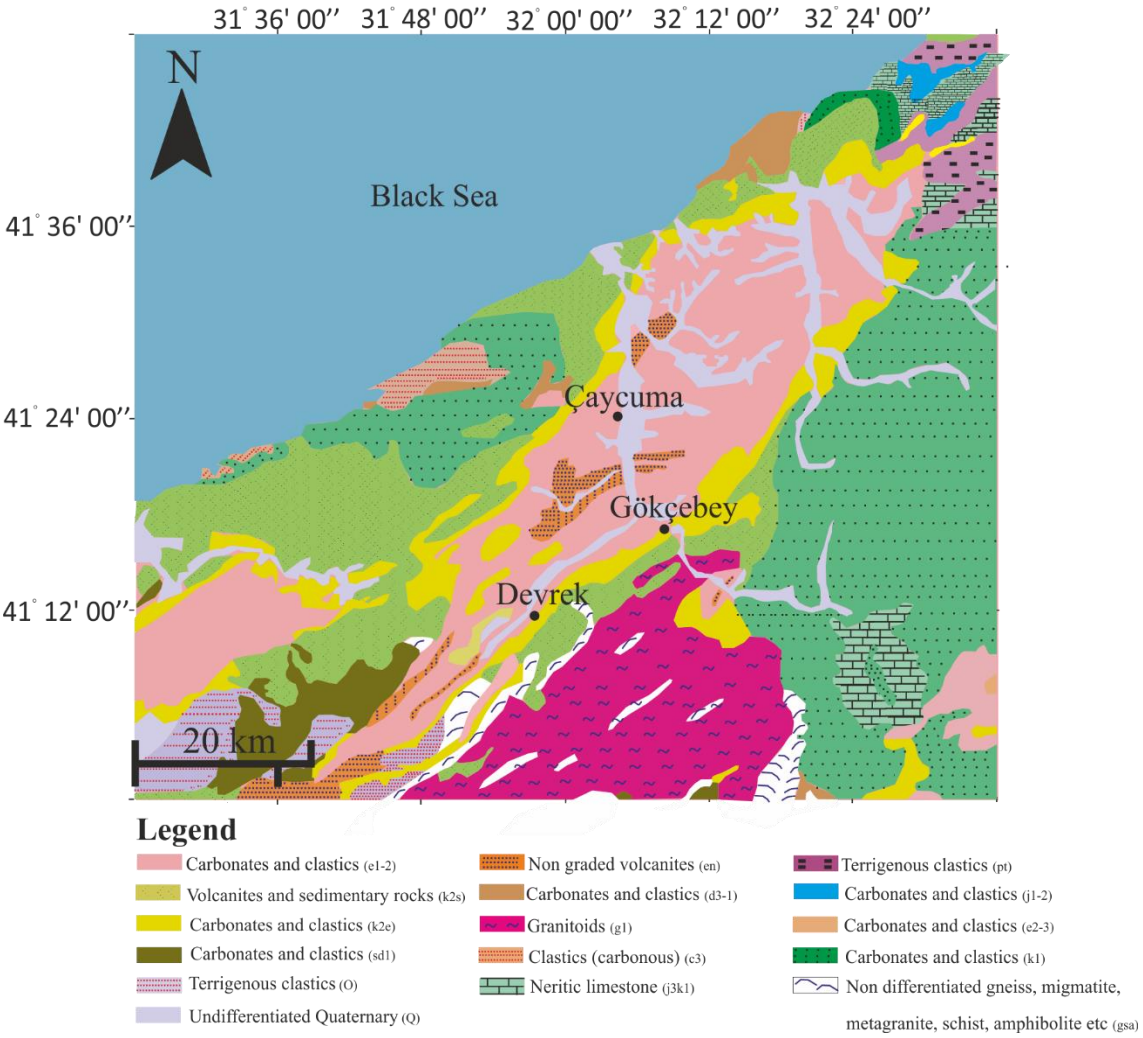

Figure 3.6. Geological map of Eocene flysch facies and its close surrounding (Modified after Akbaş et al., 2011; Duman et al., 2005a).

Eocene flysch facies are shown as a light pink colour at the centre of the map (Figure 3.6). Mudstone, claystone, sandstone alternation that shows flysch characteristics. The Eocene flysch facies are predominantly of claystone, mudstone and sandstone alternation. While sedimentology the upper part of the Eocene flysch facies includes Middle Eocene sandstone and claystone alternations (Duman et al., 2005a; Duman et al., 2005b), the middle part consists of fine-grained crystal-vitric tuffs (Akgun, Gorum and Nefeslioglu,

2021). Lytic tuff, andesitic tuff breccias and volcanoclastic sandstone and siltstones are observable in the lower part of the middle part (Akgun, Gorum and Nefeslioglu, 2021). In the lowest part of series can be defined as turbidite facies alternates with pebble, sandstone, and shale (Akgun, Gorum and Nefeslioglu, 2021). This unit is mentioned in studies as the Çaycuma Formation which was named by Tokay (1954). In this region, there is a higher likelihood of shallow landslides occurring in sandstone interbeds containing shale and mudstone (Duman et al., 1998). Görüm et al. (2019) stated that Eocene clastic and carbonate rocks are prone to landslide occurrence. Lithological properties can also affect the landslide runout behavior (Zeng et al., 2021). Coarse soils are more prone to inducing landslides compared to fine soils (Luino et al., 2022). Sandstone and shale are observable lithological unit in the Figure 3.7. Greyish-purple limestones are interbedded shales (Figure 3.7).

Figure 3.7. A general view within the boundaries of Eocene flysch facies.

Figure 3.8 is important in providing information about the geology surrounding Eocene flysch facies. As seen from the Figure 3.8a and Figure 3.8b represent the undifferentiated Quaternary. The landslide potential of this geological unit is low. Figure 3.8c shows non graded volcanics. According to the geological unit, the possible of triggering landslides is higher for non graded volcanics than undifferentiated Quaternary.

(a)

(b)

(c)

Figure 3.8. Field photographs taken around the study area: (a,b) Undifferentiated Quaternary, (c) Non-graded volcanites.

3.3. Seismicity of the Study Area

Seismicity of the study area and its immediate surrounding should be evaluated in order to focus on sensivity of the study area with respect to seismic effect. Active faults examination for the study area and its vicinity is also first and critical step in order to examine seismicity of the study area. Devrek fault, Yığılca fault, Karabük fault, and North Anatolian Fault Zone (NAFZ) segments, which are Gerede, Yeniçağ and Düzce, are active faults that should be examined more detailed for study area (Emre et al., 2018). Devrek, Yığılca and Karabük faults are shown in purple color of line, whereas other faults are shown with red color line in Figure 3.9. While Devrek fault is located in the study area boundary, Yığılca fault is very close (approximately 5 km) to study area boundary. In addition, it is possible to detect that when compared with other faults, North Anatolian Fault Zone (NAFZ) segments and Karabük fault are a little farther to study area. However, they are also important faults for study area and should not be neglected their seismic effects. Figure 3.9, which clarifies the distribution of active faults location, was obtained from AFAD official web-page. Red rectangle represents the approximate position of the Eocene flysch facies.

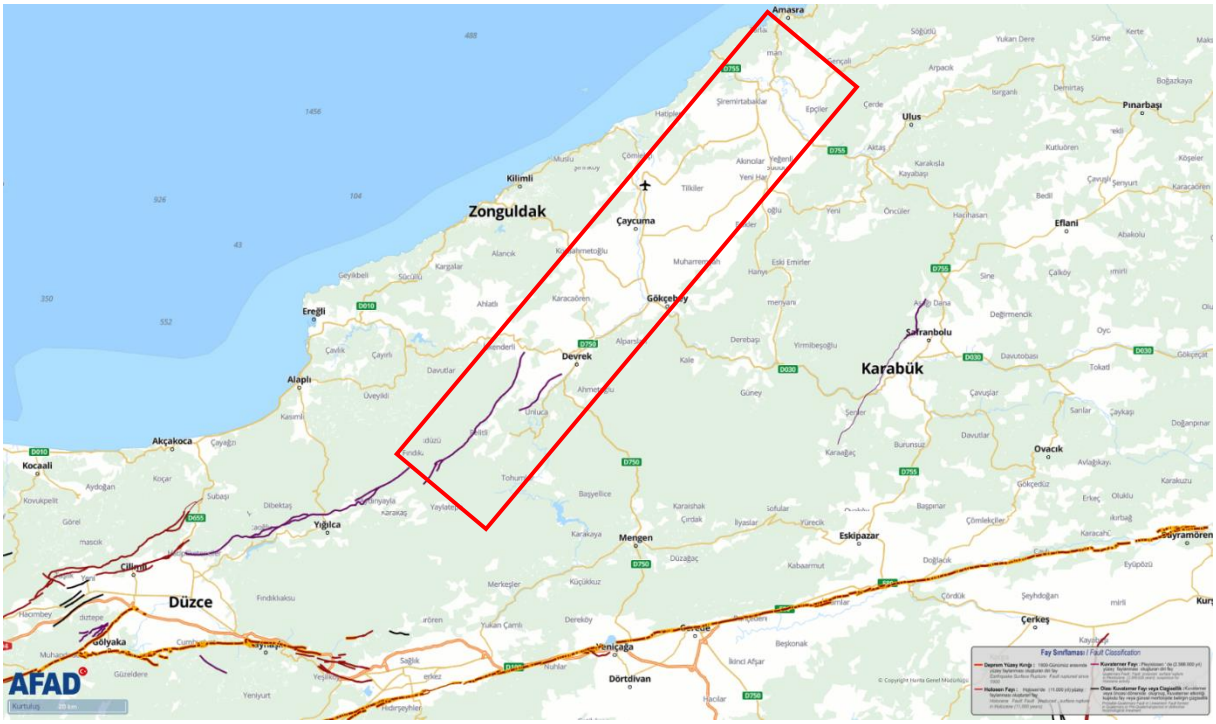

Figure 3.9. Active faults (Available online: https://deprem.afad.gov.tr/event-catalog. accessed on: 12.12.2023).

Devrek Fault, is a Quaternary right lateral strike-slip fault about 29 km length, its possible moment magnitude on fault is estimated as Mw=6.79 which is calculated from Wells and Coppersmith (1994) empirical approach (Emre et al., 2018).

Yığılca Fault, is a Quaternary reverse fault about 42 km length (Emre et al., 2018). The empirical approach proposed by Wells and Coppersmith (1994) suggests the possible moment magnitude on fault as Mw=6.98 (Emre et al., 2018).

Karabük Fault is a Quaternary reverse fault about 29 km length, possible moment magnitude on fault as Mw=6.80 is estimated by using Wells and Coppersmith (1994) empirical approach (Emre et al., 2018).

NAFZ Gerede and Yeniçağ Segments are right lateral strike-slip fault segments about 31 km and 37 km length, respectively (Emre et al., 2018). Both of them are earthquake ruptures (Emre et al., 2018). Wells and Coppersmith (1994) empirical approach estimates that both segments' possible moment magnitude on fault is 7.69 (Emre et al., 2018). NAFZ Düzce Segmenti is also right lateral strike-slip fault segments about 40 km length. Unlike Gerede and Yeniçağ Segments, its possible moment magnitude on fault is 6.95 according to Wells and Coppersmith (1994) empirical approach (Emre et al., 2018).

Faults should also be evaluated according to maximum occurrence magnitude in order to prepare detailed seismic analyses. Recorded earthquake epicentres which are having a radius of 100 km in a circular area were investigated. The study area is very large; therefore, approximate centre which is determined according to study area's start point and end point is chosen to evaluate within the 100 km radius area. Earthquake catalog data is obtained from Boğaziçi University Kandilli Observatory and Earthquake Research Institute Regional Earthquake-Tsunami Monitoring and Evaluation Center (http://www.koeri.boun.edu.tr/sismo/zeqdb/). Distribution of earthquakes epicentres having magnitude of 4.0 and higher than between years 1900-2023 was shown in Figure 3.10. The circles shown as earthquake markers in the legend section on the map in Figure 3.10; while radius sizes represent the earthquake magnitude, different colours show depth information.

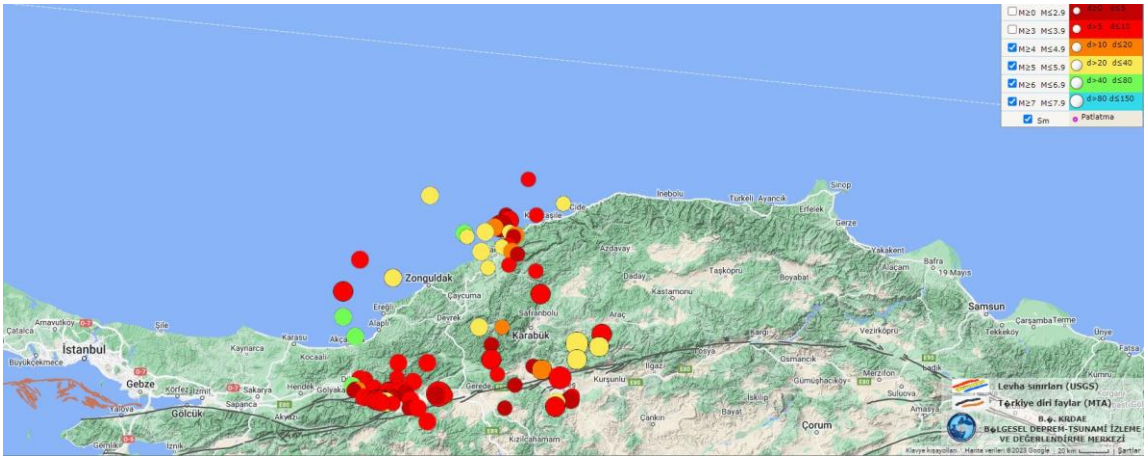

Figure 3.10. Distributions of earthquakes and faults (Available online: http://www.koeri.boun.edu.tr/sismo/zeqdb/default.asp. Accessed on: 12.12.2023).

Distribution of earthquakes having magnitude of 4.0 and higher than between years 1900-2023 was evaluated with respect to frequency histogram shown in Figure 3.11. Earthquake magnitudes were grouped as $4.0 \leq xM < 4.5$, $4.5 \leq xM < 5.0$, $5.0 \leq xM < 5.5$, $5.5 \leq xM < 6.0$, $6.0 \leq xM < 6.5$, $6.5 \leq xM < 7.0$ and $xM \geq 7.0$ in order to determine the frequency trend of earthquake for the study area. Figure 3.11 shows that while the number of earthquake magnitudes is highest in the range of $4.0 \leq xM < 4.5$, high-risk earthquake magnitudes which are $xM = 7.0$ and above are rare for the study area.

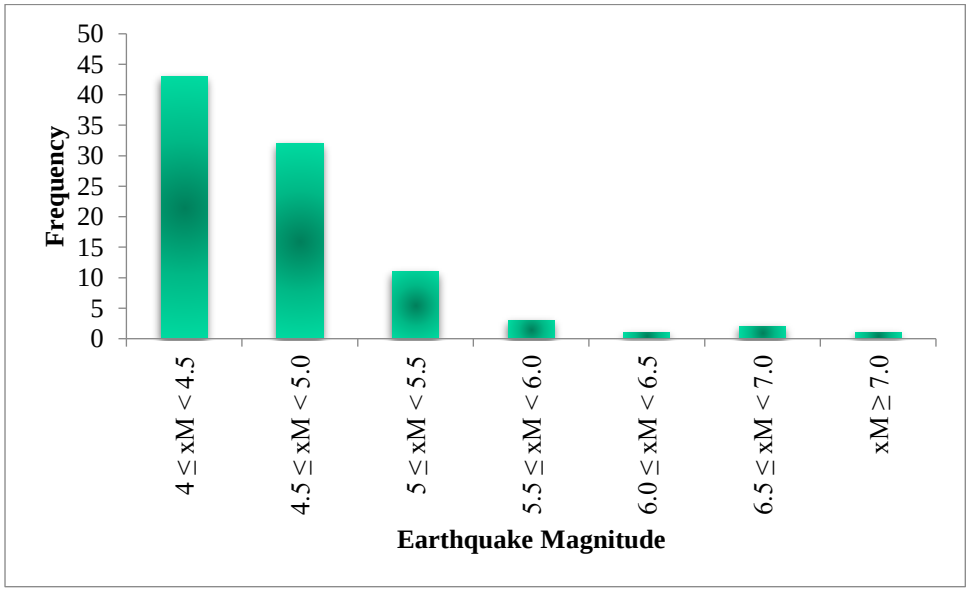

Figure 3.11. Frequency histogram of earthquakes magnitude in terms of xM.

Table 3.1 represents earthquake magnitude is 5.0 and above in the vicinity of the study area. In the region, there are earthquakes occurring during the instrumental period, which are considered moderate and high in intensity. The earthquake of 1968, which occurred during the instrumental period, is associated with the study area and its immediate surroundings. This earthquake led to the loss of 24 lives and resulted in a large number of injuries and material damages (İRAP Bartın, 2022).

Table 3.1. Instrumental period earthquakes which were xM>=5.0 (Available online: http://www.koeri.boun.edu.tr/sismo/zeqdb/default.asp Accessed on: 12.12.2023).

Date	Lat.*	Long.*	Depth (km)	xM	Mw	Location
1999.11.17	40.8	31.46	9	5.0	-	Kizilagil- (Bolu) [North West 5.9 Km]
1999.11.12	40.75	31.36	10	5.0	-	Yesiltepe-Kaynasli (Duzce) [North West 2.0 Km]
1999.11.12	40.75	31.45	10	5.2	-	Elmalik- (Bolu) [North 2.2 Km]
1999.11.12	40.75	31.4	10	5.2	-	Dariyeribakacak-Kaynasli (Duzce) [East 1.2 Km]
1968.09.03	41.81	32.39	5	6.5	6.0	Amasra (Bartin) [North 7.0 Km]
1957.05.26	41.42	31.09	10	5.2	5.2	Akçakoca Açiklari-Düzce (Karadeniz)
1953.09.07	41.09	33.01	40	6.0	6.0	Soganli-Ovacik (Karabük) [South West 1.9 Km]
1951.08.14	41.08	33.18	40	5.2	5.2	Cerciler-Arac (Kastamonu) [South West 1.6 Km]
1951.08.13	40.88	32.87	10	6.9	6.6	Kuzoren-Cerkes (Çankiri) [South East 2.8 Km]
1949.05.13	40.94	32.71	20	5.3	5.3	Incebogaz-Eskipazar (Karabük) [West 0.3 Km]
1947.12.19	40.71	32.82	10	5.2	5.2	Kisac-Cerkes (Çankiri) [South West 0.6 Km]
1945.03.08	41.85	32.44	10	5.3	5.3	Akkonak-Amasra (Bartin) [North West 8.4 Km]
1944.02.10	41	32.3	10	5.5	5.5	Ilyaslar-Mengen (Bolu) [North 4.1 Km]
1944.02.02	40.74	31.44	40	5.3	5.3	Elmalik- (Bolu) [North West 1.4 Km]
1944.02.01	41.4	32.7	10	5.5	5.5	Incecay-Safranbolu (Karabük) [North West 2.5 Km]
1944.02.01	40.7871	31.8723	10	7.2	6.8	Ulumescit-(Bolu)
1940.02.01	41	33	30	5.2	5.2	Erkec-Ovacik (Karabük) [North West 0.9 Km]
1919.06.09	41.16	33.2	10	5.8	5.8	Okcular-Arac (Kastamonu) [South East 1.3 Km]

*****Latitude: Lat. and Longitude: Long.

When studies on landslides triggered by earthquakes are examined in the literature, it is observed that landslides are triggered by earthquakes of various magnitudes. For instance, many shallow landslides were triggered after twins 2023 Kahramanmaraş earthquakes in Türkiye (Mw = 7.7 Pazarcık and Mw = 7.6 Elbistan) (Cetinkaya et al., 2023; Gokceoglu, 2023; Görüm et al., 2023; Karakas et al., 2024). Earthquake magnitudes such as Mw = 6.8 and Mw = 7.8 (Chen et al., 2020b), Mw = 6.6 (Yunus et al., 2023), Mw = 7.1 (Salinas-Jasso et al., 2023), Mw = 7.2 (Havenith et al., 2022) and Mw = 7.9 (Fan et al., 2023) led to shallow landslide occurrence in different studies. Plenty of shallow landslides triggered by the earthquake with a magnitude of 7.4 that occurred in Taiwan have been recorded (Milliyet Daily Newspaper, 2024). Martino et al. (2022) studied on shallow landslides which were triggered with 5.1 magnitude in their study area. This is why earthquakes with a magnitude of 5 or greater are shown in the Table 3.1. However, it should be noted that even an earthquake magnitude such as 4 has the potential to trigger a shallow landslide, if the saturation is high. "AFAD Earthquake Hazard Map of Türkiye Interactive Web Application" enables to examine Peak Ground Acceleration (PGA) values in the study area (Figure 3.12). The location latitude' and longitude' data need to be entered into the web application to investigate the PGA.

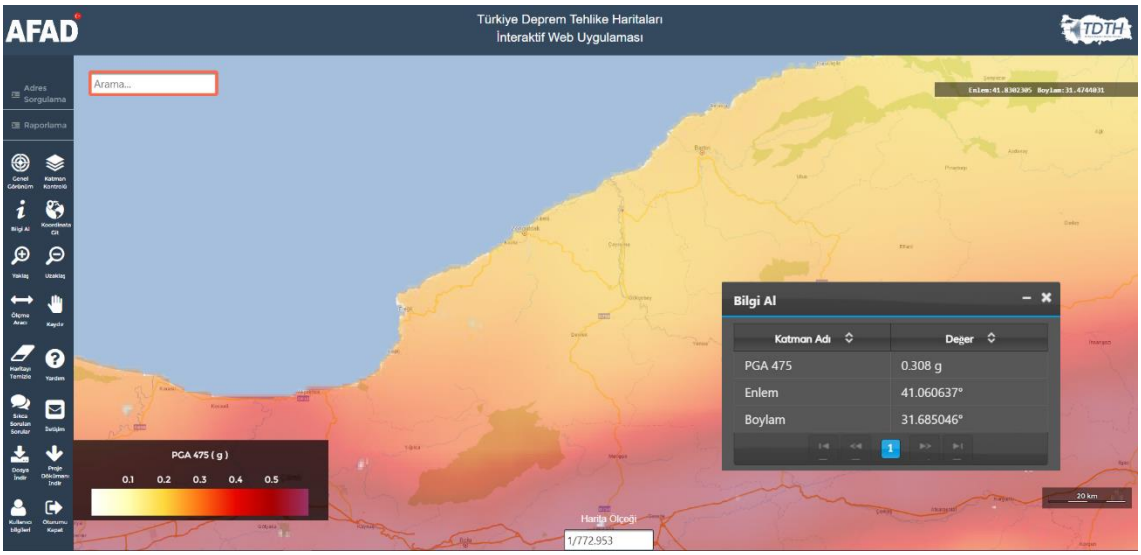

Figure 3.12. The representation of finding PGA values from AFAD Earthquake Hazard Map of Türkiye Interactive Web Application.

Random 15 points were selected to investigate seismic effect of the study area with respect to PGA values (Table 3.2). While random points were selected, it was also considered such as an active fault vicinity. As can been seen from Figure 3.13, SW part of study area PGA values are higher because of the effects of the active faults. While observed maximum PGA value is 0.316, the minimum PGA value is 0.213. PGA values enable to predict landslide prone regions (Tanyaş and Lombardo, 2019). In the study of Moses (2017); despite PGA $\geq$ 0.3g was the threshold of the occurring of earthquake induced landslides, one landslide was detected where PGA $\leq$ 0.3g. In addition, 0.05g is also considered as the minimum PGA value in order to cause landslide (Tanyaş and Lombardo, 2019). However, it should be investigated on majorly occurring of landslide events occurred area by considering threshold PGA value (Tanyaş and Lombardo, 2019). 0.15 g and 0.12 g are the thresholds PGA in the studies of Mark et al. (2017) and Tanyaş and Lombardo (2019), respectively. Shallow landslides occurred in regions where PGA exceeds 0.2 g in the study of Shao, Ma and Xu (2023). Therefore, if PGA values are scrutinized, it is possible to be evaluated that the study area may also be prone to earthquake-induced landslides.

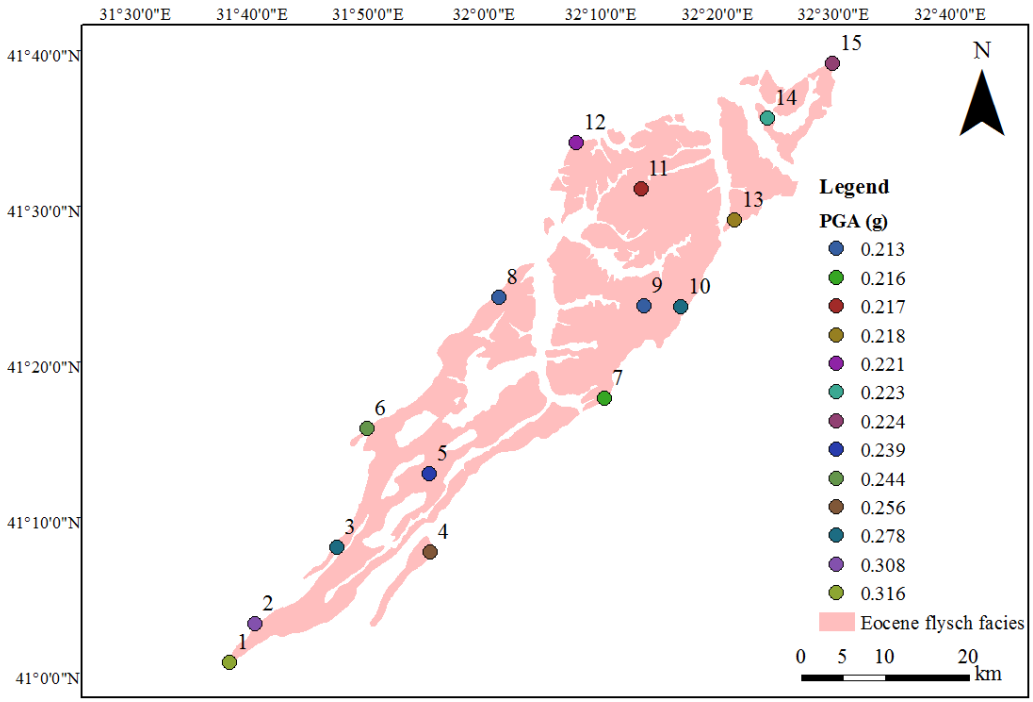

Figure 3.13. 15 randomly selected points distributions and their PGA values, which were obtained from AFAD Earthquake Hazard Map of Türkiye Interactive Web Application in Eocene flysch facies.

Table 3.2. 15 randomly selected points latitudes/longitude and their PGA values, which were obtained from AFAD Earthquake Hazard Map of Türkiye Interactive Web Application in Eocene flysch facies.

Point Number	Latitude	Longitude	PGA (g)
1	41.018885	31.649578	0.316
2	41.060637	31.685046	0.308
3	41.143763	31.799420	0.278
4	41.140144	31.931400	0.256
5	41.223889	31.929284	0.239
6	41.271231	31.840603	0.244
7	41.306647	32.177211	0.216
8	41.413776	32.025174	0.213
9	41.406174	32.232817	0.213
10	41.404981	32.284933	0.278
11	41.531070	32.226452	0.217
12	41.580017	32.133591	0.221
13	41.498367	32.360219	0.218
14	41.608116	32.406128	0.223
15	41.666896	32.498657	0.224

3.4. Land Use and Vegetation

The key to preparation of realistic site characterization is to the more detailed research about land use and vegetation. Spatial distribution of land-use changes should have been examined in that are influencing to interpret the occurrence of rainfall-triggered landslides. In the study of Asada and Minagawa (2023), grasslands and shrubs forest have higher probability of shallow landslides than coniferous forest, broadleaf forests and broadleaf secondary forests. Jiang et al. (2023) stated that broad-leaved forest, coniferous forest, shrub, meadow, grassland, and alpine vegetation are prone to occurring of shallow

landslides. While land use promises better susceptibility analyses, they are also the subject of many concerns because they are evaluated as dynamic factors which are easily affected by human activities. Corine Land Cover 2018- 100-meter GeoTiff raster file was downloaded in order used to examine land use of the study area. The current CLC 2018 version is v.2020_20u1 promises information about the detail study area land use (Figure 3.14). Information obtained from Corine Land Cover (2018) data indicate that complex cultivation patterns, non-irrigated arable land, broad-leaved forests, land principally occupied by agriculture with significant areas of natural vegetation and mixed forests are dominant in the study area (Figure 3.14).

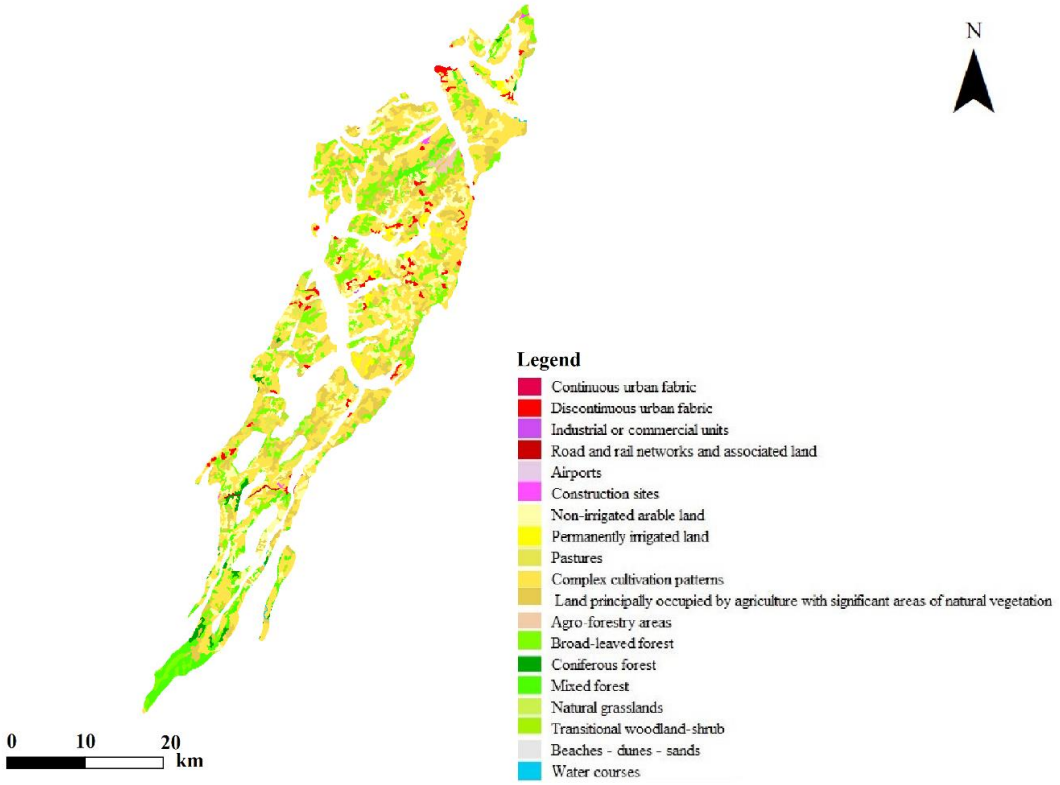

Figure 3.14. The land use map of the Eocene flysch facies (Corine Land Cover, 2018).

The chart below (Figure 3.15) shows that the proportion of main land cover in Eocene flysch facies. The pie chart elucidates that Eocene flysch facies have been dominantly covered by six distinct type of land cover. Forest vegetation and agriculture land are observable in the study area (İRAP Bartın, 2022; İRAP Zonguldak, 2021).

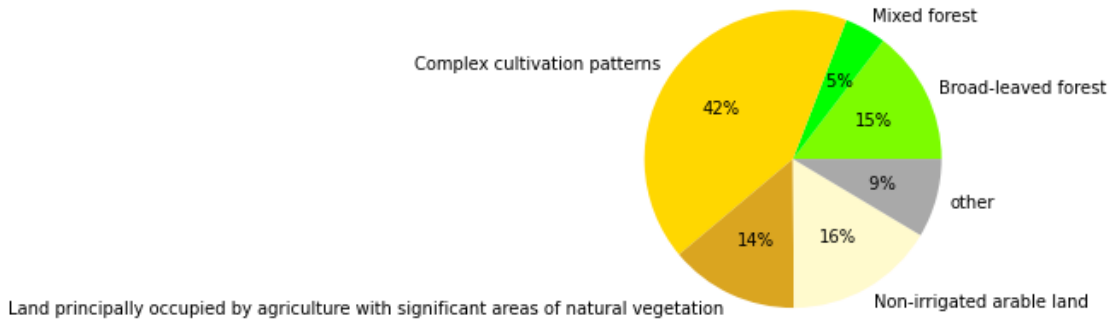

Figure 3.15. Graphical distribution of the land cover of the Eocene flysch facies (Corine Land Cover, 2018).

3.5. Climate and Precipitation

Eocene flysch facies, located in the Western Black Sea region, has been examined according to climate and precipitation in this part of the dissertation. Since the majority of the Eocene flysch facies are within the boundaries of Bartın and Zonguldak provinces, climate and precipitation assessments related to Bartın and Zonguldak provinces have been taken into account in this research.

First of all, Zonguldak and Bartın are influenced by the temperate Black Sea climate (İRAP Bartın, 2022; İRAP Zonguldak, 2021). Zonguldak, where every season is rainy and mild, does not experience a dry season (İRAP Zonguldak, 2021). The summers are cool, and the winters are mild and rainy in Bartın (İRAP Bartın, 2022). Bartın and Zonguldak were also evaluated in terms of Köppen climate classification. While Zonguldak is chrazterized by “Cfa”, Bartın is represented by “Cfb” according to Köppen climate classification (Turkish State Meteorological Service, 2016). It should be remembered that “C” warm temperature; “f” fully humid; “a” hot summer; “b” warm summer (Kottek et al., 2006). Cfa is characterized that while summer is very hot, climate is warm in winter. Cfa also indicates that climate is also rainy for all season. Unlike Cfa, Cfb is charazterized that climate is warm for both winter and summer. Climate is rainy for all season in both characterizations.

Secondly, precipitation trend was also scrutinized for both cities. Rainfall characteristic may give an inclue of the occurrence of landslides. Table 3.3, which was obtained from

Turkish Meteorological Service online portal, shows the historical precipitation and temperature for Zonguldak and Bartın cities. Figure 3.16 is the graphical representation of the information in Table 3.3 in terms of average precipitation and temperature values. The most rainfall is observed during the autumn and winter seasons for both cities. Rainfall increases from south to north within the Zonguldak province (İRAP Zonguldak, 2021).

Table 3.3. Monthly mean precipitation and temperatures for Zonguldak (1939-2022) and Bartın (1961-2022) (Turkish Meteorological Service, 2022).

ZONGULDAK (1939 - 2022)	**1**	**2**	**3**	**4**	**5**	**6**	**7**	**8**	**9**	**10**	**11**	**12**
Average Temperature (°C)	6.2	6.3	7.5	11.2	15.4	19.6	21.9	22	18.9	15.3	11.9	8.5
Average Max. Temperature (°C)	9.2	9.6	10.9	14.8	18.9	23.1	25.2	25.4	22.5	18.7	15.3	11.6
Average Min. Temperature (°C)	3.5	3.5	4.6	8	12.2	16	18.1	18.3	15.4	12.3	8.9	5.7
Average of Monthly Total Precipitation (mm)	140.4	99.4	98.1	64.4	54.7	74.6	68.9	83.2	103.4	145.3	139.4	153.8
BARTIN (1961 - 2022)	**1**	**2**	**3**	**4**	**5**	**6**	**7**	**8**	**9**	**10**	**11**	**12**
Average Temperature (°C)	4	4.9	7.2	11.4	15.9	19.8	22	21.9	18	13.8	9.2	5.9
Average Max. Temperature (°C)	9.3	10.7	13.4	18.1	22.4	26.2	28.3	28.5	25.2	20.7	16.1	11.3
Average Min. Temperature (°C)	0.4	0.7	2.5	6.0	10	13.6	15.8	15.7	12.2	8.9	4.6	2.1
Average of Monthly Total Precipitation (mm)	120.9	86.6	79.0	58.6	54.5	76.0	62.2	76.1	86.3	108.3	112.6	132.0

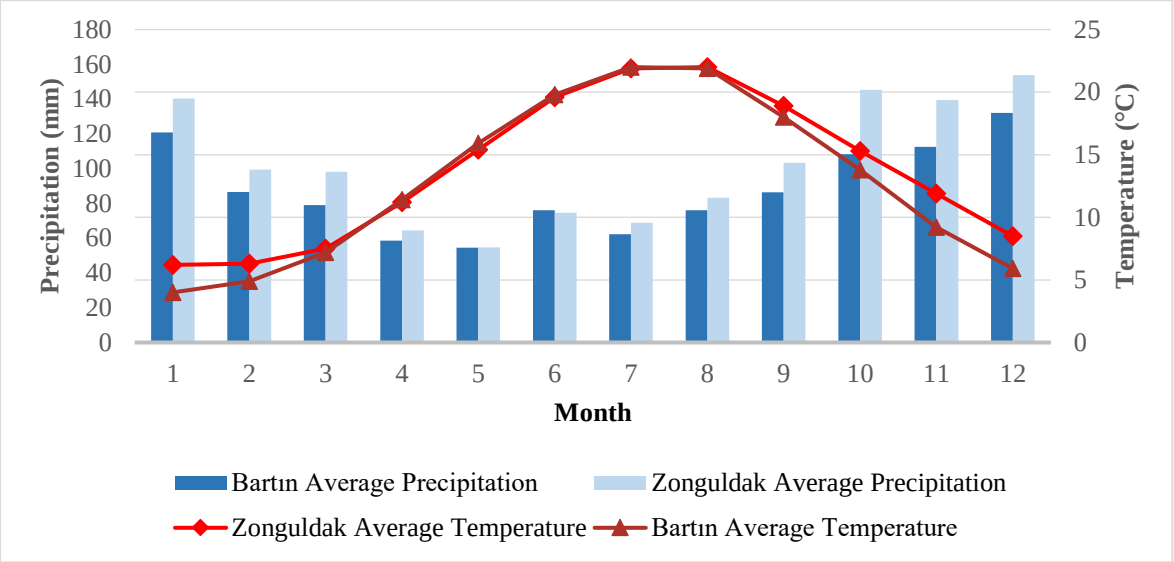

Figure 3.16. Monthly mean precipitation and temperatures for Zonguldak (1939-2022) and Bartın (1961-2022) (Turkish Meteorological Service, 2022).

Climate change may induce sudden shifts in regional weather patterns. It is necessary to examine the sudden shift with respect to rainfall data in order to fulfil needs of the future landslide's researches. In fact, with changing climate conditions effects continuing to emerge across the world, extreme rains which to cause landslides disasters also increase number of the potential flow regions. Loeche et al. (2022) state that if the slope gradient value is between 10º and 20º and the annual rainfall exceeds 800 mm, the probability of triggering a landslide is high for their study area where in a location close to the study area. There is also an assessment available in the literature for the vicinity of the region in terms of landslide and rainfall relationships. Taskiran, Alli and Yilmaz (2023) claimed that landslides may occurrence when the rainfall intensity is about less than 10 mm/h continues for such as at least 0.85 h for Bartin/Ulus in dry periods. In contrast, in wet periods, if rainfall continue 0.36 h, rainfall intensity can be much higher that 1 mm/h (Taskiran, Alli and Yilmaz, 2023). The analysis of the significant amount of rainfall observed in the last 5 years in cities Bartın and Zonguldak, as well as the rainfall data from other meteorological stations within the study area boundaries, has been examined from Table 3.4. In Table 3.4, the data up to 2022 were obtained from the Turkish State Meteorological Service Daily Historical Precipitation, while the rainfall data for the year 2023 were obtained from Turkish State Meteorological Service Daily Total Precipitation (mm) which can be daily monitored from the online portal. The median and mean value

of extreme precipitations for last 5 years presented in Table 3.4 are about 87 and 93 mm, respectively. Table 3.4 also clarifies that researchers have been observed records extreme rainfalls during seasons of summer for two years in this area. The rainfall data analysis showed that the maximum monthly rainfall occurs in June, July, August and September which coincides with the landslide occurrence in this area.

Table 3.4. Historical extreme precipitations observations at meteorological stations from recorded data (Turkish Meteorological Service).

Date	Station	Daily Precipitation (mm)
24.06.2018	Bartın, Merkez, Bartın	81
22.08.2019	Zonguldak, Merkez, Zonguldak	89
08.07.2020	Zonguldak, Merkez, Zonguldak	77
13.08.2021	Zonguldak, Merkez, Zonguldak/Beycuma	126
13.08.2021	Zonguldak, Devrek, Devrek	76
25.06.2022	Bartın, Merkez, Bartın	89
27.06.2022	Bartın, Merkez, Bartın	80
28.06.2022	Zonguldak, Devrek, Devrek/AcısuTepesi Radar Sahası	142
28.06.2022	Zonguldak, Merkez, Zonguldak	89
28.06.2022	Zonguldak, Gökçebey	94
20.06.2023	Zonguldak, Çaycuma, Çaycuma	89
09.07.2023	Zonguldak, Devrek, Devrek/AcısuTepesi Radar Sahası	85
09.07.2023	Zonguldak, Gökçebey, Gökçebey	71
09.07.2023	Zonguldak, Merkez, Zonguldak	75
09.07.2023	Zonguldak, Merkez, Zonguldak/Beycuma	115
09.07.2023	Zonguldak, Çaycuma, Çaycuma	82
10.07.2023	Bartın, Merkez, Bartın	85
10.07.2023	Zonguldak, Merkez, Zonguldak/Beycuma	89
10.07.2023	Zonguldak, Çaycuma, Çaycuma	99
10.07.2023	Zonguldak, Gökçebey	112
10.07.2023	Zonguldak, Devrek, Devrek	94
10.07.2023	Zonguldak, Devrek, Devrek/AcısuTepesi Radar Sahası	152
10.07.2023	Zonguldak, Devrek, Devrek/Eğerci Beldesi	85
04.09.2023	Zonguldak, Gökçebey	71
04.10.2023	Zonguldak, Merkez, Zonguldak	79
19.11.2023	Zonguldak, Merkez, Zonguldak/Beycuma	80
19.11.2023	Zonguldak, Çaycuma, Çaycuma	76
19.11.2023	Zonguldak, Merkez, Zonguldak	111

The planned start year in the climate change analyses for the future step of the study is chosen as 2025. The year determined for the time period of 30 years ago is 1995. Distributions of days with or without precipitation in the 1995-2022 period at the meterological stations were shown in Figure 3.17 for both cities. It has been noticed that the ratio of rainy days in the evaluations made for the two cities is similar according to the determined time period.

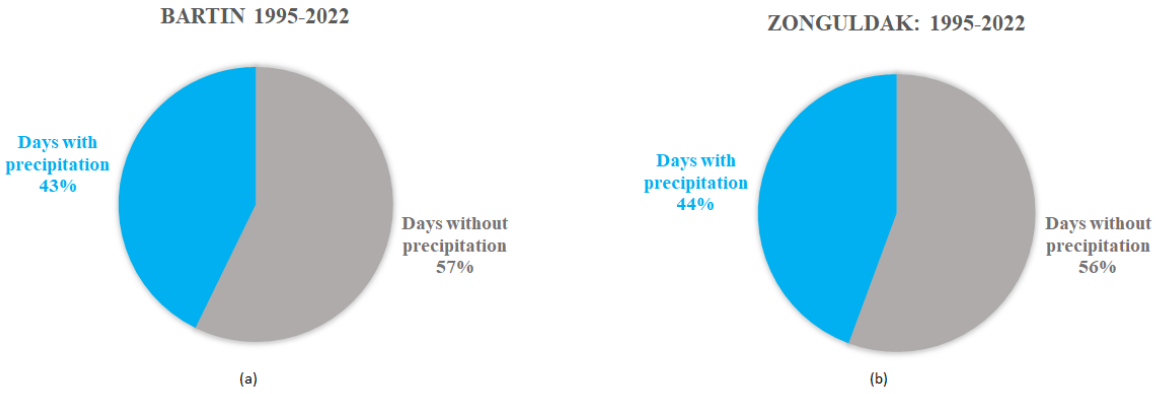

Figure 3.17. Examination of precipitation days percentages for both cities in the timeframe of 1995-2022 (Turkish Meteorological Service Historical Data).

The reason for using data from stations Zonguldak and Bartın is that these two stations have long-term historical data available for this area. Most of the stations shown in Table 3.4 do not have long-term historical data. The map showing the locations of Zonguldak and Bartın stations, which will be used in the following analyses, is presented in Figure 3.18.

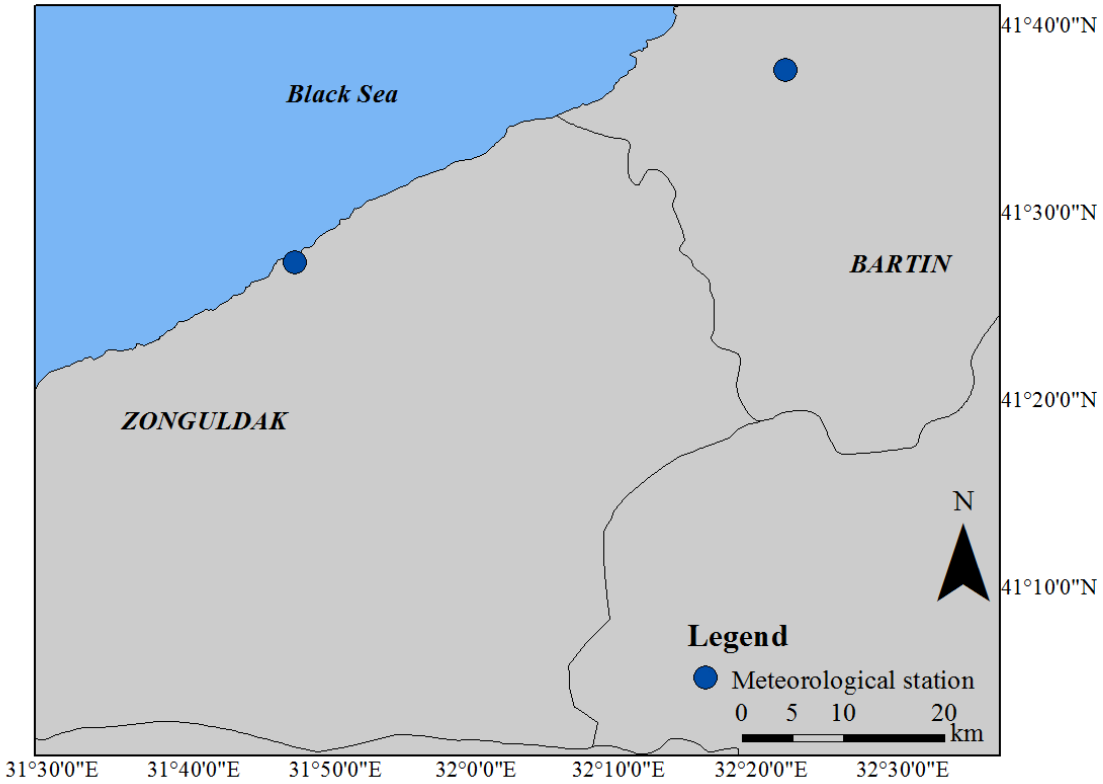

Figure 3.18. Locations of the meteorological stations.

CCSM4 which is obtained from NCAR provide available both monthly and annual RCP scenarios precipitation data which are for two stations. Data is accessible on the website of "https://gis.ucar.edu/inspector". It is necessary to characterize future climatic disposition with respect to RCP 4.5 and 8.5 precipitations over Eocene flysch facies in order to determine possible failure initiations. It is obvious that future precipitation data is uncertain, nevertheless, it is possible that uncertainties is explained by evaluating the RCP scenarios median precipitation values in this study scope. Mean seasonal rainfall was also used for projected rainfall analysis in the study of Ferrer et al. (2022).

The study periods are organized to cover a 20-year time span for following steps. The division of the time period covers over 19 or 20 years: from 2025 to 2044, from 2044 to 2063, from 2063 to 2082 and from 2082 to 2100 in this study. Table 3.5 shows the median trend of the RCP 4.5 and 8.5 precipitations for determined time ranges in terms of both annual and monthly. These data are critical because they will be used in the interpolation of the future precipitation within the scope of this study.

Table 3.5. Median precipitation for determined time frame (NCAR).

MEDIAN PRECIPITATION (mm)				
Period	**Scenario**	**Time**	**Location**	
			Bartın	**Zonguldak**
2025-2044	4.5	Month	55	91
	4.5	Year	650	996
	8.5	Month	55	85
	8.5	Year	658	991
2044-2063	4.5	Month	53	88
	4.5	Year	657	980
	8.5	Month	51	83
	8.5	Year	620	935
2063-2082	4.5	Month	53	85
	4.5	Year	647	984
	8.5	Month	52	79
	8.5	Year	631	928
2082-2100	4.5	Month	54	85
	4.5	Year	642	983
	8.5	Month	50	75
	8.5	Year	611	906

The selection of an appropriate interpolation technique is important in the study. This obtained data will used in the prediction of shallow landslides initiations. They might show a spatially heterogeneous distribution. Inverse Distance Weighted (IDW) interpolation was used to analyse general precipitation trends because IDW interpolation proves more effective in a heterogenous environment (Sun et al., 2019). IDW stands out as the preferred method when compared to MA and Kriging, thanks to its efficient

processing time and satisfactory precision (Maleika, 2020). The spatial distributions of RCP scenarios rainfalls applied in studies of Mohamed Yusof et al. (2024) and Nasidi et al. (2021) by using IDW. They are clear example studies by previous literature. It is critical to make correct choice of reference precipitation dataset with respect to determining whether precipitation from monthly or annual should be used. Taking into account necessary of analysing daily precipitation data, using the precipitation data from mothly scenarios will be closer to reality compared to data obtained from annual precipitation in this study. Rainfall maximum maps are interpolated using IDW methods for the study area in this study. The study area receives a monthly median precipitations (mm) are shown in Figure 3.19 and Figure 3.20, which display the spatial distribution of RCP 4.5 and 8.5 scenarios precipitation values by using IDW method interpolation in terms of determined time range.

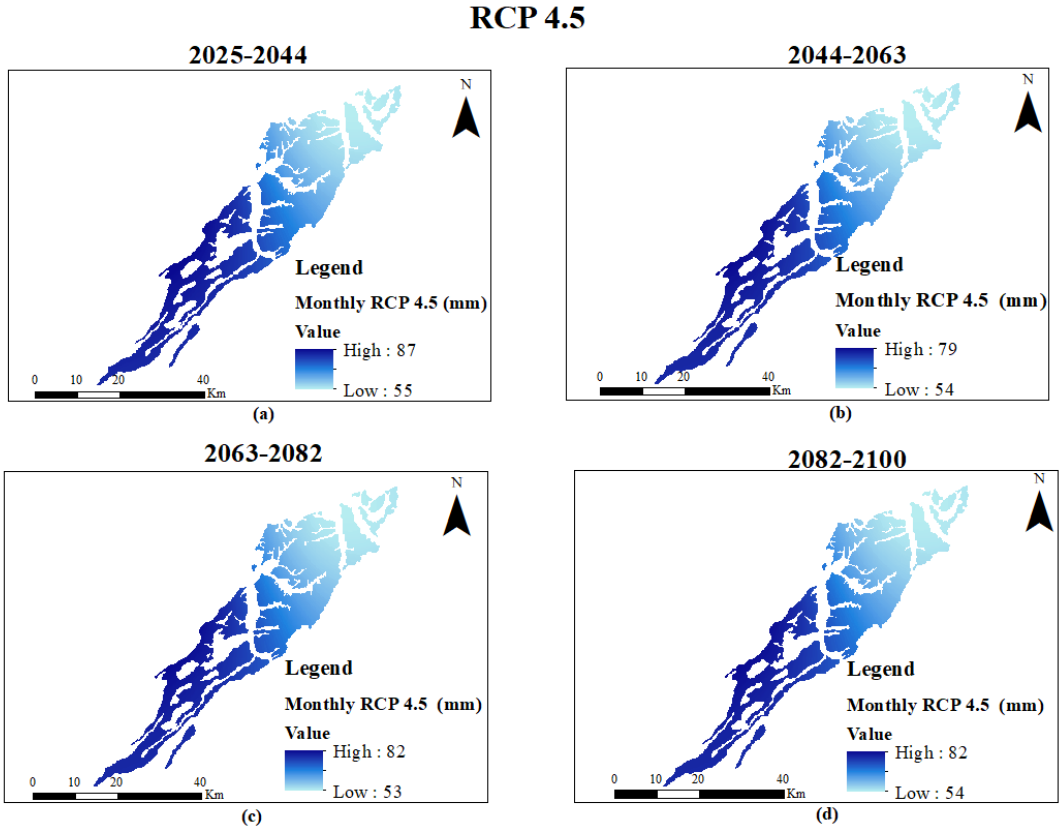

Figure 3.19. RCP 4.5 projected precipitations, which were prepared in accordance with IDW interpolation, for specific time intervals: (a) 2025-2044, (b) 2044-2063, (c) 2063-2082 and (d) 2082-2100 (NCAR).

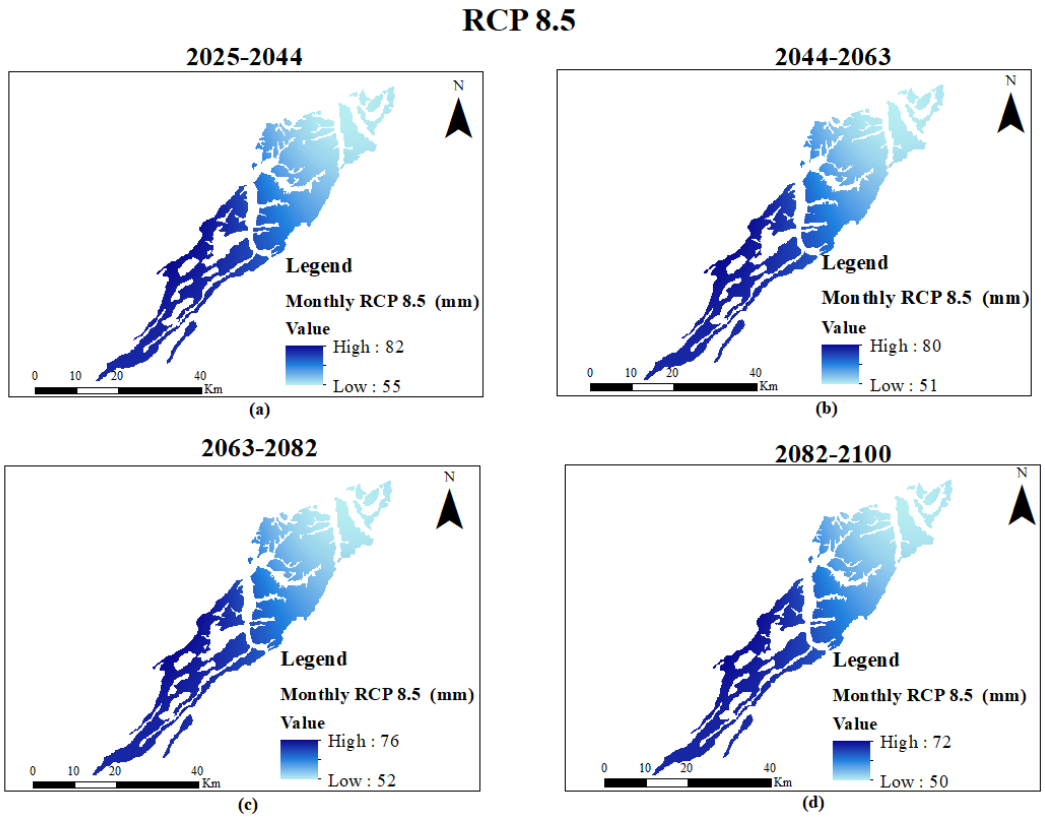

Figure 3.20. RCP 8.5 projected precipitations, which were prepared in accordance with IDW interpolation, for specific time intervals: (a) 2025-2044, (b) 2044-2063, (c) 2063-2082 and (d) 2082-2100 (NCAR).

These analyses are important because possible heavy rainfall threshold value will also suggest probable shallow landslide initiations in the study area prone to landslide phenomena in the future step of the study.

3.6. Division of Sub-basins and Their Geomorphological Characteristics

Parameter selection in large areas are more difficult. Therefore, the study area was separated into three sub-basin by evaluating the watershed in the region (Figure 3.21). ArcGIS software with the “Flow Direction” and “Basin” tools were used for this step. These tools offer immense satisfaction about identifying ridge lines between basins (ESRİ). These ridge lines also enable to see that the flow direction changes at the boundaries (ESRİ). An analysis aimed at minimizing the number of basins was conducted, and sub-basins were identified based on the criterion of changing flow direction. Sub-basins are Egerci basin at the south (269 km^2), Beycuma basin in the middle (311 km^2), Ihsanoglu basin at the north (297 km^2) (Komu, Nefeslioglu and Gokceoglu, 2024).

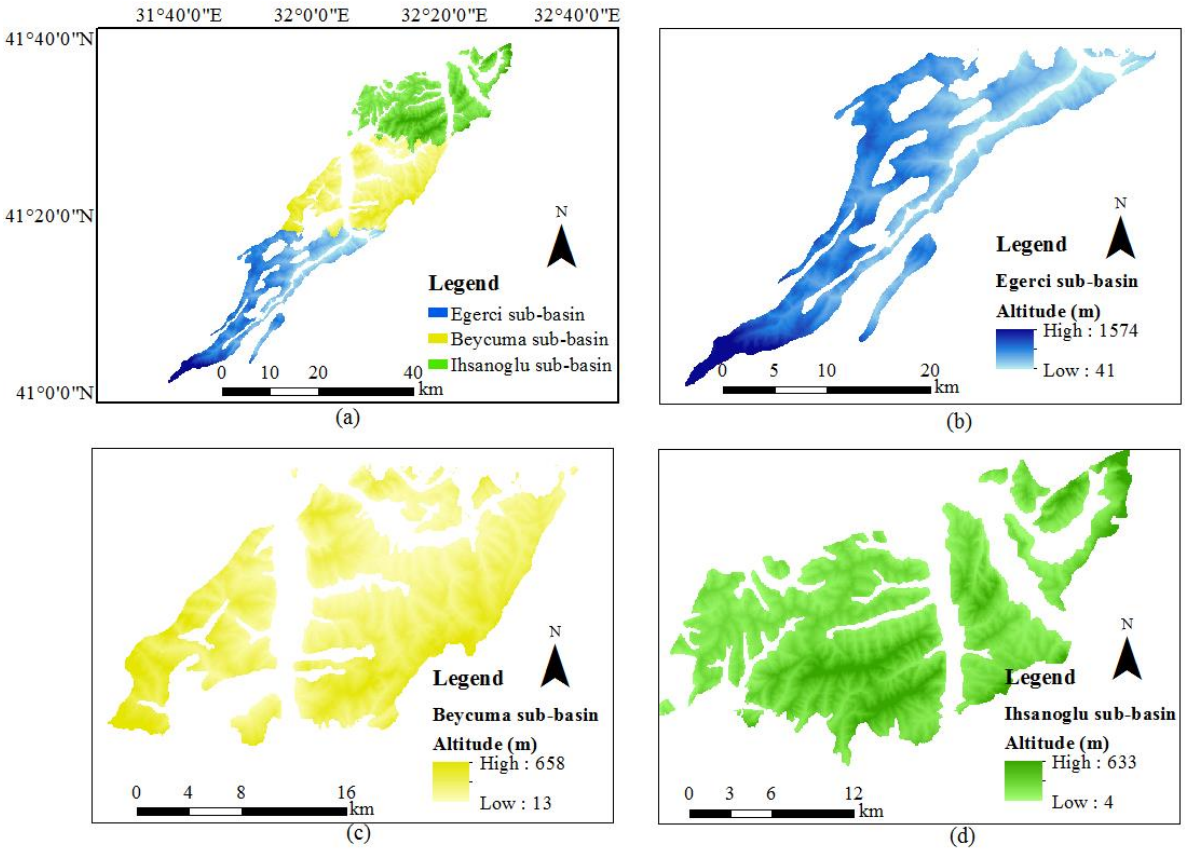

Figure 3.21. (a) Division of the sub-basins in Eocene flysch facies, (b) Egerci sub-basin, (c) Beycuma sub-basin, and (d) Ihsanoglu sub-basin (Komu, Nefeslioglu and Gokceoglu, 2024).

Table 3.6 gives information about sub-basins in terms of geomorphological characteristics.

Table 3.6. Descriptive statistics of the topographic parameters for the three sub-basins (Komu, Nefeslioglu and Gokceoglu, 2024).

Sub-basin	Statistics	A (m)	SG (°)	SA (°)	PLC	PRC	CI	CD	TWI	SLF	CNBL (m)	CND (m)	VD (m)
Egerci	Min.	41	0	0	-0.01	-0.01	-92	0	2	0	41	-49	-3
	Max.	1,574	60	6.28	0.01	0.012	96	20	21	38	1,382	449	549
	Mean	444	15	3.25	0	0	0	0	7	5	381	64	236
	Median	425	14	3.04	0	0	0	0	6	4	369	49	229
	Std. Deviation	259	8	1.91	0.002	0.002	8	1	2	3	233	60	133
Beycuma	Min.	13	0	0	-0.01	-0.01	-100	0	3	0	13	-27	0
	Max.	658	52	6.28	0.008	0.009	100	19	20	24	444	304	277
	Mean	170	11	3.27	0	0	0	0	7	3	129	41	140
	Median	158	9	3.33	0	0	0	0	7	2	118	32	146
	Std. Deviation	91	6	1.91	0.001	0.001	9	1	2	2	69	38	61
Ihsanoglu	Min.	4	0	0	-0.01	-0.02	-98	0	2	0	6	-39	0
	Max.	633	70	6.28	0.017	0.021	92	32	20	30	284	468	339
	Mean	121	11	3.35	0	0	0	0	7	3	79	42	117
	Median	104	10	3.43	0	0	0	0	6	2	69	32	117
	Std. Deviation	71	7	1.83	0.001	0.001	10	1	2	2	43	42	51

Abbreviations	Altitude: A, Slope gradient: SG, Slope Aspect: SA, Plan Curvature: PLC, Profile Curvature: PRC, Convergence Index: CI, Closed Depression: CD, Topographic Wetness Index: TWI, Slope Length Factor: SLF, Channel Network Base Level: CNBL, Channel Network Distance: CND, Valley Depth: VD

4. SHALLOW LANDSLIDES IN THE STUDY AREA

Eocene flysch facies are consistently influenced by landslide disasters. It is possible to detect that loose material is abundant in these regions. Considering the heavy rainfall in the area, it not surprises to claim that this formation is a severe disaster zone with respect to especially shallow landslides. It may be feasible to observe recurring shallow landslides which are caused by heavy rainfall in this region. The main reasons for the high incidence of landslides in 1:500,000 scale Zonguldak maps (Duman et al., 2005a) are primarily due to climatic characteristics, the widespread exposure of landslide-prone fragmented units on the surface, and rugged terrain conditions (Çan et al., 2013). Eocene flysch facies are located in the Zonguldak maps boundary with respect to Duman et al. (2005a). The landslide occurrence density map prepared by Gokce (2008) indicates that the study area is evaluated as having very high landslide density. Görüm (2019) also stated that the landslide density is high in Bartın. Akgün et al. (2021) pointed out that slide type landslides are generally observed in Eocene flysch formation. It was highlighted in previous studied that heavy rainfalls cause flow type landslides in these formation (Can et al., 2005; Akgün et al., 2021). Duman et al. (2005a) reported that shallow and deep landslides occurred in this formation. Duman et al. (2005a) also pointed out that shallow landslides frequently occur on low slope gradient areas lower than 10^{o} in this formation. Debris flows are also observable in slide masses and drainage paths. It is important to detect them in a short time because wet climatic condition causes disappearance of traces (Duman et al., 2005a). The significance of two key research points of this chapter can be summarised as: (i) construct the shallow landslide inventory map and (ii) prepare the shallow landslide susceptibility map using LR models.

4.1. Shallow Landslide Inventory Map

It can be noted that a landslide inventory map reveals the history of landslides and provide clue about possible preceded landslide areas. Landslide inventory maps are actually a practical way of communication to encourage researchers for making a decision about landslides and conveying recent information to engineers who study on landslide hazards or risks. In other words, inventory maps of landslides are crucial as a fundamental infrastructure used in susceptibility and hazard analyses.

The landslide inventory was completed with the data obtained from satellite images and field observations in many works (Kritos and Davies, 2015; Bera, Melo and Guru, 2021; Putra et al., 2022). Google Earth images were also used for shallow landslides inventories in the previous studies (Bera, Melo and Guru, 2021; Gaidzik and Ramírez-Herrera, 2021; Kasahara, Gonda and Huvaj, 2022; Dias, Dias and Grohmann, 2023; Licata et al., 2023; Thein et al., 2023) Although satellite images and Google Earth images have been upgraded in recent years in order to detect shallow landslides by peering into the past, it is necessary state that some shallow landslides may not be well documented and mostly go unnoticed. It is undeniable fact that some details about shallow landslides' parts such as skarn and toe may not be clear from the satellite images. In this study, past occurred landslides spatial distributions were detected by using high-resolution Google Earth images, which enable to display various historical records of shallow landslides spanning different years, and Sentinel 2 images. In order to prepare high quality of the shallow landslide inventory, satellite imageries, achieve inventories (MTA), historical event reports (AFAD), newspaper, media archives and recent literature (Can et al. 2005; Duman et al., 2005a, 2005b; Duman et al., 2011; İRAP Bartın, 2022; İRAP Zonguldak, 2021) were also reviewed. Short field observations were also done to identify the study area in terms of shallow landslides. The shallow landslides that have occurred in the study area generally originating from the geological and geomorphological structure of the region. Landslides in Zonguldak province are mainly found in the Çaycuma Formation, which is defined by the Eocene age (İRAP Zonguldak, 2021). Landslides have occurred between Devrek and Çaycuma, predominantly in the southern parts of the province, with a northwest-southeast orientation (İRAP Zonguldak, 2021). It has been observed that the majority of landslides in the region occur as flow-type of landslides, especially following heavy rainfall events (Figure 4.1). It is observed that landslides in this area tend to occur as debris flows.

Landslides occurring were more attributed to meteorological factors rather than seismic activity between 1985 and 1998 (İRAP Bartın, 2022). Figure 4.1 shows that shallow landslides events triggered by recorded extreme precipitation in May 1998 in the Egerci sub-basin. It has been postulated that landslides may venture society in terms of social and economic aspects of the community in Eocene flysch facies.

Figure 4.1. Some typical triggered shallow landslides view in the study area after May 1998 rainfall from Google Earth image.

The landslide percentages observed within geological formations and the landslide intensities associated with these formations were evaluated using the 1/500,000 scale Türkiye Landslide Inventory Maps Special Publication Series (Duman et al., 2005a). It can be evaluated that Eocene flysch facies are critical lithology in terms of landslides occurrence (Duman et al., 2005a). When the key findings about the lithology and their triggerence of shallow landslides was reviewed in the literature, it was inferred from previous studies that shallow landslides frequently occur in clay, sandstone and mudstone. (Roccati et al., 2019; Roccati et al., 2020; Di Napoli et al., 2021; Guo et al., 2022; Wiaja et al., 2022; Falconi et al., 2023; Guo et al., 2023; Wang et al., 2024). This information is consistent with the findings about shallow landslides and their lithology of this thesis. Shallow landslide occurrence tendency is high in sandstone interbeds with shale and mudstone in this region (Duman et al., 1998). Figure 4.2 and Figure 4.3, which were obtained in the field, show the tendency of prone to shallow landslide occurrence in the study area.

Figure 4.2. Some field photographs of tendency of observation of shallow landslides in the study area.

Figure 4.3. Some field photographs of tendency of observation of shallow landslides in the study area.

Considering 262 shallow landslides were mapped in order to make strides on their runout distances. These shallow landslides are presented with respect to their sub-basins in Figure 4.4.

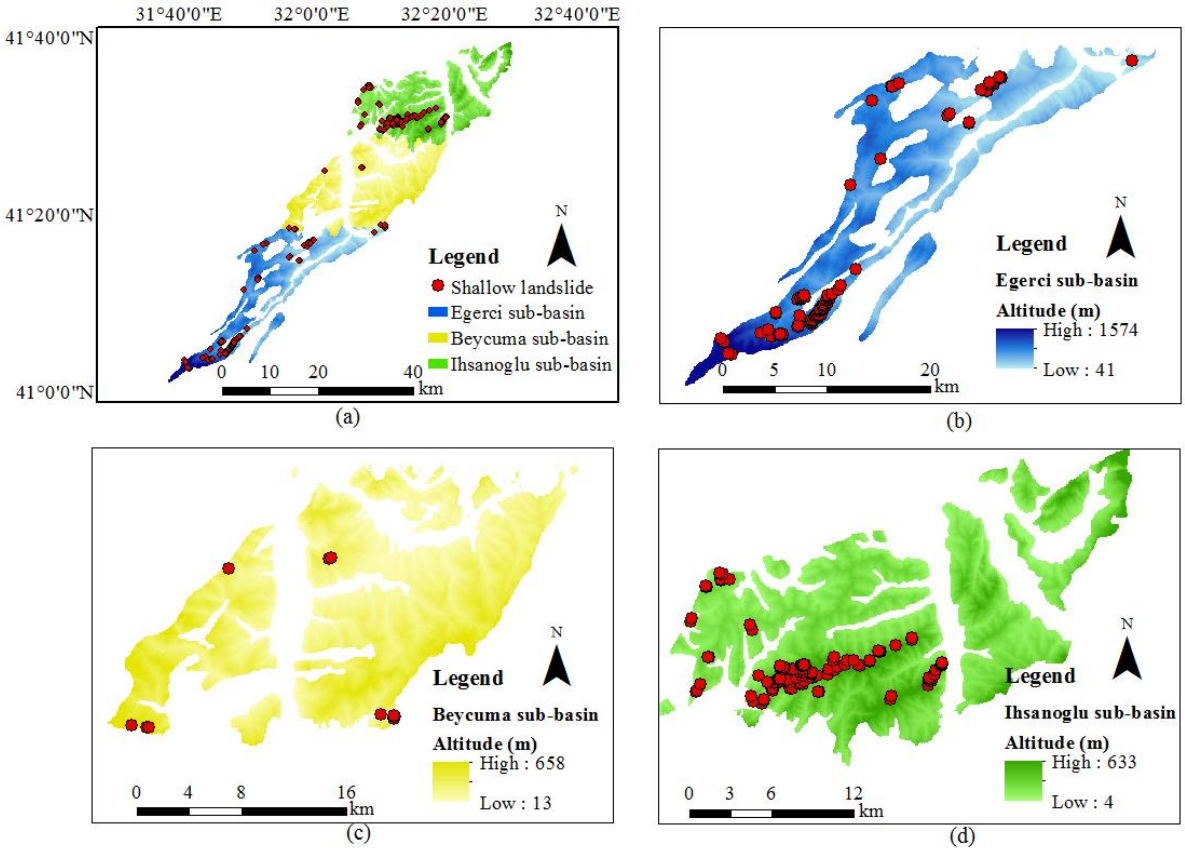

Figure 4.4. Shallow landslides inventory distributions in sub-basins.

The shallow landslide inventory map indicates that shallow landslides are 42.4% in Egerci sub-basin, 5.7% in Beycuma sub-basin and 51.9% Ihsanoglu sub-basin (Figure 4.5). More than half of the detected shallow landslides (~52%) were detected in Ihsanoglu sub-basin.

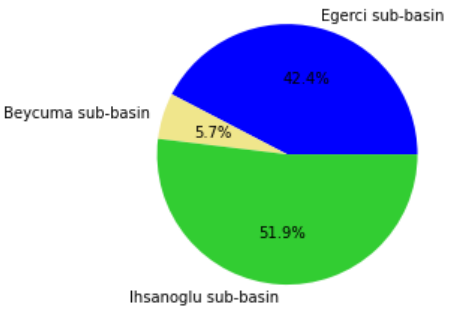

Figure 4.5. The percentage distribution data in the entire landslide inventory with respect to sub-basins.

Investigated shallow landslides were classified based on geometric characteristics such as their travel angles, failure depths and observed runout distances. First, the volume and area relations proposed by Hovius, Stark and Allen (1997) after Jaboyedoff et al. (2020) and semi ellipsoid approach were utilized to decision on the failure depths. Each sub basin failure depths were also presented separately. Results indicate that shallow landslides failure depths are smaller than 5 m (Zaruba and Mencl, 1969) in Eocene flysch facies. In fact, the highest failure depth is observed in the Egerci sub-basin within Eocene flysch facies border and its maximum failure depth is 3.2 m. In order to evaluate the study area in terms of their geometric attributes, descriptive statistics informations are shown in Table 4.1 in terms of the diverged sub-basins. Descriptive statistics might aid in the interpretation of historical events in records. Observed median runout distances according to sub-basin have been taken into account in the decision of spatial resolution cell in order use in further model analyses.

Table 4.1. Descriptive statics for the constructed landslide inventories for the sub-basins.

Sub-basin	**N**	**Statistics**	**Area (m^2)**	**Failure depth (m)**	**Travel angle (°)**	**Observed runout distance (m)**
Egerci	111	Min.	21	0.2	1	7
		Max.	4116	3.2	49	122
		Mean	536	1.0	23	53
		Median	344	0.9	24	47
		Std. Deviation	572	0.5	12	29
Beycuma	15	Min.	23	0.2	4	7
		Max.	1843	2.1	28	83
		Mean	376	0.9	13	36
		Median	258	0.8	13	31
		Std. Deviation	438	0.5	8	20
Ihsanoglu	136	Min.	7	0.1	1	5
		Max.	1710	2.1	32	122
		Mean	140	0.5	11	25
		Median	65	0.4	10	17
		Std. Deviation	226	0.3	7	21

Figure 4.6 represents the histogram of the landslide inventory in terms of A (m^2), D (m), L (m) and TA (º) for each sub-basins.

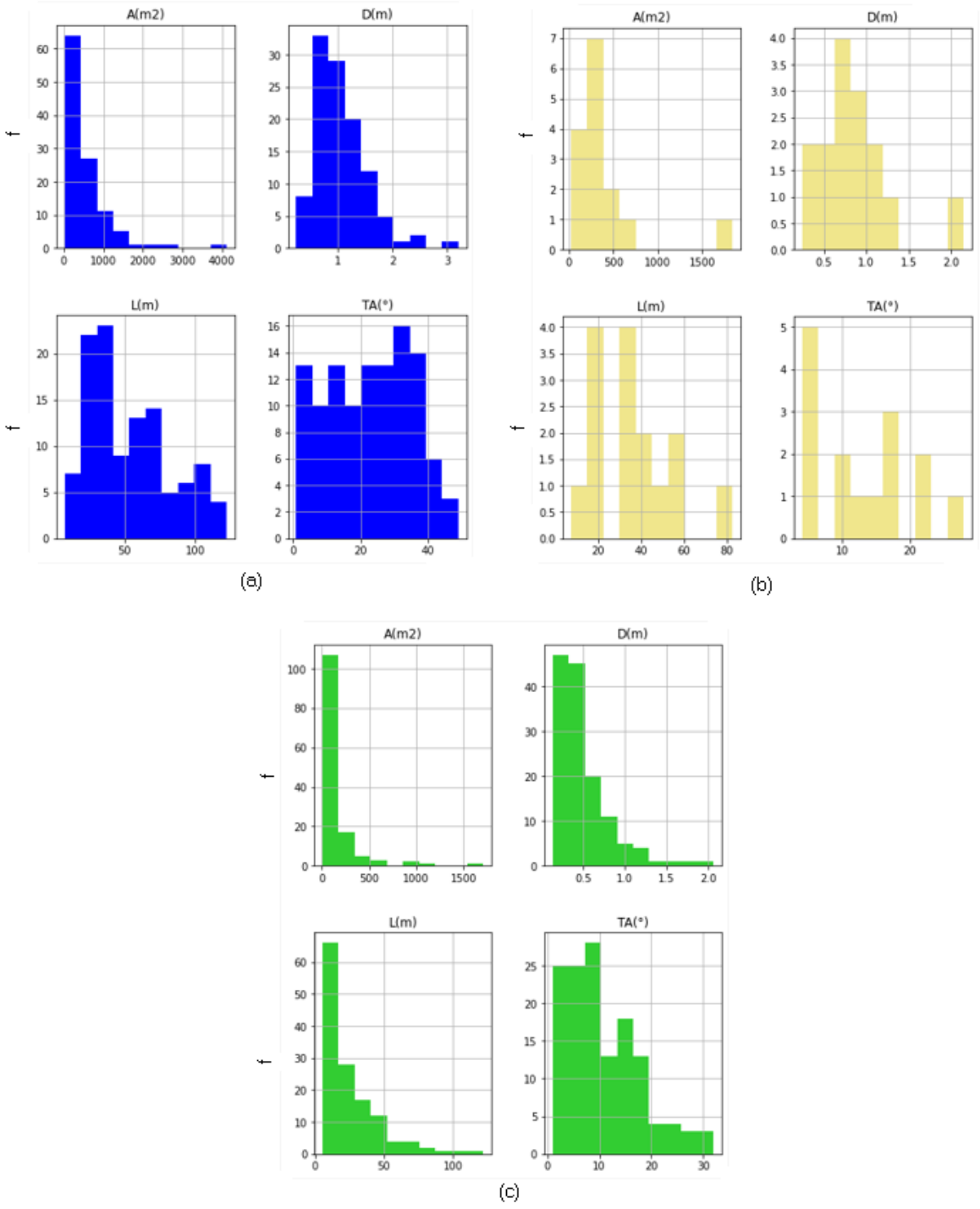

Figure 4.6. Graphical representations of sub-basins in terms of A (m^2), D (m), L (m) and TA (˚).

Figure 4.7 a and Figure 4.7 b represent the trigged shallow landslides after heavy rainfall on November 2023. Figure 4.7 offers admittedly compelling proof that shallow landslides persist due to excessive rainfall in the area. The field photographs also show the calculated runout distances of the movement in Figure 4.7. They were measured as 4 m, 6 m, 7 m, 10 m and 12 m (Figure 4.7). It can be also admitted that their observed runout distances are consistent with Table 4.1.

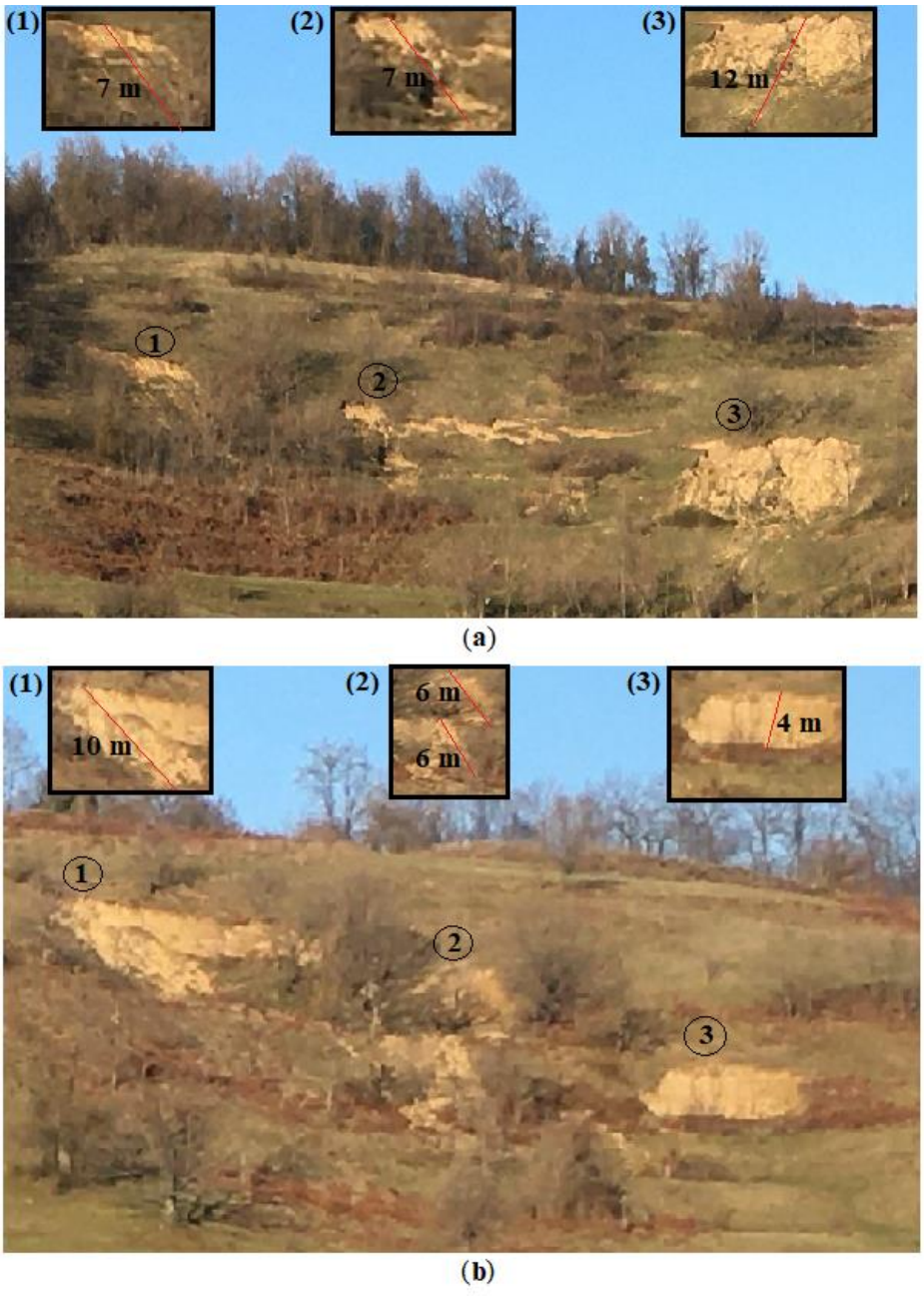

Figure 4.7. Some typical triggered shallow landslides view in the study area: (a-b) after November 2023 rainfall from field photographs.

4.1.1. Limitation of Landslide Inventory

Some situations may negatively impact the creation of the landslide inventory. Firstly, it is necessary to mention that prepared current landslide inventories by MTA/AFAD/ ARAS are not available for public. They can be examined from published existing reports (MTA online portal; İRAP Zonguldak, 2021; İRAP Bartın, 2022; Duman, Can and Emre, 2011). Furthermore, MTA offers researchers to see landslides up to 2005. In fact, although this landslide inventory map consists of many past landslides, it does not include all the past landslides during the years between 2005 and up to now. In addition, it is very difficult to detect some old landslides for especially forest region due to rapid growing of the trees. If the shallow landslide initiations are at small depths, the forest grows rapidly and causes the tracks to disappear (Andrewwinner and Chandrasekaran, 2021; Koshimizu and Uchida, 2023). Lack of high quality of satellite images, or aerial photographs are also main restriction of the preparation of detailed landslide inventory. Besides, although some of them can be detected in the field, it is critical to consider that their locations may be inaccessible because of the forest. Human effects are also not negligible with respect to landslide volume or deposition area. Finally, heavy rainfalls might impair the chance of finding a new clue in the field from past disasters.

4.2. Shallow Landslide Susceptibility Map

While researchers describe the number of studies about the runout analyses as rare in the literature, they are aware that such analyses might become more widespread day by day. Preparation of the landslide susceptibility map is suitable and basic way to acquire runout distance of shallow landslide in a runout assessment. There are many ways to prepare shallow landslides susceptibility maps. However, it should not be neglected that preparation of the landslide susceptibility mapping method changes over time due to rapidly improved technology such as artificial intelligence among scientific literature. Especially using machine learning in landslides susceptibility analyses has been increasingly preferred alternative in recent studies. Therefore, a Python machine learning with open-source codes library employed for this research during preparation of shallow landslides susceptibility maps. Logistic regression method also enables to study with strong forecast in several machine learning research, which are interested in preparation of shallow landslides susceptibility maps (Nefeslioglu and Gokceoglu, 2011; Kalantar et

al., 2018; Sevgen et al., 2019; Nhu et al., 2020; Xion et al., 2020; Crawford et al., 2021; Crawford et al., 2022; Dashbold, Bryson and Crawford, 2022; Nwazelibe, Unigwe and Egbueri, 2022; Qiu et al., 2022; Zhang et al., 2022a; Zydroń, Demczuk, and Gruchot, 2022; Gu et al., 2023; Song et al., 2023; Liu et al., 2024). Flow type of shallow landslide susceptibility mapping was prepared using logistic regression in the study of Polykretis and Chalkias (2018), Nhu et al. (2020) and Nwazelibe, Unigwe and Egbueri (2022). Since study area was chosen considering natural geological boundaries, the geological units throughout the Eocene flysch facies are the same. The study of Nwazelibe, Unigwe and Egbueri (2022), which shows similarity in terms of landslides occurred in the geological unit which is Eocene-aged Ameki-Bende formation, was successfully utilized machine learning logistic regression.

In carry out preparation of landslides susceptibility map, it is necessary to reckon with wide range of factors. First of all, The Shuttle Radar Topography Mission Digital Elevation Model (SRTM DEM) converted to a 25 x 25 m grid cell for following analyses: slope gradient and slope aspect, plan and profile curvature, convergence index, closed depressions, topographic wetness index (TWI), slope length factor, channel network base levels, channel network distance and valley depth (Table 3.3). Their coordinate systems are same as WGS 1984 UTM zone 36N. These parameters were obtained in SAGA GIS in order to evaluate the geomorphometric features of for separately each sub-basin in Eocene flysch facies. Land cover data which is obtained from Corine Land Cover (CLC 2018). Sentinel-2 imageries were used in Normalized Difference Vegetation Index (NDVI) analyses. Band 8 is used as Near Infrared Band (NIR), while band 4 is utilized as Red Band (Red) of the Sentinel-2 image in Equation 4.1.

$$NDVI = (NIR - Red) / (NIR+Red) \quad (4.1)$$

Geology is fixed and defined as Eocene flysch facies by Akbas et al. (2011) for each sub-basin. The prepared landslides inventory was also used in susceptibility analyses. Considering to rapid advances in machine learning, it will be expected to prepare more detailed susceptibility maps in order to be used in detailed runout analyses. It is necessary to remember that Table 3.3, which was shown in previous chapter, represents the predisposing factors of the shallow landslide susceptibility map.

Conforti and Ietto (2021) state that slope gradient, TWI, soil texture and lithology were acknowledged as being the most significant predisposing factors of the shallow landslide susceptibility mapping.

The selection of training and testing data has a significant impact on creating a successful shallow landslide susceptibility map (Pawluszek-Filipiak and Borkowski, 2020; Can, Kocaman and Gokceoglu; 2021; Ado et al., 2022). 80:20 ratio (Polykretis and Chalkias, 2018; Karakaş et al., 2020; Xie et al., 2021a; Xie et al., 2021b; Ghasemian et al., 2022 and Ling et al., 2022) and 70:30 ratio (Nam and Wang, 2020; Wang, Liu and Liu, 2020; Akinci, 2022; Zhang et al., 2022a; Zydroń, Demczuk, and Gruchot, 2022; Achu et al., 2023; Kaya-Topaçli, Ozcan and Gokceoglu, 2024) are frequently used for training and test data selection in the previous studies. For instance, 80:20 ratio manifests in previous researches that the dataset was also split into training (80%) and testing (20%) subsets (Polykretis and Chalkias, 2018; Karakaş et al., 2020; Xie et al., 2021a; Xie et al., 2021b; Ghasemian et al., 2022 and Ling et al., 2022). Aktas and San (2019) also attempted to develop a landslide susceptibility map using an automatic sampling algorithm by altering the ratio of the training and testing. Ado et al. (2022) also tried to find the best ratio by changing traning test ratio in the landslide susceptibility analyses.

The division of samples between training and testing sets was established at an 80:20 ratio in this study. The training and testing data were underwent using the 'the_train_test_split' and 'cross_val_score' functions from the scikit-learn, which is an open-source machine learning library for Python (Komu, Nefeslioglu and Gokceoglu, 2024). A a result, shallow landslide susceptibility maps were visualized using the ArcGIS 10.8.2 software in this study. They were separately crafted by using LR method for the sub-basins are given in Egerci (Figure 4.8), Beycuma (Figure 4.9) and Ihsanoglu (Figure 4.10). There are three classes in the shallow landslide susceptibility maps. (0-0.4) means that shallow landslide susceptibility is low (green color). Moderate (0.4-0.7) probability of shallow landslide susceptibility is represented with yellow color. Red color represents the high (0.7-1) probability of shallow landslide occurrences on the map.

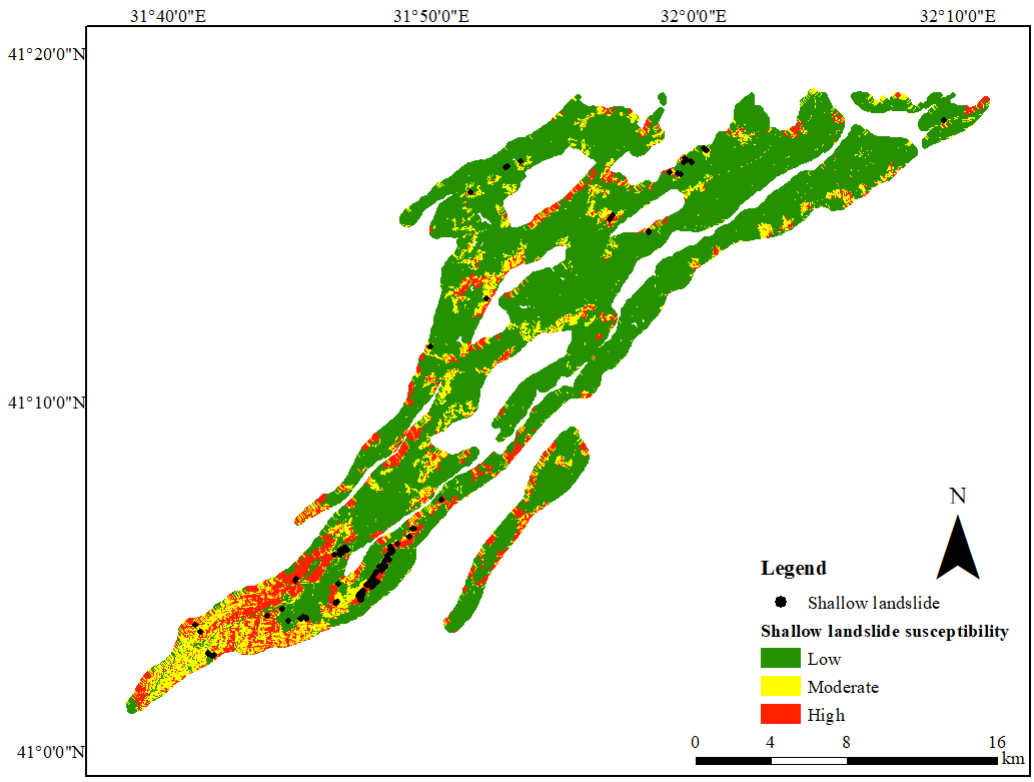

Figure 4.8. Landslide susceptibility maps produced by using LR for Egerci sub-basin.

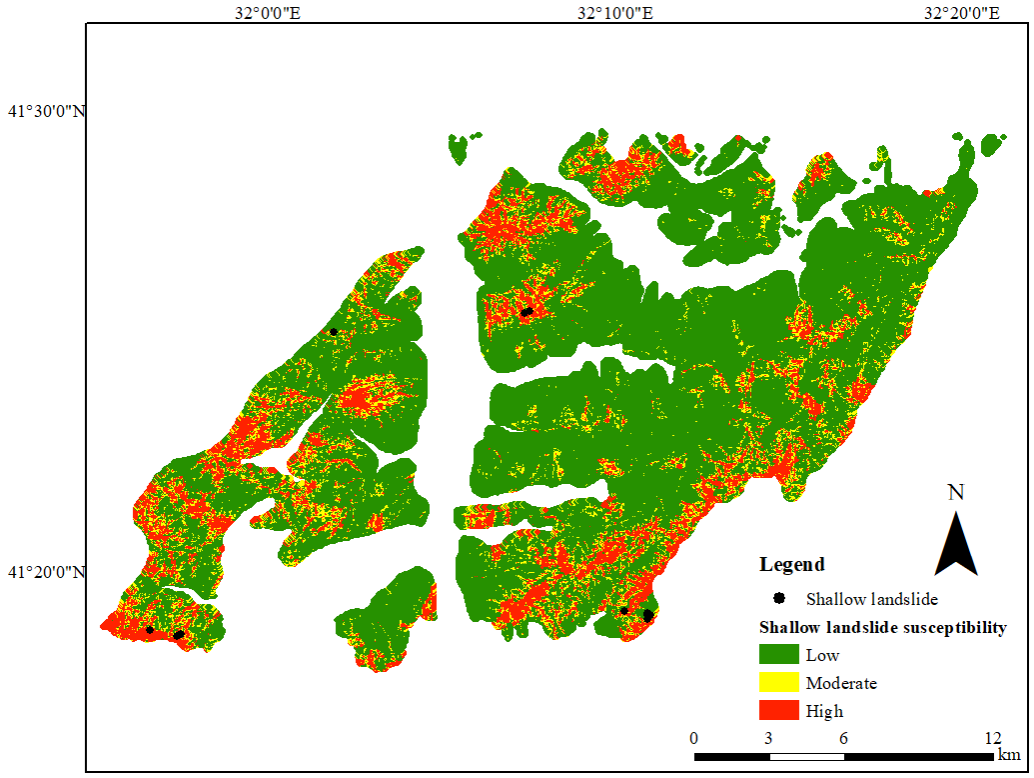

Figure 4.9. Landslide susceptibility maps produced by using LR for Beycuma sub-basin.

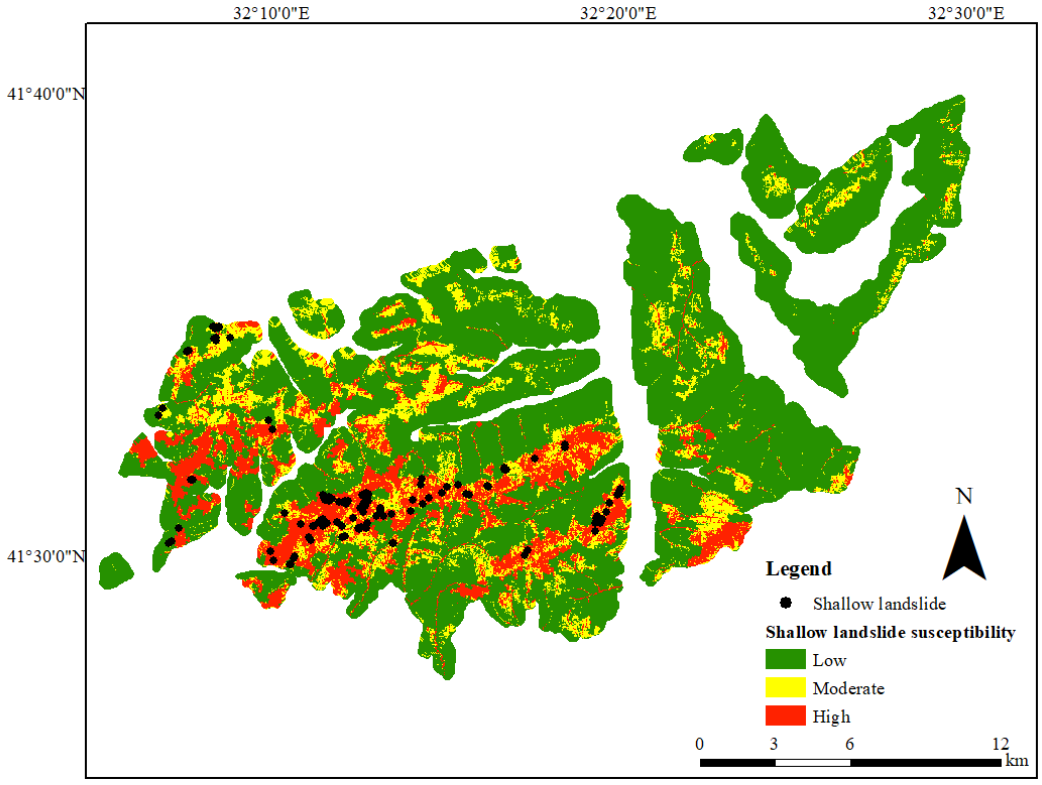

Figure 4.10. Landslide susceptibility maps produced by using LR for Ihsanoglu sub-basin.

5. RUNOUT ANALYSIS OF SHALLOW LANDSLIDES

The stages of the presented chapter are (i) introduce Flow-R software, (ii) demonstrate the measurement of runout distance of shallow landslide, (ii) perform back analyses for decision of peak velocity, (iii) examine the effects of changing travel angle for understanding of runout distance, (iv) interrogate DEM spatial resolution for the study area, and (v) probe of runout maps in terms of detecting shallow landslide initiations, evaluating propagation stage and exploring their results.

5.1. Flow-R software

Runout distances in Eocene flysch facies have not yet been subjected to scientific scrutiny in terms of using the empirical modelling up to now. Therefore, an empirical model was utilized by employing the Flow-R 1.0.0 software (Figure 5.1) in order to analyse the runout distances in Eocene flysch facies. It was carried out the review and execution of the Flow-R software algorithms within thesis organization.

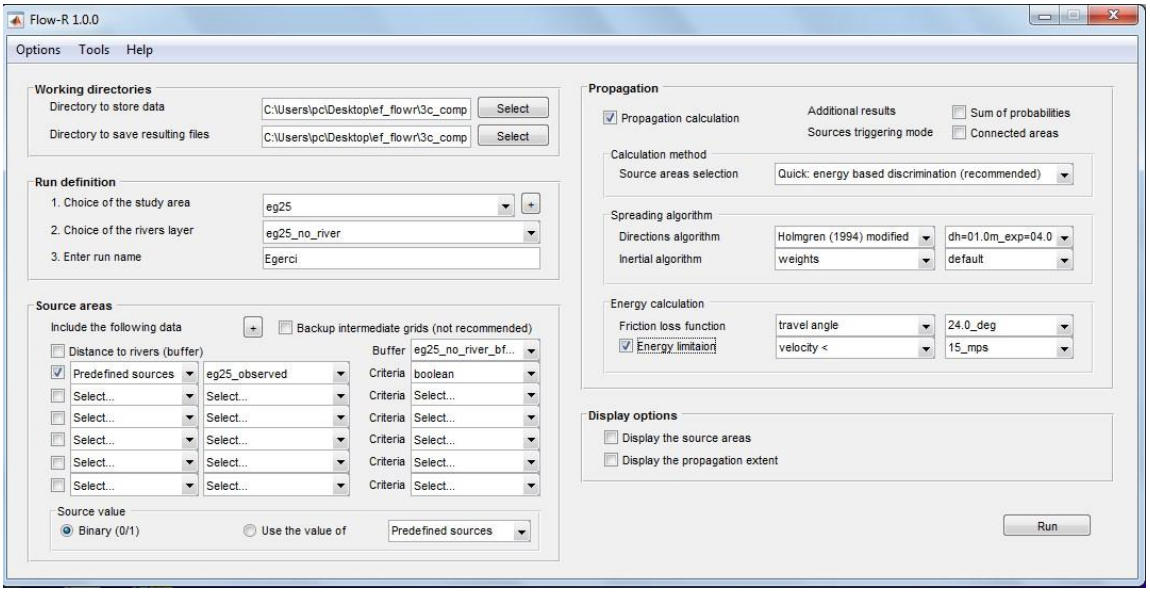

Figure 5.1. A glimpse of the Flow-R 1.0.0 software interface (Horton et al., 2013).

There are many important points that need to be considered by utilizing the Flow-R. First, data should be imported to ASCII format to Flow-R. The conversion to ASCII format was conducted using the ArcGIS software in this study. In the ASCII format, "−9999" gives the information about no data.

Second, it is necessary to arrange that prepared data set resolutions and their coordinate systems should be same. While the projection coordinate system was set to: 'WGS 1984 UTM Zone 36N', the spatial resolution was 25 m for all sub-basin. Therefore, all data for sub-basins should be converted into same coordinate system and spatial resolution.

Third, source area determination in software interface represents the shallow landslide initiations in this study. Although Flow-R enables to automatically detect possible failure initiations, it is possible to integrate the user defined failure initiations into Flow-R. It should be reminded that pre-defined failure initiations are significant for this study scope.

Finally, spreading algorithm and energy calculation are critical part of the propagation stage. Modified Holmgren flow direction algorithm and SFLM were chosen for runout distance modelling. Detailed parameter selections for each algorithm are crucial for accurate modelling in propagation stage. While "dh" and "x" parameters are used during Modified Holmgren flow direction, SFLM is based on travel angle. The parameter of "x" provides the opportunity to test about flow direction effects in the runout analyses. dh accounts for DEM roughness effects (Horton et al., 2013). It is critical to decide the correct reach or travel angle because determination of the suitable travel angle is also important to detect the landslide character. Checking the travel angles on the basin, it is hard to decide whether they will represent the real conditions of the study area. Flow-R 1.0.0 software interface enables to make some alterations within numerous parameters options immediately.

The previous Flow-R studies propagation parameters differences can also be diverged, as tabulated in Table 5.1. Table 5.1, summarizes the state of Flow-R parameters in previous studies, mainly aimed at showing the main trend of parameters. Travel angle (º), x, dh (m) and Vmax (m/s) have been presented for each research in the Table 5.1. While these

data provide a general idea for frequently preferred parameters, this research adheres to on-site analyses. Although it will be demonstrated in the following subsequent subsections, it is necessary to highlight that obtained parameters align with the parameters commonly used in the literature.

Table 5.1. Previous Flow-R studies with propogation parameters.

Authors	x	dh (m)	TA (°)	V (m/s)
Horton et al. (2013)	4	1	11;7	15
Park, Lee and Woo (2013)	4	-	13	28
Pastorello, Michelini and D'Agostino (2017)	0.7;20	1	10;11	20
Rahman, Ahmed and Di (2017)	-	-	15	15
McCoy (2019)	4	2	10	15
Sturzenegger et al. (2019)	1	2	5	15
Paudel (2019)	1 to 50	0.25 to 70	1 to 50	1 to 50
Do, Yin and Guo (2020)	1	1	5	5
Polat and Erik (2020)	6	1	-	-
Ali et al. (2021)	4	-	12	10
Bera, Melo and Guru (2021)	4	-	5	13
Charbel and El Hage Hassan (2021)	6	-	5	-
Giano, Pescatore and Siervo (2021)	1	1.5	-	8
Jiang et al. (2021)	-	-	9	25
Liu et al. (2022)	4	2	13	44
Putra et al. (2022)	50;4;20	1;4;1	2;2;5	15;36;40
Xu et al. (2022)	4	2	11	15
Sharma et al. (2023)	4	2	11	15

As seen from the Table 5.1, the parameter x is generally considered as 4 in the previous studies. In contrast to x, it is difficult to say that there is a dominant utilized value for dh. The frequency of the usage of values "1" and "2" for dh is almost the same. The values of "15" for maximum speed and "11" for travel angle are frequently preferred in past studies (Table 5.1). It is note that the model parameters used in previous studies will be re-evaluated by comparing them with the parameters determined for this study in the subsequent impending sections.

5.2. How to Measure of Runout Distances?

Google Earth images and model results enable to measure and compare the runout distances. While Figure 5.2a is obtained from Google Earth images, Figure 5.2b is the representation of the modelling of landslide in the Flow-R. Figure 5.2c also represents an example measurement of the runout distance of shallow landslide. The shallow landslide runout was also measured as 190 meters in Figure 5.2a, whereas Figure 5.2c indicates that same landslide runout distance was calculated as 195 meters in the Flow-R model. Therefore, measurement data show that model results are suitable to original data. The maximum distance probability has been symbolised using a two interval colours, in which the pink colours represent those with the low probability of runout extent, whereas the cherry red colours are the high probability of runout extent. While low probable cells (0 - 0.5) mean the maximum distance probability lower than 50%, cherry red colour cells (0.5 - 1) accounts for the maximum distance probability higher than 50%.

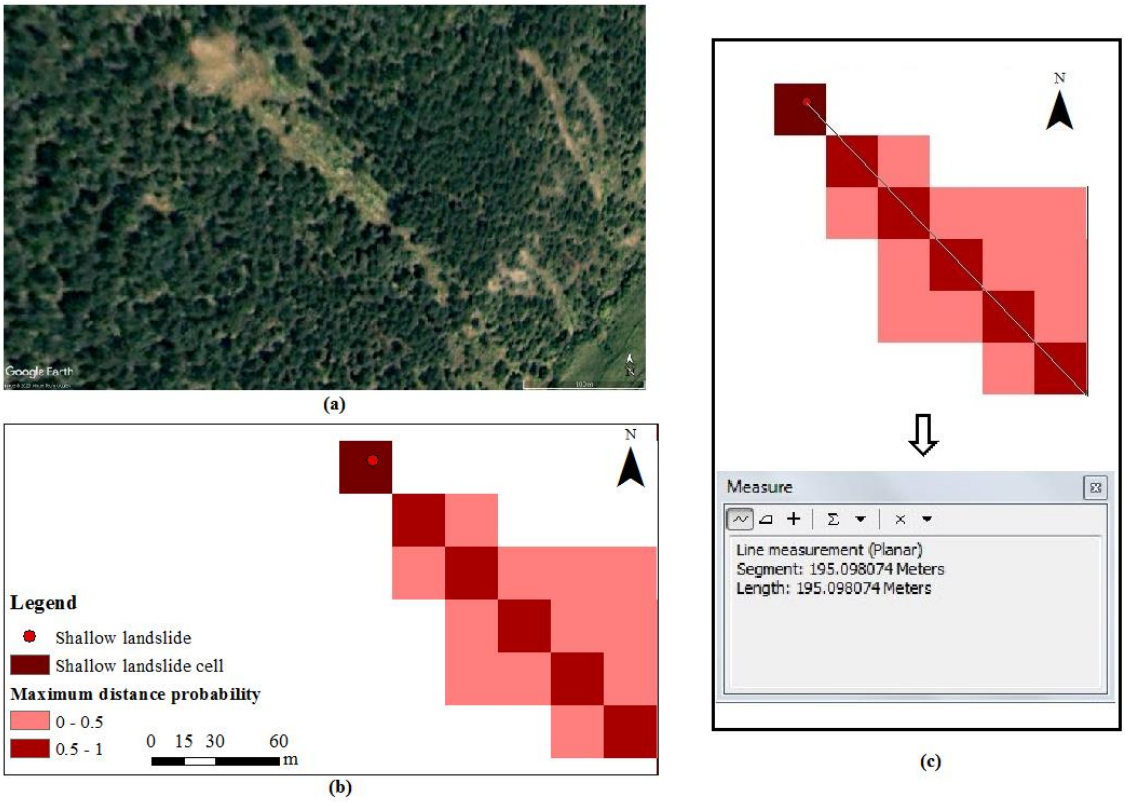

Figure 5.2. Illustration of the runout distance measurement.

5.3. Decision of Velocity Using Back Analyses

Due to the effect of velocity on runout distances, back analysis should be scrupulously completed. A back-analysis was performed by considering actual landslides to predict the parameter velocity in this study. To obtain the more detailed information of the landslide maximum velocity limit in the study area, the shallow landslides that occurred in May 1998 were used for testing of the potential exhaustive runout distances. Figure 5.3 represents an illustration of runout distances for v = 1 m/s, v = 5 m/s, v = 10 m/s, v = 15 m/s and v = 16 m/s. While Figure 5.3a shows the field appearance of the modeled landslide, the same landslide has been modeled using different velocity values to show and compare the extent of propagation in Figure 5.3b, 5.3c, 5.3d, 5.3e, and 5.3f. Relation between shallow landslide modeled runout distance in Flow-R and max velocity proved accurately with R^2 of 0.91 (Figure 5.4).

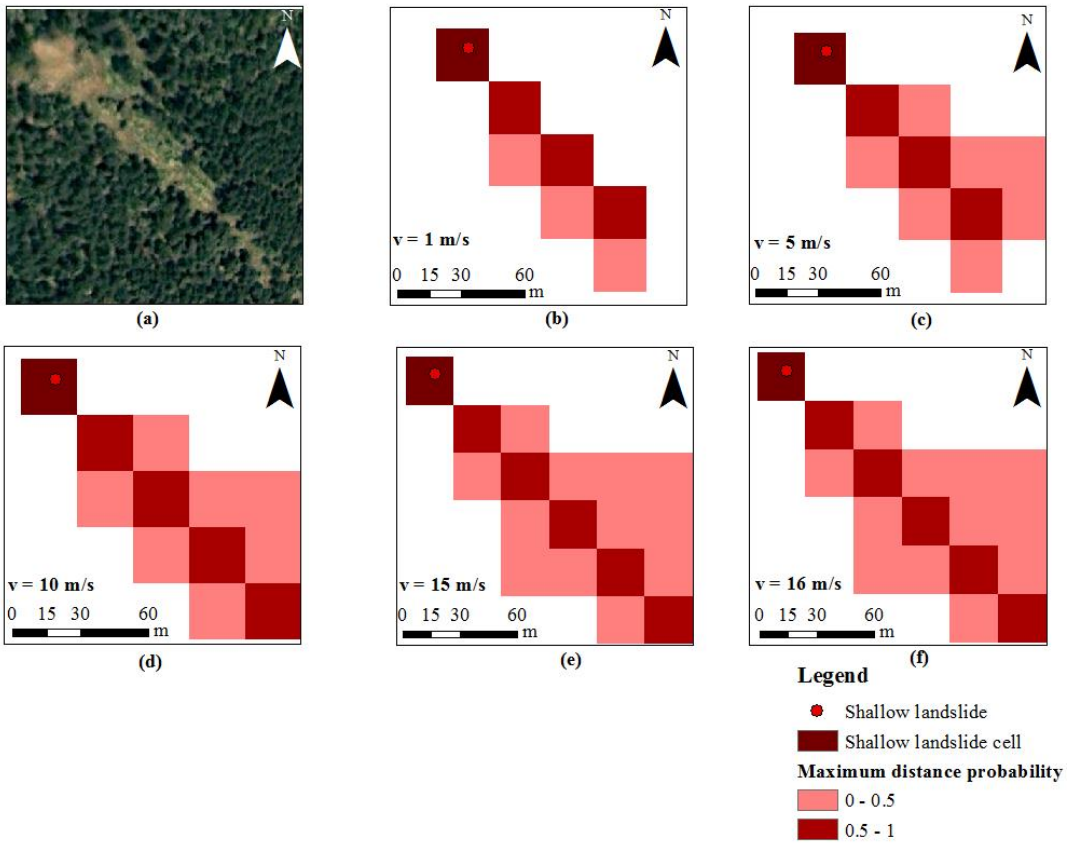

Figure 5.3. Illustration of runout distances by modifying velocity.

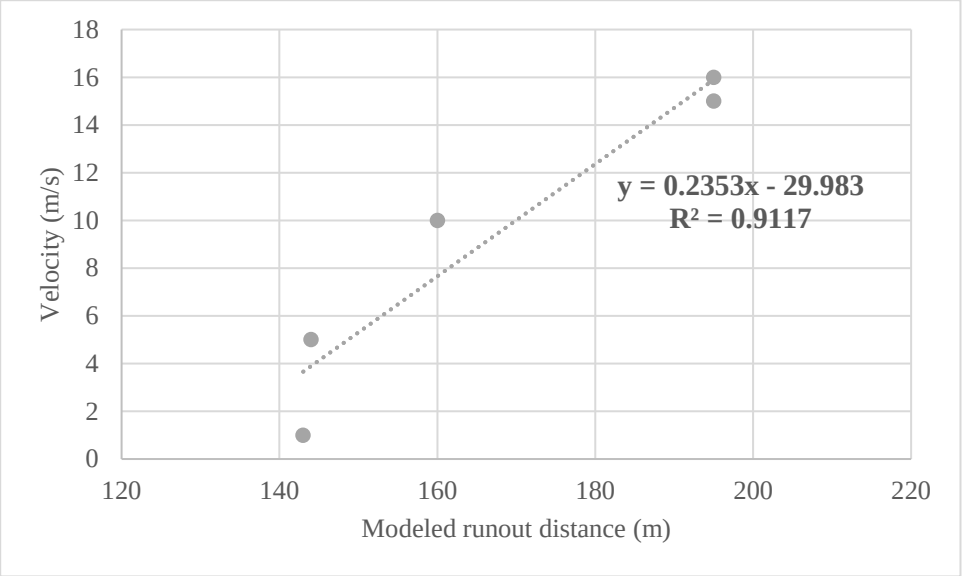

Figure 5.4. Cross correlations of modeled runout distance and velocity.

The observed real runout distance is measured as 190 meters. When Figure 5.4. equation is used in order to find model v (m/s), V=15 m/s will be found ideal Vmax for analyses.

Based on the observations of the residents regarding disasters such as landslides that occurred in May 1998 in the area, it was determined that a velocity parameter of 15 m/s could be considered suitable for the shallow landslides in the Eocene flysch facies.

The examples used for the shallow landslide velocity parameter in the literature have also been examined. Literature reviews dwell on that the shallow landslide exhibits a velocity profile spanning from 0 m/s to 21 m/s (Marinelli et al., 2022). Velocity peak data is marked as approximately 19 m/s for shallow landslides in the study of Marinelli et al. (2022). The study of Prochaska et al. (2008) observed debris flow velocities ranging from 5 to 15 m/s. 8.4 m/s was also detected as the maximum velocity of the shallow landslides in the study of Vegliante et al. (2024). Gokceoglu et al. (2005) observed the velocity of the rapid landslides as 6 m/s in their study area. The speed was observed as 17.5 due to the sandy gravel being subjected to more friction in the study of Yang et al. (2019).

5.4. Decision of Travel Angle Effects on Results

Travel angle is an important parameter of impacting on runout results. Therefore, effects of altering the travel angle were investigated to account for the process and the factor of influencing it. A smaller travel angle is associated with a more extensive runout distance. If the travel angle is determined as smaller than 27 degrees, rainfall-triggered landslides tend to demonstrates a relatively high degree of mobility (Panday and Dong, 2021). In this study, an evaluation was aimed to be made over selected travel angles in order to better understand the effect of travel angle. To illustrate, two specific travel angles, which are 24º (Figure 5.5a) and 11º (Figure 5.5b) are independently identified and measured the probable runout distances on the hazard of shallow landslides. Figure 5.5 shows that if travel angle increases, runout distances will reduce. It is note that while model results are obtaining, other parameters are same except for travel angle. Consequently, travel angle and runout distance are inversely proportional to each other that when the travel angle decrease, the runout distance increases (Zhao, Aman and Kowalski, 2021).

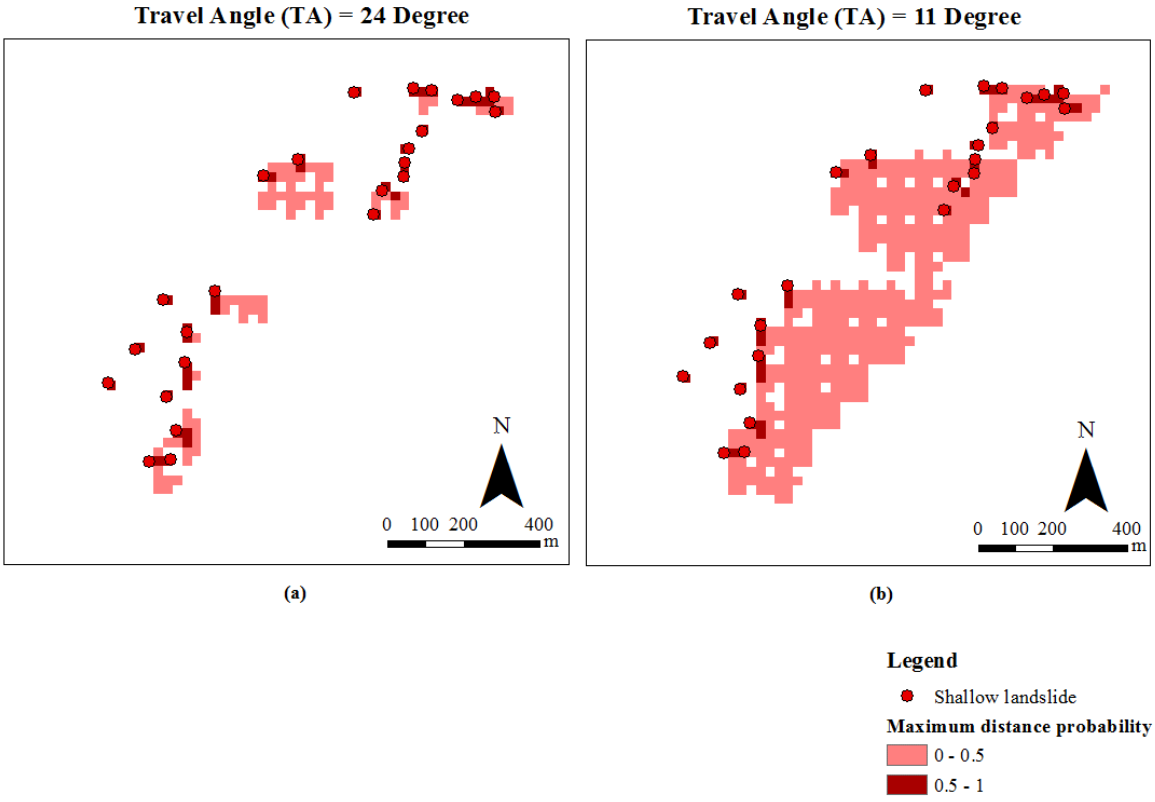

Figure 5.5. Travel angle effects on runout distances.

5.5. DEM Effects on Runout Distances

Analyses results show that the resolution is also critical for runout analyses. For an accurate representation of the shallow landslide runout distance, the correct spatial resolution needs to be employed. It was decided that 25 m spatial resolution can be used in the analyses. At this stage of the dissertation, question mark about whether 25 m spatial resolution is appropriate or not will be elaborated. A sample analysis has been completed for a landslide identified in the study area with resolutions of 25 m and 10 m by using Flow-R 1.0.0 (Figure 5.6).

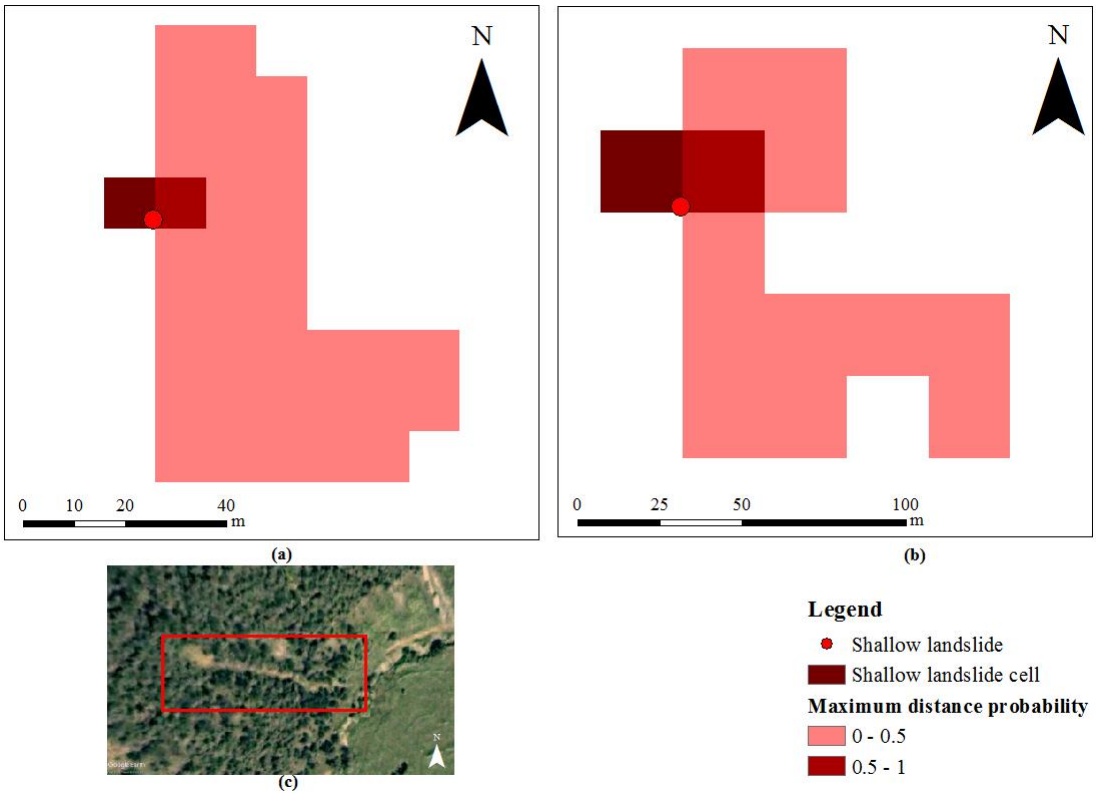

Figure 5.6. Comparison of runout distance models with 10 m and 25 m DEM: (a) 10 m DEM (b) 25 m DEM (c) field view of shallow landslide.

In this case, it is necessary to remember that the aim was to make predictions for as wide areas to the fullest extent possible. Analyses for the prepared landslide prepared inventory were applied by classifying the basin with respect to 3 classes in order to check suitability of 25 m spatial resolution. When prepared inventory mean and median observed runout distances are analysed for Eocene flysh facies, they are 45 and 31 (m). It might be also

grasped that mean observed runout distances values of all three sub-basins are also greater than or equal to 25 m (Table 4.1). Therefore, it is possible to study with 25 m resolution DEM for runout analyses. Nevertheless, Flow-R might not start a flow if runout results are less than 20 meters. Therefore, it was proved that runout results may be affected by resolution. Furthermore, it was intriguing that it is also possible to detect runout distance such as less than 20 meters, if the flow is started to observation for another landslide.

The runout distance models in Figure 5.6 clearly illustrate that if DEM effects are analysed by using a spatial distribution of 10 m and 25 m resolution, landslide runout distance results will be affected as expressed by the original developer of the software Horton et al. (2013). Therefore, it is clear that a 10 m spatial resolution provides a more detailed evaluation in terms of possible runout distance in this study. However, determining possible shallow landslide initiations is crucial in this research as emphasized in earlier sections of the dissertation. Shallow landslide initiations are described as source area in the software interface. If source area has more cells, Flow- R may not work for 10 m resolution. Therefore, analyses have also been conducted for randomly selected landslides in smaller areas. Although presented landslides were randomly selected in the same sub-basin, it is necessarily emphasized that that their locations are very close to each other. Table 5.2 and Table 5.3 compare the randomly selected landslides with respect to observed runout distances in the field and modelled by 10 m and 25 m spatial resolutions. In addition, the cross relationships between 10 m and 25 m spatial resolutions are a prominent part of predicting the power of the models. Therefore, Figure 5.7 and Figure 5.8 employed to give information about the cross-corelation of observed and modelled runout distances for randomly selected shallow landslides at 10 m and 25 m resolutions in the same sub-basin. While Figure 5.7 had R^2 greater than 0.77 and 0.60 for 10 m and 25 m spatial resolutions, respectively. 0.80 and 0.71 are R-squared values on graphs at 10 m and 25 m spatial resolutions in Figure 5.8. It has been concluded that data with a 10 m spatial resolution makes more successful predictions. However, it can be said that the results at a 25 m resolution are also successful with respect to Figure 5.7 and Figure 5.8.

Table 5.2. Comparison of observed and modelled runout distances for randomly selected shallow landslides at 10 m and 25 m resolutions in the Egerci sub-basin.

Shallow Landslide ID	Observed runout distance (m)	10 m resolution	25 m resolution
1	90	70	110
7	111	104	191
12	75	45	61
22	70	35	50
30	11	20	40
175	24	23	43
178	28	31	51
180	23	32	85
182	35	36	57
183	94	113	100
200	31	31	27
204	49	41	45
213	25	33	30
223	33	36	40

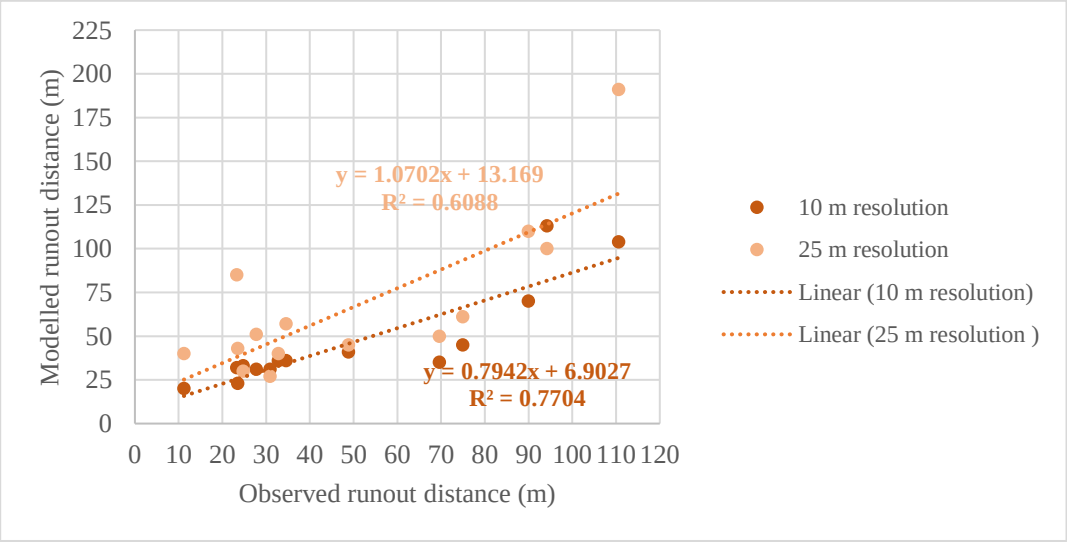

Figure 5.7. Comparison of observed and modelled runout distances for randomly selected shallow landslides at 10 m and 25 m resolutions in the Egerci sub-basin.

Table 5.3. Comparison of observed and modelled runout distances for randomly selected shallow landslides at 10 m and 25 m resolutions in the Ihsanoglu sub-basin.

Shallow Landslide	Observed runout distance (m)	10 m resolution	25 m resolution
142	136	180	175
143	18	55	50
144	7	50	85
145	16	82	85
251	31	35	46
252	55	58	63
225	11	33	35
261	10	24	25
262	9	20	25
241	8	5	10
246	13	15	25

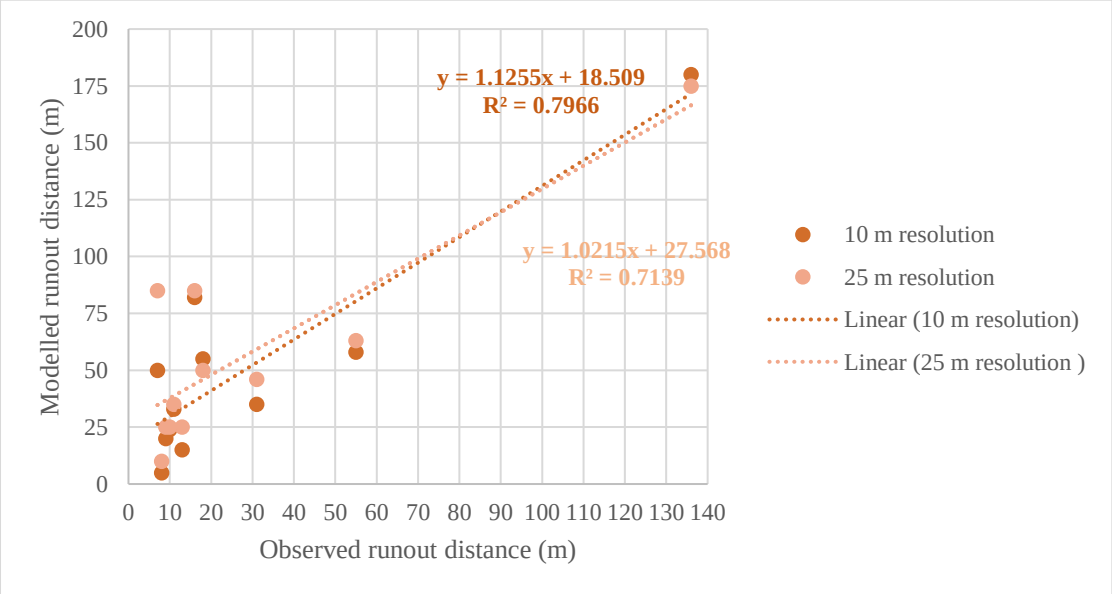

Figure 5.8. Comparison of observed and modelled runout distances for randomly selected shallow landslides at 10 m and 25 m resolutions in the Ihsanoglu sub-basin.

5.6. Probable Landslides Runout Distance Assessment

The movement of shallow landslide mass from its shallow landslide initiation points to deposition area with affected by slope geometry and amount of mass characterizes the propagation stage (Cuomo, 2020). First, the accurate determination of shallow landslide initiations will be the premise for ensuring accurate runout distance assessment for sub-basins in this study scope. Second, parameters, which depended on exhaustive analyses and researches for previous shallow landslides in the sub-basins, will be set to accurately model of the propagation stage. Finally, presented maximum probable runout distance results will be a prime issue in the upcoming potential shallow landslides dangers to refrain from negatives in sub-basins.

5.6.1. Shallow Landslides Initiations Detection

It is not possible to neglect that if shallow landslides runout distance cannot be estimated, shallow landslides may increasingly start to pose a big problem. Therefore, some critical strategies have become applied in order to estimate the runout distance of shallow landslides. For instance, the preparation of susceptibility map gives the runout analyses a quite valuable boost in terms of deciding shallow landslides initiations. Can et al. (2005) and Xu et al. (2022) note that if the study area is highly susceptible to shallow landslides, possibility of shallow landslides initiations has high in these areas. For example, shallow landslides, which occurred in May 1998 because of extreme precipitation event, are prevalently visible in high susceptible areas in Eocene flysch facies (Can et al., 2005). Taking into account the information in the previous sentences, is possible to say that the most basic way to interaction between shallow landslides initiations and their runout distance is to attain competence in preparation of landslide susceptibility map to perform runout analyses. Thus, determination of the susceptibility threshold has more important role in this study in order to detect high susceptible areas. In fact, this stage can be acknowledged as a critical step to detect an initial point for the suitable assessment of shallow landslides occurrence in terms of being capable to determine a cell by taking in account of many parameters. Separately prepared frequency histograms of the shallow landslide susceptibility values for three sub-basins give opportunity to decide on threshold value (Figure 5.9). The black arrows indicate the susceptibility value to be considered for determining the critical threshold value for sub-basins in the Figure 5.9.

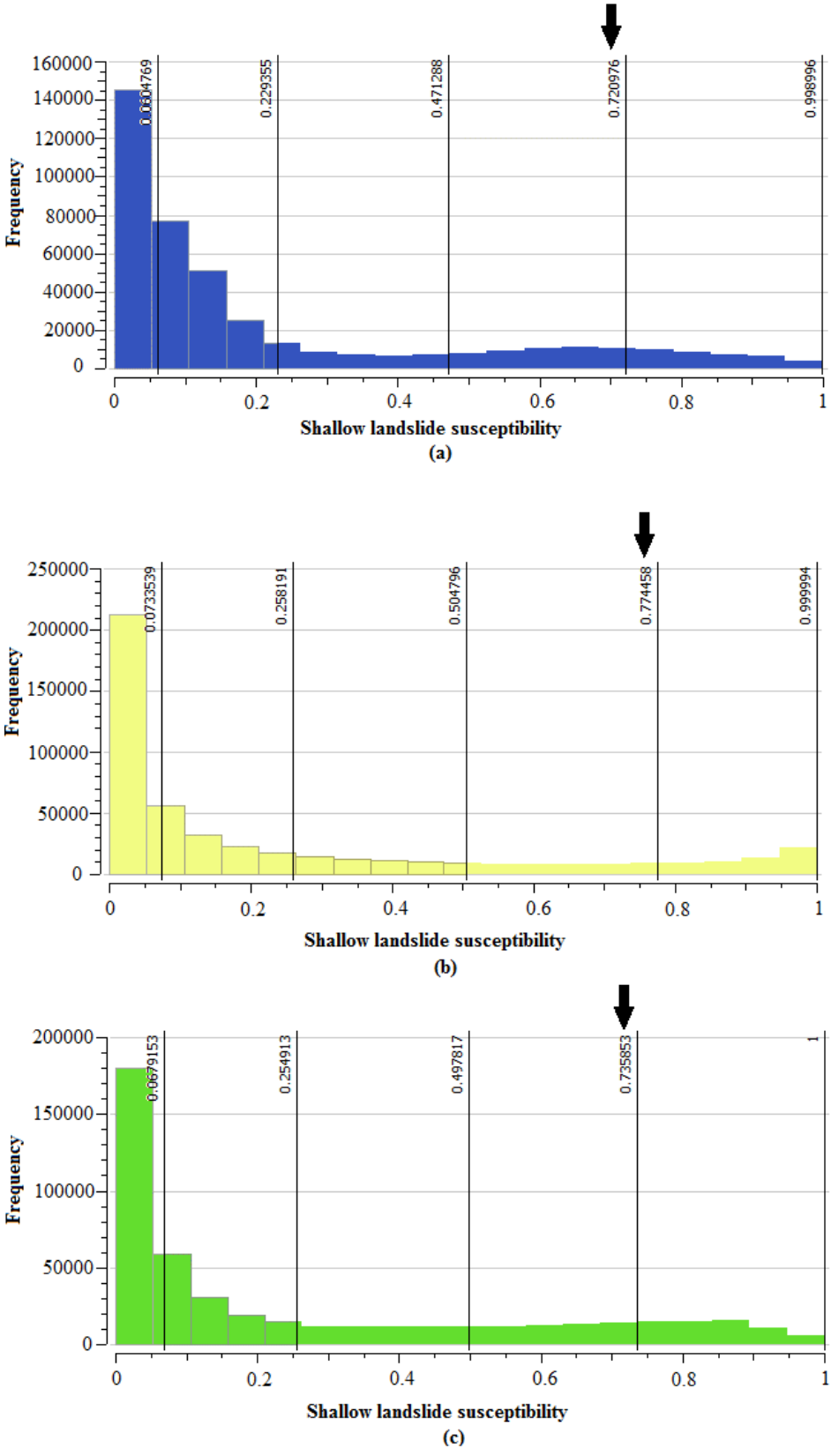

Figure 5.9. Threshold selection for initiating shallow landslides in sub-basins: (a) Egerci sub-basin, (b) Beycuma sub-basin, and (c) Ihsanoglu sub-basin.

It is wise to err on the side of caution by choosing threshold as 0.70 in terms of not neglect to any potential shallow landslide's initiations. It should not be forgetten that this value is as an important assumption to be used in the runout modeling process. Thus, it is supposed that if shallow landslides susceptibility grid cells are equal or higher than 0.70, they are selected as shallow landslides initiations. Mapped shallow landslides are also considered as pre-defined shallow landslide initiations in this study. Table 5.4 gives information about shallow landslide initiations statistic in terms of their altitude and slope gradient values in three sub-basins. Statistics on the distributions of detected possible shallow landslides initiations at different altitudes demonstrate that if shallow landslides possible initiations are analysed in terms of their median altitude values, shallow landslides occurrences possibilities altitudes have been observed at 607 m, 250 m and 154 m for Egerci, Beycuma and Ihsanoglu sub-basins, respectively (Table 5.4). In addition, when examining the median slope gradient values, the possibilities of shallow landslide occurrences have been observed at 23º, 15º and 13º for the Egerci, Beycuma, and Ihsanoglu sub-basins, respectively.

Table 5.4. Shallow landslide initiations statistic in terms of their altitude and slope gradient values.

Sub-basin	**Statistics**	**Altitude (m)**	**Slope Gradient (˚)**
Egerci	Mean	641	23
	Median	607	23
Beycuma	Mean	254	16
	Median	250	15
Ihsanoglu	Mean	164	14
	Median	154	13

It is noticeable that literature reviews indicate that debris flows usually occur in areas characterized by a slope gradient exceeding 15° (Takahashi, 1981; Rickenmann and Zimmermann, 1993). 15° was also used as a threshold of debris flow scarps (Jiang et al., 2021; Sharma et al., 2023). The slope gradient values range of (17°–38°) generally represent the rainfall-triggered landslides (Panday and Dong, 2021). Not only may slope gradient be equal to or less than 40º but also equal to or more than 15º (McCoy, 2019). The slope gradient is between 20.1º and 30º is detected for shallow landslides initiations

in the analysis of Dias, Dias and Grohmann (2023). The many of shallow landslides initiated on slope gradients with 20.1º –40º (Dias and Grohmann, 2024). As the types of the shallow landslide's initiations are slightly diverse in terms of their land use, it is possible classify them. CLC (2018) data indicate that these detected initiations are observed in broad-leaved forests for three sub-basins. The pie charts elucidate the proportion of shallow landslides initiations land cover types (Figure 5.10). The highest amounts of shallow landslides initiations have been observed by broad-leaved forest for Beycuma and Ihsanoglu sub-basins, which accounted for 55% and 62%, respectively. Conversely, mixed forest cover has highest proportion about 47% of shallow landslides initiations in Egerci sub-basin, followed by broad-leaved forest at 31%.

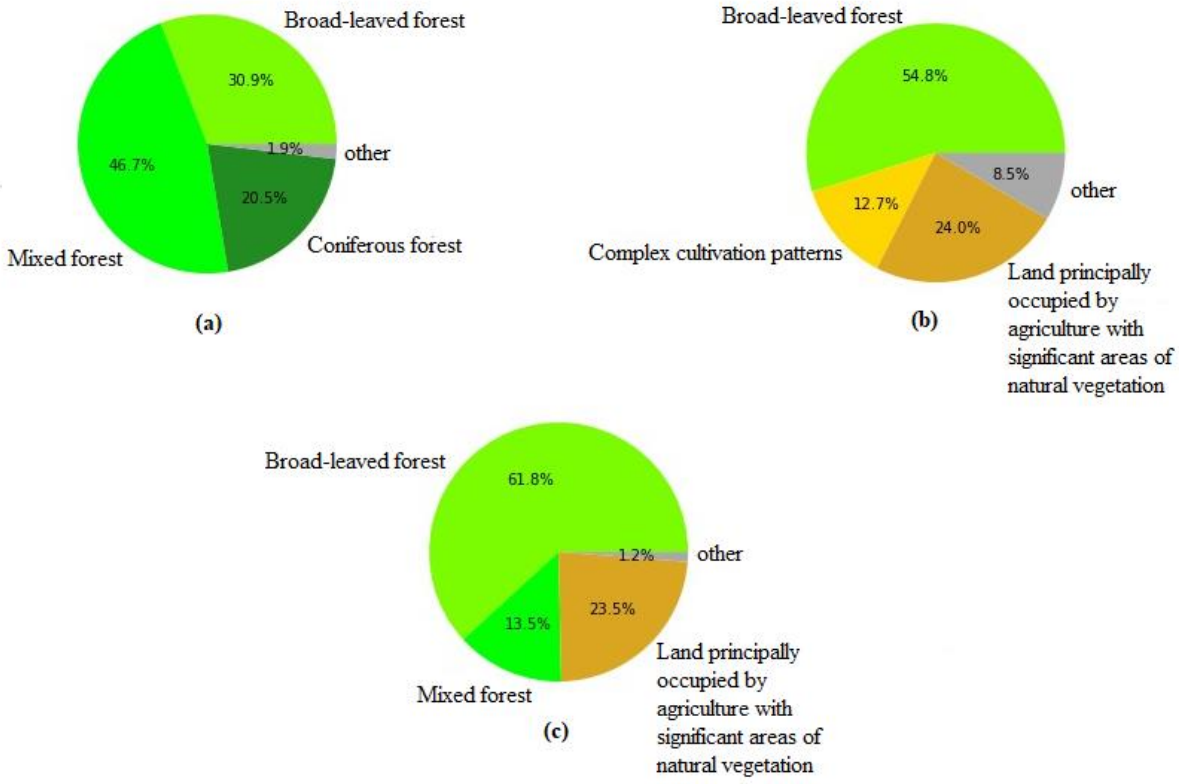

Figure 5.10. Shallow landslide initiations distributions in terms of land use: (a) Egerci sub-basin, (b) Beycuma sub-basin, and (c) Ihsanoglu sub-basin.

Landslide scarps are observable in coniferous forest and broad-leaved forest (Jiang et al., 2023; Nishioka et al., 2023; Takaoka, 2023). Shallow landslides are mainly triggered in mixed forest and broad-leaved forest (Roccati et al., 2021). It is obvious that shallow

landslides initiations are profuse in broad-leaved forest for three sub-basins (Figure 5.10) in this study. Coniferous forests might not lessen the threat of the landslides (Zhang et al., 2022b). Therefore, it is not surprise that shallow landslides initiations probability is about 21% in coniferous forest (Figure 5.10a).

5.6.2. Propagation

Although parameter selections may be complicated process, selecting the accurate parameters and professionally interpreting their results will be a crucial in terms of future further investigations. Flow-R aims to increase the reliability of analyses by providing a wide range of the parameter selection options. Therefore, models can be painstakingly adjusted to better fit a specific landslide type such as shallow landslides and debris flow in order to represent accurately their runout distances in Eocene flysch facies' sub-basins. Intending it to resemble real event conditions more closely. Uncertainty about the flow type of landslides whether they are debris flow or shallow landslide leads to using different parameters when performed to within the two configurations in this study. Therefore, runout distances have been computed for shallow landslides and debris flow parameters, separately. x, dh and TA and velocity values assigned to each sub-basin employed in debris flow and shallow landslides runout distance assessment is given Table 5.5.

Table 5.5. The model parameters utilized in Flow-R in this study.

Sub-basin	Landslide	Flow direction algorithm	x	dh (m)	TA (°)	Velocity (m/s)
Egerci	Debris flow	Modified Holmgren	4	1	24	15
	Shallow landslides	Modified Holmgren	25	1	24	15
Beycuma	Debris flow	Modified Holmgren	4	1	13	15
	Shallow landslides	Modified Holmgren	25	1	13	15
Ihsanoglu	Debris flow	Modified Holmgren	4	1	10	15
	Shallow landslides	Modified Holmgren	25	1	10	15

Horton et al. (2021) propose that x can be used as 4 for debris flow, whereas it can be selected as 22 to 26 for shallow landslides. In the study of Park, Lee and Woo (2013), McCoy (2019), Ali et al. (2021) and Jiang et al. (2021), x was utilized as 4 for debris flow. dh was widely preferred as 1 in several studies (Do, Yin and Guo, 2020; Giano, Pescatore and Siervo, 2021; Putra et al., 2022). dh can be commonly used as 1 for both shallow landslides and runout simulation analyses (Horton, Oppikofer and Michoud, 2021) because its decision is not depended on landslide type. Travel angle changes between sub-basins. It also allows to see how to vary slope gradient in the Eocene flysch facies. For this study, the preferred angles are as follows: TA: 24º for Egerci sub-basin, TA: 13º for Beycuma sub-basin, and TA:10º for Ihsanoglu sub-basin. Frequently preferred travel angles in the other studies were as follows: 4° (Kritos and Davies, 2015; Marchesini et al., 2024), 5° (Lari et al., 2011; Sturzenegger et al., 2019; Do, Yin and Guo, 2020), 7° (Prochaska et al., 2008; Horton et al., 2013), 9° (Jiang et al., 2021), 10° (McCoy, 2019), 11° (Rickenmann and Zimmermann, 1993; Huggel et al., 2002; Horton et al., 2013; Park, Lee and Woo, 2013; Pradhan et al., 2017), 12° (Ali et al., 2021), 13° (Park, Lee and Woo, 2013), 13.02º (Pradhan, 2021), 22° (Perzl et al., 2017) and 30° (Marchesini et al., 2024). The value chosen for Vmax (m/s) is 15. In addition, 5 m/s (Do, Yin and Guo, 2020), 10 m/s (Ali et al., 2021), 15 m/s (Horton et al., 2013; McCoy, 2019; Horton et al., 2021; McParland et al., 2021; Xu et al., 2022), 16 m/s (Nie, Lie and Xu., 2022), 20 m/s (Pastorello, Michelini and D'Agostino, 2017), and 25 m/s (Jiang et al., 2021) were used in the studies for Vmax.

5.6.3. Results

This analysis aims to estimate possible landslides runout distances based on the potential failure initiations that leads to propagation. Two runout models, which were fostered by using different parameter configuration such as shallow landslides and debris flow, were built with Flow-R 1.0.0 to compare their runout results. Flow-R is a distributed empirical modelling program offering propagation stages to analyse runout distances for both parameters' configurations. Therefore, whether parameter selection with respect to shallow landslides and debris flow can provide difference or not in this section will be discussed. Despite completing runout distances assignments by using different dh and x parameters for both of them, the resulting runout distributions are consistent each other.

The distributions in runout distance results models which are prepared by debris flow parameters and shallow landslide parameters are generally similar. Rather than use the fixed determined one parameter for the landslides occurs in the study area, considering both parameter configurations in runout modelling gives an opinion of runout distance patterns based on how shallow landslides and debris flow parameters affect to runout distance.

It should be remembered that possible failure initiations were well described in the earlier section. Pink colour shows the low probable cells (0-0.5), which indicate the maximum distance probability lower than 50%. Unlike pink cells, cherry red colour cells (0.5-1) denote the maximum distance probability higher than 50%. The simulated shallow landslide maximum probability areas cover smaller area than maximum debris flows probability areas.

Figure 5.11 and 5.12 aim to show quick examination of spatial impact of the probability of the maximum runout distances in three sub-basins for both parameters configurations. Detailed and larger views have also been provided separately in the impending figures.

Results indicate that models obtained by using both parameters configuration have the capacity to cover extensive distances, exhibiting max velocity at 15 m/s. Simulated runout distances by debris flow parameters are bigger than simulated runout distances by shallow landslides parameters at noticing small changes in results displayed in Figure 5.11 and 5.12. According to both model configurations, it can be inferred from that Figure 5.11 and 5.12 the possible damages of shallow landslides are discernibly concentrated in specific regions within the sub-basin.

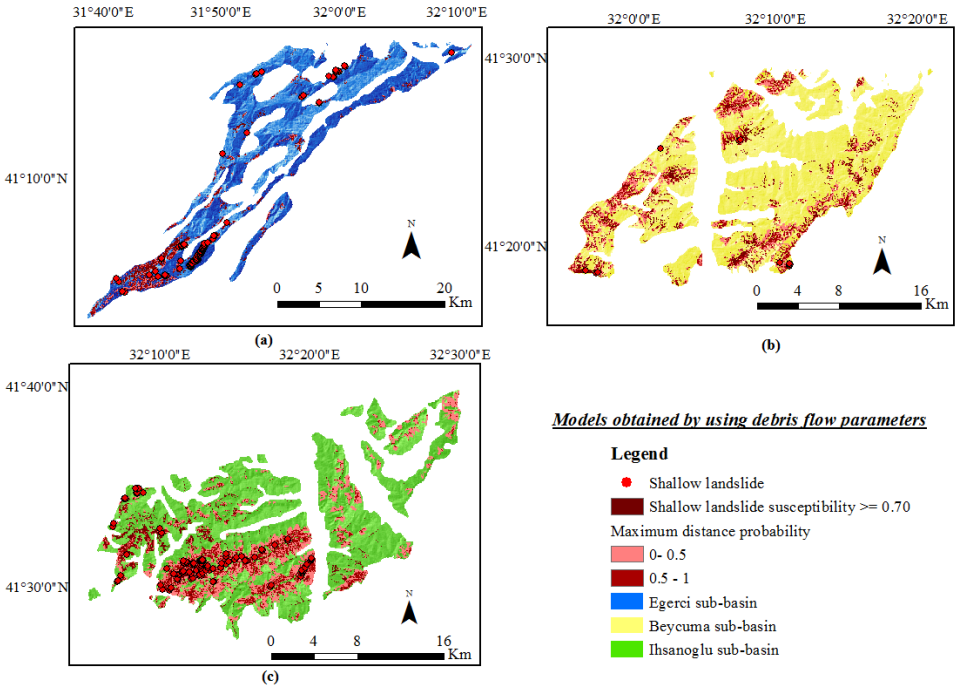

Figure 5.11. Probable maximum runout distance models by using debris flow parameters: (a) Egerci sub-basin, (b) Beycuma sub-basin and (c) Ihsanoglu sub-basin.

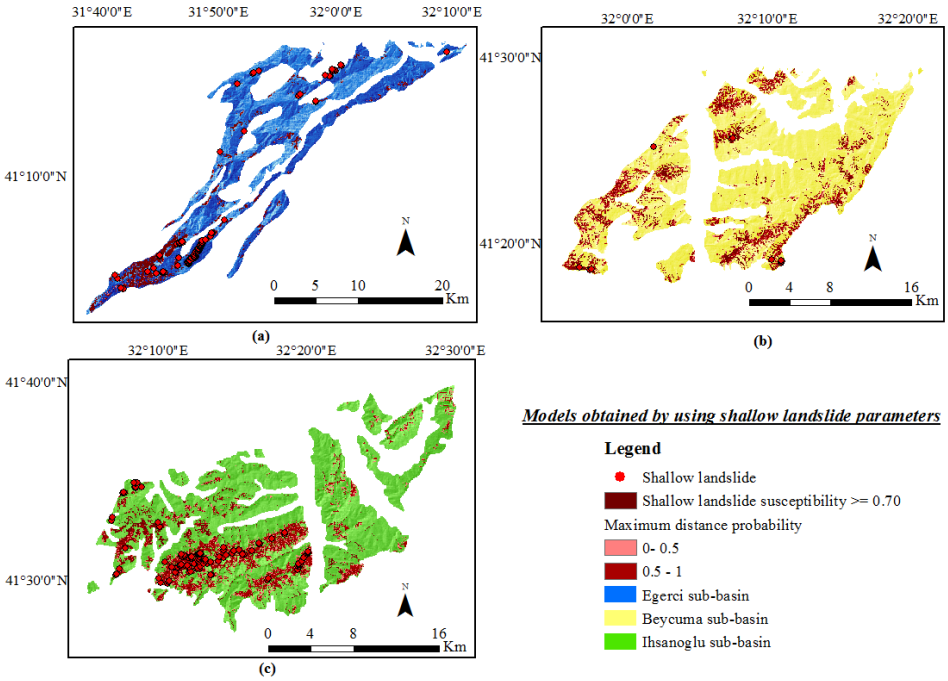

Figure 5.12. Probable maximum runout distance models by using shallow landslide parameters: (a) Egerci sub-basin, (b) Beycuma sub-basin and (c) Ihsanoglu sub-basin.

The performance of the empirical model on runout distances has been tested by considering the observed runout distances values. Runout models which were prepared by debris flow parameters and shallow landslide parameters exhibit approximately same performance. If runout distance models are prepared by using debris flow parameters for Egerci sub-basin, Beycuma sub-basin and Ihsanoglu sub-basin, coefficient of determination level is 0.61, 0.49 and 0.79, respectively (Figure 5.13).

Nevertheless, if the runout distance model is prepared by using shallow landslide parameters for Egerci sub-basin, Beycuma sub-basin and Ihsanoglu sub-basin, coefficient of determination levels is 0.59, 0.53 and 0.70, respectively (Figure 5.13).

In addition, if the assessment of runout distances is considered in terms of both model parameters in general view of Eocene flysch facies, both models yield similar coefficient of determination levels, 0.64 and 0.62. Coefficient of determination level attests to the similarity between both parametrization in the study.

Potential runout distances of debris flows or shallow landslides from possible shallow landslides initiations have been investigated in Figure 5.14, 5.15, 5.16, 5.17, 5.18 and 5.19. These figures have been prepared for a clearer examination of the sub-basins depicted in Figure 5.11 and Figure 5.12.

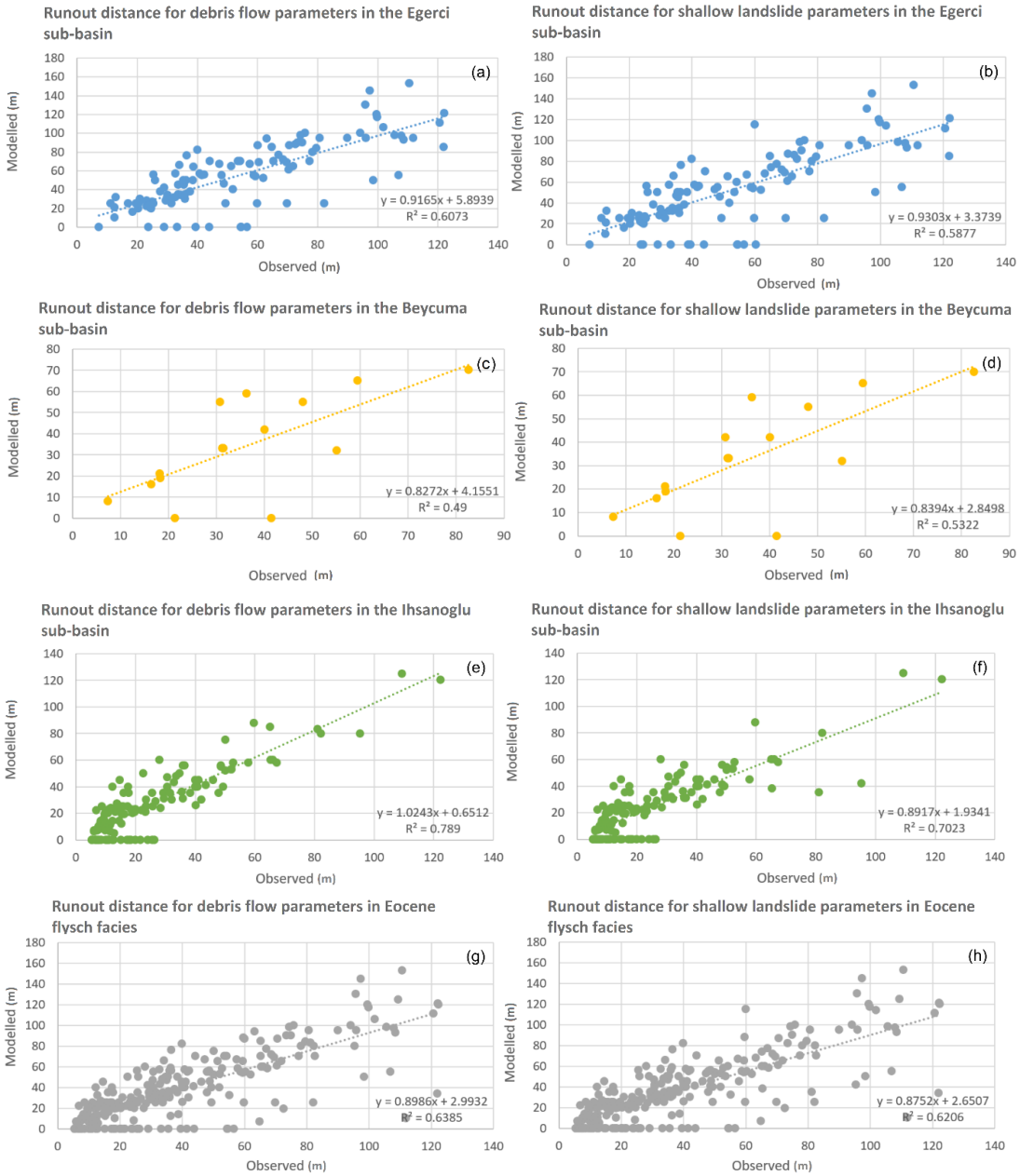

Figure 5.13. Cross-correlations between the runout distances observed and those predicted by employing the parameters of the debris flow and shallow landslide models: (a-b) in the Egerci sub-basin; (c-d) in the Beycuma sub-basin; (e-f) in the Ihsanoglu sub-basin; and (g-h) in Eocene flysch facies (Komu, Nefeslioglu and Gokceoglu, 2024).

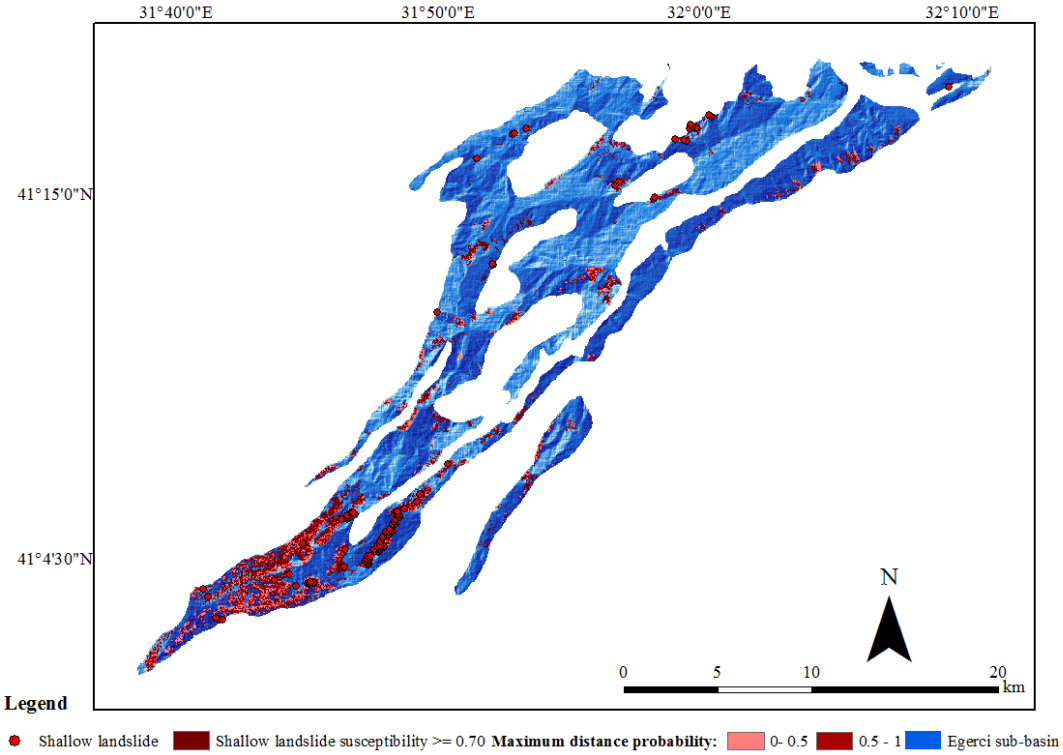

Figure 5.14. The model obtained by using debris flow parameters in Egerci sub-basin.

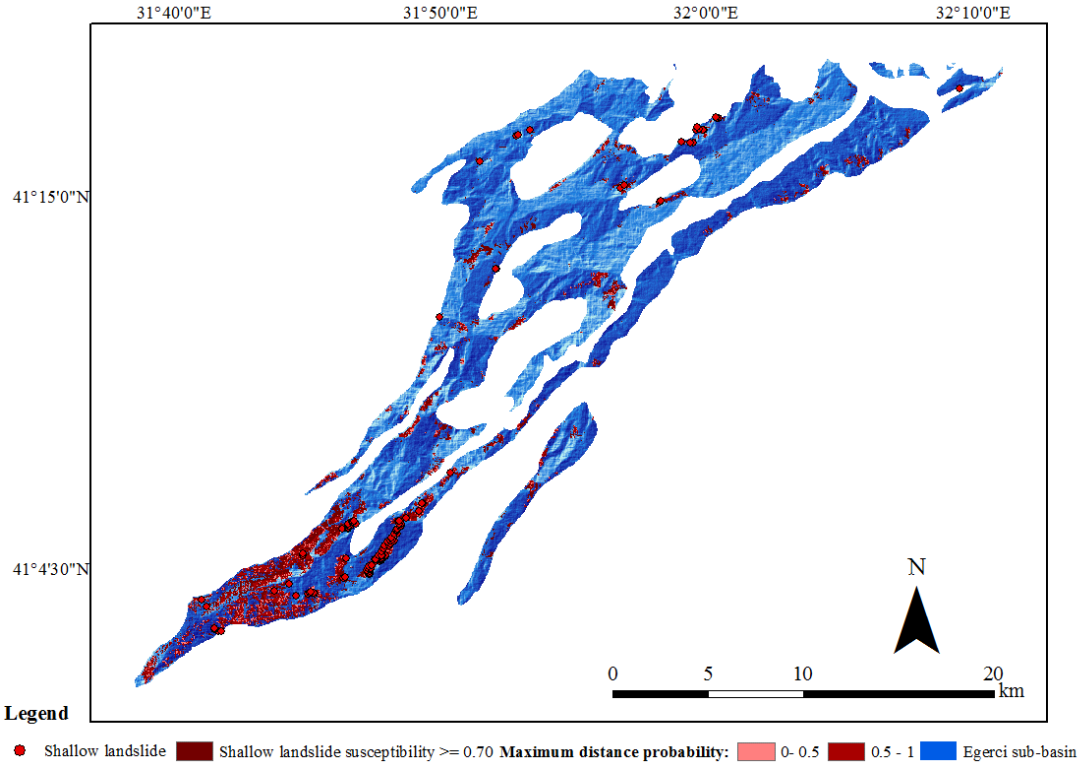

Figure 5.15. The model obtained by using shallow landslide parameters in Egerci sub-basin.

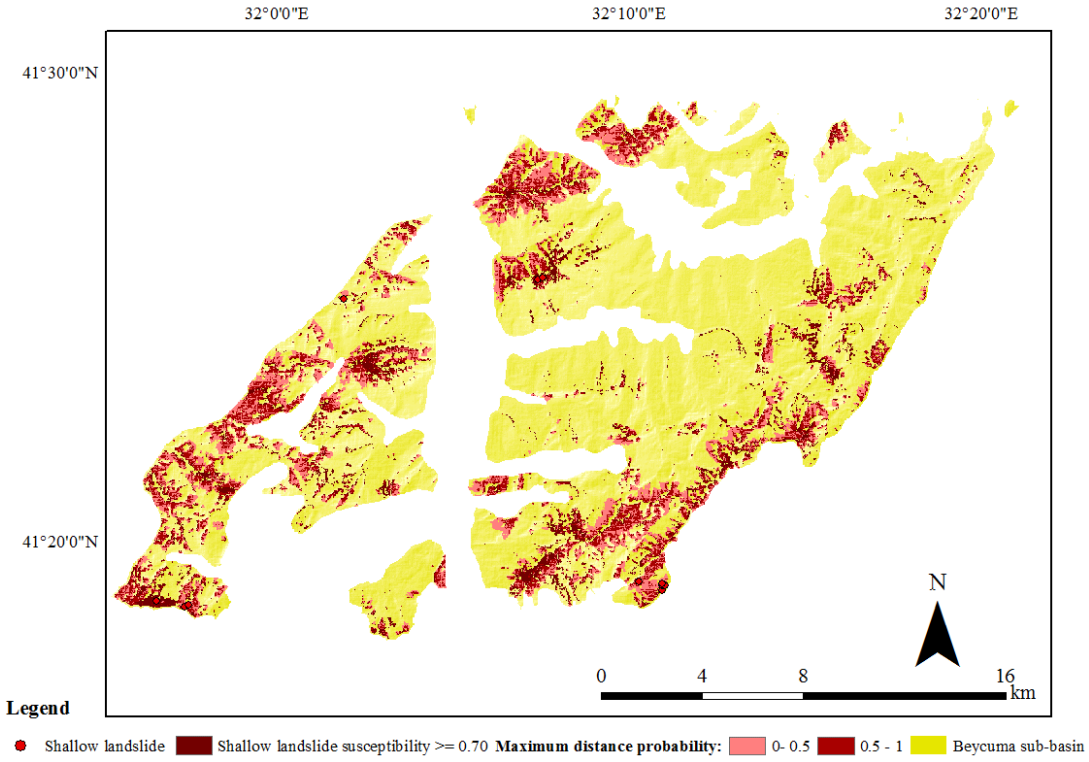

Figure 5.16. The model obtained by using debris flow parameters in Beycuma sub-basin.

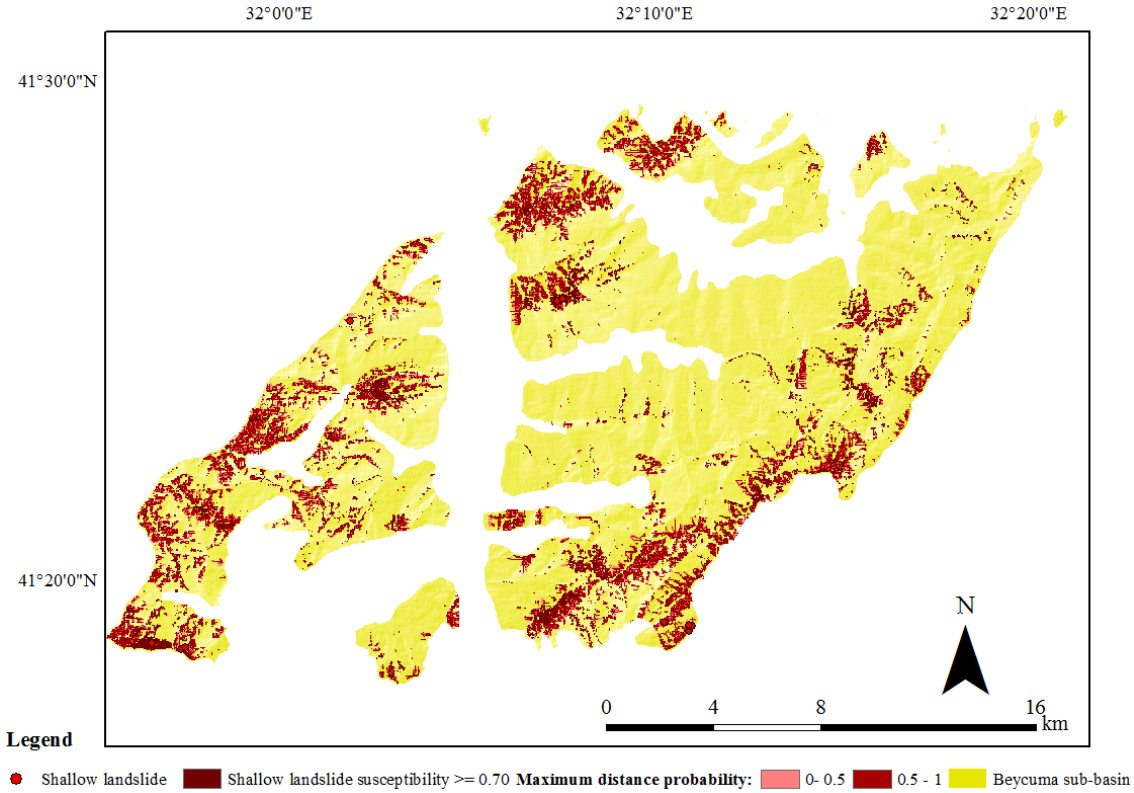

Figure 5.17.The model obtained by using shallow landslide parameters in Beycuma sub-basin.

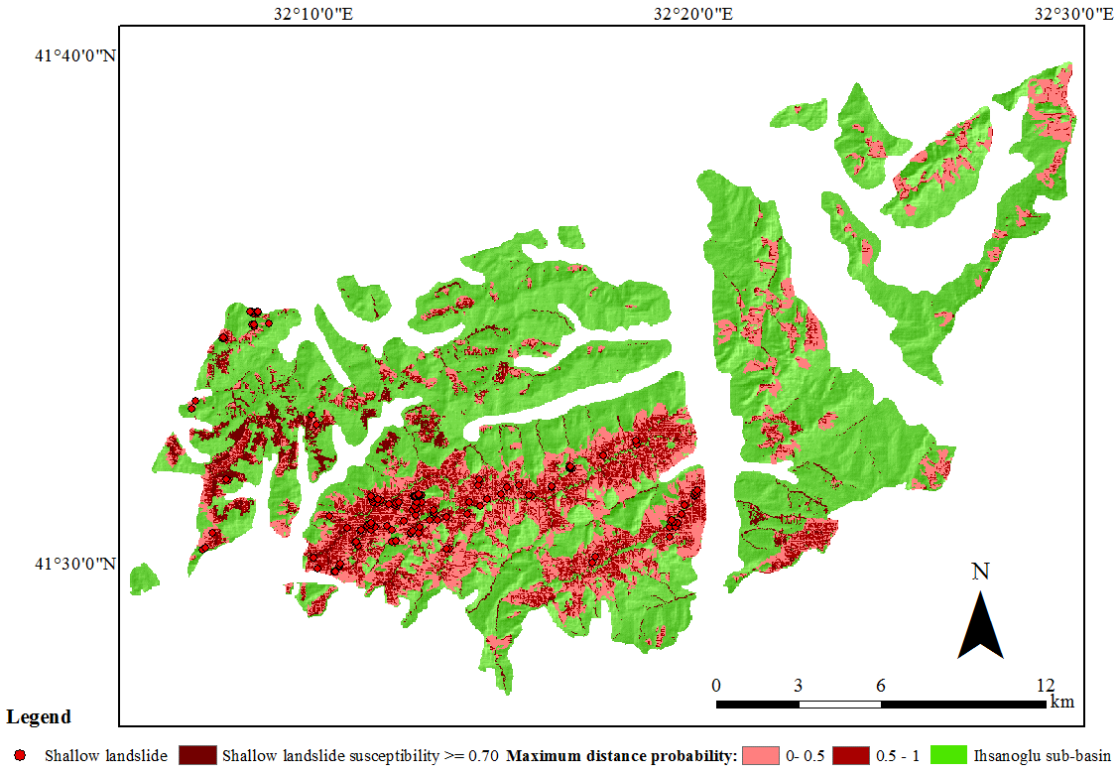

Figure 5.18.The model obtained by using debris flow parameters in Ihsanoglu sub-basin.

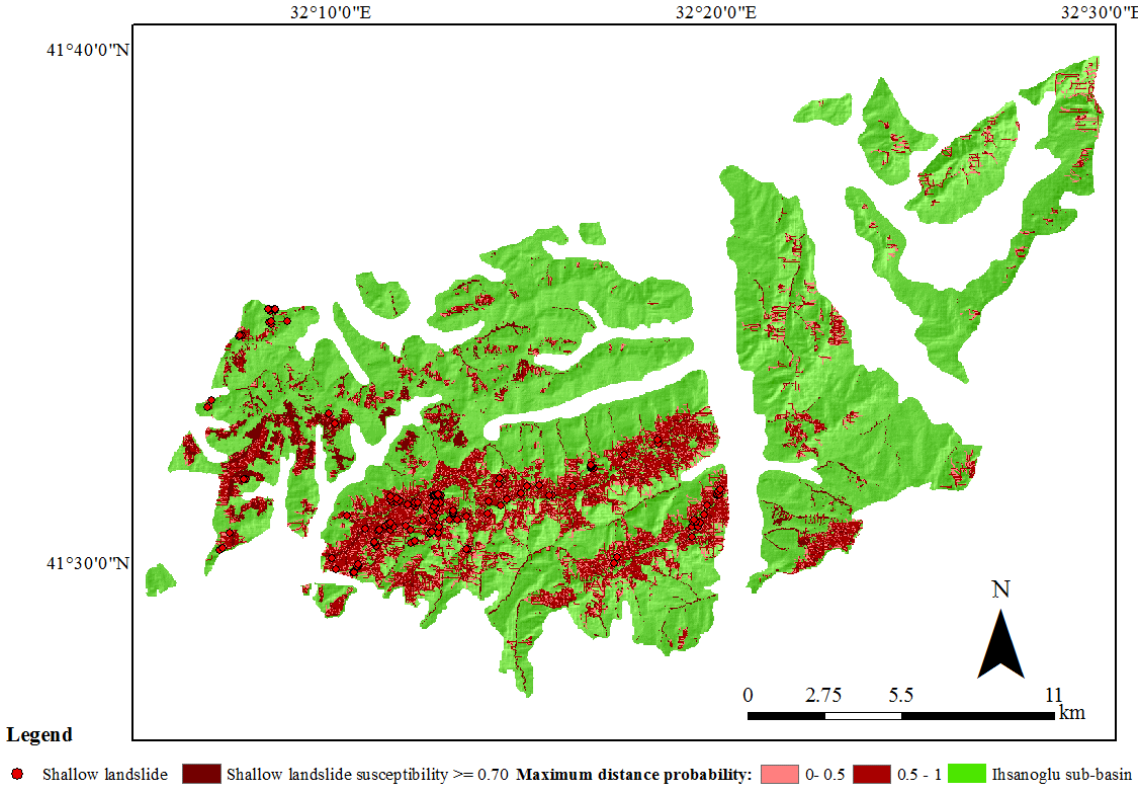

Figure 5.19. The model obtained by using shallow landslide parameters in Ihsanoglu sub-basin.

These results were critical because advanced runout models were tested with real-time data integration and customized parameters for predictive analysis. Obtained results have good estimation accuracy, meaning that runout model results can be used in developing future disaster management strategies such as protecting the city's transport network (Ali et al., 2021; Jian et al., 2021).

Figure 5.20, Figure 5.21, and Figure 5.22 provide a comparative presentation for two models parameter sets to depict the probable maximum distance in close detail.

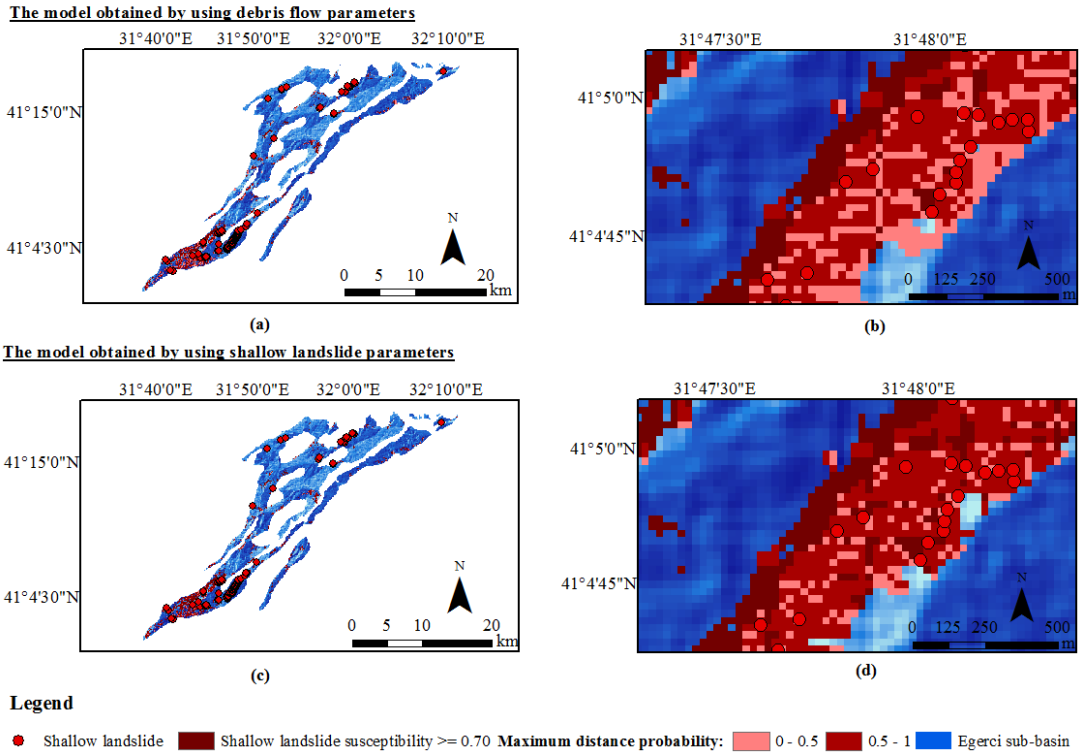

Figure 5.20. Models depicting maximum distance probabilities and detailed spatial distributions in the Egerci sub-basin (a-b) by using the debris flow parameters; (c-d) by using shallow landslide parameters (Komu, Nefeslioglu and Gokceoglu, 2024).

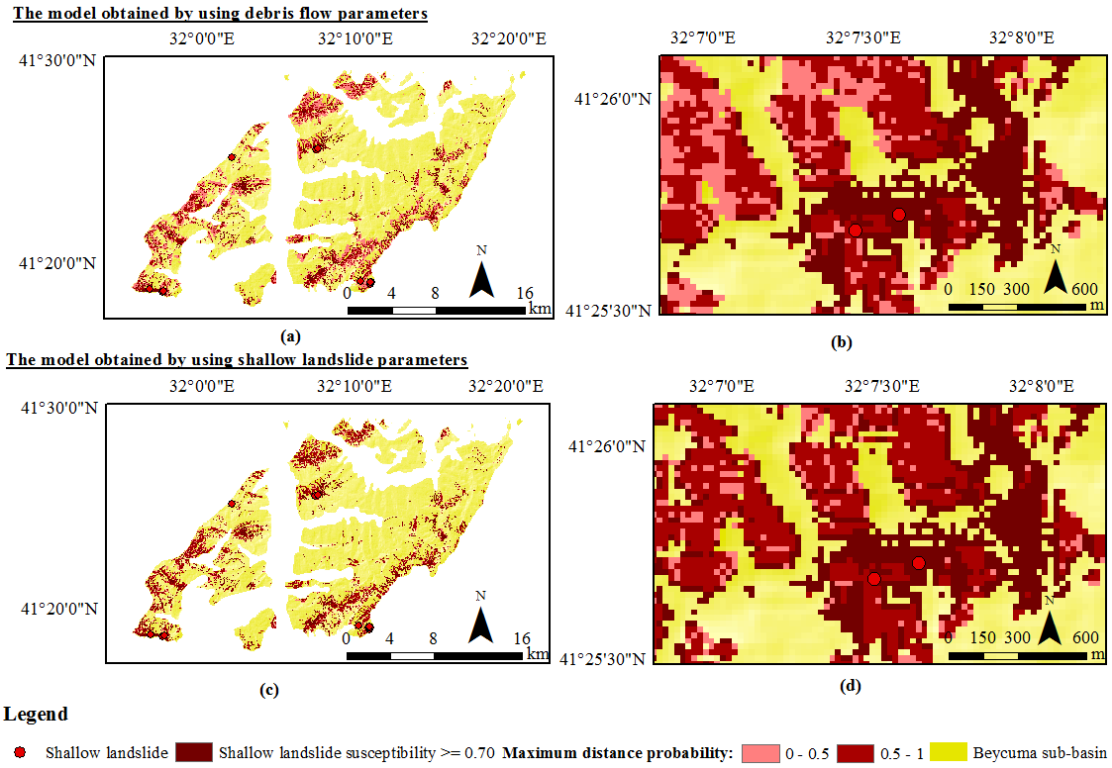

Figure 5.21. Models depicting maximum distance probabilities and detailed spatial distributions in the Beycuma sub-basin: (a-b) by using the debris flow parameters; (c-d) by using the shallow landslide parameters (Komu, Nefeslioglu and Gokceoglu, 2024).

Nearly simultaneous events of diverse flow types in nearby areas can result in the amalgamation and joint propagation of multiple shallow landslide mass (Cuomo, 2020). The proximity of two possible shallow landslide source areas to each other may lead to an intense effect in the sub-basins in terms of long runout distance (Figure 5.20, Figure 5.21 and Figure 5.22).

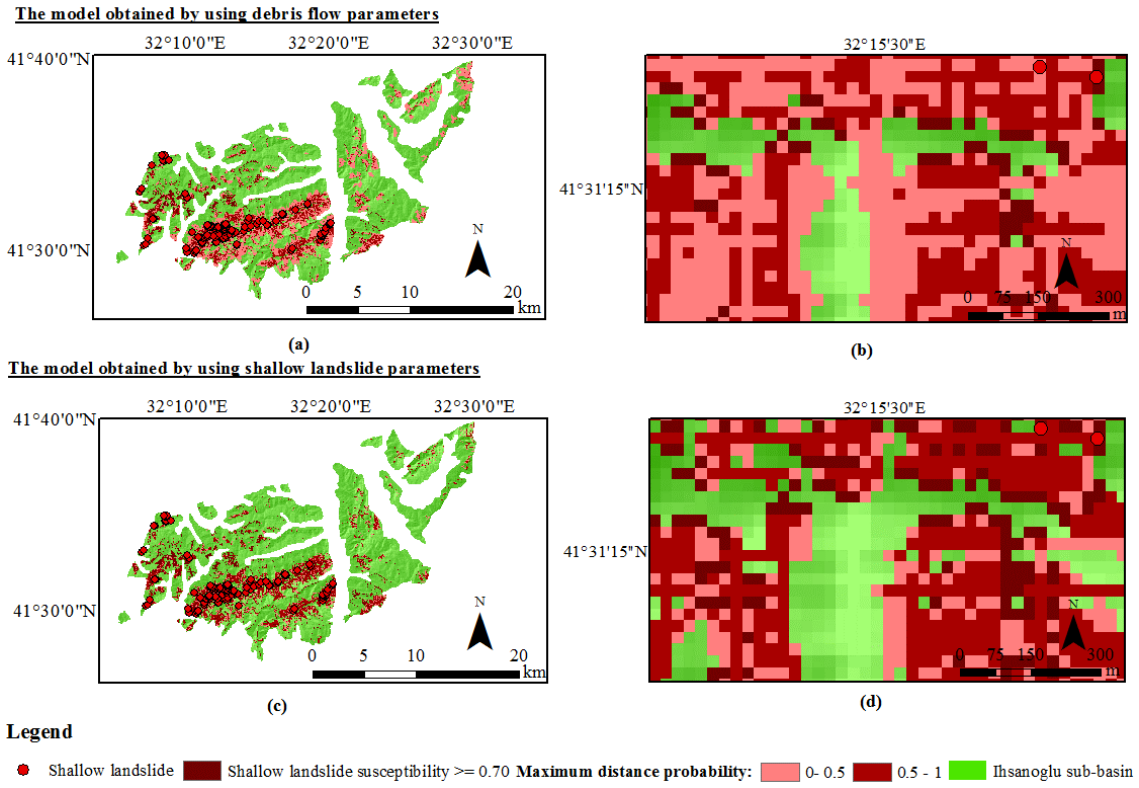

Figure 5.22. Models depicting maximum distance probabilities and detailed spatial distributions in the Ihsanoglu sub-basin: (a-b) obtained by using the debris flow parameters; (c-d) by using the shallow landslide parameters (Komu, Nefeslioglu and Gokceoglu, 2024).

Horton et al. (2021) proposed that 8 m/s is the acceptable velocity limitation for mudflows. Therefore, a back analysis is critical for this study. 15 m/s was used in the analyses. The learning objective of the velocity effect in the analyses is to account for relationships between them by illustrating example probable runout distance (Figure 5.23). The other parameters have been used as parameters used in shallow landslide modelling (x=25, dh=1). The maximum velocity values of 8 m/s and 15 m/s were used to estimate shallow landslide runout distances and compared to evaluate this individuality. This velocity comparison analysis can effectively provide that if velocity increases, runout distances will increase. Therefore, not only x parameter but also velocity parameter at runout distance analyses has a critical role in analyses in terms of influencing the runout distance results. Therefore, the determination of the maximum velocity limitation has an important role in the analyses. If the velocity increases, the runout

distance will increase linearly. The probable model results shown in Figure 5.23 accounts for in the case of V= 15 and 8 m/s of landslide velocity. Figure 5.23 depicts that velocity is obviously a key marker of runout distances analyses.

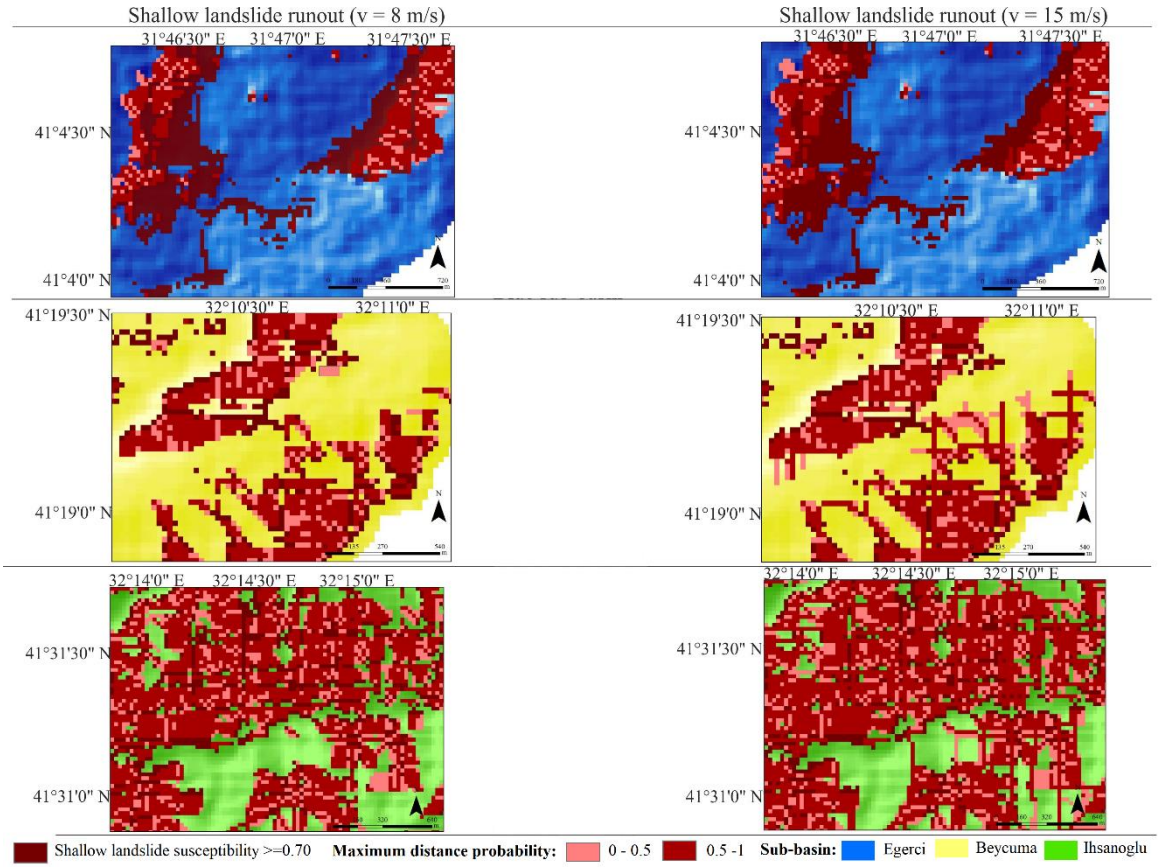

Figure 5.23. Evaluation of the effect of the maximum velocity limitation for the shallow landslide runout distance determinations.

Simulation of models graphs which give information about distribution of failure initiation, maximum distance probability, enable to not only visualize runout distance percentage distribution and but also analyse the relationships between runout distances, failure initiations and sub-basins with respect to percentage distributions (Figure 5.24). While runout distance models prepared by debris flow parameters were shown in Figure 5.24a, 5.24c and 5.24e, runout distance models prepared by shallow landslide parameters were shown in Figure 5.24b, 5.24d and 5.24f. Graphs clarifies that despite of the fact that sub-basins are prone to shallow landslides or debris flow, the affected area of shallow landslides or debris flow can be accounted for having a small pie. The debris flow model's runout zones occupy 17%, 30%, and 40% for Egerci, Beycuma and Ihsanoglu sub-basin

respectively. In contrast, the shallow landslides model's runout zones cover 16%, 26%, and 32% for Egerci, Beycuma and Ihsanoglu sub-basin, respectively.

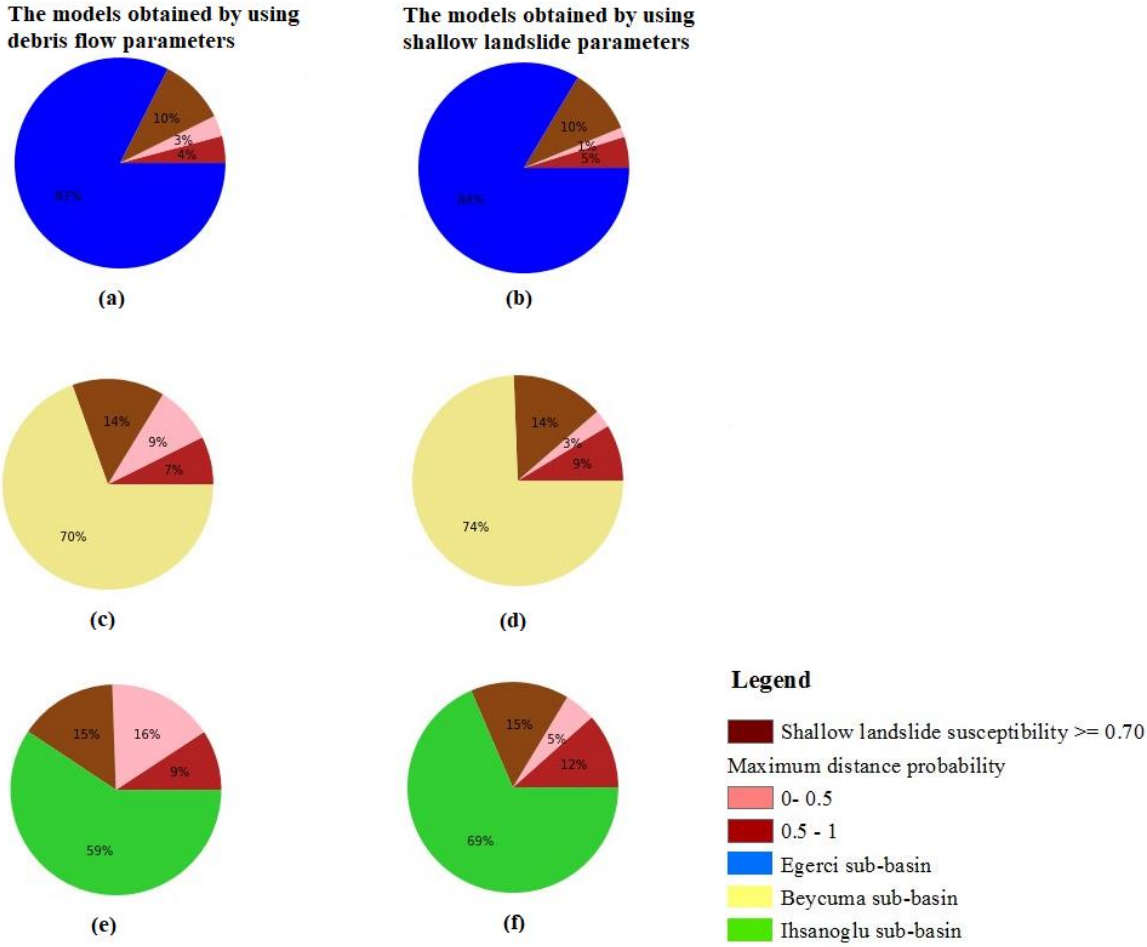

Figure 5.24. The models obtained by using the debris flow and shallow landslide model parameters: (a-b) in the Egerci sub-basin, (c-d) in the Beycuma sub-basin and (e-f) in the Ihsanoglu sub-basin.

It should be made clear that if simulated results are comprehensively examined, all three sub-basins will have exposed to negative effect of landslide hazard in case of sudden shallow failures. Modelled runout results illustrate that landslides may reach several residential areas, transportation networks, and temples. Figure 5.24 is very notable because with help of these demonstration, importance of analysing of the runout distance is beginning to realize so that researches can stay at high alert to identify and mitigate the shallow landslides or debris flow hazards.

6. RUNOUT ANALYSIS OF SHALLOW LANDSLIDES BY INCLUDING RCP SCENARIOS

Prepared runout hazard maps by considering RCP scenario precipitation values are intended to aid engineer in understanding of the potential dangers in terms of the shallow landslides at the sub-basins. This research part is especially covered an attempt to give insight on climate change effects on landslide runout distance by evaluating RCP scenarios precipitation values. This chapter mainly offers sequential steps in order to analyse and describe future shallow landslides runout distances. Firstly, evaluation of RCP precipitation trends will have role in detection of possible future failure initiations. Secondly, initiation points will be evaluated by considering climate change scenarios and LR susceptibility analyses. Finally, possible shallow landslide initiations will be also used in detection of potential maximum runout distances by employing empirical Flow-R 1.0.0 software.

6.1. Evaluation of the RCP Precipitation Scenarios

The aim of this sub-chapter is to quantify the critical precipitations of RCP precipitation scenarios to trigger shallow landslides. It is primarily essential to perform evaluations of RCP precipitation and meteorological station observations in order to identify the amount of precipitation that may cause potentially shallow landslides.

Turkish State Meteorological Service's historical meteorological station observations enabled to investigate extreme rainfalls in the study area. Although many factors trigger to extreme rainfall, climate change leads to inescapably extreme rainfall (Ahmad Tarmizi et al., 2019). While anomalous changes in climate lead to frequency and intensity of rainfall, it is not surprise that plenty of shallow landslides are happened in hillsides regions due to extreme rainfalls (Ortiz-Giraldo, Bitero and Vega, 2023; Thomas et al., 2023). In other words, heavy rainfalls in a brief time of range will induce plenty of shallow landslide's events (Thomas et al., 2023). Shallow landslides and mud-debris flows especially triggered by extreme rainfall events (Luino et al., 2022; Bi et al., 2023). However, obtaining weather data that accurately reflects the precise meteorological conditions at landslide locations is consistently a hurdle in research focused on

determining rainfall thresholds for triggering landslides (Wang, Otto and Scherer, 2021). In the western parts of the Black Sea, the flow type of landslides is triggered by heavy and intense rainfall (Ocakoglu et al., 2002; Ercanoglu and Gokceoglu, 2004; Can et al., 2005; Akgun, Gorum and Nefeslioglu, 2021). Therefore, it is also obvious that the intensity of precipitation that accumulated Eocene flysch facies have the capability of frightening in terms of occurring possible sudden fast landslides.

It is possible to provide an overview about the estimation of critical quantities of precipitation trigger for assessing possible landslide hazards. According to European Commission (2021), 30 years period is the main standard reference period in order to calculate climate normal for the specific area. Many climate researches focus on 30 years period in order to evaluate the climate effects (Ruosteenoja, Jylhä and Kämäräinen, 2016; Anjum, Ding and Shangguan, 2019; Wang et al., 2019; Gao, Booij and Xu, 2020; Bekele, Haile and Rientjes, 2021; Gumus et al., 2023; Jemec Auflič et al., 2023; Volpe et al., 2023) Nevertheless, 20 years reference period has been used in recent studies (European Commission, 2021; Doulabian et al., 2021; Kim, Jung and Kim, 2023). 14 years reference observation period was also used in the study of Andrade et al. (2021). It has been decided to conduct RCP precipitation analyses in periods of 20 years. Therefore, 2025-2044, 2044-2063, 2063-2082, and 2082-2100 are specific time periods in which the study should be examined. In this part of the thesis, meteorological historical data and Community Climate System Model (CCSM4) which based on their RCP 4.5 and RCP 8.5 precipitation values, will be compared in terms of precipitations. In fact, Figure 6.1 represents the correlation of between the meteorological station precipitations and RCP precipitations in years of 1995-2022. The correlation between observed and modelled has been taken into consideration in the study for future step of the study. Using linear statistical relationships in order to investigate relationships between RCP scenarios and Meteorological station' values is much easier, faster and more practicable as compare to other method. While it is true that extreme precipitations trigger shallow landslides, it is difficult to determine whether it will be the annual data or monthly data triggering them in the future that has a more significant impact on shallow landslides. RCP precipitation scenarios data like monthly can used in shallow landslides detection analyses with respect to informing the future precipitation trends in this study.

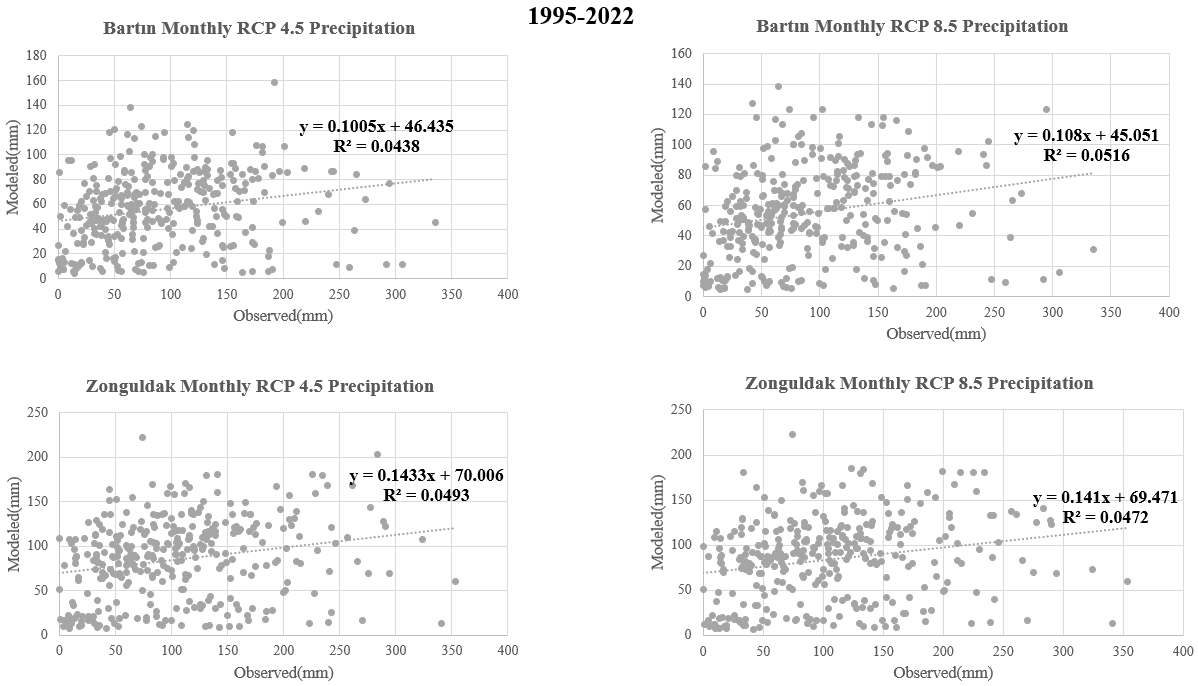

Figure 6.1. Comparison of observed and modelled RCP 4.5 and RCP 8.5 precipitations scenarios for both cities in between 1995-2022.

Propagation distance for shallow landslides and flow-type landslides that can reach exorbitant speeds and travel long distances due to heavy rainfall (Poltnig et al., 2016). Table 6.1 illustrates the data from meteorological and RCP models, depicting the total precipitation for the month in which a landslide was triggered by excessive rainfall. When the meteorological data evidence is rigorously elucidated, Western part of the Black Sea in Türkiye has experienced increasingly extreme heavy rains in recent years. Some parts of areas of Eocene flysch facies experienced extreme summer rain in June 2022 and in August 2021. Therefore, it is necessary to warn about shallow landslides threats to Eocene flysch facies in Türkiye will increase because of extreme heavy rains which are caused by climate change. Observed values represent those extreme heavy rainfalls which were obtained from meteorological data at precipitation stations, trigger shallow landslide events. Extreme rainfall values for the month it occurred that were shown in Table 6.1 to clarify the climate and rainfall characteristic of study area. According to detailed and meticulous researches, these extreme rains inevitably caused to many shallow landslides. This is expected to continue well into the future. Therefore, an integrated approach to climate change RCP precipitations scenarios and observed meteorological value is essential in order to determine the critical threshold.

Table 6.1. Comparison of observed and modelled RCP 4.5 and RCP 8.5 precipitations scenarios for both cities in terms of extreme events (Turkish Meteorological Service).

Year	Month	City	Monthly Prep. (mm)	RCP 4.5 Prep. (mm)	RCP 8.5 Prep. (mm)
1998	May	Bartın	450	92	94
2009	July	Bartın	305	77	78
2009	September	Bartın	188	65	65
2013	October	Bartın	265	73	74
2015	October	Bartın	273	74	75
2016	August	Bartın	187	65	65
2017	June	Bartın	67	53	52
2017	August	Bartın	76	54	53
2018	June	Bartın	102.2	57	56
2019	August	Bartın	69	53	53
2021	August	Bartın	715	118	122
2022	June	Bartın	693	116	120
1998	May	Zonguldak	230	103	102
2009	July	Zonguldak	168	94	93
2009	September	Zonguldak	167.3	94	93
2013	October	Zonguldak	324	116	115
2015	October	Zonguldak	241	105	103
2016	August	Zonguldak	134	89	88
2017	June	Zonguldak	135	89	89
2017	August	Zonguldak	113	86	85
2018	June	Zonguldak	32.6	75	74
2019	August	Zonguldak	161	93	92
2021	August	Zonguldak	526	145	144
2022	June	Zonguldak	864	194	191

It is necessary to remember that climate model precipitations depend on the uncertainties. In addition, bias of downscaling problem exists in this stage. To simplify the assessment of RCP 4.5 and 8.5 scenarios extreme events effect, median values are used to catch best predictions. Table 6.2 shows the median values of the extreme precipitation events for both cities with respect to RCP 4.5 and 8.5 scenarios.

Table 6.2. RCP 4.5 and 8.5 median precipitation values by considering extreme events for both cities in order to detect threshold value.

Scenario		**Bartın**	**Zonguldak**
RCP 4.5	Median	69 mm	94 mm
RCP 8.5	Median	70 mm	93 mm

It should be careful that estimation of future climate precipitation threshold is still highly ambiguous. Despite facing numerous challenges about the determination of future threshold, it could be prescribed to decide the threshold as 81 mm for both scenarios by using Figure 6.1 graphs. In fact, when mean values are calculated by taking into account both cities median RCP 4.5 and 8.5 values, they are 82 and 81 mm, respectively. Therefore, RCP critical threshold was chosen as 81 mm for both scenarios. It should not be forgotten that this value is an assumption. Nevertheless, this threshold value is logic when the literature is reviewed. For instance, in the study by Bainbridge et al. (2022), it was suggested that observational antecedent rainfall (>62 mm) is considered to be the critical indicator when shallow landslides occur. In the study of Volpe et al. (2023), maximum rainfall intensities are 3 mm/h and 2.29 mm/h for RCP 4.5 and RCP 8.5 scenarios in 2041–2070 period, respectively. This stage of thesis emphasizes the significance of the combining data set, including precipitation data, to analyse the runout distances.

6.2. Determinations of Shallow Landslides Initiations by Considering RCP Precipitation Scenarios

In this section, implemented stages of the determination of failure initiations which are affected by RCP precipitation scenarios will be presented. Although runout distance

estimation is the most important goal, possible shallow landslide initiations detections are equally significant for this study. It necessarily notes that detection of failure initiations by taking into account RCP precipitation values is not only highly ambiguous but also very arduous. Detection of failure initiations are built by assigning a critical threshold to potential failure initiations based on determined susceptible areas. They have been rolled to scrutiny with investigating on runout distance. Because of runout assessment dependency on failure initiations in this study scope, determination of shallow landslide initiations has led to more concern about their distributions in the future analyses by using RCP scenarios. It is very critical to be scrupulous when choosing a threshold determination of the hazard map to determine the failure initiations accurately. The determined shallow landslides initial points which were detected in previous section, will be used by combining with critical threshold RCP precipitation scenarios in order to apply same runout strategy to detect possible runout distances. In order words, climate projections of precipitation data and previous detected cells, which are equal to or more than 0.70 susceptible, are the main determining factor of the possible future landslides initiations. Each determination of the failure initiation process is repeated for all determined these years. Because of increasing of the frequency of the extreme rainfall events in Eocene flysch facies, many landslides like a flow type of landslides will still be triggered. It is also predicted that shallow landslide events that will be triggered by rainfall mainly cluster in Egerci and Beycuma sub-basins, where the observation of probability of extreme monthly precipitation is high. It will be expected that some shallow landslides initiations are substantially diminishing. This decrement can result on considering RCP scenarios precipitation values. It has been clarified which determined RCP scenarios and periods had the greatest influence on shallow landslide runout distance in the sub-basins. Analyses indicate the reduction of failure initiations for future periods in the study area. Figure 6.2 shows figuring out possibility of decreasing number of shallow landslides initiations for future years. Regardless of whether landslides are type of shallow landslides or debris flow, will be dense for Egerci and Beycuma sub-basins in the period of 2025-2044 (Figure 6.2). It is increased the accuracy of the probable shallow landslide's initiations by the coincidence of shallow landslide susceptibility and RCP precipitation threshold in this study scope. By 2100, the number of possible shallow landslide initiation is expected to decrease for both sub-basins. In fact, they will be almost 267 and 1411 for Egerci and Beycuma sub-basins, respectively.

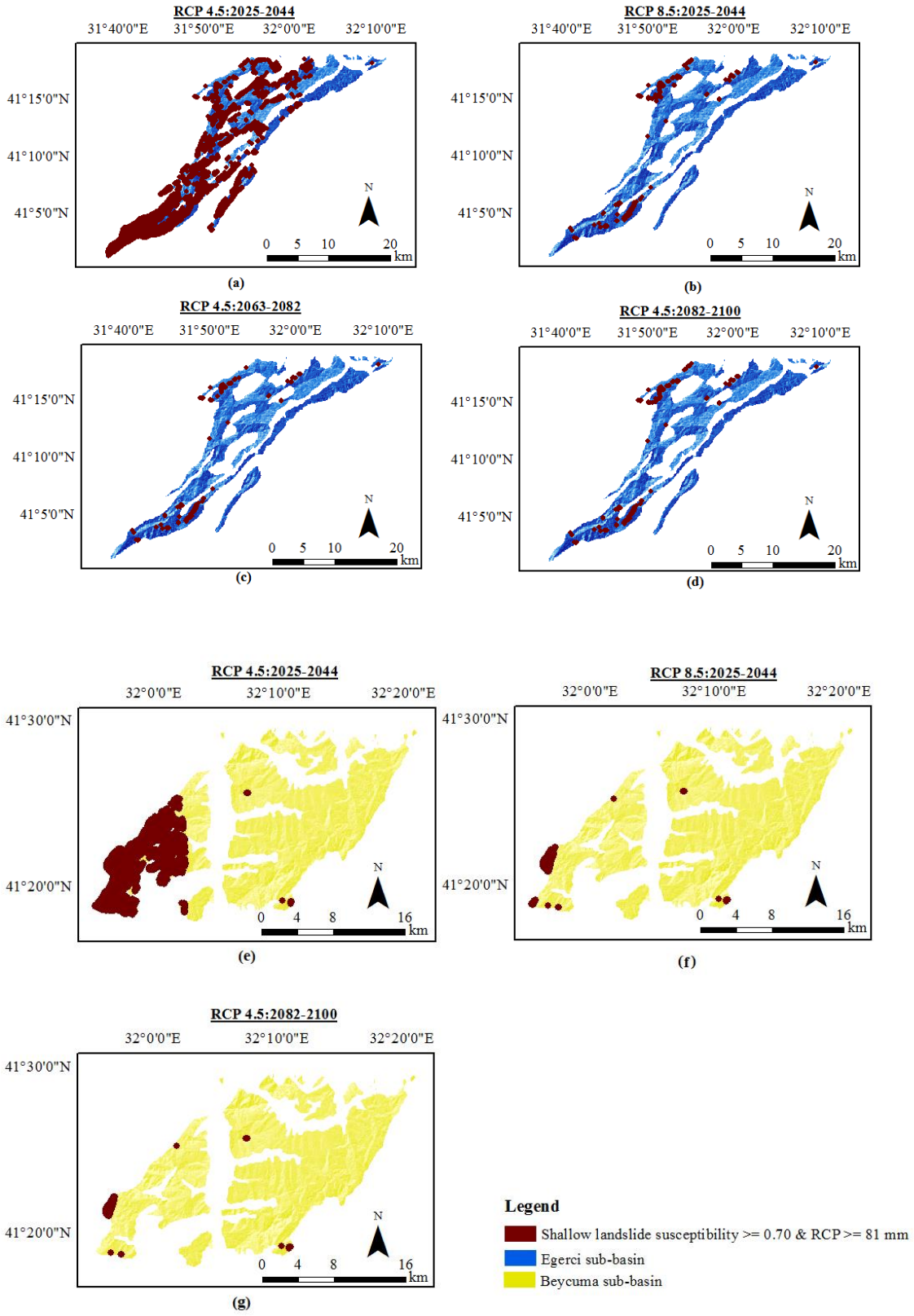

Figure 6.2. Identification of shallow landslide initiations influenced by RCP 4.5 and 8.5 scenarios, delineated within the sub-basins: (a-d) Egerci sub-basin and (e-g) Beycuma sub-basin (Komu, Nefeslioglu and Gokceoglu, 2024).

The bar charts show drop in the number of shallow landslides initiations in determined time range (Figure 6.3). They also enable to compare how many shallow landslides initiations were used for estimation of runout distances analyses in different time periods in Egerci and Beycuma sub-basins. It is noteworthy that RCP 4.5 (2025-2044) and RCP 8.5 (2025-2044) exhibit significant disparities about possible shallow landslide initiations number. Shallow landslides initiations in Beycuma sub-basin are distinctive through years rather than other sub-basin in terms of its numbers. Although there is a sharp decrease in shallow landslide initiations in Beycuma sub-basin with considerably lower shallow landslides initiations from initial condition to RCP 4.5 (2025-2044), numbers of initial shallow landslides initiations are as close as numbers of RCP 4.5 (2025-2044) shallow landslides initiations in Egerci sub-basin.

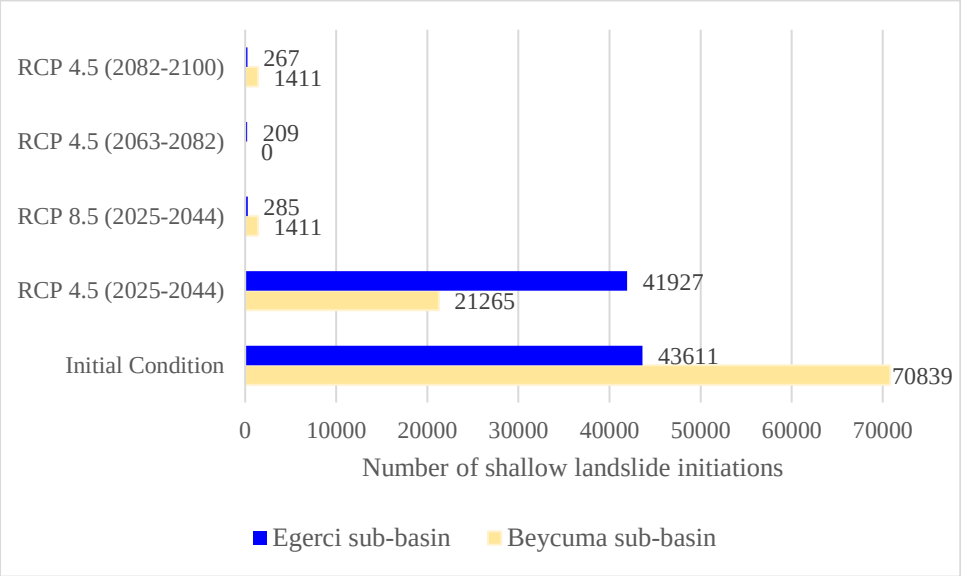

Figure 6.3. Number of possible shallow landslide initiations.

This study aligns with the findings of Ageenko et al. (2022) and Beroya-Eitner et al. (2023) indicating a decrease in landslide susceptibility across RCP scenarios. Park et al. (2024) also reached that shallow landslide occurrences are projected to be less frequent in the period of 2040-2049. The possible shallow landslides initiations have been examined in more detail with respect to their altitude, slope gradient and land use. Table 6.3 and Table 6.4 indicate the altitude and slope gradient of mean and median values of the probable failure initiations in terms of different periods.

Table 6.3. Possible shallow landslide initiations altitude mean and median values for all determined periods.

Sub-basin	Statistics Altitude (m)	RCP 4.5_2025_2044	RCP 8.5_2025_2044	RCP 4.5_2063_2082	RCP 4.5_2082_2100
Egerci	Mean	656	587	577	586
	Median	621	597	594	596
Beycuma	Mean	309	415	-	405
	Median	306	406	-	408

When reckoning with the initial analysis values, future shallow landslide initiations' altitudes are expected to be higher in Beycuma sub-basin (Table 6.3). On the contrary, the probability of shallow landslides occurring will be high even at lower altitude in Egerci sub-basin. Shallow landslides initiations slope gradient median values fluctuate between 23 to 6 or 5 degrees in different time periods in the Egerci sub-basin, while they remain about 16 degrees for determined time periods in the Beycuma sub-basin (Table 6.4).

Table 6.4. Possible shallow landslide initiations slope gradient mean and median values for all determined periods.

Sub-basin	Statistics Slope Gradient (°)	RCP 4.5_2025_2044	RCP 8.5_2025_2044	RCP 4.5_2063_2082	RCP 4.5_2082_2100
Egerci	Mean	23	9	8	10
	Median	23	6	5	6
Beycuma	Mean	16	17	-	16
	Median	16	16	-	16

The pie graphs below show land cover of shallow landslides initiations in Egerci and Beycuma sub-basins as percentage (Figure 6.4 and Figure 6.5). Although initial analyses indicate that the frequency of potential landslide initiation points is high at broad-leaved forests, the probability of landslides occurring at broad-leaved forests in Beycuma sub-basin is diminishing (Figure 6.5). Despite the fact that shallow landslide occurrence will decrease in broad-leaved forest for Egerci sub-basin, but it can be informed that there will also be a greater decrease in mixed forest and coniferous forest in the Egerci sub-basin.

Schwaab et al. (2020) state that the broad-leaved forest susceptibility will reduce. Yu et al. (2021) claimed that the broad-leaved susceptibility will decrease in 2030s and the 2080s in accordance with RCP 8.5 scenarios. Malla, Neupane and Köhl (2023) suggested that coniferous forest will be changed into broad-leaved forest or vice versa in the 2041-2060 in accord with RCP 4.5 scenarios. Nevertheless, shallow landslides initiations of land cover will remain unchanged for future periods in the study of Jemec Auflič et al. (2023).

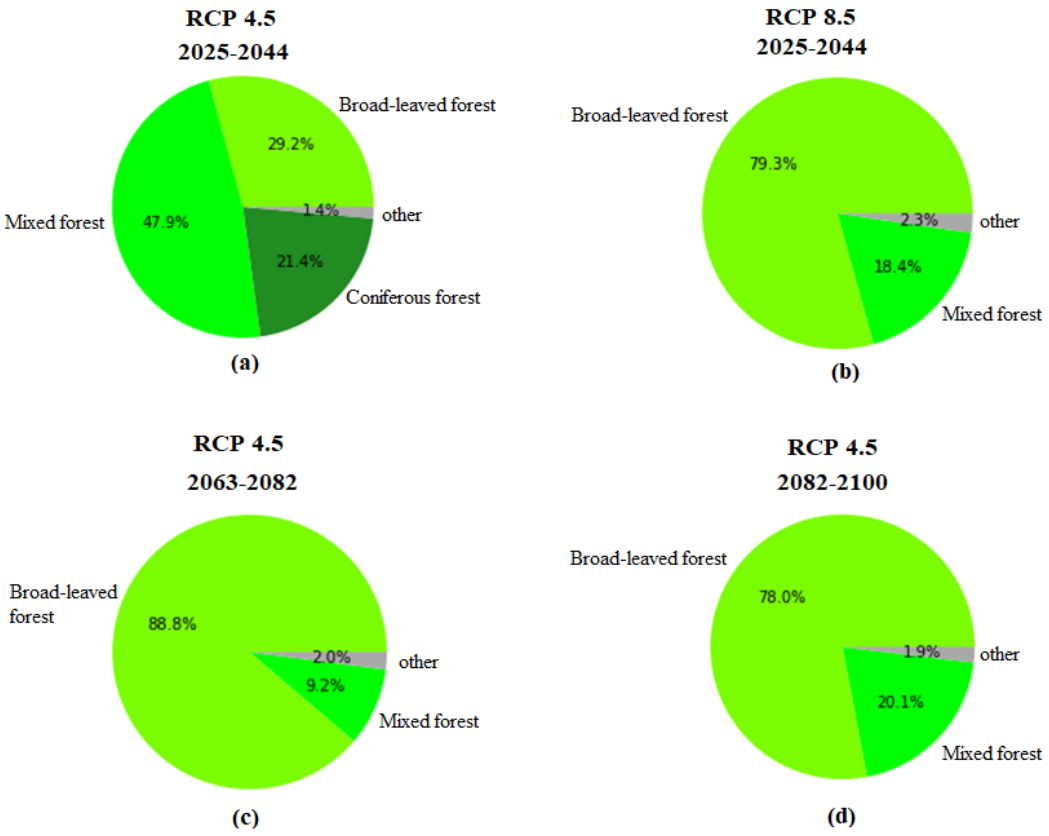

Figure 6.4. Relationships between shallow landslide initiations and land-cover Egerci sub-basin: (a) RCP 4.5 (2025-2044), (b) RCP 8.5 (2025-2044), RCP 4.5 (2063-2082) and RCP 4.5 (2082-2100) (Corine Land Cover, 2018).

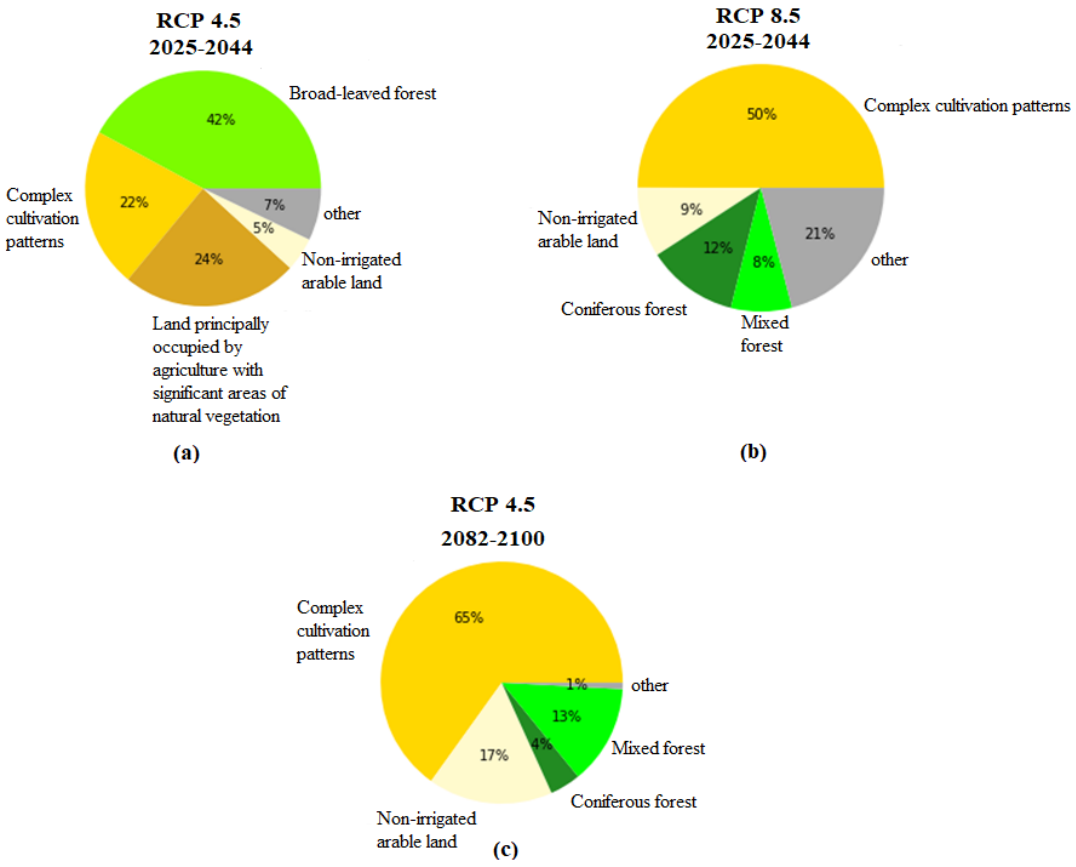

Figure 6.5. Relationships between shallow landslide initiations and land-cover for Beycuma sub-basin: (a) RCP 4.5 (2025-2044), (b) RCP 8.5 (2025-2044), and (c) RCP 4.5 (2082-2100) (Corine Land Cover, 2018).

This chapter aimed to give information about how extreme precipitation in terms of analysing extreme RCP precipitation values. The relationships between RCP scenarios and possible shallow landslide initiations are presented in mapped formats, they become highly informative to give an insight into possible mitigations of possible future shallow landslides.

6.3. Assessment of Climate Change Scenarios Propagation

In this chapter relationships between RCP scenarios and shallow landslides runout distance will be elucidated by considering changes in their shallow landslide's initiations. This chapter also discusses how make progress in evaluating the RCP scenarios precipitation value in order to detect runout distances by considering the empirical model.

RCP precipitation effects are mainly considered in order to predict the possible runout distances in this part of the study. LR with ML and RCP critical threshold precipitation value were utilized for potential shallow landslides failure initiations. Each sub-basin was presented separately for the determined time frame in order to predict the possible shallow landslide runout distances. Multiple simulation options were tried to observe shallow landslides runout distances. The model results have visualized ranging from 0.5 to 1 explain that runout probability is higher than 50%. The runout probability results with shown ranging from 0 to 0.5, on the other hand, can be interpreted that runout probability is lower than 50%. Feasible runout distance results were visualized in Figure 6.6, Figure 6.7, Figure 6.8, Figure 6.9, Figure 6.10, Figure 6.11 and Figure 6.12. Difficult as it may seem, linking between prediction of shallow landslides of runout distances and RCP precipitation values are actually possible with these models. They provide guidelines for possible landslides runout prone areas to evaluate hazards in the future. It is note that prepared runout maps enable to make complex estimation processes understandable to researchers at all levels of expertise. Additionally, the comparisons between them are clear using maps and graphs in terms of identifying the areas potentially threatened by shallow landslides. Thus, all these related data enable to optimally provided the better understood of the runout distances impact areas for the determined time periods. Results indicate that Egerci and Beycuma sub-basins runout distances will still be examined as a problem in the future. In contrast, the possible runout distance trend for Ihsanoglu sub-basin varied drastically over the period. Ihsanoglu sub-basin, where multiple runout susceptibility zones are likely in initial analyses, will not prone to runout susceptibility of shallow landslides because of not detected possible shallow landslide initiations in the future periods. Decreasing of number of shallow landslides undoubtedly plays a crucial role in reducing total runout distances. The given maps illustrate the possible changes experienced by Egerci and Beycuma sub-basins landslides from 2025 to 2044, 2082-2100 according to RCP 4.5 and RCP 8.5 scenarios (Figure 6.6, Figure 6.7, Figure 6.8, Figure 6.9, Figure 6.11 and Figure 6.12). Figure 6.10 also represents the future runout distances for RCP 4.5: 2063-2082 scenario in Egerci sub-basin. These maps enable to portend possible damages in terms of shallow landslides runout distances. Runout distances are likely to have extensive in the sub-basin Egerci sub-basin according to future RCP scenarios. Plausible worst scenario (RCP 8.5) can be evaluated only time frame of 2025-2044 in terms of probable maximum distances for both sub-basins.

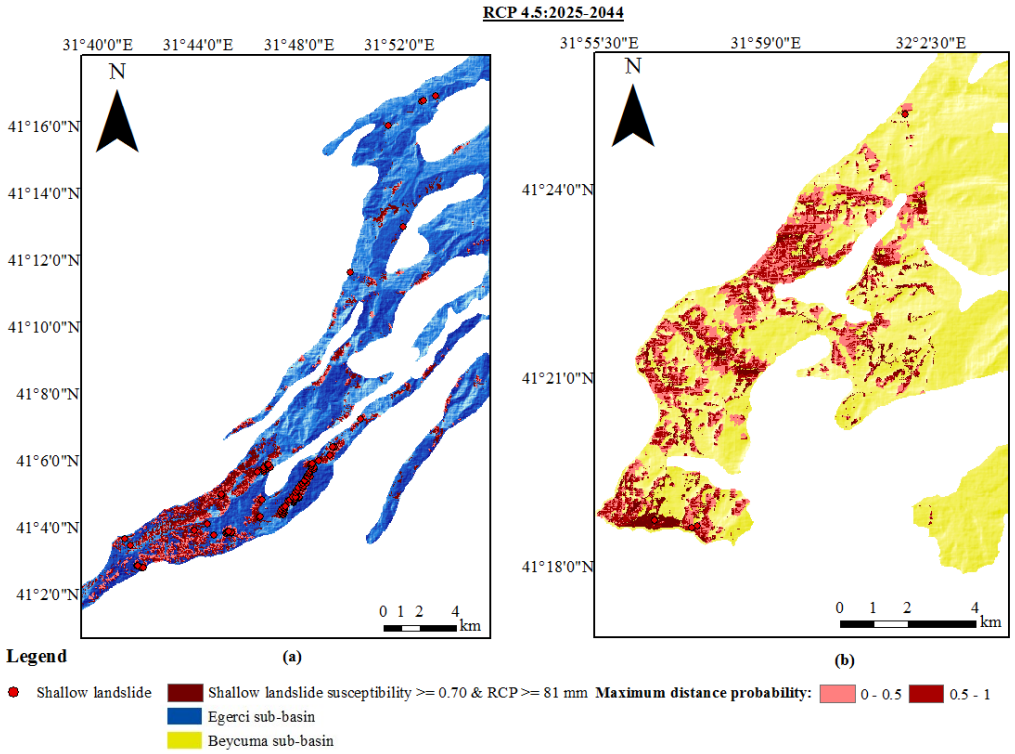

Figure 6.6. Probable runout distances models by using the debris flow parameters for RCP 4.5: 2025-2044: (a) Egerci sub-basin, (b) Beycuma sub-basin.

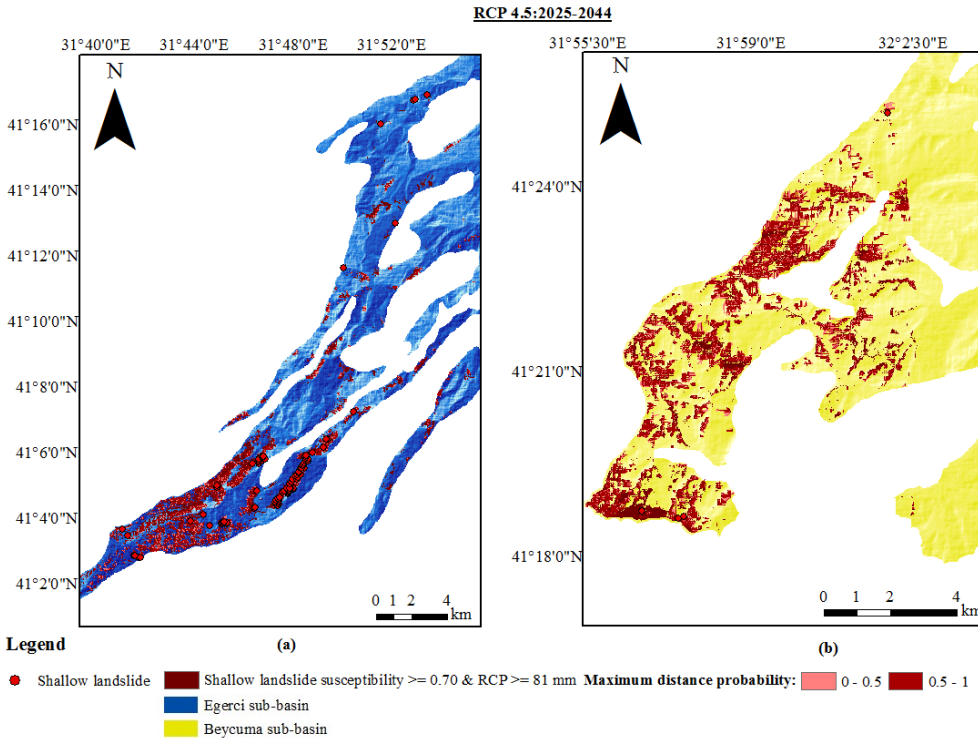

Figure 6.7. Probable runout distances models by using the shallow landslide parameters for RCP 4.5: 2025-2044: (a) Egerci sub-basin, (b) Beycuma sub-basin.

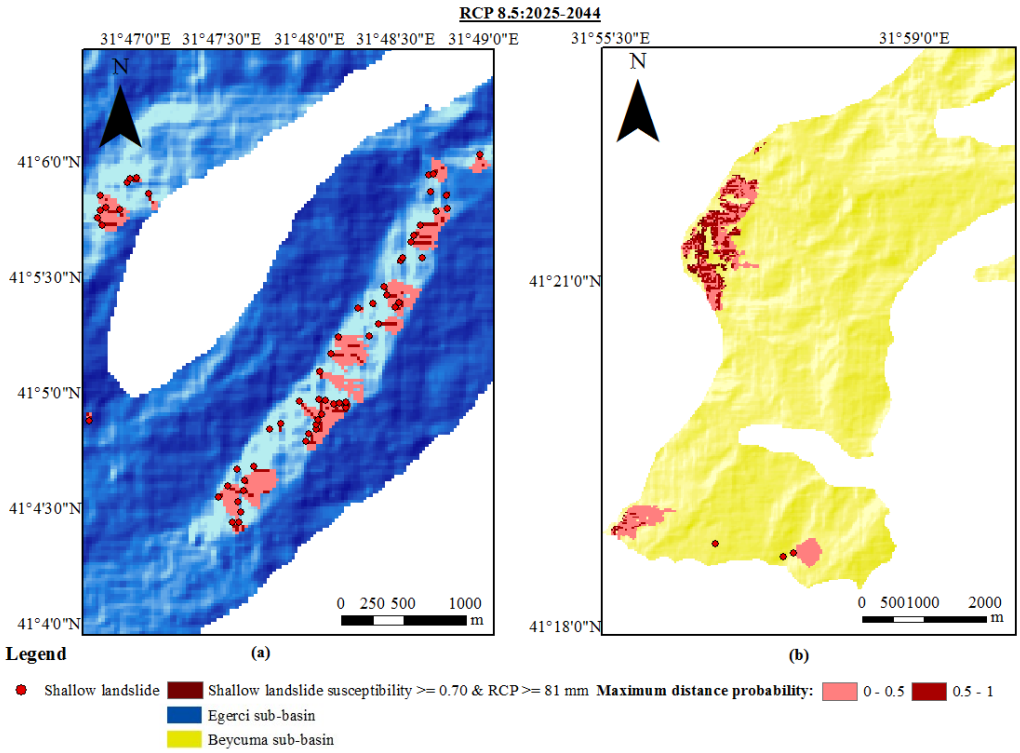

Figure 6.8. Probable runout distances models by using the debris flow parameters for RCP 8.5: 2025-2044: (a) Egerci sub-basin, (b) Beycuma sub-basin.

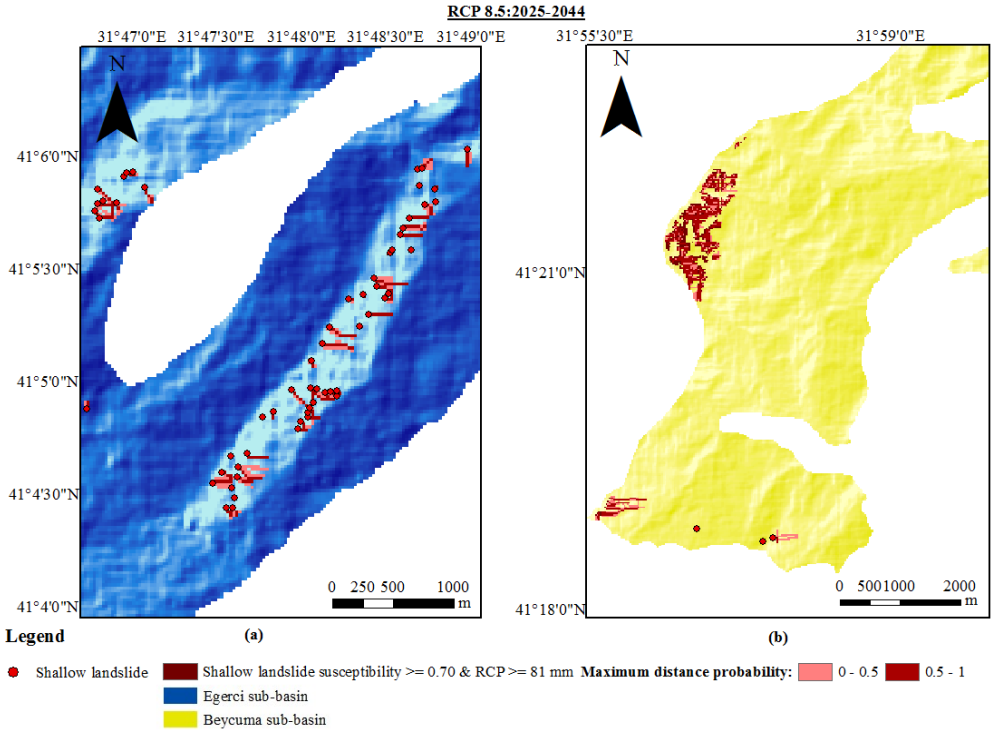

Figure 6.9. Probable runout distances models by using the shallow landslide parameters for RCP 8.5: 2025-2044: (a) Egerci sub-basin, (b) Beycuma sub-basin.

The empirical runout analyses have been revealed that RCP 4.5: 2025-2044 is the most critical time frame for runout distances (Figure 6.6 and Figure 6.7). Probable shallow landslides initiations in the both sub-basins for RCP 8.5: 2025-2044 are smaller than RCP 4.5: 2025-2044 and runout distances are supposed to be correspondingly smaller (Figure 6.8 and Figure 6.9). After the time interval of 20 years to 2044, there was a dramatic shift in runout distances for all sub-basins. In anticipation of the RCP: 2044-2063 model results suggesting the absence of shallow landslides initiations, their runout distance could not be observed for all sub-basins. Beycuma sub-basins' runout affected areas are not included in Figure 6.10 because no problem will be expected in terms of shallow landslide runout distance in the Beycuma sub-basin for RCP 4.5: 2063-2082 scenario. The results show that RCP 4.5: 2082-2100 model results present a greater number of failure initiations than results of RCP 4.5: 2063-2082 model in Egerci sub-basin. Therefore, their runout impacted areas are also smaller in the RCP 4.5: 2063-2082 models in Egerci sub-basin.

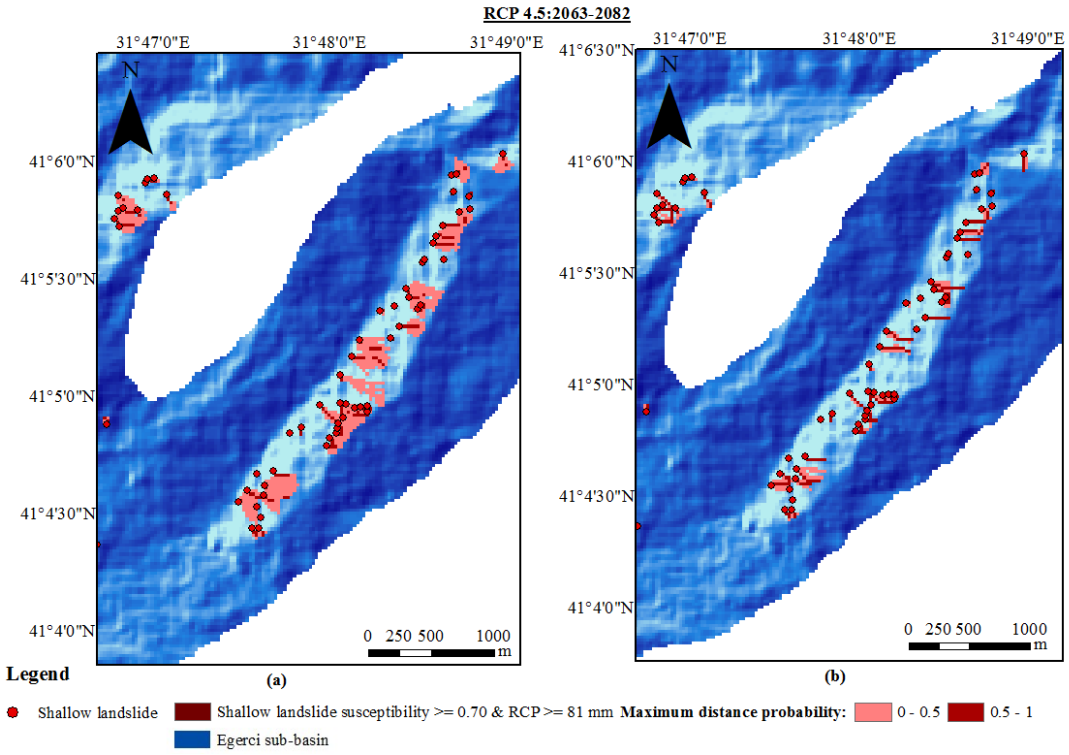

Figure 6.10. Probable runout distances models for RCP 4.5: 2063-2082 in Egerci sub-basin, (a) by using the debris flow parameters; (b) by using the shallow landslide parameters.

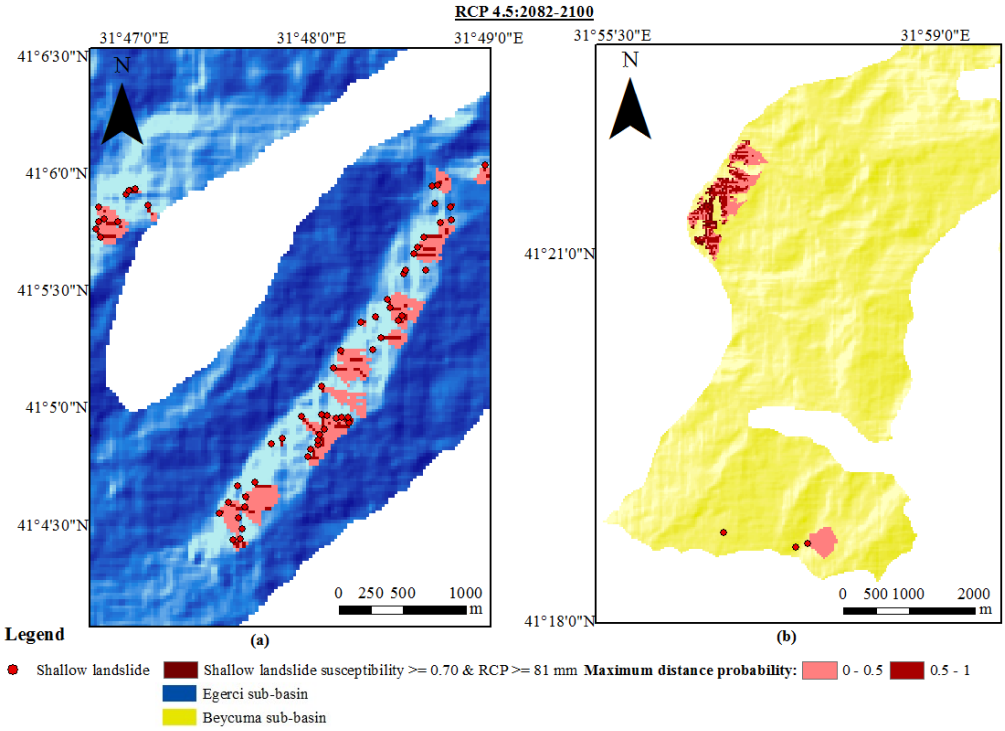

Figure 6.11. Probable runout distances models by using the debris flow parameters for RCP 4.5: 2082-2100: (a) Egerci sub-basin, (b) Beycuma sub-basin.

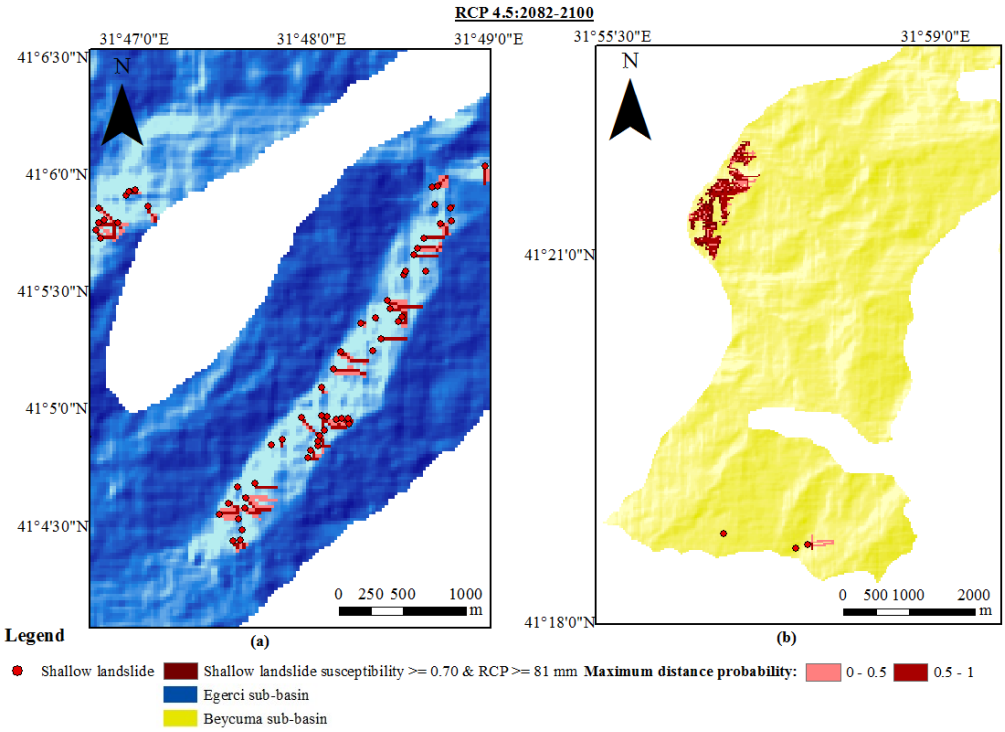

Figure 6.12. Probable runout distances models by using the shallow landslide parameters for RCP 4.5: 2082-2100: (a) Egerci sub-basin, (b) Beycuma sub-basin.

Represinting with pie charts about runout distances, possible failure initiations and remaning area in sub-basins is one among many scientific visualization that contribute to fostering of effectively comparisons. The pie charts also enable to compare the expenditure of runout distances of modelling of shallow landslides and debris flows parameters for determined time intervals in Egerci and Beycuma sub-basins. The pie charts primarily give information in percentage terms about the shallow landslides initiations and their runout distances over determined time intervals. It is obvious fact that in sub-basins, detecting future possible number of shallow landslide initiations have a great importance. Unlike Figure 6.13, in the Figure 6.14, 6.15, and 6.16, the values of shallow landslides initiations and runout distances have a relatively small percentage. The percentage of failure initiations and probable maximum distances noticeably dropped at the end of the given periods. Researchers have been inferred from how the relationship between landslides and RCP scenarios might be changed in their own study area. Lim and Kim (2022) also claim that landslide risk for 2050 will be not more different than 2011 for RCP 8.5 scenarios in their study area. However, significant reductions about possible shallow landslides occurences are expected for 8.5 scenario in the Eocene flysch facies' sub-basins. Nefros et al. (2023) revealed that period 2030–2060 is more cirtical for landslide occurrence in terms of RCP 4.5 and 8.5 scenarios. Janized et al. (2023) also claimed that the regions with very high landslide susceptibility for RCP 8.5 scenario will be higher in 2090 compared to the years 2030, 2050, and 2070. Although there is an observed increase compared to the years 2063-2082 for Egerci and Beycuma sub-basins, it cannot be said that the highest landslide problem for these sub-basins will occur at the end of the century (2082-2100). Mohamed-Yusof et al. (2024) also claimed that in forthcoming period of 2070–2099, although the landslide density will decrease, very high susceptible areas in the prepared landslide susceptibility map will increase for RCP 4.5 and RCP 8.5 scenarios. Jemec Auflič et al. (2023) informed that shallow landslides prone areas will increase in 2041-2070 and 2071-2100 with respect to RCP 4.5 and RCP 8.5 scenarios. Wijaya et al. (2022) is expected that the landslide susceptibility will increase in time horizons 2030s, 2050s, and 2080s for both scenarios. On the contrary, Ageenko et al. (2022) claimed that the landslide susceptibility will lessen for RCP 8.5 scenario in the period of 2071-2100. The landslide susceptibility will decrease for both RCP 4.5 and RCP 8.5 in the period of 2046-2065 in the study of Beroya-Eitner et al. (2023). Unlike this thesis results, it will be expected that the reductions of possible landslide occurrences

in the RCP 4.5 scenario will be greater than the reductions in the 8.5 scenario in the study of Beroya-Eitner et al. (2023).

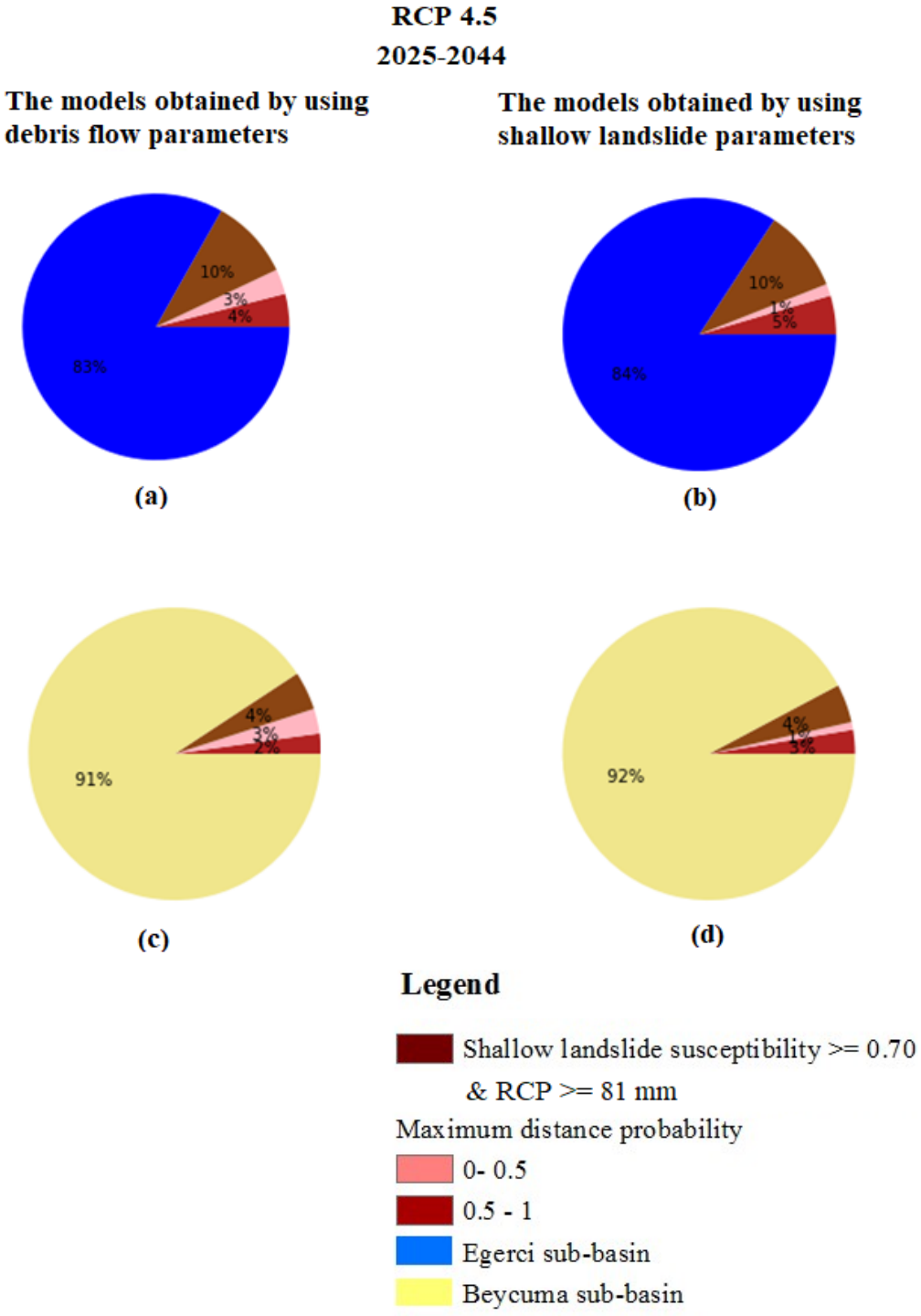

Figure 6.13. Pie charts of runout distances for RCP 4.5: 2025-2044.

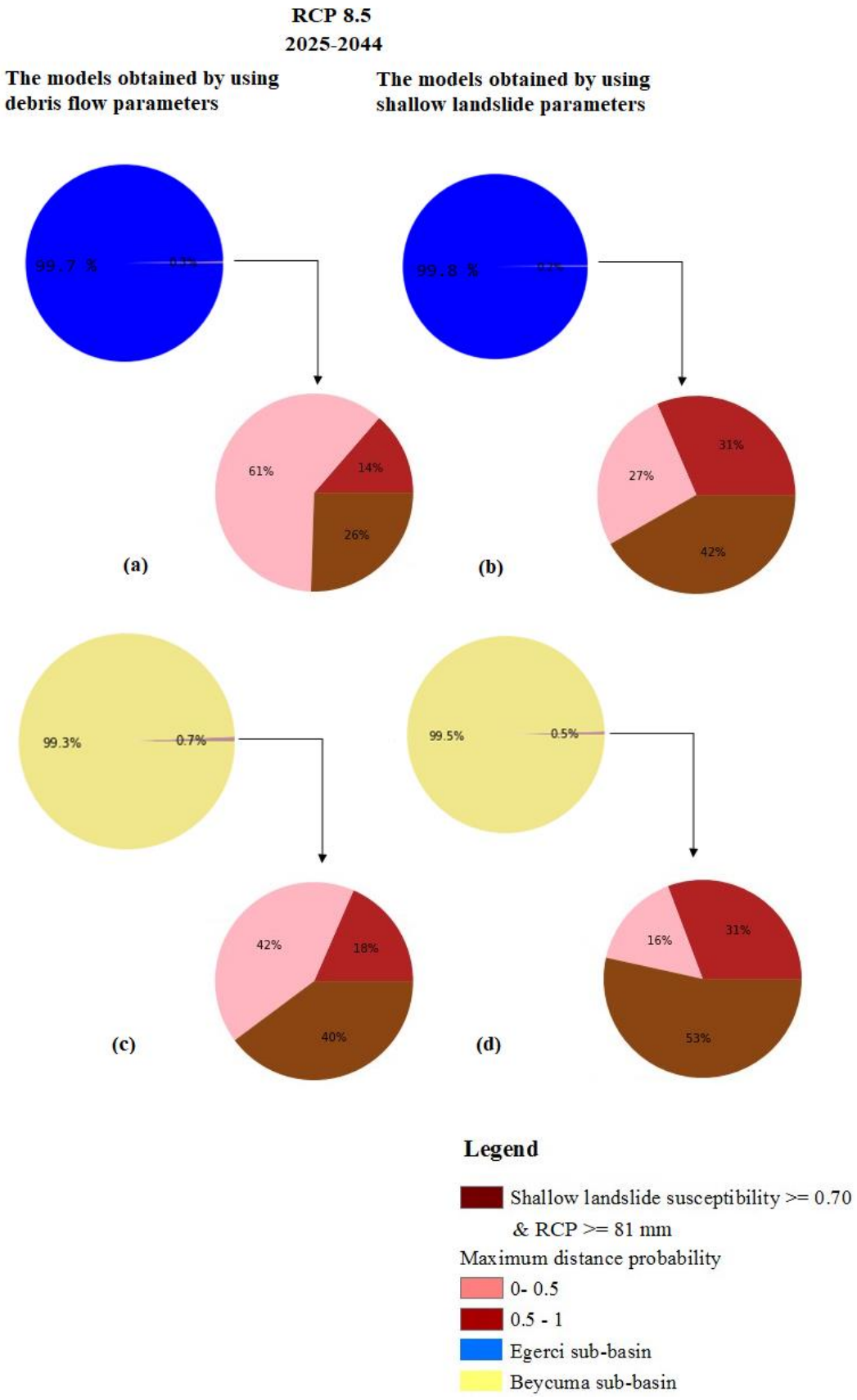

Figure 6.14. Pie charts of runout distances for RCP 8.5: 2025-2044.

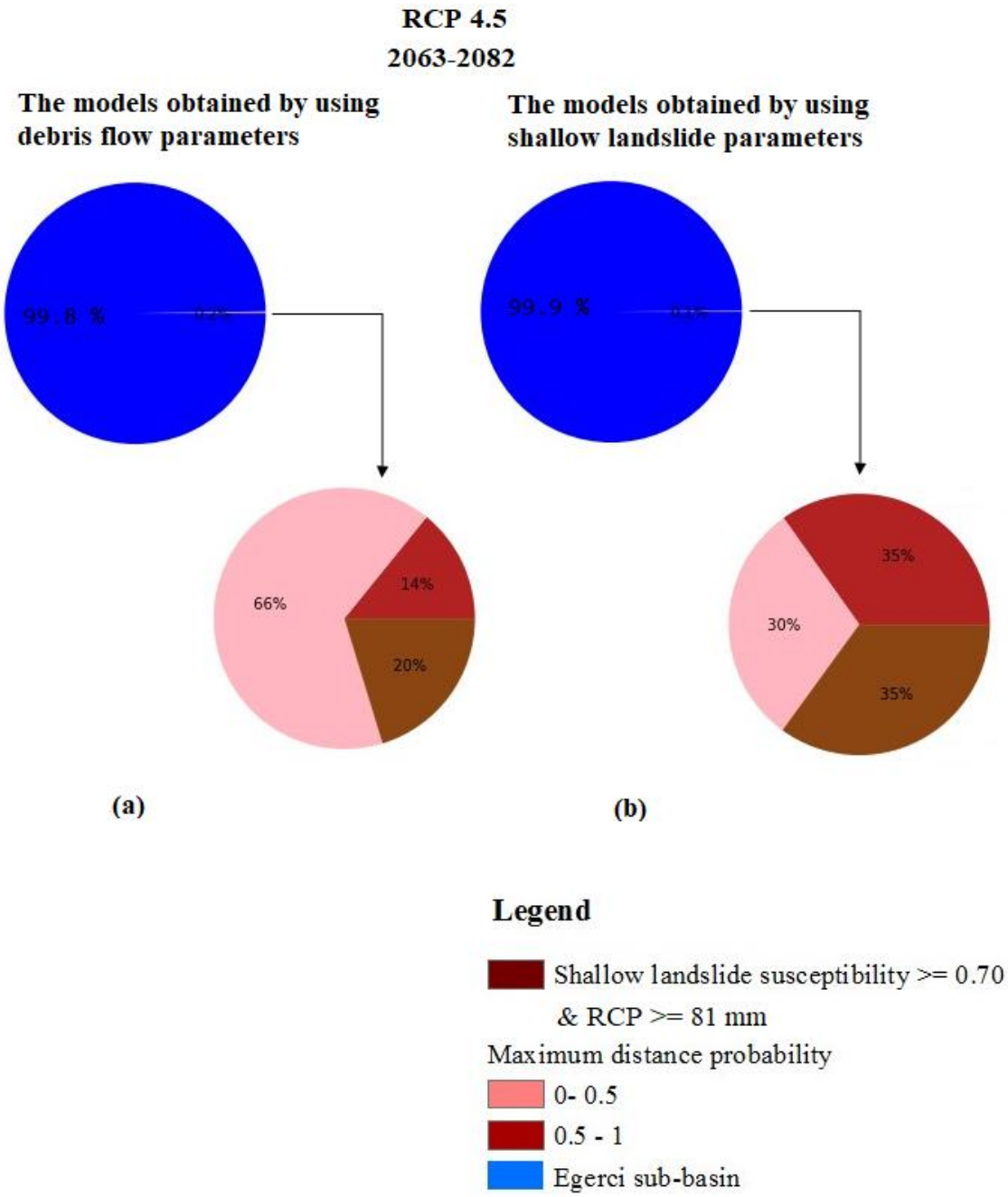

Figure 6.15. Pie charts of runout distances for RCP 4.5: 2063-2082.

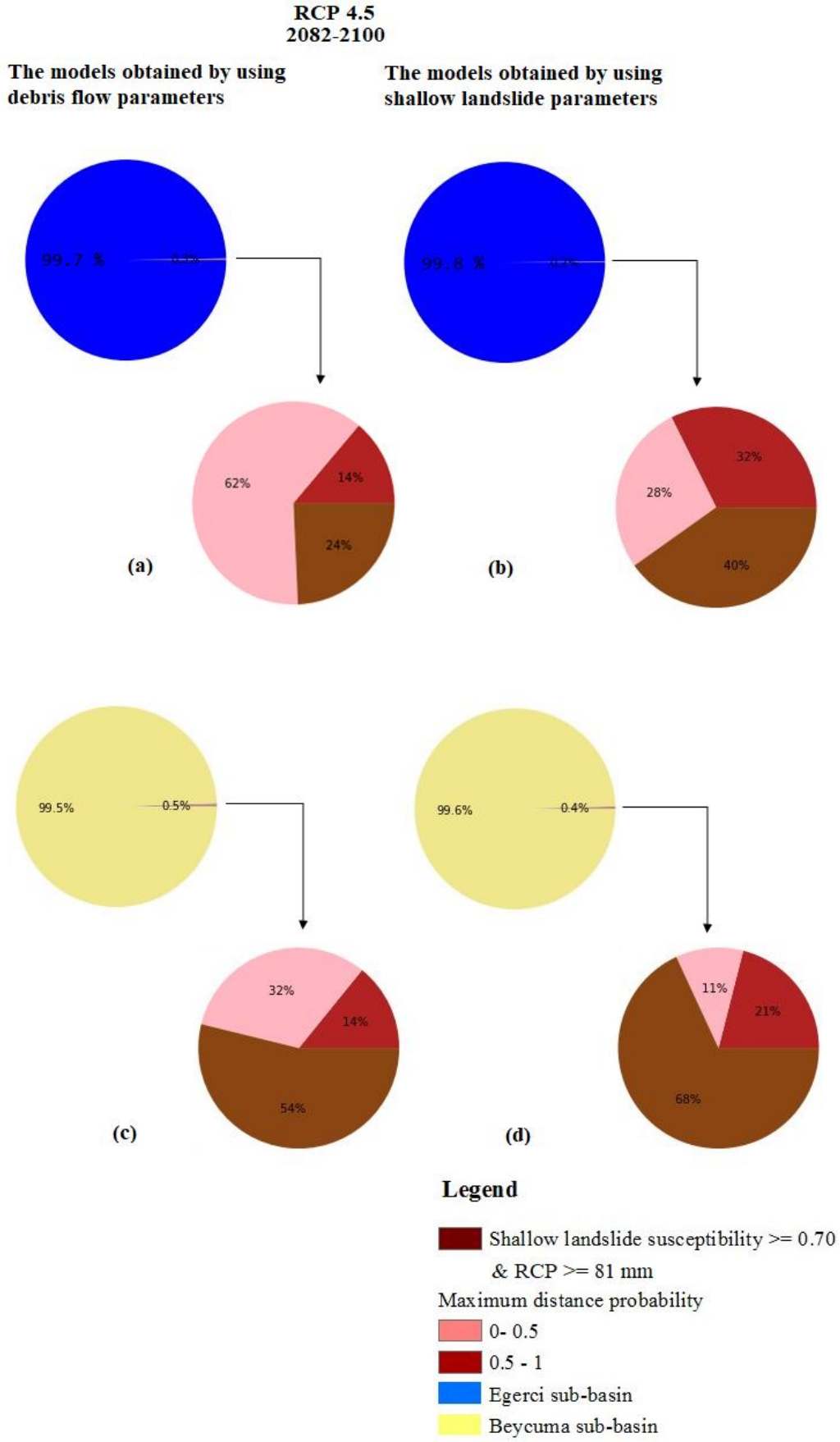

Figure 6.16. Pie charts of runout distances for RCP 4.5: 2082-2100.

Models have been carried out to decide future runout distances for the determined periods and, although possible hazard areas vary according to specifically detected shallow landslides initiations, the general trend is quite definite to decrease. To compare critical areas over the years, it is essential to analyse notable differences across all periods. Figure 6.17 and Figure 6.18 enable the examination of differences over the years in terms of runout distances for both model parameters. These figures are important to indicate the most critical locations for these years in both sub-basins in terms of shallow landslides occurrence and their possible runout distances. The runout impacted area will decrease in the period of 2025-2044 due to reducing in failure initiations and their runout distances, which can be explained with climate change severe influences on precipitations. Figure 6.17 shows that the Egerci sub-basin will be highly prone areas to shallow landslides runout distances for RCP 4.5: 2025-2044. It is also noticed that Egerci and Beycuma sub-basin share akin trends in determined periods in terms of reducing runout area. Under RCP 4.5 scenarios failure initiations in 2025-2044 will present more increases than under RCP 8.5 scenarios in Egerci sub-basin. In Beycuma sub basin, especially RCP 4.5 scenarios will be more different than RCP 8.5 scenarios. Shallow landslide initiations in RCP 4.5 scenario, which depends on RCP 4.5 precipitation values, are likely to decreases, downward trend is examinable from the Figure 6.18 for Beycuma sub-basin. Additionally, it can be inferred from the results that when an examination is conducted based on periods for both basins, the areas that could be potentially dangerous in terms of propagation distance are generally similar to each other determined periods, except for scenario RCP4.5: 2025-2044 (Figure 6.17 and Figure 6.18).

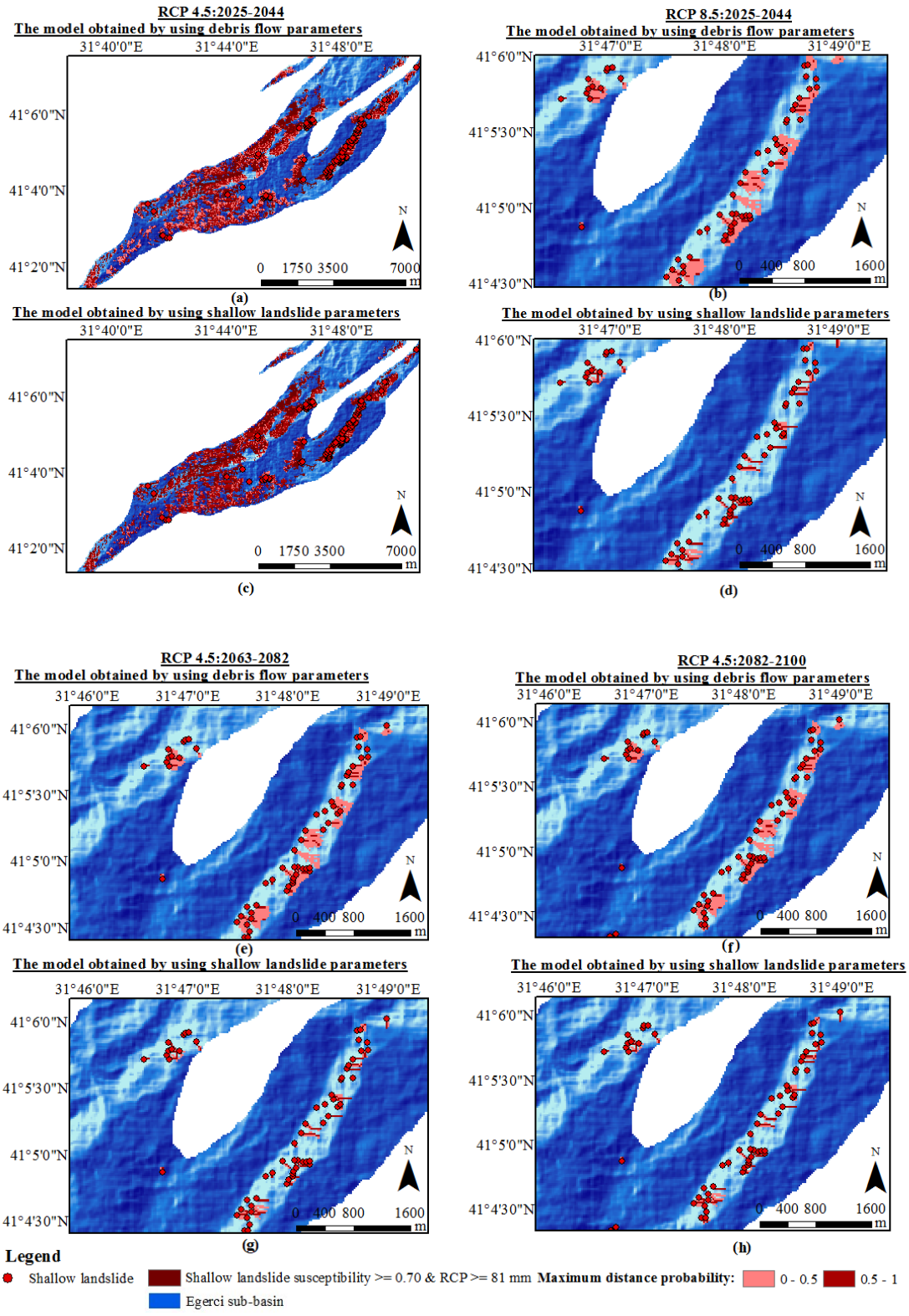

Figure 6.17. Runout models comparison in terms of diverged time period in Egerci sub-basin: (a, c) RCP 4.5: 2025-2044, (b, d) RCP 8.5: 2025-2044, (e, g) RCP 4.5: 2063-2082 and (f, h) RCP 4.5: 2082-2100 (Modified after Komu, Nefeslioglu and Gokceoglu, 2024).

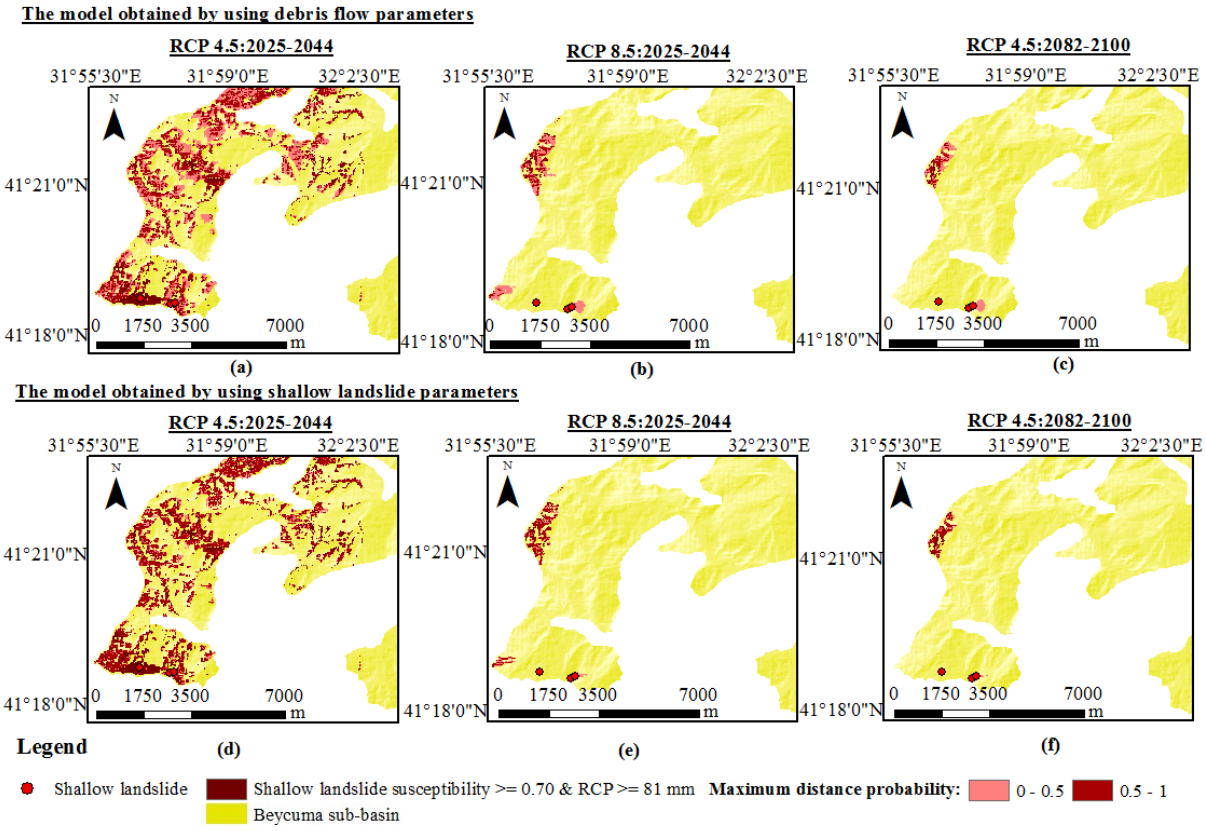

Figure 6.18. Runout models comparison in terms of diverged time period in Beycuma sub-basin: (a, d) RCP 4.5: 2025-2044, (b, e) RCP 8.5: 2025-2044, and (c, f) RCP 4.5: 2082-2100 (Komu, Nefeslioglu and Gokceoglu, 2024).

In this section of the thesis, the data from Table 6.5, Figure 6.19 and Figure 6.20 provide the opportunity to make numerical evaluations regarding the prepared maps in addition to observation-based evaluation previously made from the map figures. It is possible to make predictions about how the variation in runout distance areas trends by interpreting the distribution of shallow landslide areas since it cannot be negligible of the runout dependency on failure initiations. Probable runout impacted areas will decrease in sub-basins at the climate scenarios. The evidence substantiates that decline in the failure initiations lead to decrease in runout areas (Table 6.5). In addition, debris flow runout areas (146 km^2) are comparatively much higher than shallow landslides runout areas (101 km^2). It is expected for RCP 4.5: 2025-2044 that there is a small drop of approximately 1 km in debris flow runout area in Egerci sub-basin.

Table 6.5. Comparisons of runout areas for both parameters models in all sub-basins.

		Egerci sub-basin	**Beycuma sub-basin**	**Ihsanoglu sub-basin**
Debris flow runout area (km^2)	Initial Condition	19.7	50.7	75.8
	RCP 4.5 (2025-2044)	18.9	15.6	0
	RCP 8.5 (2025-2044)	0.52	1.3	0
	RCP 4.5 (2063-2082)	0.514	0	0
	RCP 4.5 (2082-2100)	0.52	0.756	0
Shallow landslide runout area (km^2)	Initial Condition	16.7	35.5	48.6
	RCP 4.5 (2025-2044)	16.1	10.9	0
	RCP 8.5 (2025-2044)	0.249	0.768	0
	RCP 4.5 (2063-2082)	0.243	0	0
	RCP 4.5 (2082-2100)	0.249	0.413	0

Figure 6.19 and 6.20 enabled to compare years in terms of identifying probable runout areas for both parameters set. The bar charts also compare the runout area of sub-basins in initial analyses and project future time intervals for RCP 4.5: 2025-2044, RCP 8.5: 2025-2044, RCP 4.5: 2063-2082 and RCP 4.5: 2082-2100. The decrease in the runout affected areas between initial conditions and the periods of RCP 4.5: 2025-2044 could be discernible. In the future RCP 4.5: 2025-2044 scenarios, Beycuma's runout area will be expected to moderately decrease, while Egerci's runout areas will be anticipated to remain relatively same. Unlike Egerci' and Beycuma's runout areas, Ihsanoglu' runout areas will never be observed for all future time interval for both model parameters results.

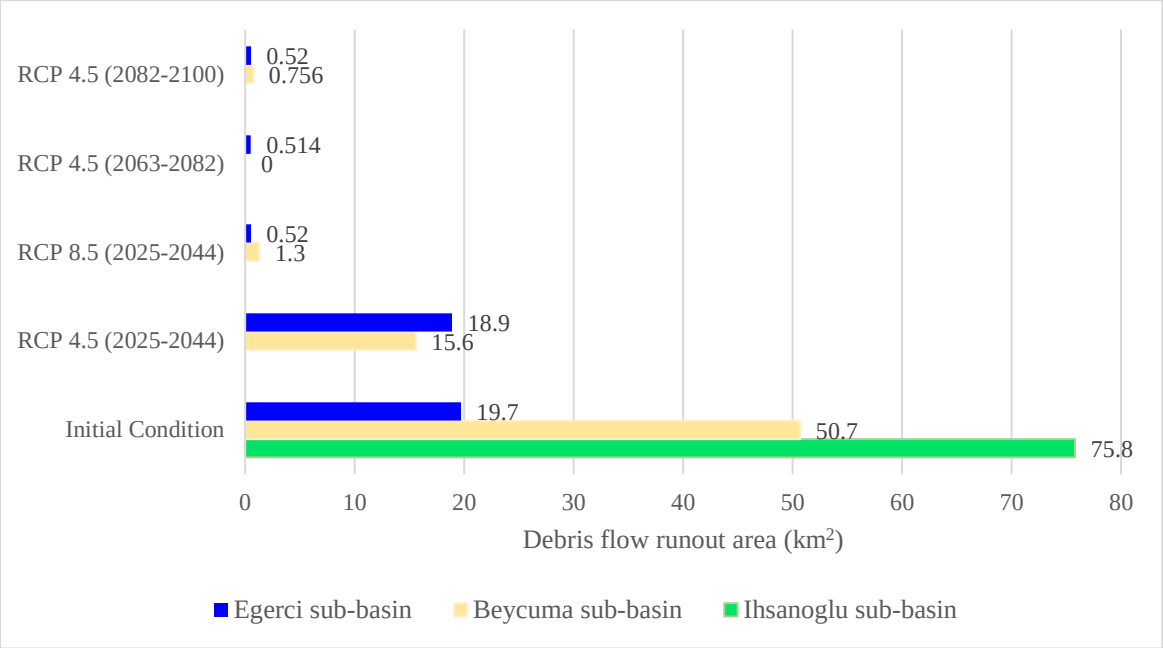

Figure 6.19. Graphical comparisons of debris flow runout areas for all sub-basins.

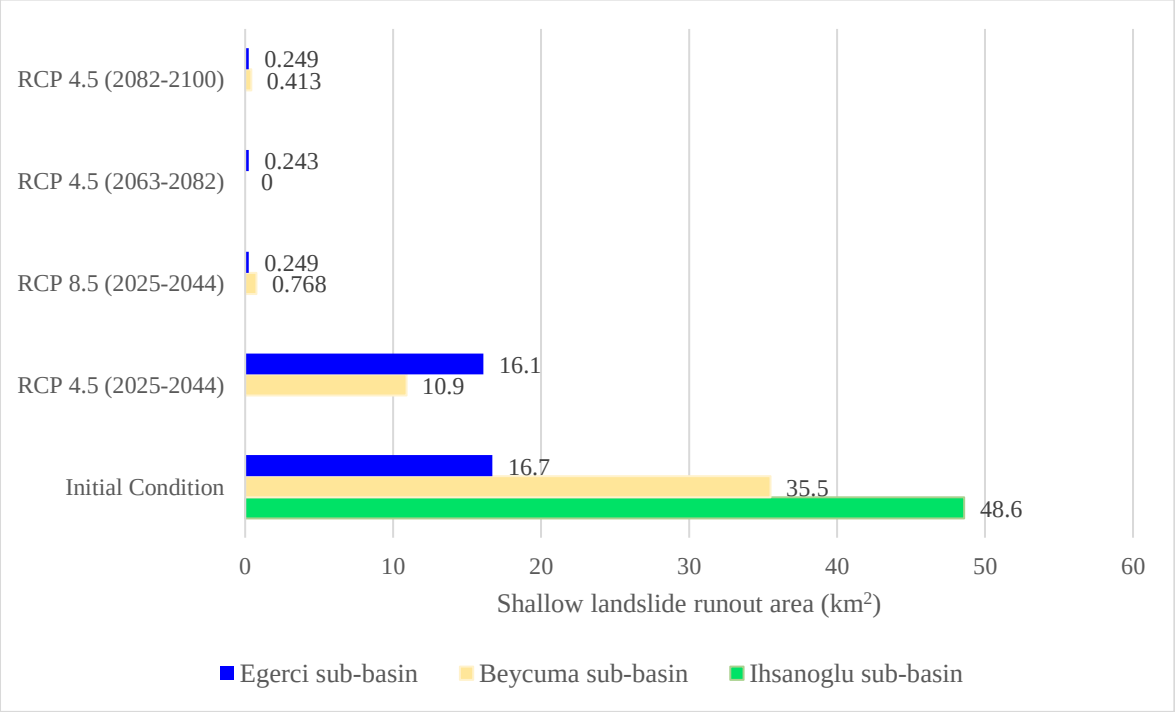

Figure 6.20. Graphical comparisons of shallow landslide runout areas for all sub-basins.

Finally, this section aimed to show whether the influence of RCP precipitation scenarios is questionable on shallow landslides runout distances or not. How the shallow landslides runout distances have changed at the specific location with respect to considering the RCP precipitation scenarios. It is possible to expect that the study area may be extensively damaged by shallow landslides in the future. It is possible to mention that it is a very critical improvement to predict future changes in runout distances of shallow landslides by considering empirical methods for linking with RCP precipitation scenarios. The model results offer valuable advice and guidance on the level of possible runout distances whether this is congruent with the level of hazards. The findings of this study can be valuable and crucial for governmental authorities, strategists, decision-makers, scholars, and land-use planners within the examined region for a better future by providing landslide safety (Wang, Otto and Scherer, 2021). The reliability of the outcome's hinges on the precision of the data and the methodology employed for data analysis (Wang, Otto and Scherer, 2021).

The results presented in this section are prepared according to the RCP models. Therefore, it should be warned that if the RCP scenarios do not unfold as expected, variations may occur in the outcomes.

7. DISCUSSSION

Shallow landslides have started to be considered severe natural disasters hazards in the present-day world. When a terrible landslide disaster event occurs, it is possible to observe that while residents are grappling with negative effects of shallow landslides challenges, researchers are trying to reap the benefits by collecting the shallow landslide related data in order to prepare detailed hazard map for future disasters. At this stage, it is pivotal for researchers to rigorously collect all data and consult residents' observations in order to prepare a shallow landslide inventory, as it will have an important role in the future studies. Runout distances of shallow landslides are also critical information for these researches because these key finds enable to take necessary measures. Therefore, a crucial perennial management plan that details how to deal with possible shallow landslides runout, can be effectively prepared without overlooking the details. Unless prepared detailed hazard maps which include runout distance, natural disaster of landslide may dangerous for citizens. This is a good example addressing the importance of this topic that while many developed countries have detailed hazard map, numbers of natural shallow landslides disaster victims are increasing in some countries where such hazard map is lacking. There are some critical points that need to be discussed for this study are summarized below:

Determining whether the prepared inventory is suitable for the characterization of shallow landslides was pivotal. Therefore, the relationships between the shallow landslide area, volume, runout distance, and depth were empirically calculated, providing evidence that supports the assertion of shallow landslides based on their depth. These analyses have bolstered the reliability of the inventory.

Determination of suitable runout distance method was necessary to achieve a correct shallow landslide moving. It is essential to acknowledge that the empirical method has given comprehensive performance with good prediction and less calculation time in this study. Empirical-statistical methods will continue to attract more attention and proliferate rapidly in the future runout distance assessments. Flow-R 1.0.0 software enabled to

prepare runout probability map. Thanks to Flow-R software, determination of runout probability significant improvements in runout analyses.

It should not be neglected that focusing of determination of shallow landslide initiations, which is a comprehensive survey, is the first and an important step in this study in order to accomplish an appropriate modelling stage. In fact, possible shallow landslide initiation detection and estimation of the propagations of shallow landslides initiations are integrated steps based on the shallow landslide susceptibility in this study. Machine learning logistic regression method for the landslide susceptibility map preparation was able to improve accuracy and efficiency in identifying possible failure initiations. Although Flow-R software enables to automatically detect initiations, it doesn't consider the effects of the rainfall, vegetation, and loose source materials (Yin, Zhou and Peng, 2023). Failure initiations were determined by Flow-R in the study of Horton et al. (2013), Park, Lee and Woo (2013), Jiang et al. (2021), Xu et al. (2022), Sharma et al. (2023), Giano, Pescatore and Siervo (2021), Charbel and El Hage Hassan (2021) and Do et al. (2020). In addition, user-defined initiations gave valuable results in the study of Pastorello, Michelini and D'Agostino (2017), McCoy (2019), Paudel (2019), Polat and Erik (2020), Ali et al. (2021), Bera, Melo and Guru (2021), Putra et al. (2022), and Liu et al. (2022). User-defined initiations by considering flow accumulation and slope gradient (Pastorello, Michelini and D'Agostino, 2017), the landslide susceptibility map (Paudel, 2019) and sentinel images (Putra et al., 2022), remote sensing and slope angle distribution (Ali et al., 2021) and GPS and multi-temporal satellite images (Bera, Melo and Guru, 2021), considering the landslide susceptibility map, and previous studies and D-InSAR technology (Liu et al., 2022). Note that shallow landslides initiations, were associated with the shallow landslide susceptibility >=0.70 and past detected shallow landslides, were used as user-defined initiations in this study. Shallow landslides initiations detection results indicate that broad-leaved forests are dominantly covering the shallow landslide initiations for Beycuma and Ihsanoglu sub-basin. Unlike the other two sub-basin, shallow landslides initiations coved by mixed forests stand out in Egerci sub-basin in the initial analyses. Recent runout model results also show that runout distances of shallow landslides have had potential extensive damages on both natural and human made systems. Although many highways, bridge, electrical transmission lines are designed to withstand the shallow landslides, severe shallow landslides may damage them. In fact,

shallow landslides directly threaten the safety of the not only transportation roads and but also residents. The shallow landslide occurrence is one of serious the geological disasters in the study area. Therefore, it is very critical to detection of vulnerable areas in terms of shallow landslides hazards. It has become clear that this area will need a master disaster management strategy.

In addition, the model results, based on the subject of climate change, which is another significant part of the dissertation, have been thoroughly examined in following statements. There has been observed many shallow landslides which are triggered because of extreme weather events in recent years. Therefore, it is necessary to investigate that whether there has been a salient increase the number of shallow landslides events or not. Climate researchers also warns that climate change would have wide ranging effects on shallow landslides. How a changing climate will affect shallow landslides runout distance is not only stay an important investigation question and but also briefly outlined by developing a practical approach in this study. On improving shallow landslides resilience in the face of climate change is possible by evaluating with RCP precipitation scenarios. Therefore, RCP precipitation scenarios were considered in this study analyses. Detection of potential runout distances of shallow landslides by connecting with RCP scenarios was particularly attractive to researcher to bring out the best that hazards will be estimated. It is possible to claim that the evaluation of the RCP precipitation values is valuable contribution to shallow landslides the future runout distance estimation in this study because this study offers a view about assessing climate change and shallow landslide runout topics together. These values were utilized together with previous detected probable initiations which were obtained from shallow landslides susceptibility analysis. RCP scenarios for climate change in Eocene flysch facies indicate a decrease in precipitations which will cause a decrease in shallow landslides initiations. It should be also noted that shallow landslides initiations depend on RCP scenarios precipitations changing at determined time ranges while keeping others criteria at their same values in this study. Therefore, the validity and suitability of the scenarios were deeply questioned. This part of the study reveals that in Ihsanoglu sub-basin, shallow landslides, which triggered by precipitation, will not occur since shallow landslides initiations will not be observable according to RCP precipitation scenarios in the all determined periods. The divergences between shallow landslides initiations which including the effects of RCP

4.5 and 8.5 precipitation scenarios for Egerci sub-basin and Beycuma sub-basin are clear. Landslide initiations decreased with time and became by far the least frequent or even absent event at the 2044-2063 period for sub-basins. However, when seen as a whole, it is apparent that possible landslide initiations will rise again after 2044-2063 timeframe in both sub-basins. Obtained results obviously indicate that short after a detection of failure initiations for possible landslide events, some areas will experience significant landslide runout distance, in the majority of periods, will reduce over time. Extreme precipitation events have become more frequently occur in Türkiye. However, it was revealed that if the general rainfall frequency tends to decrease, landslides frequency will also decrease. The proposed runout model can not only give a view of the examination of climate change by considering RCP scenarios precipitation values but also prove the model success by obtaining reasonably results in empirical methods. Therefore, obtained predictive models might assist in mitigating potential landslide hazards in the future. Nevertheless, there are some critical points that need to be separately emphasized in below:

First, the cautionary runout model results highlight potential shallow landslides runout distances associated with RCP scenarios. Therefore, it is possible to highlight that the implementation of preparation of hazard maps by integrate RCP precipitation scenarios and shallow landslides runout distances can give opportunity the deeper analyses.

Second, RCP precipitation runout models depends on the CCSM4 model data in this study. Unlike ensemble of models from CMIP5, CCSM4's monthly and annual data can be obtained from the NCAR website. However, CMIP5 data is also used many climate researches (Okkan and Kirdemir, 2016; Yunus et al., 2021; Wijaya et al., 2021; Jemec Auflič et al., 2023). If data which composed of ensemble of models from CMIP5, is used for this study, it should be considered and evaluated only annual data changes because of data availability or limitation. For instance, data can be obtained that annual precipitation data of 2025-2044 compared to the reference period 1986-2005 for CCSM4 and CMIP5. It is possible to find them by comparing data; however, CMIP5 needs initial precipitation so it leads to many blunders. Even if initial conditions can be assumed, make comparisons based on the data from the CCSM4 model.

Third, when separately conducting an assessment of CCSM4 RCP 4.5 and 8.5 scenarios annual data for shallow landslides initiations detection, although the omission of this study due to heightened uncertainty, requisite investigations have been undertaken.

Fourth, the longer sub-basins are exposed to precipitations, the more likely it is for them to become tended to occurring landslides. Therefore, it is not really surprising that landslides frequencies were high in the past. Comparisons of the extreme precipitation's values in May 1998 and November 2023, which triggered shallow landslides in the study area, were an important piece of evidence supporting the information about landslides frequency changes trends. Wang et al. (2024) showed evidence of frequency of shallow landslides occurring in 2014 was higher than the frequency of shallow landslides occurring in 2021 for their study area.

Fifth, among those three sub-basins, Ihsanoglu sub-basin were determined to have the highest impacted area from runout distances in the initial analyses. The sub-basin might not be affected by shallow landslides because possible shallow landslides initiations in this sub-basin could not detect to estimate probable mobility in the RCP precipitation scenarios. Nevertheless, Ihsanoglu sub-basin will be probably not affected the landslides problems in the future that it is a debatable topic because while other sub-basins will be affected landslide problem in the future, it is not possible. However, landslide frequency decrement is not surprise.

Finally, the prediction of the future runout distance possibilities with RCP climate change scenarios is a significant distinguishing feature of this study from other studies. On the other hand, it is necessarily highlighted that results were the broadcasted images with respect to probable runout distances based on RCP climate change scenarios by using empirical-statistical method. RCP 4.5 and 8.5 precipitation scenarios have direct effects on determination of shallow landslides initiations and their runout distances. Therefore, if future events deviate from the envisioned scenarios, the outcomes are susceptible to change in terms of both failure initiations and their runout distances.

Consequently, it is pivotal to highlighting that runout analyses have given rise to a comprehensive assessment in the study. Demonstration of shallow landslide runout may be the easiest way to resilience of the hazards. There is growing evidence that detecting of landslide runout distances enable to fix the problems because well visualised runout views can help researchers recognize whether they should take time to take precautions or not because preparation of hazard management framework is more necessary than previously thought in the landslide's literature. Therefore, this study vindicates that runout analysing is useful for future hazard management studies. This study also helps to acknowledge software contribution to analyses in terms of improving the excess time consumption at which researchers can evaluate the probability of runout distance of shallow landslides. Runout distances have not been ruled out in many studies. Taking into account the success of the analyses results, runout will be more considered in many researches because runout distance probability with susceptible areas enable to make taking decision on dangerous regions more practical.

7.1. Limitations of Study

All assessments made within the Ph.D. thesis are based on the detailed information provided in the relevant sections, relying on various sources, and the databases they have created as a result of these sources. All limitations applicable to these data, along with potential deficiencies and inaccuracies within the data, may impact the assessment results presented in this thesis. Furthermore, variations in such as topographic and climatic conditions over time due to natural processes and/or human factors might lead to differences in the results presented within the thesis. Undetected shallow landslides are a significant problem. Although disappearance of traces of some shallow landslides have challenged, many clues shallow landslides still exist to determine the runout distance of shallow landslides for back analyses. Preferred runout method might be also often considered to be extremely advantageous but in fact, they may have complex constructed process that are acknowledge as their disadvantages during the studies.

In addition, preparation of the susceptibility map, which have an important role in detection of failure initiations, was not attempted with other machine learning models rather than LR in this study. Although it is difficult to decide exact the best machine

learning approach to reliably forecast of landslide susceptibility mapping, several ML methods can be compared and selected optimal method (Ghasemian et al., 2022).

Moreover, DEM resolution is an important factor to accurately measure runout distances (Charbel and El Hage Hassan, 2021). Although a low spatial resolution is prevailing and acceptable such as 25 m among the researches, it should be noted that a high spatial resolution data such as 10 m is more accurate with respect to reliable estimation of runout distance (Horton et al., 2013). Models are also affected by variations in DEM data in this study. Working with very high-resolution data has led to the observation of events on the computer that were not predictable. If it is possible to possess a robust computational computer, more reliable results may also more promptly be provided. Furthermore, due to computational difficulties, it has been observed that dividing the area may be more adventageous. Runout distance results have also been examined by dividing the area into 5 and 7 sub-basins. Nevertheless, considering that the area does not show significantly different characteristics, it has been deemed appropriate to continue the research by dividing it into the minimum number of sub-basins. At this stage, the question of whether sub-basins can also be examined together has arisen by considering determined a criteria such as topography. However, as there was an intention to distinguish based on sub-topographic sub-basins, the areas within the divided basins did not decrease adequately. This is anticipated to pose computational challenges in the study.

In addition, in some small area observations in back analyses, determined failure initiations were not able to show propagation stage both at 10 m and 25 m spatial resolution in some areas. National or environmental features may stop the propagation by blocking and deflecting because DEM don’t show the bare Earth surface (Putra et al., 2022).

Moreover, Feranie et al. (2021) also claimed that volume might shows decreasing change, if the rainfall intensity increases in the area. It leads to decrease of shallow landslides runout distance and maximum velocity.

Furthermore, learning about relation between RCP precipitation and landslides runout in it is one of the best valuable research topics in landslides studies but there is a lot of uncertainties and downcaling bias in terms of RCP precipitation data. Considering the size of the study areas, it was not possible to use high resolution data because of the computation cost and time. Runout models, consist of RCP precipitation scenarios, assume that all other impact factors of landslides occurrence will remain unaltered. Kim, Yung and Kim (2023), Janizadeh et al. (2023) and Mohamed-Yusof et al. (2024) also discussed the same limitation in their study. They also only consider the climate change scenarios, while they neglect the other landslides occurrence factors changing. However, many factors might trigger the occurrence of shallow landslides and they might change. For instance, vegetation and human effects might cause change land use in the future. Although it was not accepted that some locations in the study area were no shallow landslide initiation points, they are likely to have shallow landslide initiation points. Roccati et al. (2021) also reached that approximately 80% of failures triggered by shallow landslides on slope gradients where no previous shallow landslides had been observed in their study area. These results warn researchers about similar type shallow landslides events and encourage to study on prioritize mitigation measures by considering these runout distance results.

8. CONCLUSION AND FUTURE WORK

8.1. Conclusions

Shallow landslides with long runout distances have increasingly jeopardized not only human safety and but also essential systems, facilities and infrastructures. This research presented a statistical-empirical runout distances modelling of shallow landslides in the Eocene flysch facies, Türkiye. Firstly, on the basis of short field survey, Google Earth imagenery, satellite images and previous studies, the shallow landslide inventory map was prepared. Secondly, Eocene flysch facies were divided into three sub-basins. They are Egerci, Beycuma and Ihsanoglu. It was also ensured that whether their statistical descriptions of the inventories are appropriate of the data resolution of the study or not. Thirdly, shallow landslides susceptibility maps were separately prepared for three sub-basins by using machine learning LR. Fourthly, shallow landslide susceptibility maps were utilized by determining the critical threshold so that probabilistic shallow landslide initiations can be detected and transformed into maps that enable to practically interpret their possible maximum runout distances. Some assumptions have been made to determine the threshold of the shallow landslide initiations from the susceptibility maps. 0.70 was assumed as the critical susceptibility value in order to be used as shallow landslides initiations in propagation analyses. Moreover, RCP 4.5 and 8.5 scenarios have been included in the work. Cells with both shallow landslide susceptibility greater than or equal to 0.70 and precipitation value greater than or equal to 81 mm were determined as shallow landslides initiations in RCP runout models. Finally, empirical-statistical models of shallow landslides were constructed in order to examine runout distances of them by calibrating the suitable parameter sets. The Modified Holmgren flow direction algorithm and SFLM parameters are a crucial indicator of the mobility in this dissertation. Runout analyses were implemented for two parameter configurations, which are debris flow and shallow landslide. While dh is equal to 1 in both model configurations, x was used as 4 and 25 for debris flows and shallow landslides, respectively in all sub-basins. Travel angles are 24º, 13º and 10º for Egerci, Beycuma and Ihsanoglu, respectively. The results of runout analyses were interpreted for both models with RCP and models without RCP. Main results are summarized as follows:

i. The detection of initial points of shallow landslides in this research was essential for observation of high runout probability zones.

ii. Although detected possible shallow landslides initiations generally tend to propagate, some initiations cannot be fully mobilized because of some reasons such as topographic obstacles.

iii. The debris flows and shallow landslides models can obtain more failure initiations with more runout distances during the initial propagation stage.

iv. The model results were tested whether the empirical runout model can correctly predict the observed runout distances. R-squared level of 0.64 and 0.62 were estimated for debris flows and shallow landslide models, respectively in Eocene flysch facies.

v. Shallow landslides initiations were ample in broad-leaved forests and mixed forests in the initial analyses. Shallow landslides initiations are generally at slope gradient degrees of 23, 15 and 13 for Egerci, Beycuma and Ihsanoglu, respectively. Additionally, in sub-basin Beycuma and Ihsanoglu, lower elevations can be considered as the initial points, while in sub-basin Egerci, the probability of shallow landslides occurring at higher elevations is higher in the initial analyses. It is necessary to recall that the studies defined as initial analyses are critical analyses that do not include RCP scenarios.

vi. When runout models by reckoning with RCP scenarios are analysed in terms of possible initiations' altitude, slope gradient and land cover, the probability of shallow landslides occurring in high-altitude areas will be higher in both Egerci and Beycuma sub-basins. In Beycuma sub-basin, significant changes in slope gradient values will be not expected at the initiation points of shallow landslide, while in the Egerci sub-basin, a significant decrease in slope gradient values compare to initial analyses will be expected. Also, it is reasonable to expect that broad-leaved forests will show decreasing trend in terms of occurring of shallow landslides in the future.

vii. Runout models were developed by considering climate change RCP scenarios. Climate changes will negatively affect the study areas in terms of rainfall triggered shallow landslides in Egerci and Beycuma sub-basins according to RCP 4.5 scenarios, especially in the 2025-2044 time period. Both analyses with RCP 4.5

and 8.5 scenarios indicate that shallow landslides initiations and their runout distances show decreasing trend in the future.

In conclusion, runout distances predictions with including RCP scenarios may offer insights into the future trajectory of disaster management in the study area. It is also believed that the results obtained from this study will contribute significantly to mitigation or preparedness strategies to be carried out by experts, aiming to circumvent the negative effects of future landslide events due to climate changes or alleviate potential losses them in the sub-basins by taking them into consideration. Therefore, it contributes to sustainable resilience of landslide hazard in this area. It will also be expected that researches which investigate the relationships between landslide runout distance and RCP scenarios, will brisk up gaining popularity among landslide researchers.

8.2. Recommendations for Further Works

It is believed that the applied methodology in this study contributes to the development of methods aimed at reducing landslide-induced damages at the sub-basin scale for future study. Prospective improvements, which can be suggested to be made in the future in order to get rid of this thesis scope's challenges and clarify the possible advancements by opening new horizons about this topic, are listed below:

i. Using different machine learning methods will be applied for this region in order to reach the best accuracy of the shallow landslide susceptibility map.
ii. If developing new climate models, which offer more detailed RCP daily forecast values, the threshold of RCP precipitation might be also investigated to get in-depth research by reaching more accurate value.
iii. PGA values in the study area show that earthquakes are the other possible reason for triggering shallow landslides. Therefore, this region can also be investigated in terms of earthquake-triggered landslide runout probability.
iv. This study area can also be investigated on wildfire triggered shallow landslides runout distances by detected of forest fire risk areas.

REFERENCES

Abraham, M.T., Satyam, N., Reddy, S.K.P. and Pradhan, B., Runout Modeling and Calibration of Friction Parameters of Kurichermala Debris Flow, India, Landslides, 18 (**2021**) 737–754.

Achu, A.L., Aju, C.D., Di Napoli, M., Prakash, P., Gopinath, G., Shaji, E.and Chandra, V., Machine-Learning Based Landslide Susceptibility Modelling with Emphasis on Uncertainty Analysis, Geoscience Frontiers, 14 (**2023**) 101657. https://doi.org/10.1016/j.gsf.2023.101657.

Adnan, M.S.G., Rahman, M.S., Ahmed, N., Ahmed, B., Rabbi, M.F. and Rahman, R.M. Improving Spatial Agreement in Machine Learning-Based Landslide Susceptibility Mapping, Remote Sens., 12 (**2020**) 3347. https://doi.org/10.3390/rs12203347

Ado, M., Amitab, K., Maji, A.K., Jasińska, E., Gono, R., Leonowicz, Z. and Jasiński, M. Landslide Susceptibility Mapping Using Machine Learning: A Literature Survey, Remote Sens., 14 (**2022**) 3029. https://doi.org/10.3390/rs14133029

AFAD, Earthquake Catalog (Available online: https://deprem.afad.gov.tr/event-catalog. Accessed on: **12 December 2023**)

AFAD Earthquake Hazard Map of Türkiye Interactive Web Application (Available online: https://www.turkiye.gov.tr/ Accessed on: **12 November 2022**)

Ageenko, A., Hansen, L.C., Lyng, K.L., Bodum, L. and Arsanjani, J.J., Landslide Susceptibility Mapping Using Machine Learning a Danish Case Study, ISPRS Int J Geo Inf, 11 (**2022**) 324. https://doi.org/10.3390/ijgi11060324

Ahmad Tarmizi, A. H., Rahmat, S.N., Abd Karim, A.T. and Tukimat, N.N.T., Climate Change and Its Impact on Rainfall, International Journal of Integrated Engineering, 11 (**2019**) 170–177.

Akbas, B., Akdeniz, N., Aksay, A., Altun, İ.E., Balcı, V., Bilginer, E., Bilgiç, T., Duru, M., Ercan, T., Gedik, İ., Günay, Y., Güven, İ.H., Hakyemez, H.Y., Konak, N., Papak, İ., Pehlivan, Ş., Sevin, M., Şenel, M., Tarhan, N., Turhan, N., Türkecan, A., Ulu, Ü., Uğuz, M.F., Yurtsever, A. and et al., 1:1250000 Olcekli Türkiye Jeoloji Haritasi: Maden Tetkik ve Arama Genel Mudurlugu Yayini, **2011**.

Akçakaya, A., Eskioğlu, O., Atay, H. and Demir, Ö., Yeni Senaryolarla Türkiye İçin İklim Değişikliği Projeksiyonları, Orman ve Su İşleri Bakanlığı Meteoroloji Genel Müdürlüğü Araştırma Dairesi Başkanlığı Klimatoloji Şube Müdürlüğü, Meteoroloji Genel Müdürlüğü Matbaası, **2013**. https://www.mgm.gov.tr/FILES/iklim/IKLIM_DEGISIKLIGI_PROJEKSIYONLARI.pdf

Akgun, A, Gorum, T. and Nefeslioglu, H., Landslide size distribution characteristics of cretaceous and eocene flysch assemblages in the Western Black Sea Region of Turkey, Understanding and Reducing Landslide Disaster Risk, Guzzetti, F., Arbanas, S.M. (Eds.), Springer, London, 299-303, **2021**. https://doi.org/10.1007/978-3-030-60227-7_33

Akinci, H., Assessment of Rainfall-Induced Landslide Susceptibility in Artvin, Turkey Using Machine Learning Techniques, Journal of African Earth Sciences 191 (**2022**) 104535. https://doi.org/10.1016/j.jafrearsci.2022.104535.

Aktas, H. and San, B.T., Landslide Susceptibility Mapping Using an Automatic Sampling Algorithm Based on Two Level Random Sampling, Computers & Geosciences: 133 (**2019**) 104329, https://doi.org/10.1016/j.cageo.2019.104329.

Alene, G.H., Vicari, H., Irshad, S., Perkis, A., Bruland, O. and Thakur, V., Realistic Visualization of Debris Flow Type Landslides Through Virtual Reality, Landslides, 20 (**2023**) 13–23. https://doi.org/10.1007/s10346-022-01948-x

Ali, S., Haider, R., Abbas, W., Basharat, M. and Reicherter, K., Empirical Assessment of Rockfall and Debris Flow Risk along the Karakoram Highway, Pakistan, Nat. Hazards, 106 (**2021**) 2437–2460. https://doi.org/10.1007/s11069-021-04549-4

Andrade, C.W.L., Montenegro, S.M.G.L., Montenegro, A.A.A., Lima, J.R.S., Srinivasan, R. and Jones, C.A., Climate Change Impact Assessment on Water Resources under RCP Scenarios: A Case Study in Mundaú River Basin, Northeastern Brazil, Int J Climatol.,41 (**2021**) E1045–E1061.

Andrewwinner, R. and Chandrasekaran, S.S., Investigation on the Failure Mechanism of Rainfall Induced Long-Runout Landslide at Upputhode, Kerala State of India, Land, 10 (**2021**) 1212. https://doi.org/10.3390/land10111212

Anjum, M.N., Ding, Y. and Shangguan, D., Simulation of the Projected Climate Change Impacts on the River Flow Regimes under CMIP5 RCP Scenarios in the Westerlies Dominated Belt, Northern Pakistan, Atmospheric Research, 227 (**2019**) 233-248.

Ansar, A.S., Sudha, S., Vinayagamoorthi, S., Menachery, M.M., and Francis, S., Landslide Classification and Prediction of Debris Flow Using Machine Learning Models, IETE Journal of Research, (**2023**) 1-17. DOI:10.1080/03772063.2023.2217802

Apriani, D.W., Credidi, C. and Khala, S., An Empirical-Statistical Model for Landslide Runout Distance Prediction in Indonesia, Tahun, 27 (**2022**) 1.

Araújo, J.R., Ramos, A.M., Soares, P.M.M., Melo, R., Oliveira, S.C. and Trigo R.M., Impact of Extreme Rainfall Events on Landslide Activity in Portugal Under Climate Change Scenarios, Landslides, 19 (**2022**) 2279–2293. https://doi.org/10.1007/s10346-022-01895-7

Arghya, A.B., Hawlader, B. and Guthrie, R., A comparison of two runout programs for debris flow assessment at the Solalex-Anzeindaz Region of Switzerland, Geohazard 8 Conference, 12-15 June, Quebec, Canada, **2022**.

Asada, H. and Minagawa, T., Impact of Vegetation Differences on Shallow Landslides: A Case Study in Aso, Japan, Water, 15 (**2023**) 3193. https://doi.org/10.3390/w15183193

Azarafza, M., Azarafza, M., Akgün, H., Atkinson, P.M. and Derakhshani, R., Deep Learning-Based Landslide Susceptibility Mapping, Scientific Reports, 11 (**2021**) 24112. https://doi.org/10.1038/s41598-021-03585-1

Baggio, T., Mergili, M. and D'Agostino, V., Advances in the Simulation of Debris Flow Erosion: The Case Study of the Rio Gere (Italy) Event of the 4th August 2017, Geomorphology, 381 (**2021**) 107664, https://doi.org/10.1016/j.geomorph.2021.107664.

Bainbridge, R., Lim, M., Dunning, S., Winter, M.G., Diaz-Moreno, A., Martin, J., Torun, H., Sparkes, B., Khan, M.W. and Jin, N., Detection and Forecasting of Shallow Landslides: Lessons from a Natural Laboratory, Geomatics, Natural Hazards and Risk, 13 **(2022)** 686-704, DOI: 10.1080/19475705.2022.2041108

Baumann, V., Wick, E., Horton, P. and Jaboyedoff, M. Debris flow susceptibility mapping at a regional scale along the National Road N7, Argentina, 2011 Pan-Am CGS Geotechnical Conference, 1-7 October, Toronto, Canada, **2011**.

Baselt, I., Queiroz de Oliveira, G., Fischer, J.-T. and Pudasaini, S.P., Evolution of Stony Debris Flows in Laboratory Experiments, Geomorphology, 372 (**2021**) 1–27.

Bekele, W.T., Haileand, A.T. and Rientjes, T., Impact of Climate Change on the Stream Flow of the Arjo-Didessa Catchment under RCP Scenarios, Journal of Water and Climate Change, 12 **(2021)** 2325-2337.

Bellugi, D.G., Milledgeb, D.G., Cuffeya, K.M., Dietricha, W.E. and Larsen, L.G., Controls on The Size Distributions of Shallow Landslides, PNAS, 118 (**2021**) e2021855118

Bera, S., Melo, R. and Guru, B., Assessment of Exposed Elements in a Changing Built Environment by Using an Integrated Model of Debris Flow Initiation and Runout (Kalimpong region, Himalaya), Bull. Eng. Geol. Environ., 80 (**2021**) 7131–7152. https://doi.org/10.1007/s10064-021-02352-w.

Bernardie, S., Vandromme, R., Thiery, Y., Houet, T., Grémont, M., Masson, F., Grandjean, G., and Bouroullec, I., Modelling Landslide Hazards Under Global Changes: the Case of a Pyrenean Valley, Nat. Hazards Earth Syst. Sci., 21 (**2021**) 147–169, https://doi.org/10.5194/nhess-21-147-2021.

Beroya-Eitner, M.A.A., Vicente, M.C.T.M., Dado, J.M.B., Dimain, M.R.S., Maquiling, J.T. and Cruz, F.A.T., Climate change as modifier of landslide susceptibility: case study in Davao Oriental, Philippines. In Progress in Landslide Research and

Technology, Alcántara-Ayala, I., et al. (Eds.), Vol. 2, Springer, Cham., **2023**. https://doi.org/10.1007/978-3-031-44296-4_12

Berti, M. and Simoni, A., DFLOWZ: A Free Program to Evaluate the Area Potentially Inundated by a Debris Flow, Comput. Geosci., 67 (**2014**) 14–23. https://doi.org/10.1016/j.cageo.2014.02.002

Bi, X., Fan, Q., He, L., Zhang, C., Diao, Y. and Han, Y., Analysis and Evaluation of Extreme Rainfall Trends and Geological Hazards Risk in the Lower Jinshajiang River, Appl. Sci., 13 (**2023**) 4021. https://doi.org/10.3390/app13064021

Blais-Stevens, A. and Behnia, P., Debris Flow Susceptibility Mapping Using a Qualitative Heuristic Method and Flow-R along the Yukon Alaska Highway Corridor, Canada, Nat. Hazards Earth Syst. Sci., 16 (**2016**) 449–462.

Bolliger, D., Schlunegger, F., and McArdell, B. W., Comparison of Debris Flow Observations, Including Fine-Sediment Grain Size and Composition and Runout Model Results, at Illgraben, Swiss Alps, Nat. Hazards Earth Syst. Sci., 24 (**2024**) 1035–1049. https://doi.org/10.5194/nhess-24-1035-2024

Calista, M., Menna, V., Mancinelli, V., Sciarra, N. and Miccadei, E., Rockfall and Debris Flow Hazard Assessment in the SW Escarpment of Montagna del Morrone Ridge (Abruzzo, Central Italy), Water, 12 (**2020**) 1206. https://doi.org/10.3390/w12041206

Can, T., Nefeslioglu, H.A., Gokceoglu, C., Sonmez, H. and Duman, T.Y., Susceptibility Assessments of Shallow Earthflows Triggered by Heavy Rainfall at Three Catchments by Logistic Regression Analyses, Geomorphology, 72 (**2005**) 250–271. https://doi.org/10.1016/j.geomorph.2005.05.011

Can, R., Kocaman, S. and Gokceoglu, C., A Comprehensive Assessment of XGBoost Algorithm for Landslide Susceptibility Mapping in the Upper Basin of Ataturk Dam, Türkiye, Appl. Sci., 11 (**2021**) 4993. https://doi.org/10.3390/app11114993

Cascini, L., Ciurleo, M. and Di Nocera, S., Soil Depth Reconstruction for the Assessment of the Susceptibility to Shallow Landslides in Fine-Grained Slopes, Landslides, 14 (**2017**) 459–471. https://doi.org/10.1007/s10346-016-0720-8

Cetinkaya, S., Ozcan N.T., Karakas G., Karakas, V. E., Kocaman, S., Gokceoglu, C., Frequency ratio assessment for landslıdes trıggered by 6 February 2023 Kahramanmaras Turkıye earthquakes between Golbası and Erkenek, International Archives of the Photogrammetry, Remote Sensing and Spatial Information Sciences, 39th International Symposium on Remote Sensing of Environment (ISRSE-39) “From Human Needs to SDGs”, 24–28 April 2023, Antalya, Türkiye, **2023**.

Chae, B.-G., Wu, Y.-H., Liu, K.-F., Choi, J. and Park, H.-J., Simulation of Debris-Flow Runout Near a Construction Site in Korea, Appl. Sci., 10 (**2020**) 6079. https://doi.org/10.3390/app10176079

Charbel, L. and El Hage Hassan, H., Mudflow Modeling Using Flow-R Software: Case Study of Ras Baalbek Basin (Lebanon), Geo-Eco-Trop, 45 (**2021**) 475–486.

Christen, M., Kowalski, J. and Bartelt, P., RAMMS: Numerical Simulation of Dense Snow Avalanches in Three-Dimensional Terrain, Cold Reg. Sci. Technol., 63 (**2010**) 1–14.

Chen, W., Chen, Y., Tsangaratos, P., Ilia, I. and Wang, X., Combining Evolutionary Algorithms and Machine Learning Models in Landslide Susceptibility Assessments, Remote. Sens., 12 (**2020a**) 3854.

Chen, L., Mei, L., Zeng, B., Yin, K., Shrestha, D.P. and Du, J., Failure Probability Assessment of Landslides Triggered by Earthquakes and Rainfall: A Case Study in Yadong County, Tibet, China, Sci. Rep., 10 (**2020b**) 16531. https://doi.org/10.1038/s41598-020-73727-4

Chen, Y., Chen, E., Zhang, J., Zhu, J., Xiao, Y. and Dai, Q., Investigation of Model Uncertainty in Rainfall-Induced Landslide Prediction under Changing Climate Conditions, Land, 12 (**2023**) 1732. https://doi.org/10.3390/land12091732

Ciervo, F., Rianna, G., Mercogliano, P. and Papa, M.N., Effects of Climate Change on Shallow Landslides in a Small Coastal Catchment in Southern Italy, Landslides, 14 (**2017**) 1043–1055. https://doi.org/10.1007/s10346-016-0743-1

Clark, B., Numerical Modelling of Debris Flow Hazards Using Computational Fluid Dynamics, Master's Thesis, Norwegian University of Science and Technology, Department of Civil and Environmental Engineering, Trondheim, Norway, **2018**.

Colorado Geological Survey, Debris and Mud Flows, https://coloradogeologicalsurvey.org/hazards/debris-flows/ (Accessed on: **21 April 2024**).

Conforti, M. and Ietto, F., Modeling Shallow Landslide Susceptibility and Assessment of the Relative Importance of Predisposing Factors, through a GIS-Based Statistical Analysis, Geosciences, 11 (**2021**) 333. https://doi.org/10.3390/geosciences11080333

CORINE Land Cover Change 2012-2018 (vector/raster 100 m), Europe, 6-yearly, CLC 2018 version v2020 20u1, https://land.copernicus.eu/pan-european/corine-land-cover/lcc-2012-2018?tab=download. (Accessed on: **16 August 2022**).

Corominas, J., The Angle of Reach as a Mobility Index for Small and Large Landslides, Canadian Geotechnical Journal, 33 (**1996**) 260–271. doi:10.1139/t96-005.

Crawford, M.M., Dortch, J.M., Koch, H.J., Killen, A.A., Zhu, J., Zhu, Y., Bryson, L.S. and Haneberg, W.C. Using Landslide-Inventory Mapping for a Combined Bagged-Trees and Logistic-Regression Approach to Determining Landslide Susceptibility in Eastern Kentucky, USA, Q. J. Eng. Geol. Hydrogeol., 54 (**2021**). https://doi.org/10.1144/qjegh2020-177

Crawford, M.M., Dortch, J.M., Koch, H.J., Zhu, Y., Haneberg, W.C., Wang, Z. and Bryson, L.S., Landslide Risk Assessment in Eastern Kentucky. USA: Developing a Regional Scale, Limited Resource Approach, Remote Sens., 14 (**2022**) 6246. https://doi.org/10.3390/rs14246246

Cruden, D.M., Varnes, D., Landslide types and processes. Landslides investigation and mitigation. Transportation research board UNRC (Eds.) Special Re., Washington, DC, 36–75, **1996**.

Cuomo, S., Modelling of Flowslides and Debris Avalanches in Natural and Engineered Slopes: A Review, Geoenviron Disasters, 7 (**2020**). https://doi.org/10.1186/s40677-019-0133-9

Çan, T., Duman, T.Y., Olgun, Ş., Çörekçioğlu, Ş., Karakaya Gülmez, F., Elmacı, H., Semi Hamzaçebi, S. and Emre, Ö., Türkiye heyelan veri tabanı, TMMOB Coğrafi Bilgi Sistemleri Kongresi, 11-13 Kasım, Ankara, Türkiye, **2013**.

Dash, R.K., Kanungo, D.P. and Malet, J.P., Runout Modelling and Hazard Assessment of Tangni Debris Flow in Garhwal Himalayas, India, Environ Earth Sci., 80 (**2021**) 338. https://doi.org/10.1007/s12665-021-09637-z

Dashbold, B., Bryson, L.S. and Crawford, M.M., Landslide Hazard and Susceptibility Maps Derived from Satellite and Remote Sensing Data Using Limit Equilibrium Analysis and Machine Learning Model, Nat. Hazards, 116 (**2022**) 235–265. https://doi.org/10.1007/s11069-022-05671-7

Demircan, M., Gürkan, H., Eskioğlu, O., Arabaci, H. and Coşkun, M., Climate Change Projections for Turkey: Three Models and Two Scenarios, Turkish Journal of Water Science & Management, 1 (**2017**) 22-43.

Dias, V.C., Dias, H.C. and Grohmann, C.H., Rainfall-Induced Debris Flows and Shallow Landslides in Ribeira Valley, Brazil: Main Characteristics and Inventory Mapping, E3S Web of Conf., 415 (**2023**) 05003. https://doi.org/10.1051/e3sconf/202341505003

Dias, H.C. and Grohmann, C.H., Standards for Shallow Landslide Identification in Brazil: Spatial Trends and Inventory Mapping, Journal of South American Earth Sciences, 135 (**2024**) 104805. https://doi.org/10.1016/j.jsames.2024.104805.

Di Napoli, M., Martire, D.D., Bausilio, G., Calcaterra, D., Confuorto, P., Firpo, M., Pepe, G. and Cevasco, A., Rainfall-Induced Shallow Landslide Detachment, Transit and Runout Susceptibility Mapping by Integrating Machine Learning Techniques and GIS-based Approaches, Water, 13 (**2021**) 488. https://doi.org/10.3390/w13040488

Djukem, D.L.W., Fan, X., Braun, A., Fan, X., Braun, A., Chevalier, M.-L., Wang, X., Dai, L., Fang, C., Zhang, X., Gorum, T., Qiang Xu, Q. and Havenith H.-B., Traditional and Modified Newmark Displacement Methods After The 2022 Ms 6.8 Luding Earthquake (Eastern Tibetan Plateau), Landslides, 21 (**2024**) 807–828. https://doi.org/10.1007/s10346-023-02194-5

Do, H.M., Yin, K.L. and Guo, Z.Z., A Comparative Study on The Integrative Ability of the Analytical Hierarchy Process, Weights of Evidence and Logistic Regression Methods with the Flow-R Model for Landslide Susceptibility Assessment, Geomat. Nat. Haz. Risk, 11 (**2020**) 2449–2485. https://doi.org/10.1080/19475705.2020.1846086

Doulabian, S., Golian, S., Toosi, A.S. and Murphy, C., Evaluating the Effects of Climate Change on Precipitation and Temperature for Iran Using RCP Scenarios, Journal of Water and Climate Change,12 (**2021**) 166–184.

Duman, T.Y., Emre, Ö., Akçay, A.E., Uysal, Ş., Özmutaf, M., Bozbay, E., Tongal, O. and Sönmez, M., Arazi Kullanım Kapasitesi Belirleme Çalışmalarında Yerbilim Verilerinin Uygulanmasına Bir Örnek: Aşağı Filyos Vadisi (Zonguldak, Batı Karadeniz), Geological Bulletin of Turkey, 41 (**1998**) 117-129.

Duman, T., Emre, O., Can, T., Nefeslioglu, H.A., Kecer, M., Dogan, A., Durmaz, S. and Ates, S., Türkiye Heyelan Envanteri Haritasi, 1/500,000 olcekli Zonguldak Paftasi, Maden Tetkik ve Arama Genel Mudurlugu (MTA) Ozel Yayinlar Serisi, 4a (**2005a**).

Duman, T.Y., Can, T., Emre, O., Kecer, M., Dogan, A., Ates, S. and Durmaz, S., Landslide Inventory of Northwestern Anatolia, Turkey, J. Eng. Geol., 77 (**2005b**) 99–114. https://doi.org/10.1016/j.enggeo.2004.08.005

Duman, T.Y., Can, T. and Emre, O., 1/1500000 Olcekli Türkiye Heyelan Envanteri Haritasi, Maden Tetkik ve Arama Genel Mudurlugu (MTA) Ozel Yayinlar Serisi, 27 (**2011**).

Durmaz, M., Hürlimann, M., Huvaj, N. and Medina, V., Comparison of Different Hydrological and Stability Assumptions for Physically-Based Modeling of Shallow Landslides, Engineering Geology, 323 (**2023**) 107237, https://doi.org/10.1016/j.enggeo.2023.107237.

Emre, Ö., Duman, T.Y., Özalp, S., Şaroğlu, F., Olgun, Ş., Elmacı, H. and Çan, T., Active Fault Database of Türkiye, Bull Earthquake Eng., 16 (**2018**) 3229–3275. https://doi.org/10.1007/s10518-016-0041-2

Ercanoglu, M. and Gokceoglu, C., Use of Fuzzy Relations to Produce Landslide Susceptibility Map of a Landslide Prone Area (West Black Sea Region, Turkey), Engineering Geology, 75 (**2004**) 229-250, https://doi.org/10.1016/j.enggeo.2004.06.001.

Erskine, R., Green, T., Ramirez, J., and MacDonald, L., Comparison of Grid-Based Algorithms for Computing Upslope Contributing Area, Water Resour. Res., 42 (**2006**) W09416, doi:10.1029/2005WR004648.

Esri, Basin (Spatial Analyst) https://pro.arcgis.com/en/pro-app/latest/tool-reference/spatial analyst/basin.htm#:~:text=The%20drainage%20basins%20are%20created,a%20ra

ster%20of%20drainage%20basins. (Accessed on: **25**(Accessed on: **16 August 2022**). **May 2022**).

European Commission, New Decade Brings Reference Period Change for Climate Data. https://climate.copernicus.eu/new-decade-brings-reference-period-change-climate-data (Accessed on: **09 October 2022**).

Fairfield, J. and Leymarie, P., Drainage Networks from Grid Digital Elevation Models, Water Resour. Res., 27 (**1991**) 709–717, doi:10.1029/90WR02658.

Falconi, L.M., Moretti, L., Puglisi, C. and Righini, G., Debris and Mud Flows Runout Assessment: A Comparison Among Empirical Geometric Equations in the Giampilieri and Briga Basins (East Sicily, Italy) Affected by the Event of October 1, 2009, Nat. Hazards, 117 (**2023**) 2347–2373. https://doi.org/10.1007/s11069-023-05945-8

Fan, X., Liu, B., Luo, J., Pan, K., Han, S. and Zhou, Z., Comparison of Earthquake-Induced Shallow Landslide Susceptibility Assessment Based on Two-Category LR and KDE-MLR., Sci. Rep., 13 (**2023**) 833. https://doi.org/10.1038/s41598-023-28096-z

Feranie, S., Khoiriyah, T.M., Jabbar, F.D.E and Tohari, A., The Effect of Rainfall Intensity to Landslide Run-Out Prediction and Velocity: A Parametric Study on Landslide Zones in West Java-Indonesia, Journal of Southwest Jiaotong University, 56 (**2021**) 6.

Ferrer, J., Guo, Z., Medina, V., Puig-Polo, C. and Hürlimann, M., A Framework to Project Future Rainfall Scenarios: An Application to Shallow Landslide-Triggering Summer Rainfall in Wanzhou County China, Water, 14 (**2022**) 873. https://doi.org/10.3390/w14060873

Fischer, F.V., Keiler, M. and Zimmermann, M., Modelling of individual debris flows using Flow-R: a case study in four Swiss Torrents, 13th INTERPRAEVENT Conference Proceedings, 30 May-2 June, Lucerne, Switzerland, **2016**.

Fischer, J.-T., Kofler, A., Huber, A., Fellin, W., Mergili, M. and Oberguggenberger, M., Bayesian Inference in Snow Avalanche Simulation with r.avaflow, Geosciences, 10 (**2020**) 191. https://doi.org/10.3390/geosciences10050191

Fornes, P., Bihs, H., Thakur, V. and Nordal, S., Implementation of non-newtonian rheology for debris flow simulation with Reef3d, E-proceedings of the 37th IAHR World Congress, 13 – 18August, Kuala Lumpur, Malaysia, **2017**.

Freeman, T.G., Calculating Catchment Area with Divergent Flow Based on a Regular Grid, Comput. Geosci., 17 (**1991**) 413–422. doi:10.1016/0098-3004(91)90048-I, 1991

Froude, M.J. and Petley, D., Global Fatal Landslide Occurrence from 2004 to 2016, Nat. Hazards Earth Syst. Sci., 18 (**2018**) 2161–2181.

Gaidzik, K. and Ramírez-Herrera, M.T., The Importance of Input Data on Landslide Susceptibility Mapping, Sci. Rep., 11 (**2021**) 19334. doi: 10.1038/s41598-021-98830-y.

Gamma, P., dfwalk – Ein Murgang-Simulationsprogramm zur Gefahrenzonierung. *Geographica Bernensia* G66, University of Bern, In German, **2000**.

Gan, J.J. and Zhang, Y.X., Numerical Simulation of Debris Flow Runout Using Ramms: A Case Study of Luzhuang Gully in China, CMES, 121 (**2019**) 981-1009. doi: 10.32604/cmes.2019.07337

Gao, C., Booij, M.J. and Xu, Y.-P., Impacts of Climate Change on Characteristics of Daily-Scale Rainfall Events based on Nine Selected GCMs under Four CMIP5 RCP Scenarios in Qu River basin, East China, Int J Climatol.,40 (**2020**) 887–907.

Gao, Y., Li, B., Zhang, H., Wu, W., Li, J. and Yin, Y., Numerical Modeling of Mixed Two-Phase in Long Runout Flow-Like Landslide Using LPF3D, Landslides (**2023a**). https://doi.org/10.1007/s10346-023-02159-8948/2006/0130.

Gao, Y., Li, J., Liu, X., Wu, W., Zhang, H. and Liu, P., Deformation Monitoring and Dynamic Analysis of Long-Runout Bedding Landslide Based on InSAR and Particle Flow Code, Remote Sens., 15 (**2023b**) 5105.https://doi.org/10.3390/rs15215105

Gariano, S.L. and Guzzetti, F., Landslides in a Changing Climate, Earth-Science Reviews, 162 (**2016**) 227-252, https://doi.org/10.1016/j.earscirev.2016.08.011.

Ghasemian, B., Shahabi, H., Shirzadi, A., Al.-Ansari., N., Jaafari, A., Geertsema, M., Melesse, A.M., Singh, S.K. and Ahmad, A., Application of a Novel Hybrid Machine Learning Algorithm in Shallow Landslide Susceptibility Mapping in a Mountainous Area, Front. Environ. Sci., 10 (**2022**) 897254. doi: 10.3389/fenvs.2022.897254.

Giano, S.I., Pescatore, E. and Siervo, V., Morphometry and Debris-Flow Susceptibility Map in Mountain Drainage Basins of the Vallo Di Diano, Southern Italy, Remote Sens., 13 (**2021**) 3254. https://doi.org/10.3390/rs13163254

Giarola, A., Meisina, C., Tarolli, P., Zucca, F., Galve, J.P. and Massimiliano Bordoni, A Data-Driven Method for the Estimation of Shallow Landslide Runout, CATENA, 234 (**2024**) 107573, https://doi.org/10.1016/j.catena.2023.107573.

Goetz, J., Kohrs, R., Parra Hormazábal, E., Bustos Morales, M., Araneda Riquelme, M. B., Henríquez, C., and Brenning, A., Optimizing and Validating the Gravitational Process Path Model for Regional Debris-Flow Runout Modelling, Nat. Hazards Earth Syst. Sci., 21 (**2021**) 2543–2562. https://doi.org/10.5194/nhess-21-2543-2021

Gokceoglu, C., Sonmez, H., Nefeslioglu, H.A., Duman, T.Y. and Can, T., The 17 March 2005 Kuzulu Landslide (Sivas, Turkey) and Landslide-Susceptibility Map of its Near Vicinity, Engineering Geology, 81 (**2005**) 65-83. https://doi.org/10.1016/j.enggeo.2005.07.011.

Gokceoglu, C., 6 February 2023 Kahramanmaraş – Türkiye Earthquakes: A general overview, The International Archives of the Photogrammetry, Remote Sensing and Spatial Information Sciences, 39th International Symposium on Remote Sensing of Environment (ISRSE-39), 24–28 April, Antalya, Türkiye, **2023**.

Google Earth Pro, https://www.google.com/earth/about/versions/#earth-pro (Accessed on: **10 March 2024**).

Gorr, A.N., McGuire, L.A., Youberg, A.M. and Rengers, F.K., A Progressive Flow-Routing Model for Rapid Assessment of Debris-Flow Inundation, Landslides, 19 (**2022**) 2055–2073. https://doi.org/10.1007/s10346-022-01890-y.

Gökçe, O., Bayındırlık ve İskan Bakanlığı Afet İşleri Genel Müdürlüğü Afet Etüt ve Hasar Tespit Dairesi İmar Planına Esas Jeolojik Jeoteknik Etüt ve PROJELER Şubesi, Projeler Şefliği, **2008**. (Accessed on: **21 March 2024**) https://www.afad.gov.tr/kurumlar/afad.gov.tr/3506/xfiles/96-2014060215311-heyelan_yogunluk_a1_olceksiz.pdf

Görüm, T., Tectonic, Topographic and Rock-Type Influences on Large Landslides at the Northern Margin of the Anatolian Plateau, Landslides, 16 (**2019**) 333–346. https://doi.org/10.1007/s10346-018-1097-7

Görüm, H., Tanyas, H., Karabacak, F., Yılmaz, A., Girgin, S., Allstadt, K.E, Süzen, M. L. and Burgi, P., Preliminary Documentation of Coseismic Ground Failure Triggered by the February 6, 2023 Türkiye Earthquake Sequence, Engineering Geology, 327 (**2023**) 107315. https://doi.org/10.1016/j.enggeo.2023.107315

Gregoretti, C., Degetto, M. and Boreggio, M., GIS-Based Cell Model for Simulating Debris Flow Runout on a Fan, Journal of Hydrology, 534 (**2016**) 326–340.

Gu, F., Chen, J., Sun, X., Li, Y., Zhang, Y. and Wang, Q., Comparison of Machine Learning and Traditional Statistical Methods in Debris Flow Susceptibility Assessment: A Case Study of Changping District, Beijing, Water, 15 (**2023**) 705. https://doi.org/10.3390/w15040705

Gumus, B., Oruc, S., Yucel, I. and Yilmaz, M.T., Impacts of Climate Change on Extreme Climate Indices in Türkiye Driven by High-Resolution Downscaled CMIP6 Climate Models, Sustainability, 15 (**2023**) 7202. https://doi.org/10.3390/su15097202

Guo, J., Wang, J., Li, Y. and Yi, S., Discussions on the Transformation Conditions of Wangcang Landslide-Induced Debris Flow, Landslides, 18 (**2021**) 1833–1843. DOI 10.1007/s10346-021-01650-4

Guo, J., Cui, Y., Xu, W., Yin, Y., Li, Y. and Jin, W., Numerical Investigation of the Landslide-Debris Flow Transformation Process Considering Topographic and Entrainment Effects: A Case Study, Landslides, 19 (**2022**) 773–788. https://doi.org/10.1007/s10346-021-01791-6

Guo, Z., Ferrer, J.V., Hürlimann, M., Medina, V., Puig-Polo, C., Yin, K. and Huang, D., Shallow Landslide Susceptibility Assessment under Future Climate and Land Cover

Changes: A Case Study from Southwest China, Geosci. Front., 14 (**2023**) 101542. https://doi.org/10.1016/j.gsf.2023.101542

Guthrie, R.H., Deadman, P., Cabrera, R. and Evans. S.G., Exploring the Magnitude-Frequency Distribution: A Cellular Automata Model for Landslides, Landslides, 5 (**2008**) 151–159. https://doi.org/10.1007/s10346-007-0104-1

Guthrie, R. and Befus, A. DebrisFlow Predictor: an Agent-Based Runout Program for Shallow Landslides, Nat. Hazards Earth Syst. Sci., 21 (**2021**) 1029–1049. https://doi.org/10.5194/nhess-21-1029-2021

Haque, U., da Silva, P.F., Devoli, G., Pilz, J., Zhao, B., Khaloua, A., Wilopo, W., Andersen, P., Lu, P., Lee, J., Yamamoto, T., Keellings, D., Wu, J.-H., Glassand, G.E., The Human Cost of Global Warming: Deadly Landslides and Their Triggers (1995–2014), Sci. Total Environ., 682 (**2019**) 673–684.

Havenith, H.-B., Guerrier, K., Schlögel, R., Braun, A., Ulysse, S., Mreyen, A.-S., Victor, K.-H., Saint-Fleur, N., Cauchie, L., Boisson, D., and Prépetit, C., Earthquake-Induced Landslides in Haiti: Analysis of Seismotectonic and Possible Climatic Influences, Nat. Hazards Earth Syst. Sci., 22 (**2022**) 3361–3384. https://doi.org/10.5194/nhess-22-3361-2022

Heim, A., 1932 Bergsturz und Menschenleben (Landslides and Human Lives), (English translation by Skermer, N.), BiTech Publishers, Vancouver, B.C., **1989**.

Hien, D.M., Hoang, N.V., Dung, M.L., Dung, L.H., Thuy, N.T., Hang, V.T., Large-scale Mapping of Landslide and Debris Flow using Flowr Model with Statistical and Machine Learning Methods, VNU Journal of Science: Earth and Environmental Sciences, 38 (**2022**) 39-62.

Holmgren, P., Multiple Flow Direction Algorithms for Runoff Modelling in Grid Based Elevation Models: an Empirical Evaluation, Hydrol. Process, 8 (**1994**) 327–334. https://doi.org/10.1002/hyp.3360080405

Hong, M., Jeong, S. and Kim, J., A Combined Method for Modeling the Triggering and Propagation of Debris Flows, Landslides, 17 (**2020**) 805–824. https://doi.org/10.1007/s10346-019-01294-5

Horton, P., Jaboyedoff, M., Rudaz, B. and Zimmermann, M., Flow-R, a Model for Susceptibility Mapping of Debris Flows and other Gravitational Hazards at a Regional Scale, Nat. Hazards, 13 (**2013**) 869–885. https://doi.org/10.5194/nhess-13-869-2013

Horton, P., Oppikofer, T. and Michoud, C., Introduction to Flow R Online tutorial © Terranum Ltd., https://www.terranum.ch/en/products/flow-r/ (Accessed on: **10 August 2022**).

Hovius, N., Stark, C.P. and Allen, P.A., Sediment Flux from a Mountain Belt Derived by Landslide Mapping, Geology 25 (**1997**) 231–234.

Huber, A., Kofler, A., Fischer, J.-Th., Kleemayr K. Projektbericht DAKUMO. Bundesforschungszentrum für Wald (BFW), Innsbruck., **2017**.

Huggel, C., Kaab, A., Haeberli, W., Teysseire, P., and Paul, F., Remote Sensing Based Assessment of Hazards from Glacier Lake Outbursts: A Case Study in the Swiss Alps, Can. Geotech. J., 39 (**2002**) 316–330, doi:10.1139/t01-099.

Huggel, C., Kääb, A., Haeberli, W., and Krummenacher, B., Regional-Scale GIS-Models for Assessment of Hazards from Glacier Lake Outbursts: Evaluation and Application in the Swiss Alps, Nat. Hazards Earth Syst. Sci., 3 (**2003**) 647–662. https://doi.org/10.5194/nhess-3-647-2003,

Hungr, O. and McDougall, S., Two Numerical Models for Landslide Dynamic Analysis, Comput. Geosci., 35 (**2009**) 978–992.

Hussain, M.A., Chen, Z., Zheng, Y., Zhou, Y. and Daud, H., Deep Learning and Machine Learning Models for Landslide Susceptibility Mapping with Remote Sensing Data, Remote Sens., 15 (**2023**) 4703. https://doi.org/10.3390/rs15194703

Iverson, R.M., Scaling and Design of Landslide and Debris-Flow Experiments: Geomorphology, 244 (**2015**) 9–20.

İRAP, Bartın İl Afet Risk Azaltma Planı, **2022**.

İRAP, Zonguldak İl Afet Risk Azaltma Planı, **2021**.

Jaboyedoff, M., Rudaz, B., and Horton, P., Concepts and parameterization of Perla and FLM model using Flow-R for debris flow, Proceedings of the 5th Canadian Conference on Geotechnique and Natural Hazards, 15–17 May, Kelowna, BC, Canada, **2011**.

Jaboyedoff, M., Carrea, D., Derron, M.H., Thierry, O., Penna, I. and Bejamin, R., A Review of Methods Used to Estimate Initial Landslide Failure Surface Depths and Volumes: Eng. Geol., 267 (**2020**) 105478. https://doi.org/10.1016/j.enggeo.2020.105478

Jakob, M. and Lambert, S., Climate Change Effects on Landslides along the Southwest Coast of British Columbia, Geomorphology, 107 (**2009**) 275–284. http://dx.doi.org/10.1016/j.geomorph.2008.12.009

Jakob, M. and Owen, T., Projected Effects of Climate Change on Shallow Landslides, North Shore Mountains, Vancouver, Canada, Geomorphology, 393 (**2021**) 107921, https://doi.org/10.1016/j.geomorph.2021.107921.

Janizadeh, S., Bateni, S.M., Jun, C., Pal, S.C., Band, S.S., Chowdhuri, I., Saha, A., Tiefenbacher, J.P. and Mosavi, A., Potential Impacts of Future Climate on the Spatio-Temporal Variability of Landslide Susceptibility in Iran Using Machine Learning Algorithms and CMIP6 Climate-Change Scenarios, Gondwana Research, 124 (**2023**) 1-17. https://doi.org/10.1016/j.gr.2023.05.003

Jemec Auflič, M., Bezak, N., Šegina, E., Frantar, P., Gariano, S.L., Medved, A., and Peternel, T., Climate Change Increases the Number of Landslides at the Juncture of the Alpine, Pannonian and Mediterranean Regions, Sci. Rep., 13 (**2023**) 23085. https://doi.org/10.1038/s41598-023-50314-x

Jenson, S.K. and Domingue, J.O., Extracting Topographic Structure from Digital Elevation Data for Geographic Information System Analysis, Photogramm. Eng. Rem. S., 54 (**1988**) 1593–1600.

Jiang, N., Su, F., Li, Y., Guo, X., Zhang, J. and Liu, X., Debris Flow Assessment in the Gaizi-Bulunkou Section of Karakoram Highway, Front. Earth Sci., 9 (**2021**) 660579. https://doi.org/10.3389/feart.2021.773619

Jiang, H., Zou, Q., Zhou, B., Jiang, Y., Cui, J., Yao, H. and Zhou, W., Estimation of Shallow Landslide Susceptibility Incorporating the Impacts of Vegetation on Slope Stability, Int. J. Disaster Risk Sci., 14 (**2023**) 618–635. https://doi.org/10.1007/s13753-023-00507-9

Ju, L-Y., Xiao, T., He, J., Wang, H-J. and Zhang, L.-M., Predicting Landslide Runout Paths Using Terrain Matching-Targeted Machine Learning, Engineering Geology, 311 (**2022**) 106902, https://doi.org/10.1016/j.enggeo.2022.106902.

Kaafarani, R., Jaoude, G.A., Wartman, J. and Tawk, M., Landslide Susceptibility Mapping Based on Triggering Factors Using a Multi-Modal Approach, Chehade, F.H., (Ed.), International Conference of Engineering Risk, Beirut, Lebanon, 3-5 April 2019, MATEC Web Conf, 281, **2019**, p. 1-8. https://doi.org/10.1051/matecconf/201928102002

Kalantar, B., Pradhan, B., Naghibi, S.A., Motevalli, A. and Mansor, S., Assessment of the Effects of Training Data Selection on the Landslide Susceptibility Mapping: A Comparison between Support Vector Machine (SVM), Logistic Regression (LR) and Artificial Neural Networks (ANN), Geomat. Nat. Haz. Risk, 9 (**2018**) 49–69. https://doi.org/10.1080/19475705.2017.1407368

Kang, D.H., Hong, M. and Jeong, S., A Simplified Depth-Averaged Debris Flow Model with Herschel-Bulkley Rheology for Tracking Density Evolution: A Finite Volume Formulation, Bull. Eng. Geol. Environ., 80 (**2021**) 5331–5346. https://doi.org/10.1007/s10064-021-02202-9

Kasahara, N., Gonda, Y. and Huvaj, N., Quantitative Land-Use and Landslide Assessment: A Case Study in Rize, Türkiye, Water, 14 (**2022**) 1811. https://doi.org/10.3390/w14111811

Karakas, G., Can, R., Kocaman, S., Nefeslioglu, H.A. and Gokceoglu, C., Landslide Susceptibility Mapping with Random Forest Model for Ordu, Turkey, Int. Arch. Photogramm. Remote Sens. Spatial Inf. Sci., XLIII-B3-2020 (**2020**) 1229-1236. 10.5194/isprs-archives-XLIII-B3-2020-1229-2020.

Karakas, G., Unal, E.O., Cetinkaya, S., Ozcan, N.T., Karakas, V.E., Can, R., Gokceoglu, C. and Kocaman, S., Analysis of Landslide Susceptibility Prediction Accuracy with an Event-Based Inventory: The 6 February 2023 Turkiye Earthquakes, Soil Dynamics and Earthquake Engineering, 178 (**2024**) 108491. https://doi.org/10.1016/j.soildyn.2024.108491.

Kaya Topaçli, Z., Ozcan, A.K. and Gokceoglu, C., Performance Comparison of Landslide Susceptibility Maps Derived from Logistic Regression and Random Forest Models in the Bolaman Basin, Türkiye, Natural Hazards Review, 25 (**2024**) 04023054. https://doi.org/10.1061/NHREFO.NHENG-1771

Keles, F. and Nefeslioglu, H.A., Infinite Slope Stability Model and Steady-State Hydrology-Based Shallow Landslide Susceptibility Evaluations: The Guneysu catchment Area (Rize, Turkey), CATENA, 200 (**2021**) 105161, https://doi.org/10.1016/j.catena.2021.105161.

Khalkhali, A.B. and Koochaksaraei, M.K., Evaluation of Limit Equilibrium and Finite Element Methods in Slope Stability Analysis Case Study of Zaremroud Landslide, Iran, Comput. Eng. Phys. Model., 2 (**2019**) 1–15.

Khan, M.A., Mustaffa, Z., A L B Balogun, A.L.B., Al-Bared, M.A.M., and Ahmad, A., Role of the Rheological Parameters in Debris Flow Modelling, IOP Conf. Series, Materials Science and Engineering, 1092 (**2021**) 012041. doi:10.1088/1757-899X/1092/1/012041

Kim, H.G., Lee, D.K., Park, C., Kil, S., Son, Y. and Park, J.H., Evaluating Landslide Hazards Using RCP 4.5 and 8.5 Scenarios, Environ. Earth Sci., 73 (**2015**) 1385–1400. https://doi.org/10.1007/s12665-014-3775-7

Kim, J. W., Jung, H. and Kim H.G., Comparative Analysis of Future Landslide Susceptible Areas Based on Climate Change Scenario Applications, J. People Plants Environ., 26 (**2023**) 565-581.https://doi.org/10.11628/ksppe.2023.26.5.565

Kritikos, T. and Davies, T., Assessment of Rainfall-Generated Shallow Landslide/Debris-Flow Susceptibility and Runout Using a GIS-Based Approach: Application to Western Southern Alps of New Zealand, Landslides, 12 (**2015**) 1051–1075. https://doi.org/10.1007/s10346-014-0533-6

KOERI (Bogazici University Kandilli Observation and Earthquake Research Institute), B.U. KOERI-RETMC Earthquake Catalog Search System, http://www.koeri.boun.edu.tr/sismo/zeqdb/indexeng.asp (Accessed on: **26 January 2024**).

Kottek, M., Grieser, J., Beck, C., Rudolf, B. and Rubel, F., World Map of the Köppen-Geiger Climate Classification Updated, Meteorol. Z., 15 (**2006**) 259-263. DOI: 10.1127/0941-2

Komu, M.P., Nefeslioglu, H.A. and Gokceoglu, C., A Review of the Prediction Methods for Landslide Runout, Proceedings, 87 (**2023**) 3. https://doi.org/10.3390/IECG2022-14604

Komu, M.P., Nefeslioglu, H.A. and Gokceoglu, C., Modeling Shallow Landslide Runout Distance in Eocene Flysch Facies Using Empirical–Statistical Models (Western Black Sea Region of Türkiye), ISPRS Int. J. Geo-Inf., 13 (**2024**) 84. https://doi.org/10.3390/ijgi13030084

Koshimizu, K. and Uchida, T., Time-Series Variation of Landslide Expansion in Areas with a Low Frequency of Heavy Rainfall, Geosciences, 13 (**2023**) 314. https://doi.org/10.3390/geosciences13100314

Kumar, A. and Sarkar, R., Debris Flow Susceptibility Evaluation—A Review, Iran J Sci Technol. Trans. Civ. Eng., 47 (**2023**) 1277–1292. https://doi.org/10.1007/s40996-022-01000-x

La Porta, G., Leonardi, A., Pirulli, M., Cafaro, F. and Castelli, F., Time-Resolved Triggering and Runout Analysis of Rainfall-Induced Shallow Landslides, Acta Geotech., (**2023**). https://doi.org/10.1007/s11440-023-01996-0

Lari, S., Crosta, G., Frattini, P., Horton, P. and Jaboyedoff, M., Regional-Scale Debris-Flow Risk Assessment for an Alpine Valley, Italian Journal of Engineering Geology and Environment, (**2011**) 933–940.

Legros, F., The Mobility of Long-Runout Landslides, Eng. Geol., 63 (**2002**) 301–331.

Li, X., Liu, H., Pan, J., Li, D. and Wang, J., Rainfall Thresholds of Shallow Landslides in Wuyuan County of Jiangxi Province, China, Open Geosciences, 12 (**2020a)** 821–831.

Li, Y., Chen, J., Zhang, Y., Song, S., Han, X., Ammar, M., Debris Flow Susceptibility Assessment and Runout Prediction: A Case Study in Shiyang Gully, Beijing, China, Int J Environ Res 14 (**2020b**) 365–383. https://doi.org/10.1007/s41742-020-00263-4

Li, B., Tang, H., Gong, W., Cheng, Z., Li, T. and Wang, L., Numerical Study of the Runout Behavior of the Kamenziwan Landslide in the Three Gorges Reservoir Region, China, Landslides, 19 (**2022**) 963–976. https://doi.org/10.1007/s10346-021-01804-4

Liang, Z., Wang, C., Ma, D. and Khan, K.U.J., Exploring the Potential Relationship between the Occurrence of Debris Flow and Landslides, Nat. Hazards Earth Syst. Sci., 21 (**2021**) 1247–1262, https://doi.org/10.5194/nhess-21-1247-2021

Licata, M., Buleo Tebar, V., Seitone, F. and Fubelli, G., The Open Landslide Project (OLP), a New Inventory of Shallow Landslides for Susceptibility Models: The Autumn 2019 Extreme Rainfall Event in the Langhe-Monferrato Region (Northwestern Italy), Geosciences, 13 (**2023**) 289. https://doi.org/10.3390/geosciences13100289

Lim, C.-H. and Kim, H.-J., Can Forest-Related Adaptive Capacity Reduce Landslide Risk Attributable to Climate Change? —Case of Republic of Korea, Forests, 13 (**2022**) 49. https://doi.org/10.3390/f13010049

Ling, S., Zhao, S., Huang, J. and Zhang, X., Landslide Susceptibility Assessment Using Statistical and Machine Learning Techniques: A Case Study in The Upper Reaches of the Minjiang River, Southwestern China, Front. Earth Sci., 10 (**2022**) 986172. doi: 10.3389/feart.2022.986172

Liu, Z., Gilbert, G., Cepeda, J.M., Lysdahl, A.O.K., Piciullo, L., Hefre, H. and Lacasse, S., Modelling of Shallow Landslides with Machine Learning Algorithms, Geoscience Frontiers, 12 (**2021**) 385-393, https://doi.org/10.1016/j.gsf.2020.04.014.

Liu, J., Wu, Y, Gao, X. and Zhang, X., A Simple Method of Mapping Landslides Runout Zones Considering Kinematic Uncertainties, Remote Sens., 14 (**2022**) 668. https://doi.org/10.3390/rs14030668

Liu, Y., Chen, J., Sun, X., Li, Y., Zhang, Y, Xu, W., Yan, J., Ji, Y. and Wang, Q., A Progressive Framework Combining Unsupervised and Optimized Supervised Learning for Debris Flow Susceptibility Assessment, CATENA, 234 (**2024**) 107560, https://doi.org/10.1016/j.catena.2023.107560.

Loche, M., Lombardo, L., Gorum, T., Tanyas, H. and Scaringi, G., Distinct Susceptibility Patterns of Active and Relict Landslides Reveal Distinct Triggers: A Case in Northwestern Türkiye, Remote Sens., 14 (**2022**) 1321. https://doi.org/10.3390/rs14061321

Luino, F., De Graff, J., Biddoccu, M., Faccini, F., Freppaz, M., Roccati, A., Ungaro, F., D'Amico, M. and Turconi, L., The Role of Soil Type in Triggering Shallow Landslides in the Alps (Lombardy, Northern Italy), Land, 11 (**2022**) 1125. https://doi.org/10.3390/land11081125

Luna, B.R.Q., Dynamic Numerical Run-Out Modeling for Quantitative Landslide Risk Assessment. Ph.D. Thesis, University of Twente, Faculty of Geo-Information Science and Earth Observation, Netherlands, **2012**.

Maleika, W., Inverse Distance Weighting Method Optimization in the Process of Digital Terrain Model Creation Based on Data Collected from a Multibeam Echosounder, Appl. Geomat., 12 (**2020**) 397–407. https://doi.org/10.1007/s12518-020-00307-6

Malla, R., Neupane, P.R. and Köhl, M. Climate Change Impacts Vegetation Shift of Broad Leaved and Coniferous Forests, Trees, Forests and People, 14 (**2023**) 100457 https ::/doi org/ 10 1016 /j tfp 2023 100457

Marc, O., Meunier, P., and Hovius., N., Prediction of the Area Affected by Earthquake-Induced Landsliding Based on Seismological Parameters, Nat. Hazards Earth Syst. Sci., 17 (**2017**) 1159-1175.

Marchesini, I., Althuwaynee, O., Santangelo, M., Alvioli, M., Cardinali, M., Mergili, M., Reichenbach, P., Peruccacci, S., Balducci, V., Agostino, I., Esposito, R., Rossi, M., National-Scale Assessment of Railways Exposure to Rapid Flow-Like Landslides, Engineering Geology, 332 (**2024**) 107474, https://doi.org/10.1016/j.enggeo.2024.107474.

Marinelli, A., Medici, C., Rosi, A., Tofani, V., Bianchini, S. and Casagli, N. Shallow Landslides and Rockfalls Velocity Assessment at Regional Scale: A Methodology Based on a Morphometric Approach, Geosciences, 12 (**2022**) 177. https://doi.org/10.3390/geosciences12040177

Martino, S., Marmoni, G.M., Fiorucci, M., Ceci, A.F., Discenza, M.E., Rouhi, J. and Tedoradze, D., Role of Antecedent Rainfall in the Earthquake-Triggered Shallow Landslides Involving Unsaturated Slope Covers, Appl. Sci., 12 (**2022**) 2917. https://doi.org/10.3390/app12062917

Maki Mateso, J.-C., Bielders, C. L., Monsieurs, E., Depicker, A., Smets, B., Tambala, T., Bagalwa Mateso, L., and Dewitte, O., Characteristics and Causes of Natural and Human-Induced Landslides in A Tropical Mountainous Region: The Rift Flank West of Lake Kivu (Democratic Republic Of The Congo): Nat. Hazards Earth Syst. Sci., 23 (**2023**) 643–666. https://doi.org/10.5194/nhess-23-643-2023

McCoy, K.M. Debris-flow susceptibility mapping in Colorado using Flow-r: calibration techniques and selected examples. In Proceedings of the 7th International Conference on Debris-Flow Hazards Mitigation, 10-13 June, Golden, Colorado, USA, **2019**.

McDougall, S., 2014 Canadian Geotechnical Colloquium: Landslide runout analysis — current practice and challenges, Can. Geotech. J., 54 (**2017**) 605–620.

Melo, R., van Asch, T. and Zêzere, J.L., Debris Flow Run-Out Simulation and Analysis Using a Dynamic Model, Nat. Hazards Earth Syst. Sci., 18 (**2018**) 555–570. https://doi.org/10.5194/nhess-18-555-2018.

Menard, S., Applied Logistic Regression Analysis. Sage University Paper Series on Quantitative Applications in Social Sciences, Sage Publications No. 106, Thousand Oaks, California, USA, **1995**.

Merghadi, A., Yunus, A.P., Dou, J., Whiteley, J., ThaiPham, B., Bui, D.T., Avtar, R. and Abderrahmane, B., Machine Learning Methods for Landslide Susceptibility Studies: A Comparative Overview of Algorithm Performance, EarthSci. Rev., 207 (**2020**) 103225. https://doi.org/10.1016/j.earscirev.2020.103225.

Mergili, M, Schratz, K., Thalhammer, M., Fellin, W. and Ostermann, A., An open source model for the simulation of granular flows: first results with GRASS GIS and needs for further research, Academic Proceedings of the 2008 Free And Open Source Software for Geospatial (FOSS4G) Conference, 29 Sept–3 Oct, Cape Town, 231–238, **2008**.

Mergili, M., Integrated modelling of debris flows with Open Source GIS, Dissertation, University of Innsbruck, Austria, Faculty of Geo- and Atmospheric Sciences, **2008**.

Mergili, M., Krenn, J. and Chu, H.-J., r. randomwalk v1, A Multi-Functional Conceptual Tool for Mass Movement Routing, Geosci Model Dev, 8 (**2017**) 4027–4043. https://doi.org/10.5194/gmd-8-4027-2015

Mergili, M., Schwarz, L. and Kociu, A., Combining Release and Runout in Statistical Landslide Susceptibility Modeling, Landslides, 16 (**2019**) 2151-2165. https://doi.org/10.1007/s10346-019-01222-7

Mikoš, M. and Bezak, N., Debris Flow Modelling Using RAMMS Model in the Alpine Environment with Focus on the Model Parameters and Main Characteristics, Front. Earth Sci., 8 (**2021**) 605061. doi: 10.3389/feart.2020.605061

Milledge, D.G., Densmore, A.L., Bellugi, D., Rosser, N.J., Watt, J., Li, G. and Oven, K.J. Simple Rules to Minimise Exposure to Coseismic Landslide Hazard, Nat. Hazards Earth Syst. Sci., 19 (**2019**) 837–856.

Milliyet Daily Newspaper, Köprüde 7.4 kabusu! Tayvan'da çeyrek asrın en şiddetli depremi: Dünya izliyor. https://www.milliyet.com.tr/dunya/live-koprude-7-4-kabusu-tayvanda-ceyrek-asrin-en-siddetli-depremi-dunya-izliyor-7107345#post-3 (Accessed on: **03 April 2024**)

Mohamed Yusof, M.K.T., A Rashid, A.S., Abdul Khanan, M.F., Abdul Rahman, M.Z., Abdul Manan, W.A., Kalatehjari, R. and Dehghanbanadaki, A., Assessing the Impact of RCP4.5 and RCP8.5 Scenarios on Landslide Susceptibility Mapping Using Support Vector Machine: A case study of Penang Island, Malaysia, Phys. Chem. Earth, Parts A/B/C, 133 (**2024**) 103496, https://doi.org/10.1016/j.pce.2023.103496

Moncayo, S. and Ávila, G., Landslide travel distances in Colombia from National landslide database analysis. Progress in Landslide Research and Technology, Sassa, K., Konagai, K., Tiwari, B., Arbanas, Ž., Sassa, S. (Eds.), Vol. 1, Springer, Cham., **2023**. https://doi.org/10.1007/978-3-031-16898-7_24

Mondini, A., Guzzetti, F. and Melillo, M., Deep Learning Forecast of Rainfall-Induced Shallow Landslides, Nature Communications, 14 (**2023**) 2466. https://doi.org/10.1038/s41467-023-38135-y

Moses, D.N., Earthquake Induced Landslides. M.Sc. Thesis, Graduate School of Natural and Applied Sciences of Dokuz Eylül University, Izmir, Türkiye, **2017.**

Moss, R.H., Babiker, M., Brinkman, S., Calvo, E., Carter, T., Edmonds, J.A. and Zurek, M. Towards New Scenarios for Analysis of Emissions, Climate Change, Impacts, and Response Strategies. United States, IPCC Expert Meeting Report. Intergovernmental Panel on Climate Change, p. 34, Geneva, Switzerland, **2008**.

Motamedi, M. Quantitative Landslide Hazard Assessment in Regional Scale Using Statistical Modeling Techniques. Ph.D. Thesis, The Graduate Faculty of The University of Akron, Akron, OH, USA, **2013**.

Naemitabar, M. and Zanganeh Asadi, M., Landslide Zonation and Assessment of Farizi Watershed in Northeastern Iran Using Data Mining Techniques: Nat. Hazards, 108 (**2021**) 2423–2453. https://doi.org/10.1007/s11069-021-04805-7

Nam, K. and Wang, F., An Extreme Rainfall-Induced Landslide Susceptibility Assessment Using Autoencoder Combined with Random Forest in Shimane Prefecture, Japan, Geoenviron Disasters 7, 6 (**2020**). https://doi.org/10.1186/s40677-020-0143-7

Nasidi, N.M., Wayayok, A., Abdullah, A.F. and Kassim, M.S.M., Dynamics of Potential Precipitation Under Climate Change Scenarios at Cameron Highlands, Malaysia, SN Appl. Sci., 3 (**2021**) 334.

NCAR Geographic Information System Program. Climate Change Scenarios. https://gis.ucar.edu/inspector (Accessed on: **16 August 2022**)

Nefeslioglu, H.A. and Gokceoglu, C., Probabilistic Risk Assessment in Medium Scale for Rainfall Induced Earthflows: Catakli Catchment Area (Cayeli, Rize, Turkey), Math Probl. Eng., 2011 (**2011**) 1–21. https://doi.org/10.1155/2011/280431

Nefros, C., Tsagkas, D.S., Kitsara, G., Loupasakis, C. and Giannakopoulos, C., Landslide Susceptibility Mapping Under the Climate Change Impact in the Chania Regional Unit, West Crete, Greece, Land, 12 (**2023**) 154. https://doi.org/10.3390/land12010154

Nhu, V.-H., Shirzadi, A., Shahabi, H., Singh, S.K., Al-Ansari, N., Clague, J.J., Jaafari, A., Chen, W., Miraki, S., Dou, J., Luu, C., Górski, K., Thai Pham, B., Nguyen, H.D. and Ahmad, B.B. Shallow Landslide Susceptibility Mapping: A Comparison between Logistic Model Tree, Logistic Regression, Naïve Bayes Tree, Artificial Neural Network, and Support Vector Machine Algorithms, Int. J. Environ. Res. Public Health, 17 (**2020**) 2749. https://doi.org/10.3390/ijerph17082749

Nie, Y., Li, X. and Xu, R., Dynamic Hazard Assessment of Debris Flow Based on TRIGRS and Flow-R Coupled Models, Stoch. Environ. Res. Risk Assess, 36 (**2022**) 97–114. https://doi.org/10.1007/s00477-021-02093-y

Nikoobakht, S., Azarafza, M., Akgün, H. and Derakhshani, R., Landslide Susceptibility Assessment by Using Convolutional Neural Network., Appl. Sci., 12 (**2022**) 5992. https://doi.org/10.3390/app12125992

Nishioka, M., Inoue, H., Ota, T. and Mizoue, N., Impact of Forest Type and Age on Shallow Landslide Susceptibility a Case Study from the 2017 Heavy Rainfall in Northern Kyushu, Japan Socioeconomics, Planning, and Management, (**2023**) 389-396.

Nnanwuba, U.E., Qin, S., Adeyeye, O.A., Cosmas, N.C., Yao, J., Qiao, S., Jingbo, S. and Egwuonwu, E.M., Prediction of Spatial Likelihood of Shallow Landslide Using GIS-Based Machine Learning in Awgu, Southeast/Nigeria, Sustainability, 14 (**2022**) 12000. https://doi.org/10.3390/su141912000

Noël, F., Nordang, S.F., Jaboyedoff, M., Digout, M., Guerin, A., Locat, J. and Matasci, B. Comparing Flow-R, Rockyfor3D and RAMMS to Rockfalls from the Mel de la Niva Mountain: A Benchmarking Exercise, Geosciences, 13 (**2023**) 200. https://doi.org/10.3390/geosciences13070200

Nwazelibe, V., Unigwe, C. and Egbueri, J., Integration and Comparison of Algorithmic Weight of Evidence and Logistic Regression in Landslide Susceptibility Mapping of the Orumba North Erosion-Prone Region, Nigeria, Model Earth Syst. Environ., (**2022**). https://doi.org/10.1007/s40808-022-01549-6

Ocakoglu, F., Gokceoglu, G. and Ercanoglu, M., Dynamics of a Complex Mass Movement Triggered by Heavy Rainfall: A case Study from NW Turkey, Geomorphology, 42 (**2002**) 329-341. https://doi.org/10.1016/S0169-555X(01)00094-0.

O'Callaghan, J. F. and Mark, D. M., The Extraction of Drainage Networks from Digital Elevation Data, Comput. Vision Graph., 28 (**1984**) 328–344. doi:10.1016/S0734-189X(84)80011-0.

Oh, C.-H., Choo, K.-S., Go, C.-M., Choi, J.-R. and Kim, B.-S., Forecasting of Debris Flow Using Machine Learning-Based Adjusted Rainfall Information and RAMMS Model, Water, 13 (**2021**) 2360. https://doi.org/10.3390/w13172360

Okkan, U. and Kirdemir, U., Downscaling of Monthly Precipitation Using CMIP5 Climate Models Operated under RCPs, Meteorol. Appl., 23 (**2016**) 514–528.

Ortiz-Giraldo, L., Botero, B.A. and Vega, J., An Integral Assessment of Landslide Dams Generated by the Occurrence of Rainfall-Induced Landslide and Debris Flow Hazard Chain, Front. Earth Sci., 11 (**2023**) 1157881. doi: 10.3389/feart.2023.1157881

Pacific Climate Impact Consortium. https://pacificclimate.org/analysis-tools/pcic-climateexplorer (Accessed on: **15 October 2022**).

Panday, S. and Dong, J.J., Topographical Features of Rainfall-Triggered Landslides in Mon State, Myanmar, August 2019: Spatial Distribution Heterogeneity and Uncommon Large Relative Heights, Landslides, 18 (**2021**) 3875–3889. https://doi.org/10.1007/s10346-021-01758-7

Park, H.J., Lee, J.H. and Woo, I., Assessment of Rainfall-Induced Shallow Landslide Susceptibility Using a GIS-Based Probabilistic Approach, Eng. Geol., 161 (**2013**) 1–1. https://doi.org/10.1016/j.enggeo.2013.04.011

Park, S.J. and Lee, D., Predicting Susceptibility to Landslides under Climate Change Impacts in Metropolitan Areas of South Korea Using Machine

Learning, Geomatics, Nat. Hazards Risk, 12 (**2021**) 2462-2476. DOI: 10.1080/19475705.2021.1963328

Park, C.Y., Cho, M.G., Park, C. and Kim, H.G., Landslide Risk on Photovoltaic Power Stations under Climate Change, Geomatics, Natural Hazards and Risk, 15 (**2024**) 1, DOI: 10.1080/19475705.2023.2286904

Pastorello, R., Michelini, T. and D'Agostino, V., On the Criteria to Create a Susceptibility Map to Debris Flow at a Regional Scale Using Flow-R, J. Mt. Sci., 14 (**2017**) 621–635. https://doi.org/10.1007/s11629-016-4077-1

Paudel, B.P., GIS-Based Assessment of Debris Flow Susceptibility and Hazard in Mountainous Regions of Nepal. Ph.D. Thesis, Ottawa University, Civil Engineering Faculty of Engineering, Ottawa, Canada, **2019**.

Paudel, B., Fall, M. and Daneshfar, B., Gis-Based Assessment of Debris Flow Runout in Kulekhani Watershed, Nepal, Geotech. Geol. Eng., 39 (**2021**) 2755–2775. https://doi.org/10.1007/s10706-020-01655-1

Paul, L.R., Michel, G.P., Schwarz, H., Abatti, B.H., and Guerra Salvador, C., Comparison of Different Rheological Approaches and Flow Direction Algorithms in a Physically Based Debris Flow Model for Data Scarce Regions, Nat. Hazards Earth Syst. Sci., (**2023**). https://doi.org/10.5194/nhess-2023-119.

Pawluszek-Filipiak, K. and Borkowski, A., On the Importance of Train–Test Split Ratio of Datasets in Automatic Landslide Detection by Supervised Classification, Remote Sens., 12 (**2020**) 3054. https://doi.org/10.3390/rs12183054

Pennington, C.V.L, Bossu, R., Ofli, F., Imran, M., Qazi, U., Roch, J. and Banks, V.J., A Near-Real-Time Global Landslide Incident Reporting Tool Demonstrator Using Social Media and Artificial Intelligence, International Journal of Disaster Risk Reduction, 77 (**2022**) 103089. https://doi.org/10.1016/j.ijdrr.2022.103089.

Peres, D.J. and Cancelliere, A., Modeling Impacts of Climate Change on Return Period of Landslide Triggering, Journal of Hydrology, 567 (**2018**) 420-434, https://doi.org/10.1016/j.jhydrol.2018.10.036.

Peruzzetto, M., Mangeney, A., Grandjean, G., Levy, C., Thiery, Y., Rohmer, J. and Lucas, A. Operational Estimation of Landslide Runout, Comparison of Empirical and Numerical Methods: Geosciences, 10 (**2020**) 424. https://doi.org/10.3390/geosciences10110424

Perzl, F., Rössel, M., Lauss, E. and Neuhauser, M., Mapping of the protective function of forests in Austria against shallow landslides, 14th Congress INTERPRAEVENT, 31 May-2 June, Norway, **2021.**

Pham, Q.B., Pal, S.C., Chakrabortty, R., Saha, A., Janizadeh, S., Ahmadi, K., Khedher, K.M., Anh, D.T., Tiefenbacher, J.P. and Bannari, A., Predicting Landslide Susceptibility Based on Decision Tree Machine Learning Models under Climate

and Land Use Changes, Geocarto International, 37 (**2022**) 7881-7907. DOI: 10.1080/10106049.2021.1986579.

Pitman, E.B., Nichita, C.C., Patra, A., Bauer, A., Sheridan, M. and Bursik, M., Computing Granular Avalanches and Landslides, Phys. Fluids, 15 (**2003**) 3638–3646.

Polat, A. and Erik, D., Debris Flow Susceptibility and Propagation Assessment in West Koyulhisar, Turkey, J. Mt. Sci., 17 (**2020**) 2611-2623. https://doi.org/10.1007/s11629-020-6261-6

Poltnig, W., Bak, R., Berg, W. and Keršmanc, T., Runout-Modelling of Shallow Landslides in Carinthia (Austria), Aust. J. Earth Sci., 109 (**2016**) 59 – 67.

Polykretis, C. and Chalkias, C., Comparison and Evaluation of Landslide Susceptibility Maps Obtained from Weight of Evidence, Logistic Regression, and Artificial Neural Network Models, Nat. Hazards, 93 (**2018**) 249–274. https://doi.org/10.1007/s11069-018-3299-7

Pradhan, A.M.S., Kang, H., Lee, S. and Kim, Y., Spatial Model Integration for Shallow Landslide Susceptibility and Its Runout Using a GIS-Based Approach in Yongin, Kore, Geocarto International, 32 (**2016**) 420-441. https://doi.org/10.1080/10106049.2016.1155658

Pradhan, A.M.S. and Kim, Y.-T., Rainfall-Induced Shallow Landslide Susceptibility Mapping at Two Adjacent Catchments Using Advanced Machine Learning Algorithms, ISPRS Int. J. Geo-Inf., 9 (**2020**) 569. https://doi.org/10.3390/ijgi9100569

Pradhan, A.M.S., Quantification of Slope Unit Wise Vulnerability in Terms of Building Aggregation, WRRDC Research Letter, 07 (**2021**) 1–2.

Prochaska, A.B., Santi, P.M., Higgins, J.D., Cannon, S.H., A Study of Methods to Estimate Debris Flow Velocity, Landslides, 5 (**2008**) 431–444. https://doi.org/10.1007/s10346-008-0137-0

Pudasaini, S.P., A General Two-Phase Debris Flow Model, Journal of Geophysical Research, 17 (**2012**) F03010. doi:10.1029/2011JF002186

Putra, M., Dinata, I., Sadisun, I., Sarah, D., Aulia, A. and Sukristiyanti, S., Modeling of Individual Debris Flows Based on DEMNAS Using Flow-R: A Case Study in Sigi. Central Sulawesi, RISET Geologi dan Pertambangan, 32 (**2022**) 37–58. 10.14203/risetgeotam2022.v32.1215

Qiu, C., Su, L., Zou, Q., Geng, X., A Hybrid Machine-Learning Model to Map Glacier-Related Debris Flow Susceptibility Along Gyirong Zangbo Watershed under the Changing Climate, Science of the Total Environment, 818 (**2022**) 151752, https://doi.org/10.1016/j.scitotenv.2021.151752.

Quinn, P., Beven, K., Chevallier, P. and Planchon, O., The Prediction of Hillslope Flow Paths for Distributed Hydrological Modelling Using Digital Terrain Models, Hydrol. Process, 5 (**1991**) 59–79. https://doi.org/10.1002/hyp.3360050106

Rahman, M.S., Ahmed, B. and Di, L., Landslide Initiation and Runout Susceptibility Modeling in the Context of Hill Cutting and Rapid Urbanization: a Combined Approach of Weights of Evidence and Spatial Multi-Criteria, J. Mt. Sci., 14 (**2017**) 1919–1937. https://doi.org/10.1007/s11629-016-4220-z

RAMMS:DEBRISFLOW User Manual https://ramms.slf.ch/ramms/downloads/RAMMS_DBF_Manual.pdf. (Accessed on: **5.12.2023**)

RAMMS software, Debris Flow Theory Friction Parameters https://ramms.slf.ch/en/modules/debrisflow/theory/friction-parameters.html (Accessed on: **01.04.2024**)

Ray, A., Verma, H., Bharati, A.K., Rai, R., Koner, R. and Singh, T.N., Numerical Modelling of Rheological Properties of Landslide Debris, Nat. Hazards, 110 (**2022**) 2303–2327. https://doi.org/10.1007/s11069-021-05038-4

Rickenmann, D. and Zimmermann, M., The 1987 Debris Flows in Switzerland: Documentation and Analysis, Geomorphology, 8 (**1993**) 175–189, doi:10.1016/0169-555X (93) 90036-2.

Roccati, A., Faccini, F., Luino, F., Ciampalini, A. and Turconi, L., Heavy Rainfall Triggering Shallow Landslides: A Susceptibility Assessment by a GIS-Approach in a Ligurian Apennine Catchment (Italy), Water, 11 (**2019**) 605. https://doi.org/10.3390/w11030605

Roccati, A., Paliaga, G., Luino, F., Faccini, F. and Turconi, L., Rainfall Threshold for Shallow Landslides Initiation and Analysis of Long-Term Rainfall Trends in a Mediterranean Area, Atmosphere, 11 (**2020**) 1367. https://doi.org/10.3390/atmos11121367

Roccati, A., Paliaga, G., Luino, F., Faccini, F. and Turconi, L., GIS-Based Landslide Susceptibility Mapping for Land Use Planning and Risk Assessment, Land, 10 (**2021**) 162. https://doi.org/10.3390/land10020162

Roman Quintero, D.C., Ortiz Contreras, J.D., Tapias Camacho, M.A. and Oviedo-Ocaña, E.R., Empirical Estimation of Landslide Runout Distance Using Geometrical Approximations in the Colombian North–East Andean Region, Sustainability, 16 (**2024**) 793. https://doi.org/10.3390/su16020793

Rosser, N.J., Kincey, M.E., Oven, K.J., Densmore, A.L., Robinson, T.R., Pujara, D.S., Shrestha, R., Smutny, J., Gurung, K., Lama, S. and Dhital, M.R., Changing Significance of Landslide Hazard and Risk After The 2015 Mw 7.8 Gorkha, Nepal Earthquake, Progress in Disaster Science, 10 (**2021**) 100159.

Ruosteenoja, K., Jylhä, K. and Kämäräinen, M., Climate projections for Finland under the RCP forcing scenarios, Geophysica, 51 (**2016**) 17-50.

Salinas-Jasso, J.A., Montalvo-Arrieta, J.C. and Velasco-Tapia, F., Spatial Patterns of Shallow Landslides Induced by the 19 September 2017 Puebla-Morelos Earthquake, Mexico, Bull. Eng. Geol. Environ., 82 (**2023**) 15. https://doi.org/10.1007/s10064-022-03030-1

Schwaab, J., Davin, E.L., Bebi, P., Duguay-Tetzlaff, A., Waser, L.T., Haeni, M., and Meier, R., Increasing the Broad Leaved Tree Fraction in Europe an Forests Mitigates Hot Temperature Extremes, SciRep, 10 (**2020**) 14153. https://doi.org/10.1038/s41598-020-71055-1

Sevgen, E., Kocaman, S., Nefeslioglu, H.A. and Gokceoglu, C., A Novel Performance Assessment Approach Using Photogrammetric Techniques for Landslide Susceptibility Mapping with Logistic Regression, ANN and Random Forest, Sensors, 19 (**2019**) 3940. https://doi.org/10.3390/s19183940

Sharma, C.P., Kumar, A., Chahal, P., Shukla, U.K., Srivastava, P. and Jaiswal, M.K., Debris Flow Susceptibility Assessment of Leh Valley, Ladakh, Based on Concepts of Connectivity, Propagation and Evidence-Based Probability, Nat. Hazards, 115 **(2023)** 1833–1859. https://doi.org/10.1007/s11069-022-05619-x

Sharir, K., Simon, N. and Roslee, R., The Influence of Landslides Parameters Contributing to Runout Zones using GIS-Based Empirical Model in Kundasang, Sabah, ASM Sc. J., 11 (**2018**) 254-266.

Shirzadi, A., Bui, D.T., Pham, B.T., Solaimani, K., Chapi, K., Kavian, A., Shahabi, H. and Revhaug, I. Shallow Landslide Susceptibility Assessment Using a Novel Hybrid Intelligence Approach, Environ. Earth Sci., 76 (**2017**) 60 https://doi.org/10.1007/s12665-016-6374-y

Shirzadi, A., Soliamani, K., Kavian, H.M., Chapi, A., K., Shahabi, H., Chen, W., Khosravi, K., Thai Pham, B., Pradhan, B., Ahmad, A., Bin Ahmad, B., and Bui, D.T., Novel GIS Based Machine Learning Algorithms for Shallow Landslide Susceptibility Mapping, Sensors, 18 (**2018**) 3777. https://doi.org/10.3390/s18113777

Shao, X., Ma, S. and Xu, C., Distribution and Characteristics of Shallow Landslides Triggered by the 2018 Mw 7.5 Palu Earthquake, Indonesia, Landslides, 20 (**2023**) 157–175. https://doi.org/10.1007/s10346-022-01972-x

Smith, H.G., Neverman, A.J., Harley Betts, Raphael Spiekermann, The Influence of Spatial Patterns in Rainfall on Shallow Landslides, Geomorphology, 437 (**2023**) 108795, https://doi.org/10.1016/j.geomorph.2023.108795.

Song, K., Han, L., Ruan, D., Li, H. and Ma, B., Stability Prediction of Rainfall-Induced Shallow Landslides: A Case Study of Mountainous Area in China, Water, 15 (**2023**) 2938. https://doi.org/10.3390/w15162938

Stancanelli, L.M., Peres, D.J., Cancelliere, A. and Foti, E., A Combined Triggering-Propagation Modeling Approach for the Assessment of Rainfall Induced Debris Flow Susceptibility, Journal of Hydrology, 550 (**2017**) 130-143, https://doi.org/10.1016/j.jhydrol.2017.04.038.

Steger, S., Scorpio, V., Comiti, F., Cavalli, M., Data-Driven Modelling of Joint Debris Flow Release Susceptibility and Connectivity, Earth Surf. Process. Landf., 47 (**2022**) 2740–2764. https://doi.org/10.1002/esp.5421.

Stoffel, M., Tiranti, D. and Huggel, C., Climate Change Impacts on Mass Movements — Case Studies from the European Alps, Science of The Total Environment, 493 (**2014**) 1255-1266, https://doi.org/10.1016/j.scitotenv.2014.02.102.

Sturzenegger, M., Holm, K., Lau, C. and Jakob, M. Semi-Automated Regional Scale Debris-Flow and Debris-Flood Susceptibility Mapping Based on Digital Elevation Model Metrics and Flow-R Software. In Proceedings of the 7th International Conference on Debris-Flow Hazards Mitigation, 10-13 June, Golden, Colorado, USA, **2019**.

Sun, L., Wei, Y., Cai, H., Yan, J. and Xiao, J., Improved Fast Adaptive IDW Interpolation Algorithm based on the Borehole Data Sample Characteristic and Its Application, J. Phys.: Conf. Ser.,1284 (**2019**) 012074.

Sun, W., Bocchini, P. and Davison, B.D., Applications of Artificial Intelligence for Disaster Management, Nat. Hazards, 103 (**2020**) 2631–2689. https://doi.org/10.1007/s11069-020-04124-3

Takaoka, S., A Landscape-Level Study on Vegetation Richness of Ancient Landslide Areas, Progress in Physical Geography, 0 (**2023**) 1–15.

Tang, Q., Gratchev, I. and Ravindran, S., Effect of Rainfall Intensity on Landslide Initiation: Flume Tests and Numerical Analysis. Geotechnics, 3 **(2023)** 104-115. https://doi.org/10.3390/geotechnics3010007

Tanyaş, H. and Lombardo, L., Variation in Landslide-Affected Area Under the Control of Ground Motion and Topography, Engineering Geology, 260 (**2019**) 105229, https://doi.org/10.1016/j.enggeo.2019.105229.

Tanyaş, H., Görüm, T., Kirschbaum, D. and Lombardo, L., Could Road Constructions be More Hazardous than An Earthquake in terms of Mass Movement?, Nat. Hazards, 112 (**2022**) 639–663. https://doi.org/10.1007/s11069-021-05199-2

Taskiran, T., Alli, S. and Yilmaz, Y., Hydro–Mechanical Behaviour of a Rainfall-Induced Landslide by Instrumental Monitoring: Landslide–Rainfall Threshold of the Western Black Sea Bartin Region of Türkiye, Appl. Sci., 13 (**2023**) 8703. https://doi.org/10.3390/app13158703

Tarboton, D.G., A New Method for the Determination of Flow Directions and Upslope Areas in Grid Digital Elevation Models, Water Resour. Res., 33 (**1997**) 309–319, doi:10.1029/96WR03137.

Thein, K.S.M., Nagai, M., Nakamura, T., Phienwej, N. and Pal, I., Assessment of the Impacts of Urbanization on Landslide Susceptibility in Hakha City, a Mountainous Region of Western Myanmar, Land, 12 (**2023**) 1036. https://doi.org/10.3390/land12051036

Thomas, J., Gupta, M., Srivastava, P.K. and Petropoulos, G.P., Assessment of a Dynamic Physically Based Slope Stability Model to Evaluate Timing and Distribution of Rainfall-Induced Shallow Landslides, ISPRS Int. J. Geo-Inf., 12 (**2023**) 105. https://doi.org/10.3390/ijgi12030105.

Tian, M., Xu, J. and Li, L., Bayesian Approaches for Probabilistic Prediction of Debris-Flow Runout Using Limited Site-Specific Data Sets, International Journal of Geomechanics, 23 (**2023**) 05023007. https://doi.org/10.1061/IJGNAI.GMENG-836

Tiranti, D., Nicolò, G. and Gaeta, A.R., Shallow Landslides Predisposing and Triggering Factors in Developing a Regional Early Warning System, Landslides, 16 (**2019**) 235–251.

Tiranti, D. and Ronchi, C., Climate Change Impacts on Shallow Landslide Events and on the Performance of the Regional Shallow Landslide Early Warning System of Piemonte (Northwestern Italy), GeoHazards, 4 (**2023**) 475-496. https://doi.org/10.3390/geohazards4040027

Tokay, M., Filyos Çayı Ağzı-Amasra-Bartın-Kozcağız-Çaycuma Bölgesinin Jeolojisi, Maden Tetkik ve Arama Dergisi, 46/47 (**1954**) 46–63.

Troncone, A., Pugliese, L. and Conte, E., Rainfall Threshold for Shallow Landslide Triggering Due to Rising Water Table, Water, 14 (**2022**) 2966. https://doi.org/10.3390/w14192966

Turkish State Meteorological Service, Köppen İklim Sınıflandırmasına Göre Türkiye İklimi, Araştırma Dairesi Başkanlığı Klimatoloji Şube Müdürlüğü, **2016**.

Turkish State Meteorological Service, Maximum Rainfall Intensity and Recurrence Analysis, https://mgm.gov.tr/veridegerlendirme/maksimum-yagislar.aspx (Accessed on: **23 December 2022**).

Turkish State Meteorological Service, Daily Historical Precipitation (mm=kg/m²) OMGİ and MANUEL, **2022**.

Turkish State Meteorological Service, Daily Total Precipitation (mm), https://www.mgm.gov.tr/sondurum/toplam-yagis.aspx. (Accessed on: **21 November 2023**).

Tzabiras, J., Loukas, A., and Vasiliades, L., A Hybrid Downscaling Approach for the estimation of Climate Change Effects on Droughts Using a Geo-Information Tool. Case study: Thessaly, Central Greece, Open Geosciences, 8 (**2016**) 728-746.

Unal, E.O., Kocaman, S. and Gokceoglu, C., Impact Assessment of Geohazards Triggered by 6 February 2023 Kahramanmaras Earthquakes (Mw 7.7 and Mw 7.6) on the Natural Gas Pipelines, Engineering Geology, 334 (**2024**) 107508, https://doi.org/10.1016/j.enggeo.2024.107508.

Varnes, D.J., Slope movement types and processes. In Special Report 176: Landslides: Analysis and Control, Schuster, R.L, Krizek, R.J., (Eds.), Transportation and Road Research Board, National Academy of Science: Washington, DC, USA, 11-33, **1978**.

Vegliante, G., Baiocchi, V., Falconi, L.M., Moretti, L., Pollino, M., Puglisi, C. and Righini, G., A GIS-Based Approach for Shallow Landslides Risk Assessment in the Giampilieri and Briga Catchments Areas (Sicily, Italy), GeoHazards, 5 (**2024**) 209-232. https://doi.org/10.3390/geohazards5010011

Vicari, H., Nordal, S. and Thakur, V., The Significance of Entrainment on Debris Flow Modelling: The Case of Hunnedalen, Norway. In Challenges and Innovations in Geomechanics, IACMAG 2021. Lecture Notes in Civil Engineering, Barla, M., Di Donna, A., Sterpi, D. (Eds.), Springer, Cham., Vol. 126, **2021**. https://doi.org/10.1007/978-3-030-64518-2_60, ISBN 978-3-030-64517-5.

Volpe, E., Gariano, S.L., Ciabatta, L., Peiro, Y. and Cattoni, E., Expected Changes in Rainfall-Induced Landslide Activity in an Italian Archaeological Area, Geosciences, 13 (**2023**) 270. https://doi.org/10.3390/geosciences13090270

Wallace, C.S. and Santi, P.M., Runout Number: A New Metric for Landslide Runout Characterization, Environmental & Engineering Geoscience, 27 (**2021**) 455–470. doi: https://doi.org/10.2113/EEG-D-20-00144

Wang, R., Cheng, Q., Liu, L., Yan, C. and Huang, G., Multi-Model Projections of Climate Change in Different RCP Scenarios in an Arid Inland Region, Northwest China, Water, 11 (**2019**) 347. https://doi.org/10.3390/w11020347

Wang, Z., Liu, Q. and Liu, Y., Mapping Landslide Susceptibility Using Machine Learning Algorithms and GIS: A Case Study in Shexian County, Anhui Province, China, Symmetry, 12 (**2020**) 1954. https://doi.org/10.3390/sym12121954

Wang, X., Otto, M., and Scherer, D.: Atmospheric triggering conditions and Climatic Disposition of Landslides in Kyrgyzstan and Tajikistan at the Beginning of the 21st Century, Nat. Hazards Earth Syst. Sci., 21 (**2021**) 2125–2144. https://doi.org/10.5194/nhess-21-2125-

Wang, X.J., Wu, S.-J., Tsai, T.-L. and Yen, K.-C., Modeling Probabilistic-Based Reliability Assessment of Gridded Rainfall Thresholds for Shallow Landslide Occurrence Due to The Uncertainty of Rainfall in Time and Space, Journal of Hydroinformatics, 25 (**2023**) 706–737.

Wang, T., Dahal, A., Fang, Z., van Westen, C, Yin, K. and Lombardo, L., From Spatio-Temporal Landslide Susceptibility to Landslide Risk Forecast, Geoscience Frontiers, 15 (**2024**) 101765. https://doi.org/10.1016/j.gsf.2023.101765

Wells, D.L. and Coppersmith, K.J., New Empirical Relationships Among Magnitude, Rupture Length, Rupture Width, Rupture Area, and Surface Displacement, Bull. Seismol. Soc. Am., 84 (**1994**) 974–1002.

Wei, L., Cheng, H. and Dai, Z., Propagation Modeling of Rainfall-Induced Landslides: A Case Study of the Shaziba Landslide in Enshi, China, Water, 15 (**2023**) 424. https://doi.org/10.3390/w15030424

Wichmann, V., The Gravitational Process Path (GPP) model (v1.0) – A GIS-Based Simulation Framework for Gravitational Processes, In Geosci. Model Dev., 10 (**2017**) 3309–3327. DOI: 10.5194/gmd-10-3309-2017.

Wijaya, I.P.K., Joshi, A., Alam, M.N., Jayasinghe, S. and Laila, N, Climate Change Induced Landslide Susceptibility Assessment - for Aiding Climate Resilient Planning for Road Infrastructure: A Case Study in Rangamati District, Chittagong Hill Tracts, Bangladesh: IOP Conf. Ser., Earth Environ. Sci., 1091 (**2022**) 012010.

Xia, C. and Tian, H., A Quasi-Single-Phase Model for Debris Flows Incorporating Non-Newtonian Fluid Behavior, Water, 14 (**2022**) 1369. https://doi.org/10.3390/w14091369

Xie, W., Li, X., Jian, W., Yang, Y., Liu, H., Robledo, L.F. and Nie, W., A Novel Hybrid Method for Landslide Susceptibility Mapping-Based GeoDetector and Machine Learning Cluster: A Case of Xiaojin County, China, ISPRS Int. J. Geo-Inf., 10 (**2021a**) 93. https://doi.org/10.3390/ijgi10020093

Xie, W., Nie, W., Saffari, P., Robledo, L. F., Descote, P.-Y. and Jian, W., Landslide Hazard Assessment Based on Bayesian Optimization-Support Vector Machine in Nanping City, China, Nat. Hazards, 109 (**2021b**) 931–948. doi:10.1007/ s11069-021-04862-y

Xiong, K., Adhikari, B.R., Stamatopoulos, C.A., Zhan, Y., Wu, S., Dong, Z. and Di, B., Comparison of Different Machine Learning Methods for Debris Flow Susceptibility Mapping: A Case Study in the Sichuan Province, China, Remote Sens., 12 (**2020**) 295.

Xu, H., Su, P., Chen, Q., Liu, F., Zhou, Q. and Liu, L., Susceptibility Areas Identification and Risk Assessment of Debris Flow Using the Flow-R Model: A Case Study of Basu County of Tibet, Geoenviron. Disasters, 9 (**2022**). https://doi.org/10.1186/s40677-022-00216-3

Xu, H., He, X., Shan, F., Niu, G. and Sheng, D., 3D Simulation of Debris Flows with the Coupled Eulerian–Lagrangian Method and an Investigation of the Runout, Mathematics, 11 (**2023**) 3493. https://doi.org/10.3390/math11163493

Yang, L., Wei, Y., Wang, W. and Zhu, S., Numerical Runout Modeling Analysis of the Loess Landslide at Yining, Xinjiang, China, Water, 11 (**2019**) 1324.

Yin, H., Zhou, W. and Peng, Z., Numerical Simulation of Rainfall-Induced Debris Flow in the Hongchun Gully Based on the Coupling of the LHT Model and the Pudasaini Model, Natural Hazards, 117 (**2023**) 2553–2572.

Yu, J., Berry, P., Guillod, B.P. and Hickler, T., Climate Change Impacts on the Future of Forests in Great Britain, Frontiers in Environmental Science, 9 (**2021**) 640530. 10.3389/fenvs.2021.640530

Yunus, A.P., Fan, X., Subramanian, S.S., Jie, D. and Xu, Q., Unraveling the Drivers of Intensified Landslide Regimes in Western Ghats, India, Science of The Total Environment, 770 (**2021**) 145357, https://doi.org/10.1016/j.scitotenv.2021.145357.

Yunus, A.P., Xinyu, C., Catani, F., Subramaniam, S.S., Fan, X., Jie, D., Sajinkumar, K. S., Gupta, A. and Avtar, R., Earthquake-Induced Soil Landslides: Volume Estimates and Uncertainties with the Existing Scaling Exponents, Sci. Rep., 13 (**2023**) 8151. https://doi.org/10.1038/s41598-023-35088-6

Zahra, T., Quantifying Uncertainties in Landslide Runout Modelling. Master of Science Thesis, International Institute for Geo-Information Science and Earth Observation Enschede, The Netherlands, and Indian Institute of Remote Sensing Dehradun, India., **2010**.

Zaruba, Q. and Mencl, V. Landslides and Their Control, Elsevier: Amsterdam, **1969**.

Zeng, P., Sun, X., Xu, Q., Li, T. and Zhang, T., 3D Probabilistic Landslide Run-Out Hazard Evaluation for Quantitative Risk Assessment Purposes, Engineering Geology, 293 (**2021**) 106303. https://doi.org/10.1016/j.enggeo.2021.106303.

Zhang, Y., Ge, T., Tian, W. and Liou, Y.A., Debris Flow Susceptibility Mapping Using Machine-Learning Techniques in Shigatse Area, China, Remote Sens., 11 (**2019**) 2801.

Zhang, Y., Chen, J., Tan, C., Bao, Y., Han, X., Yan, J. and Mehmood, Q., A Novel Approach to Simulating Debris Flow Runout Via a Three-Dimensional CFD Code: A Case Study of Xiaojia Gully, Bull. Eng. Geol. Environ., 80 (**2021**) 5293–5313. https://doi.org/10.1007/s10064-021-02270-x

Zhang, S., Bai, L., Li, Y., Li, W. and Xie, M., Comparing Convolutional Neural Network and Machine Learning Models in Landslide Susceptibility Mapping: A Case Study in Wenchuan County, Front. Environ. Sci., 10 (**2022a**) 886841. doi: 10.3389/fenvs.2022.886841

Zhang, Y., Shen, C., Zhou, S. and Luo, X., Analysis of the Influence of Forests on Landslides in the Bijie Area of Guizhou, Forests, 13 (**2022b**) 1136. https://doi.org/10.3390/f13071136

Zhao, H., Amann, F. and Kowalski, J., Emulator-Based Global Sensitivity Analysis for Flow-Like Landslide Run-Out Models, Landslides, 18 (**2021**) 3299–3314. https://doi.org/10.1007/s10346-021-01690-w

Zhao, H. and Kowalski, J., Bayesian Active Learning for Parameter Calibration of Landslide Run-Out Models, Landslides, 19 (**2022**) 2033–2045. https://doi.org/10.1007/s10346-022-01857-z

Zhou, W., Fang, J., Tang, C. and Yang, G., Empirical Relationships for The Estimation of Debris Flow Runout Distances on Depositional Fans in The Wenchuan Earthquake Zone, Journal of Hydrology, 577 (**2019**) 123932. https://doi.org/10.1016/j.jhydrol.2019.123932

Zhou, W., Qiu, H., Wang, L., Pei, Y., Tang, B., Ma, S., Yang, D. and Cao, M., Combining Rainfall-Induced Shallow Landslides and Subsequent Debris Flows for Hazard Chain Prediction, CATENA, 213 (**2022**) 106199. https://doi.org/10.1016/j.catena.2022.106199

Zhu, C., He, M., Karakus, M., Cui, X. and Tao, Z., Investigating Toppling Failure Mechanism of Anti-dip Layered Slope due to Excavation by Physical Modelling, Rock Mech. Rock Eng., 53 (**2020**) 5029–5050. https://doi.org/10.1007/s00603-020-02207-y

Zhu, D., Song, K., Mu, J., Huang, H., Du, H., Ziazhuang, F. and Sun, C., Effect of Climate Change Induced Extreme Precipitation on Landslide Activity in the Three Gorges Reservoir China, Bull. Eng. Geo. Environ., 80 (**2021a**) 781–794.

Zhu, C., He, M., Karakus, M., Zhang, X. and Tao, Z., Numerical Simulations of the Failure Process of Anaclinal Slope Physical Model and Control Mechanism of Negative Poisson's Ratio Cable, Bull. Eng. Geol. Environ., 80 (**2021b**) 3365–3380. https://doi.org/10.1007/s10064-021-02148-y

Zydroń, T., Demczuk, P. and Gruchot, A., Assessment of Landslide Susceptibility of the Wiśnickie Foothills Mts. (The Flysch Carpathians, Poland) Using Selected Machine Learning Algorithms, Front. Earth Sci., 10 (**2022**) 872192. doi: 10.3389/feart.2022.872192